Controlling the structure of supramolecular fibre formation for benzothiazole based hydrogels with antimicrobial activity against methicillin resistant *Staphylococcus aureus*†

Kira L. F. Hilton, Antonis A. Karamalegkos, Nyasha Allen, Lauren Gwynne, Bree Streather, Lisa J. White, Karen B. Baker, Samantha A. Henry, George T. Williams, Helena J. Shepherd, Mark Shepherd, Charlotte K. Hind, Mark J. Sutton, Toby A. Jenkins,* Daniel P. Mulvihill,* Jennifer M. A. Tullet,* Marina Ezcurra* and Jennifer R. Hiscock*

Contents

Section 1: Summary tables of data

Table S1 - Overview of gaseous and solution state studies.

SSA	Gas Phase Dimer	K_{dim} (M^{-1})	d_H (nm)	Zeta potential (mV)	CAC (mM)	Surface tension at CAC (mN m^{-1})
1	Y	0.09 ± 1.8 %	181	-42.71	*a*	*a*
2[1]	Y	2.70 ±	300	-101	0.50	46.05
3	N	0.00 ± >0.01 %	815	-88.29	1.92[2]	56.24[2]
4	N	6.26 ± 1.0 %	115	-74.80	14.77[2]	45.16[2]
5	N	*a*	*C*	*c*	4.56[2]	44.92[2]
6	N	92.72 ± 1.3 %	127	-84.22	3.03[2]	49.90[2]
7	Y	*b*	255	-67.13	5.16[2]	66.97[2]

a – Compound is in slow exchange.
b – Multiple association events prevent data fitting.
c – Could not be calculated due to compound solubility.
Abbreviations: Critical aggregation concentration (CAC).

Table S2 - Overview of the results from quantitative ^{1}H NMR studies. Values given in % represent the observed proportion of compound that became NMR silent.

SSA	DMSO-d_6 1 % DCM (%)		D_2O 5 % EtOH (%)	
	Anionic component	Cationic component	Anionic component	Cationic component
1	0	0	62	*a*
2[1]	0	0	10	8
3	0	0	48	45
4	0	0	19	*a*
5	0	0	*b*	*b*
6	0	0	53	47
7	22	20	55	51

a – Could not be calculated due to overlapping peaks.
b – Could not be calculated due to compound solubility.

Table S3 - Overview of minimum gelation concentrations.

Salt solution	Concentration (mg/mL)						
	1	**2^3**	**3**	**4**	**5**	**6**	**7**
NaCl	*a*	1.5	*b*	*b*	*a*	*a*	1.5
KCl	*a*	2.5	*b*	*b*	*a*	*a*	*a*
$NaNO_3$	*a*	1.5	*b*	*b*	*a*	*b*	2
NaH_2PO_4	*a*	1.5	*b*	*b*	*a*	*a*	*b*
NaOBz	*a*	1.5	*a*	*b*	*a*	*b*	2
Na_2SO_4	*a*	3.5	*b*	*b*	*a*	*b*	*b*

a – Precipitation occurred at 5 mg/mL.
b – Heterogeneous mixture of gel-sol formed at 5 mg/mL.

Table S4 - Overview of melting temperature (T_m) of homogenous hydrogels at 5 mg/mL.

Aqueous salt solution	T_m (ºC)	
	2^3	**7**
NaCl	51.2 ± 0.1	37.4 ± 0.3
KCl	54.8 ± 0.1	*a*
$NaNO_3$	54.5 ± 0.2	37.2 ± 0.5
NaH_2PO_4	43.9 ± 0.1	*b*
NaOBz	52.4 ± 0.1	35.1 ± 0.1
Na_2SO_4	43.2 ± 0.1	*b*

a – Precipitation occurred at 5 mg/mL. No evidence of gel formation.
b – Heterogenous gel-sol mixture observed at 5 mg/mL.

Table S5 – Effect of SSAs on development of *C. elegans* GLO-1 mutant. Error = standard deviation.

	Control	**4**	**6**
L3	0.637 ± 0.1	0.681 ± 0.1	0.647 ± 0.1
L4	0.363 ± 0.1	0.319 ± 0.1	0.353 ± 0.1

Table S6 – Overview of brood size assay against lab strain N2 *Caenorhabditis elegans* (*C. elegans*) and knock out mutant GLO-1 *C. elegans* against OP50 *E. coli* only and OP50 *E. coli* with 0.05 % ethanol in H_2O. Error = standard deviation, control = 0.05 % EtOH.

	OP50		**0.05 % EtOH**	
	Brood size	**Error**	**Brood size**	**Error**
N2	249.53	14.88	205.07	13.15
GLO-1	216.53	11.46	189.20	18.12

Table S7 – Overview of brood size of knock out mutant GLO-1 *C. elegans* against **4** and **6**. Error = standard deviation, control = 0.05 % EtOH.

	Brood size	**Error**
4	168.86	9.69
6	156.33	9.21
Control	164.25	7.52

Section 2: Chemical experimental

General remarks: All NMR spectra were obtained using a Bruker AV2 400 MHz or AVNEO 400 MHz spectrometer. The data was processed using Topspin software. NMR Chemical shift values are reported in parts per million (ppm) and calibrated to the centre of the residual solvent peak set (s = singlet, br = broad, d = doublet, t = triplet, q = quartet, m = multiplet). Tensiometry measurements were undertaken using the Biolin Scientific Theta Attension optical tensiometer. The data was processed using Biolin OneAttension software. A Hamilton (309) syringe was used for these measurements. High resolution mass spectrometry was performed using a Brucker microTOF-Q mass spectrometer and spectra recorded and processed using Brucker's Compass Data Analysis software. DLS and Zeta Potential studies were carried out using an Anton Paar Litesizer^{TM} 500 and processed using Kalliope TM professional. Rheological measurements were recorded on an Anton Parr modular compact rheometer (MCR302) using a cylinder probe ST10-4V-8.8/97.5. UV-Vis absorbance and optical density measurements were conducted and analysed using a Clariostar plate reader and MARS data analysis software.

Quantitative ^{1}H NMR studies: The sample is prepared at a known concentration, with the T_1 relaxation time set to 60 seconds. For quantification in polar organic DMSO-*d_6* the sample is doped with 1 % DCM, for quantification in aqueous D_2O, the sample is doped with 5 % EtOH. The ^{1}H NMR resonance of the doped solvent is then integrated. To establish the proportion of SSA that has become ^{1}H NMR 'silent', the ratio of DCM : SSA is determined using the mmol – 0.08/0.0556 mmol = 1.44, which is doubled due to the two protons present in the DCM peak, giving a ratio of 1 : 2.88. The DCM CH_2 signal is then set to 2.88 and the anionic/cationic peak of SSA is integrated. If the SSA signal is less than the expected value (eg. integrates for 0.52 rather than 1), then the percentage loss is calculated (eg. 48 %). This is repeated for aqueous D_2O doped with 5 % EtOH.

Self-association constant calculation: Self-association constants were determined using Bindfit v0.5 (http://app.supramolecular.org/bindfit/).[4] All data can be accessed online using the hyperlinks provided.

Tensiometry Studies: All samples were prepared in an EtOH:H_2O (1:19) solution. All samples underwent an annealing process in which the various solutions were heated to approximately 313 K before being allowed to cool to room temperature, allowing each sample to reach a thermodynamic minimum. All samples were prepared through serial dilution of the most concentrated sample. Three surface tension measurements were obtained for each sample at a given concentration, using the pendant drop method. The average of the three values were plotted to calculate the critical aggregation concentration (CAC).

Mass spectrometry: Approximately 1 mg of each SSA was dissolved in 1 mL of methanol. This solution was further diluted 100-fold before undergoing analysis where 10 µL of each sample was injected directly into a flow of 10 mM ammonium acetate in 95 % water (flow rate = 0.02 mL/min).

DLS studies: All vials used for preparing the samples were clean and dry. All solvents used were filtered to remove any particulates that may interfere with the results obtained. Samples of differing concentrations were obtained through serial dilution of a concentrated solution. All samples underwent an annealing process, in which they were heated to 313 K before being allowed to cool to 298 K to allow each sample to reach a thermodynamic minimum. A series of 9 or 10 runs were recorded at 298 K.

Zeta potential studies: All vials used for preparing the samples were clean and dry. All solvents used were filtered to remove any particulates that may interfere with the results obtained. All samples underwent an annealing process, in which they were heated to 313 K before being allowed to cool to room temperature, allowing each sample to reach a thermodynamic minimum. The final zeta potential value given is an average of the number of experiments conducted at 298 K.

Hydrogel preparation: The appropriate aqueous salt solution (1 mL, 0.505 M) was added to the specified quantity of the SSA in a glass vial and heated to approximately 323 K until dissolved and then sealed and left at room temperature to allow gelation to occur. The samples then underwent an inversion test for the formation of a hydrogel, this was then confirmed through rheological measurements.

Annealing processes for spherical aggregate and hydrogel formation: As we have previously reported, SSAs such as those reported herein typically self-associate in polar organic solutions (DMSO) to form anionic hydrogen bonded dimers, when in 1:19 EtOH:H_2O solution these same compounds self-associate to form spherical aggregates, which we have previously shown to reach a thermodynamic minimum, following an annealing process, in which these species are heated to 313 K before being allowed to cool to room temperature (298 K).[5] However, when placed into an aqueous salt solution these same compounds are found to form fibrous structures however, this process only occurs after heating this mixture to 323 K due to the change in solvation environment and as a result of the different self-association events present.[3,6]

Rheometer hydrogel preparation and experimental: Each experiment was run in triplicate. The appropriate aqueous salt solution (1 mL, 0.505 M) was added to 5 mg of the compound in a glass vial with an internal diameter of 1 cm and heated to approximately 323 K, until dissolved. The sample was positioned on the rheometer and set with a relaxation time of 30 minutes. Oscillatory amplitude experiments maintained a frequency of 10 rad s^{-1} and were performed with the amplitude of oscillation from 0.01 % up to 100 % at 298 K. Where a gel/sol transition was not observed, the oscillation was increased to 1000 %. Oscillatory frequency sweep experiments maintained a constant shear strain (γ) with an increasing frequency from 0.01-100 rad s^{-1} at 298 K.

Fluorescence microscopy: Samples were visualised using an Olympus IX71 microscope with PlanApo 100x OTIRFM-SP 1.49 NA lens mounted on a PIFOC z-axis focus drive (Physik Instrumente, Karlsruhe, Germany), fitted onto an ASI motorised stage (ASI, Eugene, OR), with the sample holder, objective lens and environmental chamber held at the required temperature. Samples were illuminated using LED light sources (Cairn Research Ltd, Faversham, UK) with DC/ET350/50x excitation and DC/457/50m emission filters (Chroma, Bellows Falls, VT). Samples were visualised using a Zyla 5.5 (Andor) CMOS camera, and the system was controlled with Metamorph software (Molecular Devices).

Fluorescence microscopy preparation: Microscope slide prepared with chamber using a coverslip secured on three sides with double sided tape. Aqueous salt (0.505 M) added to relevant SSA (5 mg/mL) and heated to ~ 323 K and immediately transferred to prepared chamber.

Fluorescence image processing: ImageJ (FIJI) software, 64-bit windows version was used to process all fluorescent images. Final images were acquired by performing 'z stack max projection' on all the stacks of each image file (.tiff).

Quantification of SSA hydrogel fibre characteristics: To quantify the characteristics of the hydrogel fibres, fluorescence microscopy images were processed and coloured to ensure maximum contrast using ImageJ (FIJI) software. To ensure a valid representation of the fibres present, a minimum of 4 images containing at least 15 fibres each were examined. These fibres were then sorted into categories as listed below:

- **Curled** (e.g. as observed in Figure S108a): When the equivalent to a 10 nM straight line in ImageJ, drawn using a line tool, was traced over a fibre, if any deviation from a straight line was observed, the fibre was characterised as 'curled'.

- **Straight** (e.g. as observed in Figure S108b): When the equivalent to a 10 nM straight line in ImageJ, drawn using a line tool, was traced over a fibre, if no deviation from a straight line was observed, the fibre was characterised as ‘straight’.
- **Linked** (e.g. as observed in Figure S108b): When tracing a fibre in the network with a line tool in ImageJ, if an intersection between two or more fibres was observed, forming a ‘node’, the fibre was characterised as ‘linked’.
- **Independent** (e.g. as observed in Figure S106d, S111c): When tracing a fibre in the network with a line tool in ImageJ, if no intersection with another fibre was observed, the fibre was characterised as ‘independent’.

To measure the length of the fibres, nodes in linked fibre networks were used as start or end points. For independent fibres, the tapered ends of each fibre was determined to be the start and end of the fibre.

- **Short** (e.g. as observed in Figure S108b): The line tool in ImageJ was used to trace the length of the fibre. If the fibre was < 20 nm in length, it was characterised as ‘short’.
- **Long** (e.g. as observed in Figure S108a, S111c): The line tool in ImageJ was used to trace the length of the fibre. If the fibre was > 20 nm in length, it was characterised as ‘long’.

The packing density of the fibres was determined using the amount of aqueous salt solution visible in the microscopy image.

- **Densely packed** (e.g. as observed in Figure S108a, S111c): Gel fibres that were close together (<5 nm) were defined as ‘densely packed’.
- **Medium packing** (e.g. as observed in Figure S106d, S108b): Gel fibres that were further apart (5 – 20 nm), and held together through cross linking or twisted fibres, were defined as ‘medium packing’.
- **Low packing density** (e.g. as observed in Figure S107e): Gel fibres that are far apart (< 20 nm), were defined as ‘low packing density’.
- **Uniform** (e.g. as observed in Figure S108b): If the fibre is structured with a reproducible pattern, the fibres were defined as ‘uniform’.
- **Stochastic** (e.g. as observed in Figure S108a S111f, S111c): If the fibre network was not structured with no reproducible pattern present, the fibres were defined as ‘stochastic’.
- **Unidirectional** (e.g. as observed in Figure S106d): The line tool in ImageJ was used to trace the fibres, and if the fibres were > 90 % aligned in one direction, the fibres were characterised as ‘unidirectional’.
- **Multidirectional** (e.g. as observed in Figure S111f): The line tool in ImageJ was used to trace the fibres, and if the fibres were not aligned in a single direction, the fibres were characterised as ‘multidirectional’.

Preparation of 96-well microplates: Standards and supramolecular hydrogels/heterogenous gel-so mixtures (n=3) were prepared in low UV-transparent 96-well microplates. Standards or SSA in the relevant solutions (1.5 mg/mL) were transferred as 200 µL aliquots to each microplate well, at a temperature higher than the melting point.

UV-Vis spectroscopy: After preparation, the low UV-transparent 96-well microplate was transferred into the plate reader at an equilibrated temperature of 318 K and absorbance measurements taken at 5-degree decreases from 318 K to 298 K. All experiments repeated in triplicate to ensure experimental reproducibility.

Optical density (OD) spectral well scans: After preparation, the low UV-transparent 96-well microplate was transferred into the plate reader at an equilibrated temperature of 318 K and spectral well scans read through the sample at 5-degree decreases from 318 K to 298 K at $Abs._{450}$. All experiments were repeated in triplicate to ensure experimental reproducibility.

Section 3: Microbial material and methods

Preparation of Luria Broth media (LB): Yeast extract (5 g), tryptone (10 g) and NaCl (10 g) were dissolved in dH_2O (1 L) then divided into bottles and autoclaved.

Preparation of Luria Broth (LB) agar plates: Agar (15 g) was added to LB (1 L) and autoclaved. Once cool, the LB agar was poured into sterile petri dishes under sterile conditions and allowed to set. LB plates were stored at 4 °C until use.

Preparation of bacterial plates: Sterile LB agar plates were streaked using USA300 Methicillin resistant *Staphylococcus aureus* (MRSA) then incubated at 37 °C overnight.

Formation of 1 % agarose pad controls: Powdered agarose was dissolved in either dH2O or 0.505 M NaCl and microwaved. 500 µl per pad was pipetted onto a petri dish, under sterile conditions. For the 0.505 M NaCl + oxacillin control, 400 µl of 1.2% agarose in 0.505 M NaCl was mixed with 100 µl of oxacillin in 0.505 M NaCl so the final concentration of agarose was 1%, and oxacillin was 1:1 molar concentration with **7**.

Preparation of inoculum: A starter culture was made by inoculating LB media (5 ml) with at least 4 single colonies of MRSA and incubated at 37 °C overnight. The following day, a 1:100 subculture was made and incubated at 37 °C until it reached an optical density of 0.4 at 600 nm. Density was adjusted using LB to equal 0.5 McFarland standard (107 – 108 cfu/ml). A 1:1000 dilution was carried using the McFarland adjusted culture (150 µl) and LB (14.85 ml) to achieve a final cell concentration of 105 cfu/ml. All work was carried out under sterile conditions.

Surface diffusion assay: After autoclaving, LB agar was placed in a 42 °C water bath until the temperature equilibrated. The molten agar was inoculated with the MRSA subculture (see preparation of inoculum) with 15 ml culture to 200 ml agar. The subculture and agar were mixed immediately and aliquoted (20 ml) into sterile petri dishes and left to set. The set SSA gel (500 µl), +/- oxacillin, was removed from the vial in which it was made and placed in the centre of the agar, one per plate. All work was carried out under sterile conditions. The plates were incubated overnight at 37 °C and imaged the following day using a light box.

Section 4: *C. elegans* material and methods

***C. elegans* strains and husbandry**: *C. elegans* were cultured as previously described,[7] and maintained at 293 K. As wildtype *C. elegans* is intrinsically auto-fluorescent,[8] with overlapping with fluorescence properties of SSAs **2**-**7**, GH10 *glo-1(zu437)* mutants, a strain with reduced autofluorescence was used for all experiments.[9] Experimental plates with SSAs **2-7** were prepared by seeding NGM plates with 400 µL *E. coli* OP50, dried for 48 hours, followed by adding 100 µL of SSA in 5 % EtOH or a 5 % EtOH to give a final concentration of 0.10 mM SSA. Plates were incubated for an additional 48 hours before use. Synchronised *C. elegans* populations were generated by placing 20-30 adults on the experimental plates and left to lay eggs for 2-3 hours before removal.

Microscopy and Image acquisition: To prepare slides for imaging, agarose solution (2 %) was heated to 368 K, pipetted onto frosted microscope slides and flattened to form a mounted pad. SSA incubated nematodes (10 µL) were transferred to the slide, immobilised with levamisole (10 µL, 100 mM) in M9 buffer and secured with a glass cover slide. Microscopy was performed using an inverted Olympus IX81 microscope with an Andor Xyla 4.1 cMOS

camera with CoolLED illumination for desired fluorescence wavelength. All images were taken using 63x magnification and z-stacks were acquired using 20 steps of 0.75 µm each. Fluorescent images were acquired using DAPI filter (405 nm) at 200 ms exposure time, while bright-field images were acquired under bright-field light at 20 ms exposure time.

Development assay: 10 adult nematodes were left to lay eggs on NGM plates incubated with SSA or vehicle control for 3 hours at 293 K, then removed from the plate. After 52 hours an image of the plate was taken, the number of animals in L3 and L4 stages quantified, and the L3:L4 ratio calculated.

Brood size assay: 10 L4 stage nematodes were plated on individual NGM plates incubated with SSA or control. Every 24 hours each animal moved to a new experimental plate, up to 72 hours. Viable offspring on each plate were quantified and total brood size calculated.

Synchronising nematode populations: Adult *Caenorhabditis elegans (C. elegans*) (20-30) picked on a seeded NGM plate and left to lay eggs for 2-3 hours and removed.

Liquid nematode incubation with SSAs: Synchronised L4 stage nematodes were grown on NGM plates with *E. coli* OP50, 'washed off' using M9 solution and left to settle at the bottom of a sterile 15 mL falcon tube. Once settled, excess M9 solution was removed, and used to distribute the nematodes into a 96-well plate. Each well contained 60 µL M9 containing worms, 20 µL *E. coli* OP50 overnight suspension, 20 µL 5 % EtOH SSA solution / 5 % EtOH control. The microplate was then incubated at 293 K for 24 hours.

Preparation of M9 buffer: KH_2PO_4 (3 g), Na_2HPO_4 (6 g), NaCl (5 g) were dissolved in dH_2O (1 L) and autoclaved. Once cool, $MgSO_4$ (1 mL) was added to avoid precipitation.

Preparation of Nematode Growth Media (NMN): NaCl (3 g), peptone (2.5 g) and agar (17 g) were dissolved in dH_2O (0.97 L) and autoclaved. Once cool, filter sterilised KH_2PO_4 (25 mL, pH 6), $CaCl_2$ (1mL), $MgSO_4$ (1 mL) and cholesterol (1 mL) were added, and the resulting solution poured into 6 cm plates under sterile conditions.

Preparation of *Escherichia coli* (*E. coli*) suspension: *E. coli* OP50 frozen stocks were streaked onto agar plates and incubated at 37 °C Single colonies were used to inoculate 5 mL of LB and incubated at 37 °C overnight, under sterile conditions.

Seeding NGM plates: NMN agar plates were left to dry for at least 72 hours before seeding. *E. coli* OP50 (400 µL) was pipetted onto the centre of each plate and incubated at room temperature for 48 hours before use, under sterile conditions.

NGM plate incubation with SSAs: 100 µL of SSA in 5 % EtOH or a 5 % EtOH control was added to a seeded NGM plate and incubated at 293 K for 24 hours.

Section 5: Chemical structures

1

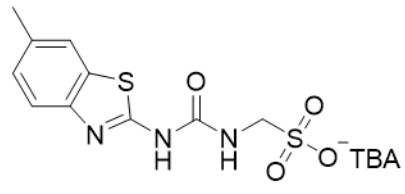

2

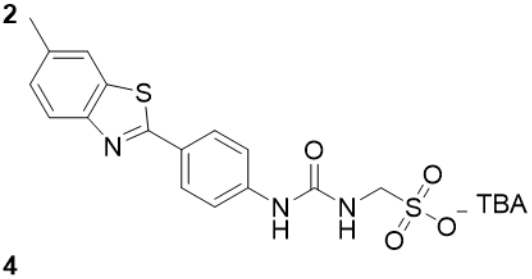

3

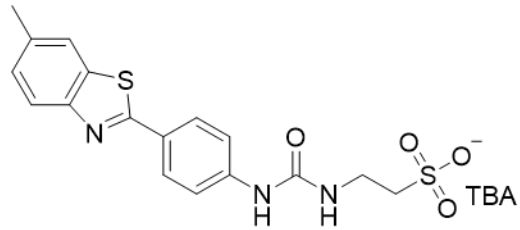

4

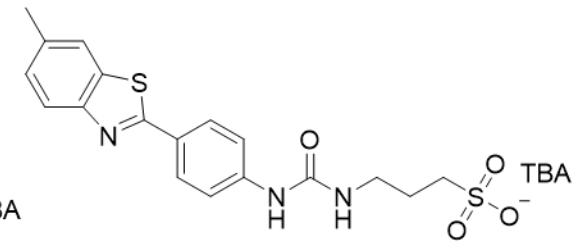

5

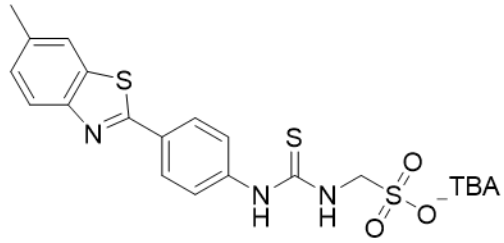

6

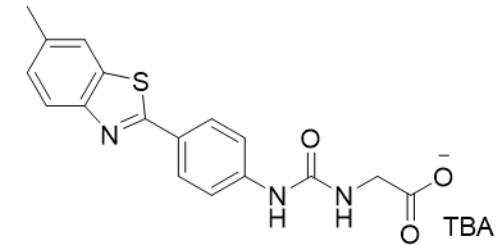

7

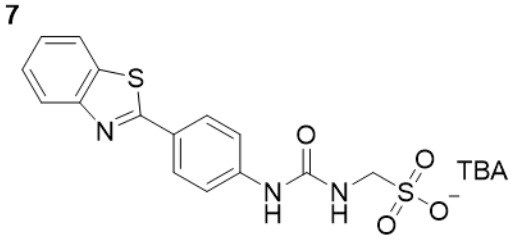

Section 6: Chemical synthesis

1: This compound was synthesized in line with previously published methods.[2] ^{1}H NMR (400 MHz, 298 K, DMSO-d_6): δ: 0.93 (t, *J* = 7.24 Hz, 12H), 1.25 – 1.35 (m, 8H), 1.52 – 1.59 (m, 8H), 2.37 (s, 3H), 3.13 – 3.17 (m, 8H), 3.91 (d, *J* = 5.88 Hz, 2H), 7.11 – 7.17 (m, 2H), 7.50 (d, *J* = 8.16 Hz, H), 7.67 (s, 1H), 10.52 (s, 1H).

2: This compound was synthesized in line with previously published methods.[1] ^{1}H NMR (400MHz, 298K, DMSO-d_6): δ: 0.93 (t, *J* = 7.24 Hz, 12H), 1.25 – 1.34 (m, 8H), 1.55 (m, 8H), 2.44 (s, 3H), 3.13 – 3.17 (m, 8H), 3.89 (d, *J* = 5.84 Hz, 2H), 6.65 (s, 1H), 7.32 (dd, *J* = 8.16, 1.2 Hz, 1H), 7.56 (d, *J* = 8.76 Hz, 2H), 7.86 (m, 4H), 9.15 (s, 1H).

3: This compound was synthesized in line with previously published methods.[2] ^{1}H NMR (400MHz, 298K, DMSO-d_6): δ: 0.93 (t, *J* = 7.36, 12H), 1.26 – 1.36 (m, 8H), 1.53 – 1.60 (m, 8H), 2.45 (s, 3H), 2.57 (t, *J* = 6.04 Hz, 2H), 3.14 – 3.18 (m, 8H), 3.39 (q, *J* = 6.32 Hz, 2H), 6.51 (t, *J* = 5.28 Hz, 1H), 7.32 (d, *J* = 8.04 Hz, 1H), 7.59 (d, *J* = 8.72 Hz, 2H), 7.85 – 7.92 (m, 4H), 9.30 (s, 1H.

4: This compound was synthesized in line with previously published methods.[2] ^{1}H NMR (400MHz, 298K, DMSO-d_6): δ: 0.90 (t, *J* = 7.28, 12H), 1.23 – 1.3231 (m, 8H), 1.49 – 1.57 (m, 8H), 1.78 – 1.83 (m, 2H), 2.42 (s, 3H), 2.54 – 2.58 (m, 2H), 3.10 – 3.21 (m, 10H), 6.73 (t, *J* = 5.64 Hz, 1H), 7.30 (dd, *J* = 8.04, 1.24 Hz, 1H), 7.61 (d, *J* = 8.80 Hz, 2H), 7.83 – 7.90 (m, 4H), 9.11 (s, 1H).

5 This compound was synthesized in line with previously published methods.[2] ^{1}H NMR (400MHz, 298K, DMSO-d_6): δ: 0.93 (t, *J* = 7.28, 12H), 1.26 – 1.35 (m, 8H), 1.52 – 1.60 (m, 8H), 2.46 (s, 3H), 3.13 – 3.18 (m, 8H), 4.09 (s, 0.6H), 4.32 (s 1.4H), 7.34 (dd, *J* = 8.44, 1.48 Hz, 1H), 7.70 – 8.00 (m, 6.7H), 8.71 (s, 0.3H), 10.21 (s, 0.6H), 11.05 (s, 0.2H).

6: This compound was synthesized in line with previously published methods.[2] ^{1}H NMR (400MHz, 298K, DMSO-d_6): δ: 0.92 (t, *J* = 7.28, 12H), 1.25 – 1.34 (m, 8H), 1.51 – 1.58 (m, 8H), 2.44 (s, 3H), 3.12 – 3.16 (m, 8H), 3.39 (d, *J* = 3.48 Hz, 2H), 6.92 (s, 1H), 7.31 (d, *J* = 8.52 Hz, 1H), 7.72 – 7.90 (m, 6H), 10.49 (s, 1H).

7: This compound was synthesized in line with previously published methods.[2] ^{1}H NMR (400MHz, 298K, DMSO-d_6): δ: 0.93 (t, *J* = 7.32, 12H), 1.26 – 1.35 (m, 8H), 1.52 – 1.60 (m, 8H), 3.13 – 3.17 (m, 8H), 3.90 (d, *J* = 5.68 Hz, 2H), 6.65 (s, 1H), 7.41 (t, *J* = 7.76 Hz, 1H), 7.51 (t, *J* = 7.84 Hz, 1H), 7.57 (d, *J* = 8.44 Hz, 2H), 7.95 – 8.00 (m, 3H), 8.09 (d, *J* = 7.92 Hz, 1H), 9.18 (s, 1H).

Section 7: NMR data

Characterisation data

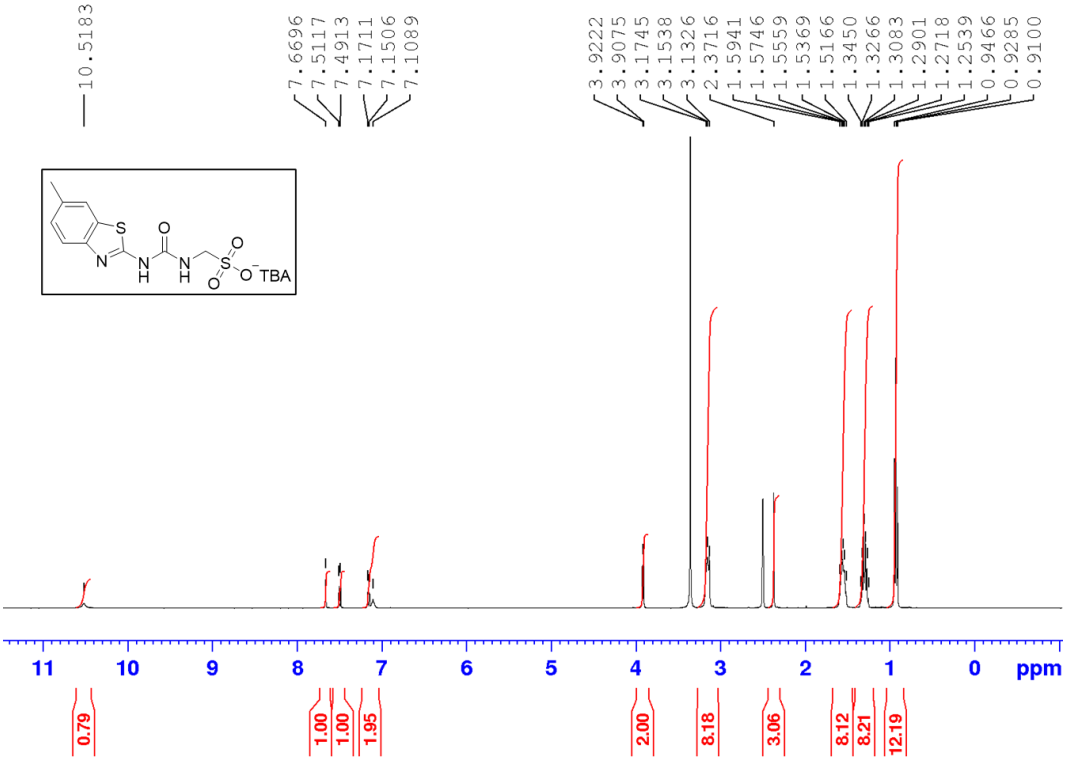

Figure S1 - ^{1}H NMR of SSA **1** in DMSO-d_6 conducted at 298 K.

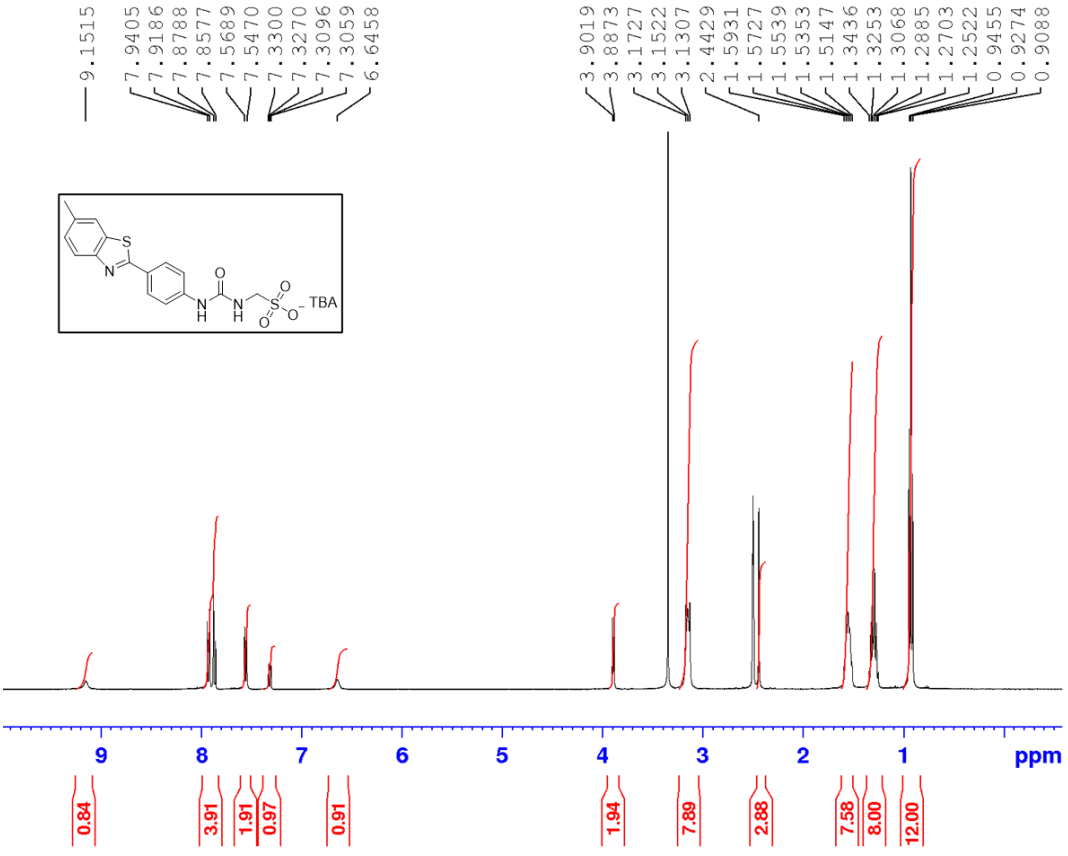

Figure S2 - ^{1}H NMR of SSA **2** in DMSO-d_6 conducted at 298 K.

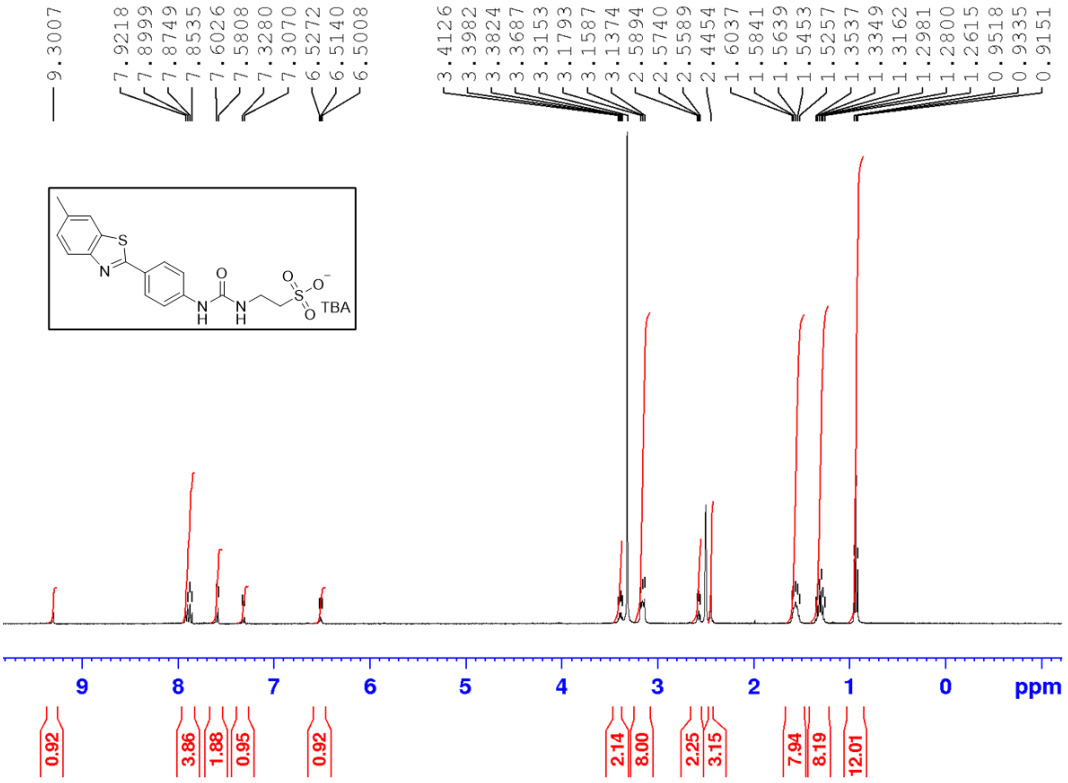

Figure S3 - ^{1}H NMR of SSA **3** in DMSO-d_6 conducted at 298 K.

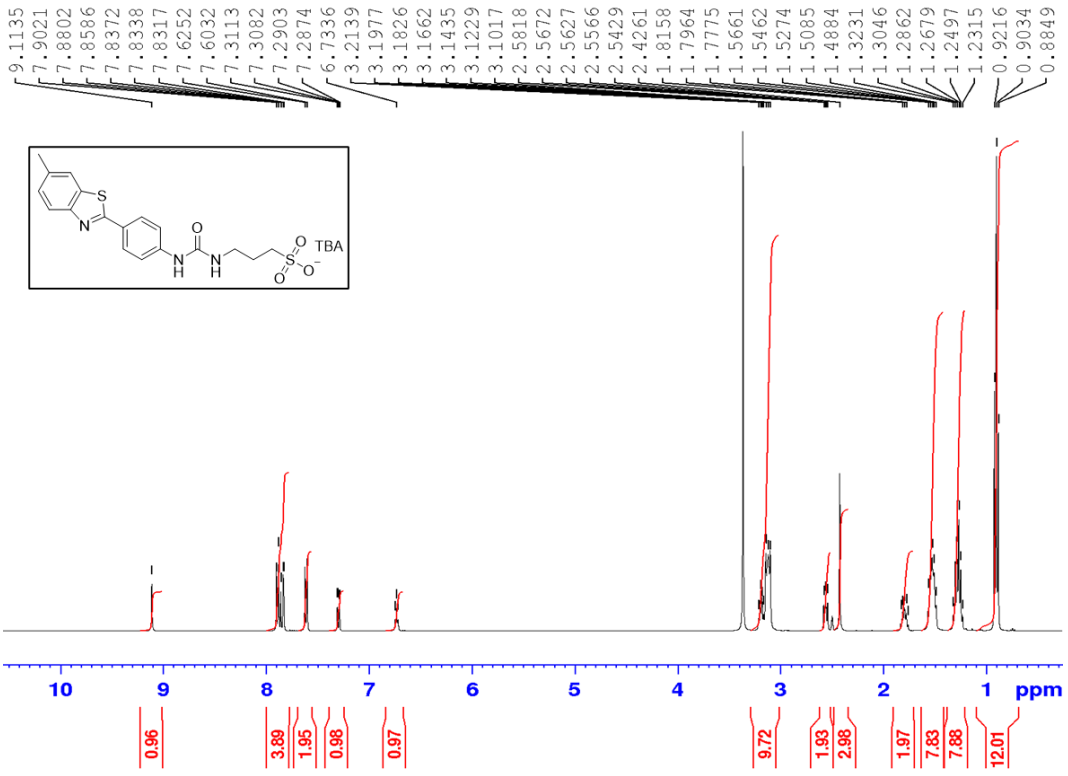

Figure S4 - ^{1}H NMR of SSA **4** in DMSO-d_6 conducted at 298 K.

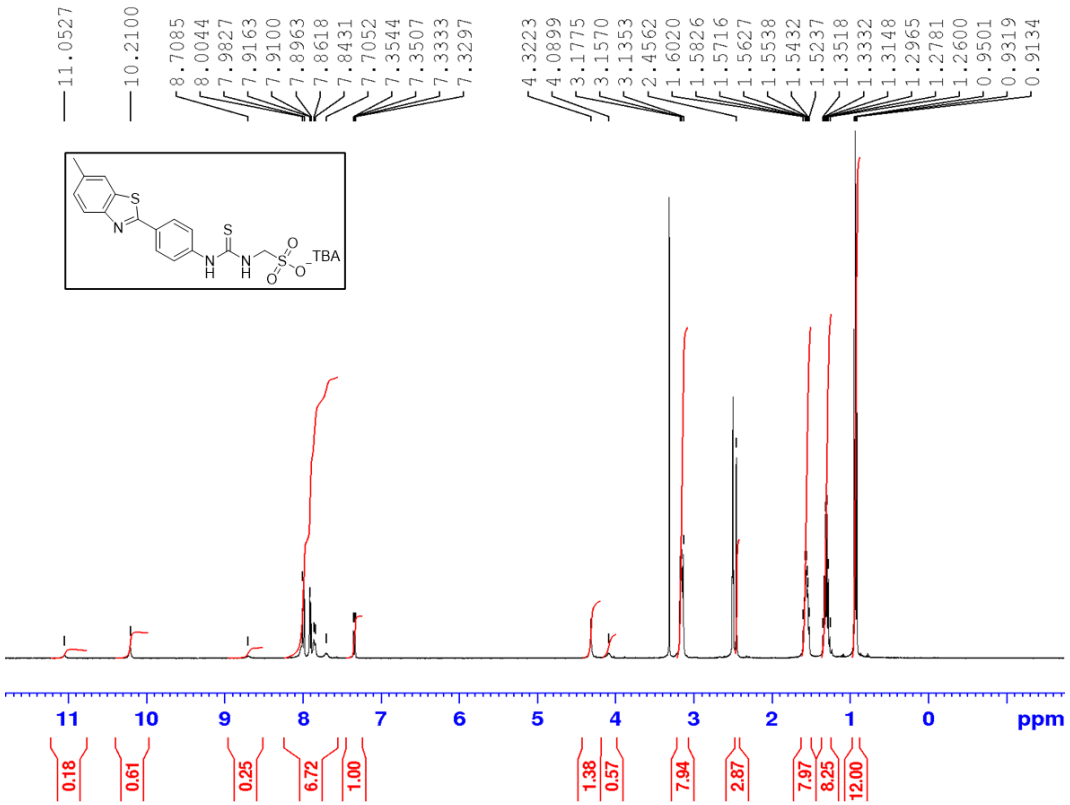

Figure S5 - ^{1}H NMR of SSA **5** in DMSO-d_6 conducted at 298 K.

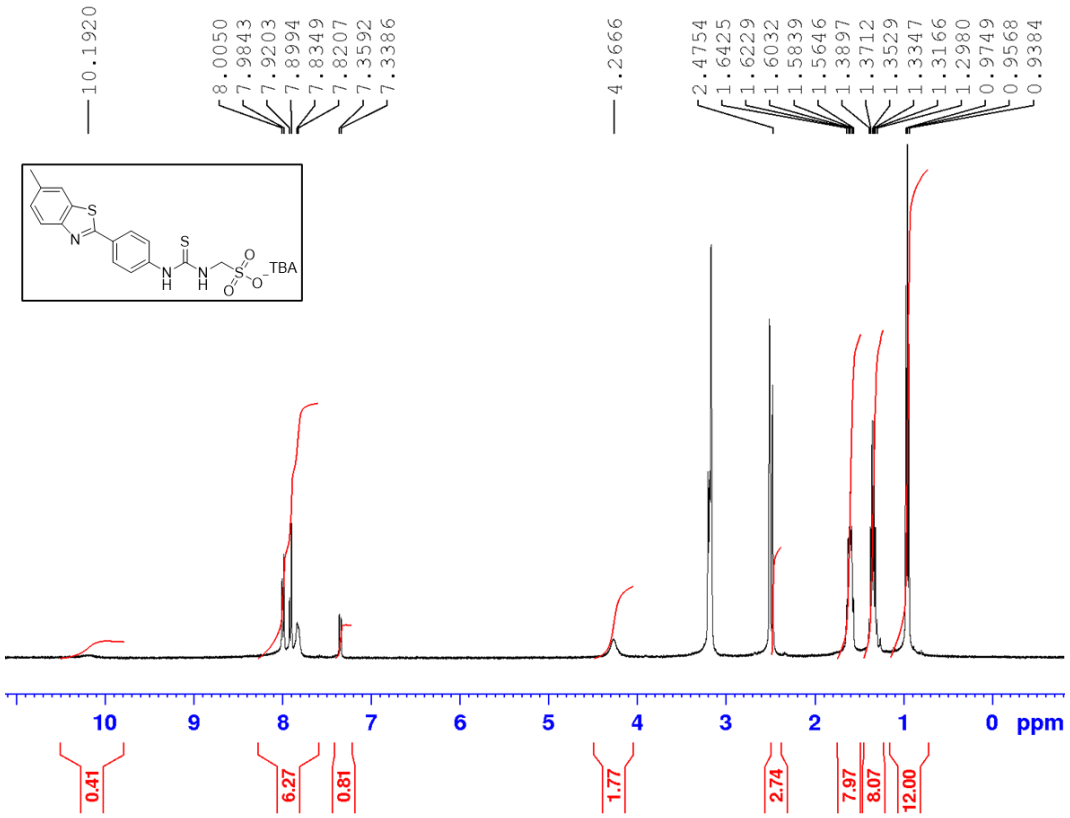

Figure S6 - ^{1}H NMR of SSA **5** in DMSO-d_6 conducted at 333 K.

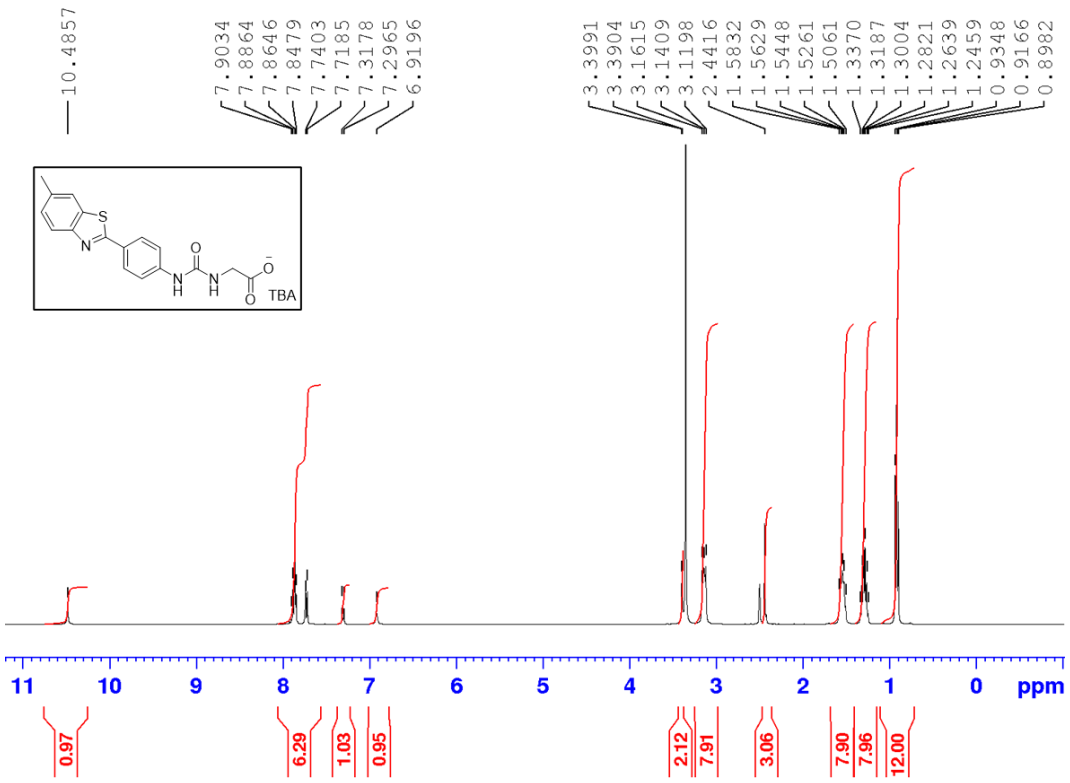

Figure S7 - ^{1}H NMR of SSA **6** in DMSO-d_6 conducted at 298 K.

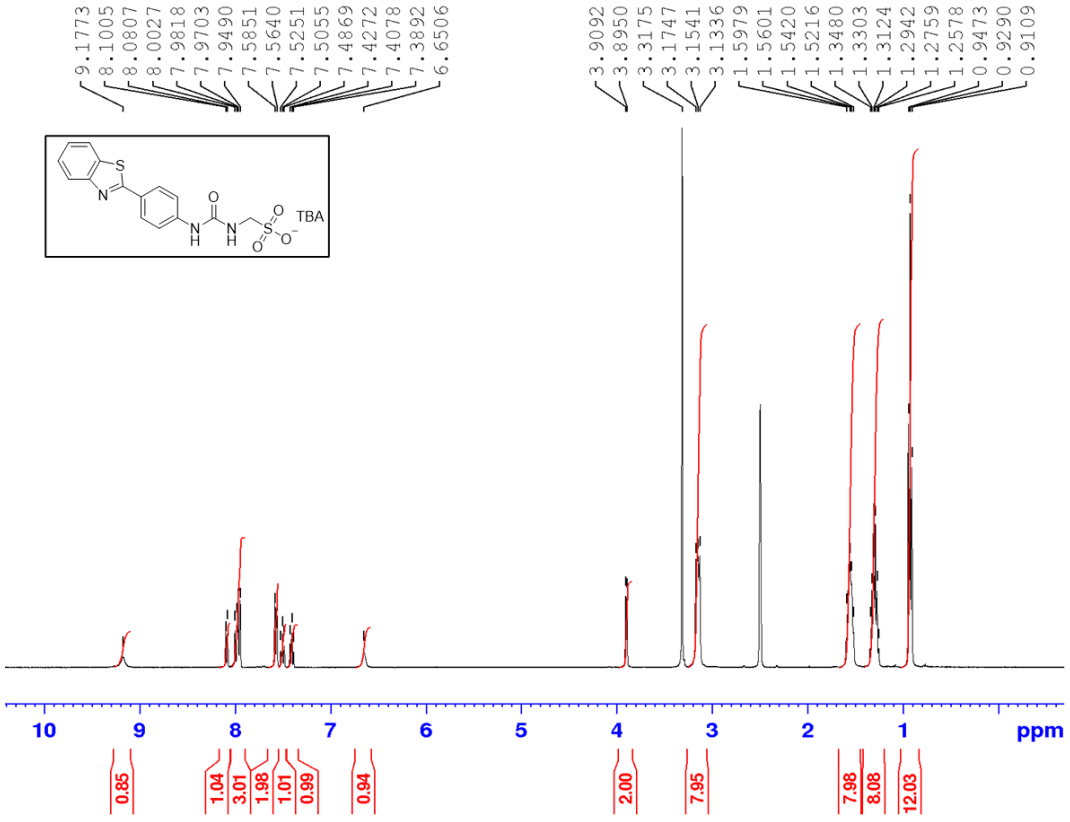

Figure S8 - ^{1}H NMR of SSA **7** in DMSO-d_6 conducted at 298 K.

qNMR data

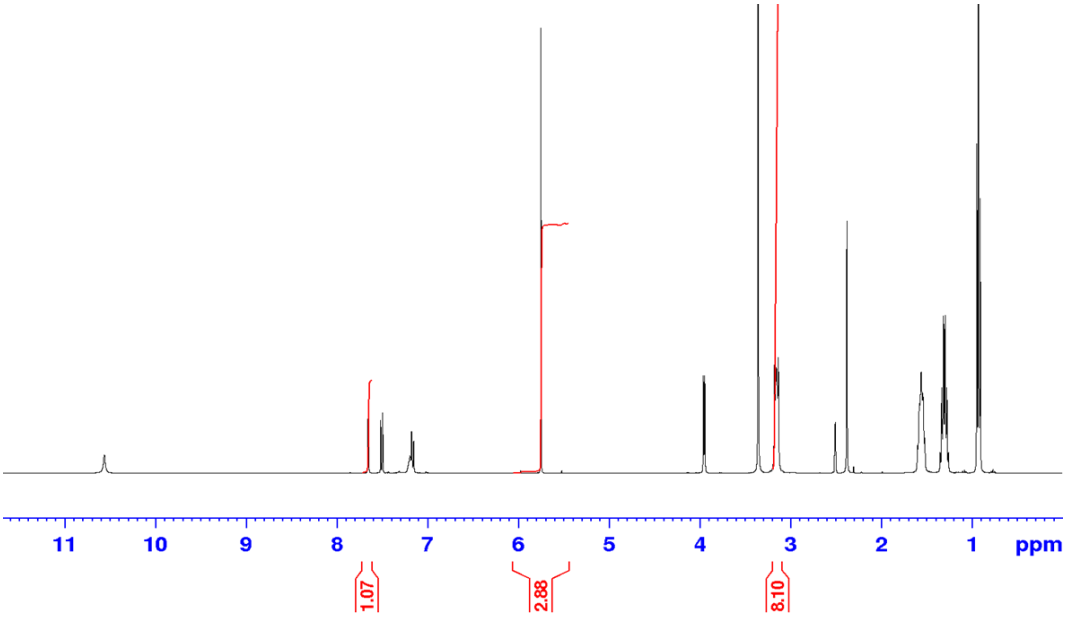

Figure S9 - ^{1}H NMR spectrum (d_1 = 60 s) of SSA **1** (112 mM) in DMSO-d_6/1.0 % DCM. Comparative integration indicates 0 % of the anionic and cationic component of **1** has become NMR silent.

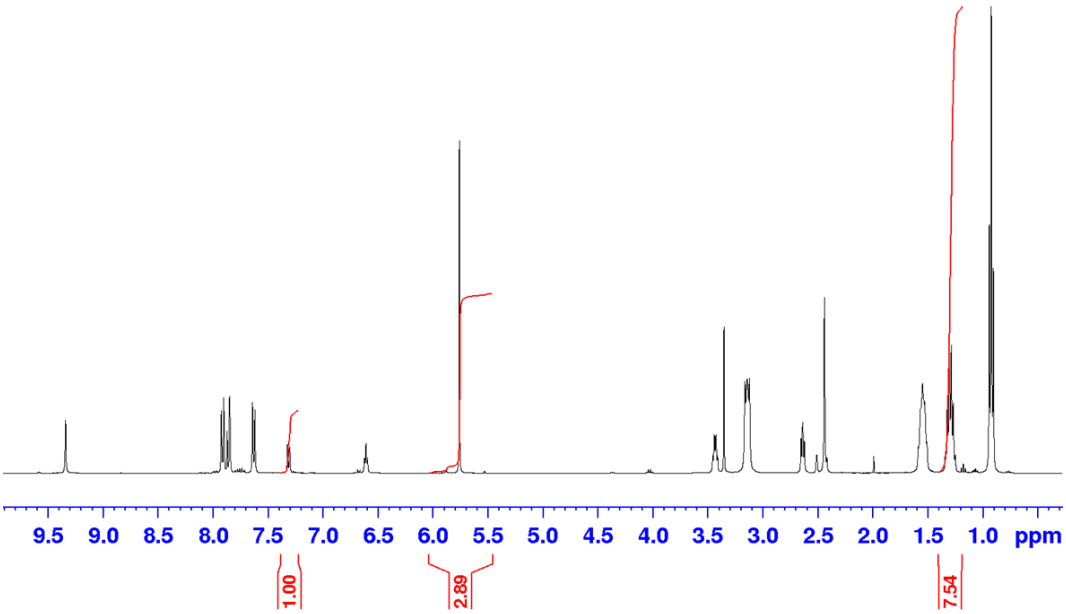

Figure S10 - ^{1}H NMR spectrum (d_1 = 60 s) of SSA **3** (112 mM) in DMSO-d_6/1.0 % DCM. Comparative integration indicates 0 % of the anionic and cationic component of **3** has become NMR silent.

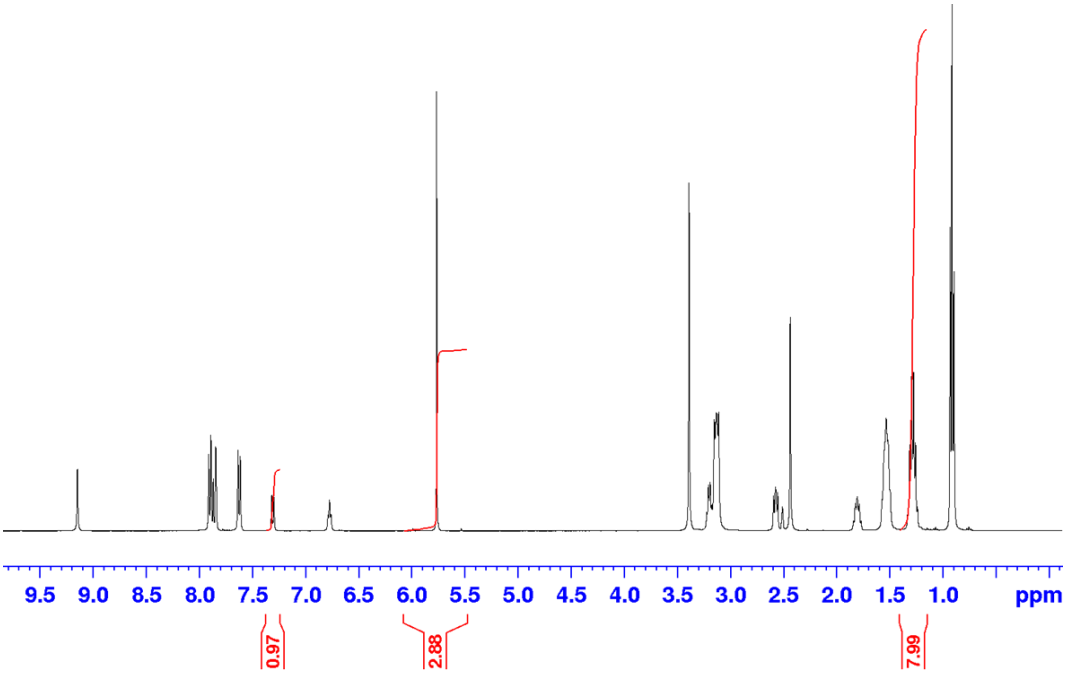

Figure S11 - ^{1}H NMR spectrum (d_1 = 60 s) of SSA **4** (112 mM) in DMSO-d_6/1.0 % DCM. Comparative integration indicates 0 % of the anionic and cationic component of **4** has become NMR silent.

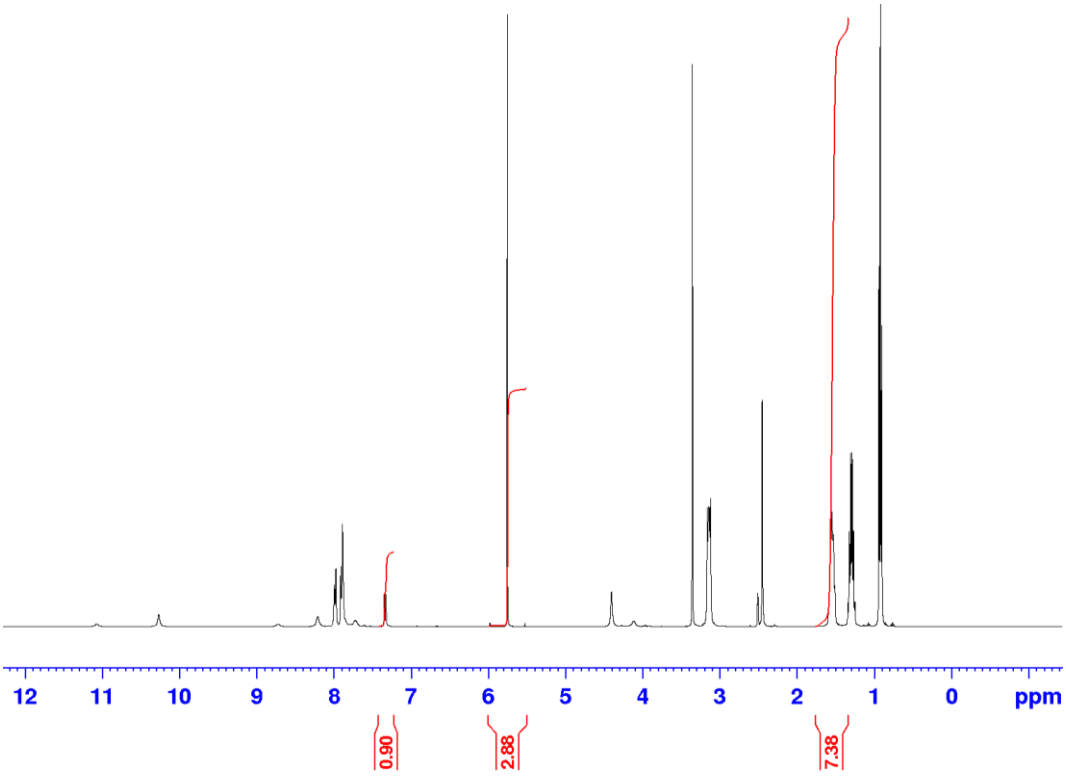

Figure S12 - ^{1}H NMR spectrum (d_1 = 60 s) of SSA **5** (112 mM) in DMSO-d_6/1.0 % DCM. Comparative integration indicates 0 % of the anionic and cationic component of **5** has become NMR silent.

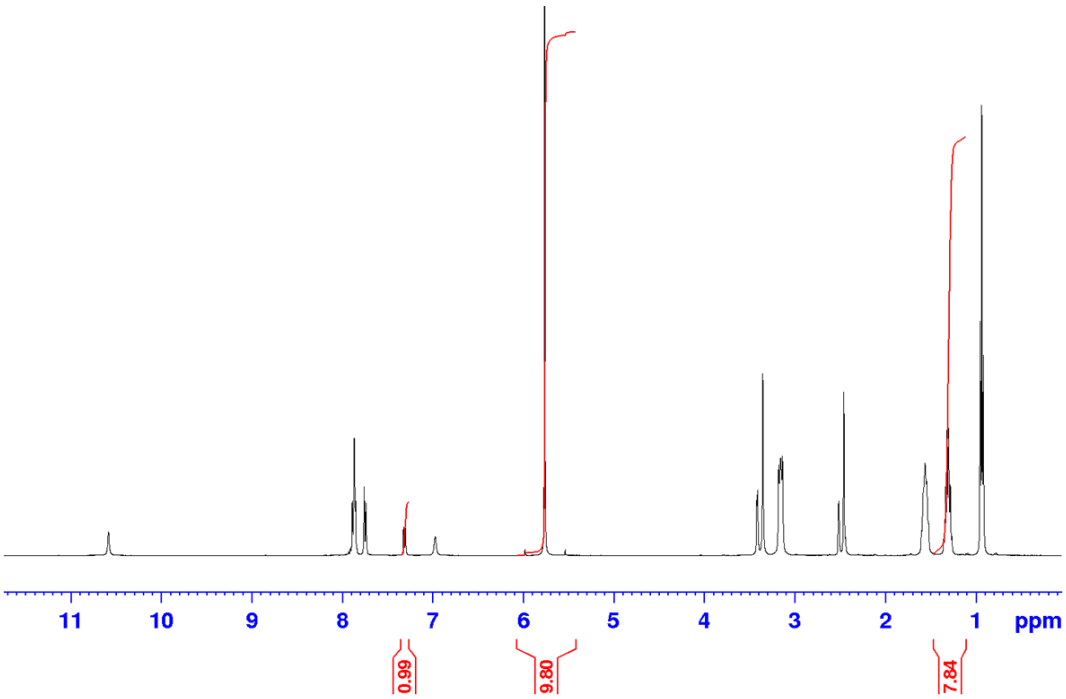

Figure S13 - ^{1}H NMR spectrum (d_1 = 60 s) of SSA **6** (17 mM) in DMSO-d_6/1.0 % DCM. Comparative integration indicates 0 % of the anionic and cationic component of **6** has become NMR silent.

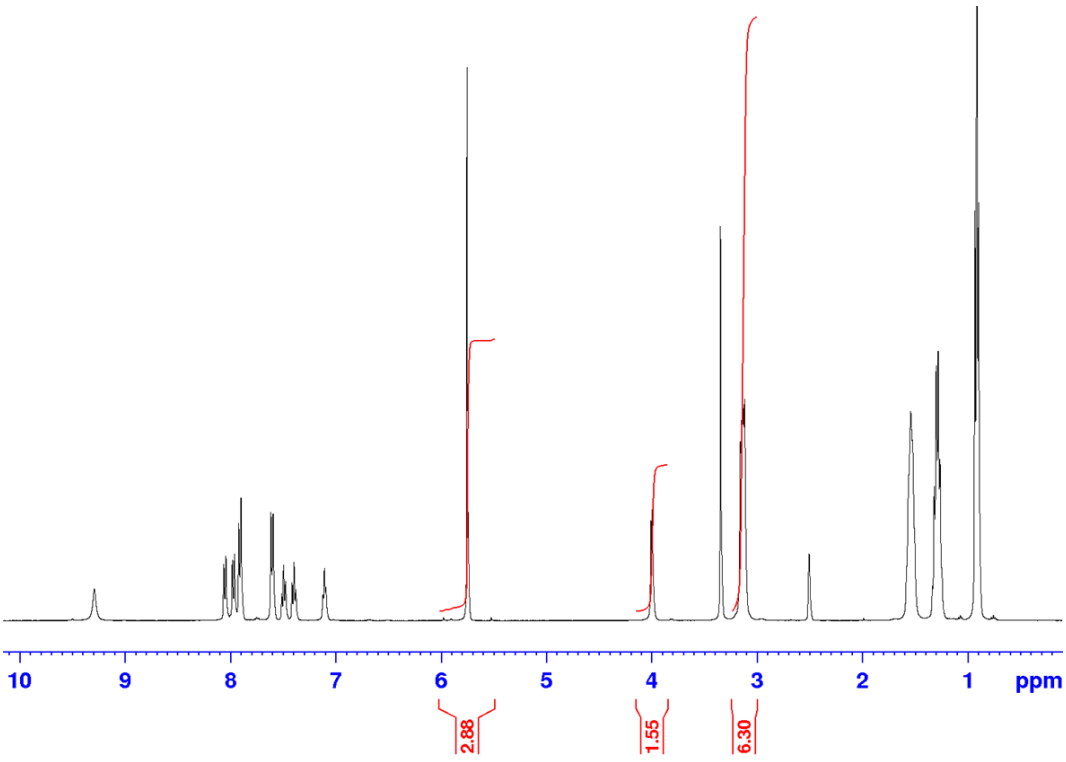

Figure S14 - ^{1}H NMR spectrum (d_1 = 60 s) of SSA **7** (112 mM) in DMSO-d_6/1.0 % DCM. Comparative integration indicates 23 % of the anionic component and 21 % of the cationic component of **7** has become NMR silent.

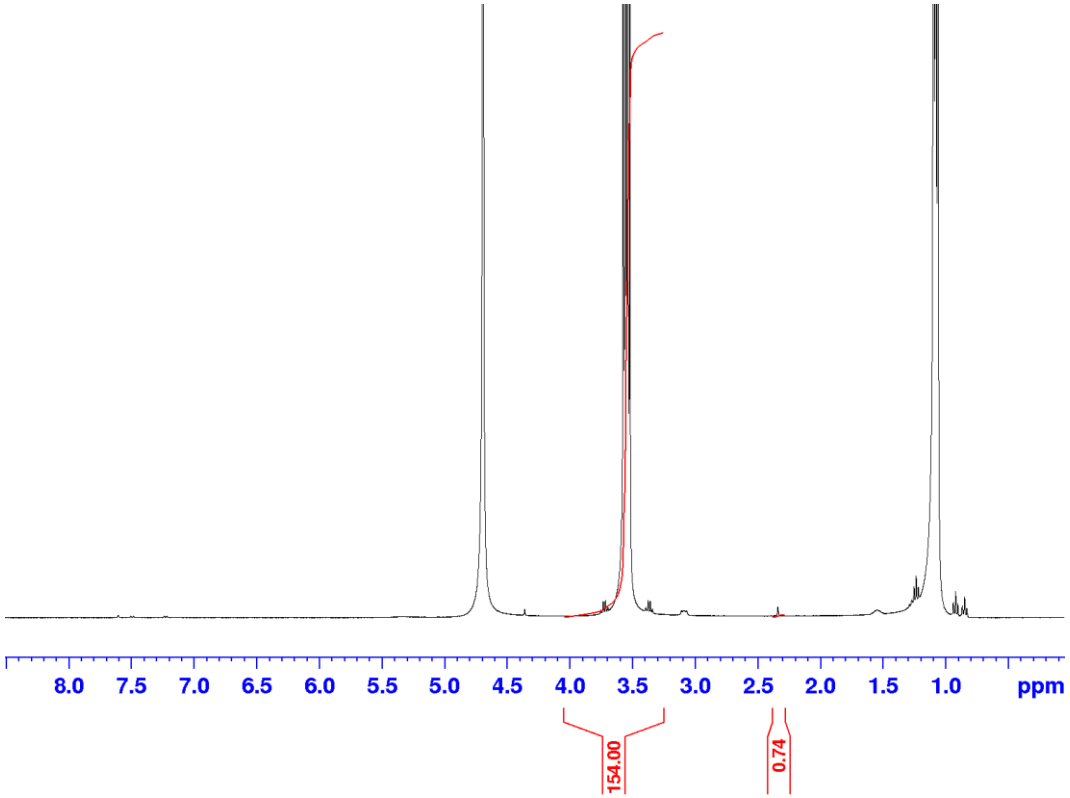

Figure S15 - ^{1}H NMR spectrum (d_1 = 60 s) of SSA **1** (5.56 mM) in D_2O/5.0 % EtOH. Comparative integration indicates 65 % of the anionic component of **1** has become NMR silent.

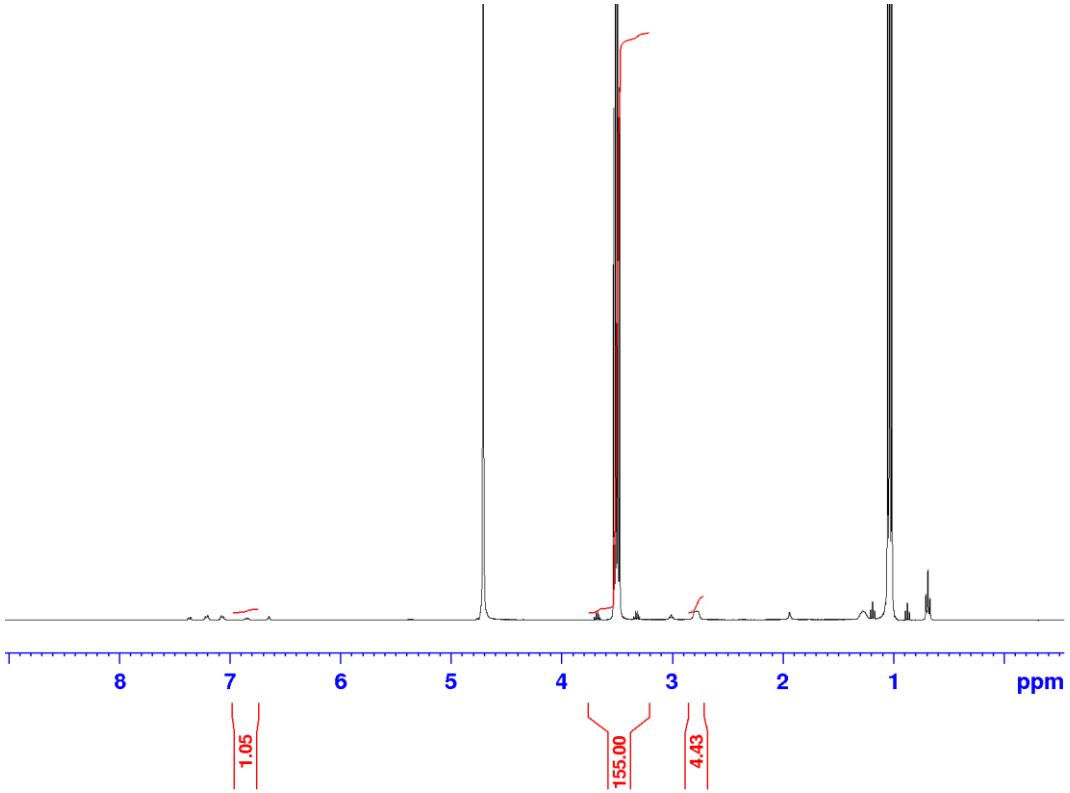

Figure S16 - ^{1}H NMR spectrum (d_1 = 60 s) of SSA **3** (5.56 mM) in D_2O/5.0 % EtOH. Comparative integration indicates 48 % of the anionic component and 45 % of the cationic component of **3** has become NMR silent.

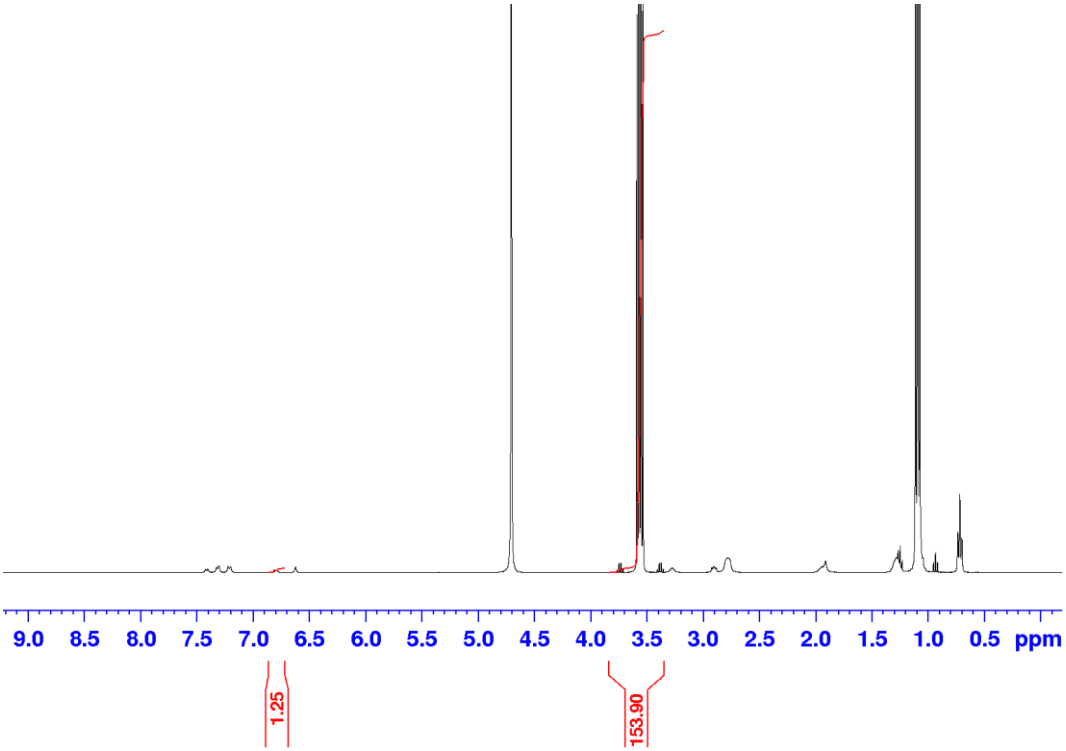

Figure S17 - ^{1}H NMR spectrum (d_1 = 60 s) of SSA **4** (5.56 mM) in D_2O/5.0 % EtOH. Comparative integration indicates 38 % of the anionic component of **4** has become NMR silent.

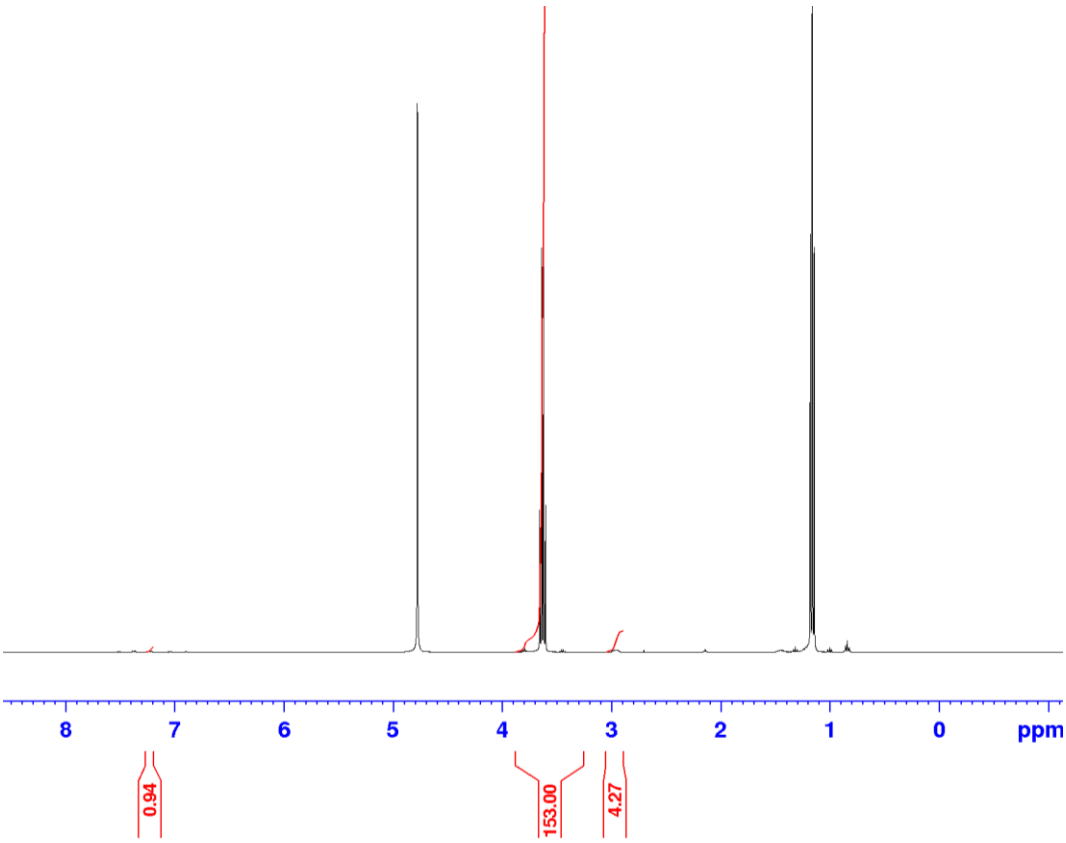

Figure S18 - ^{1}H NMR spectrum (d_1 = 60 s) of SSA **6** (2.78 mM) in D_2O/5.0 % EtOH. Comparative integration indicates 53 % of the anionic component and 47 % of the cationic component of **6** has become NMR silent.

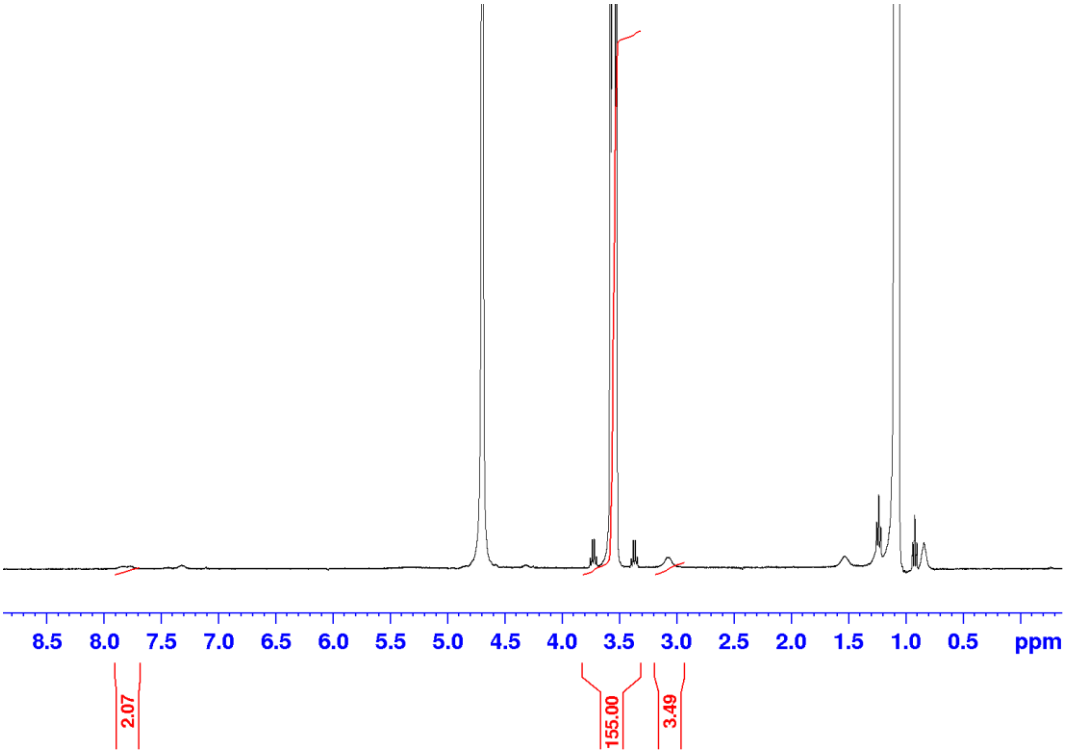

Figure S19 - ^{1}H NMR spectrum (d_1 = 60 s) of SSA **7** (5.56 mM) in D_2O/5.0 % EtOH. Comparative integration indicates 48 % of the anionic component and 56 % of the cationic component of **7** has become NMR silent.

^{1}H NMR self-association study data

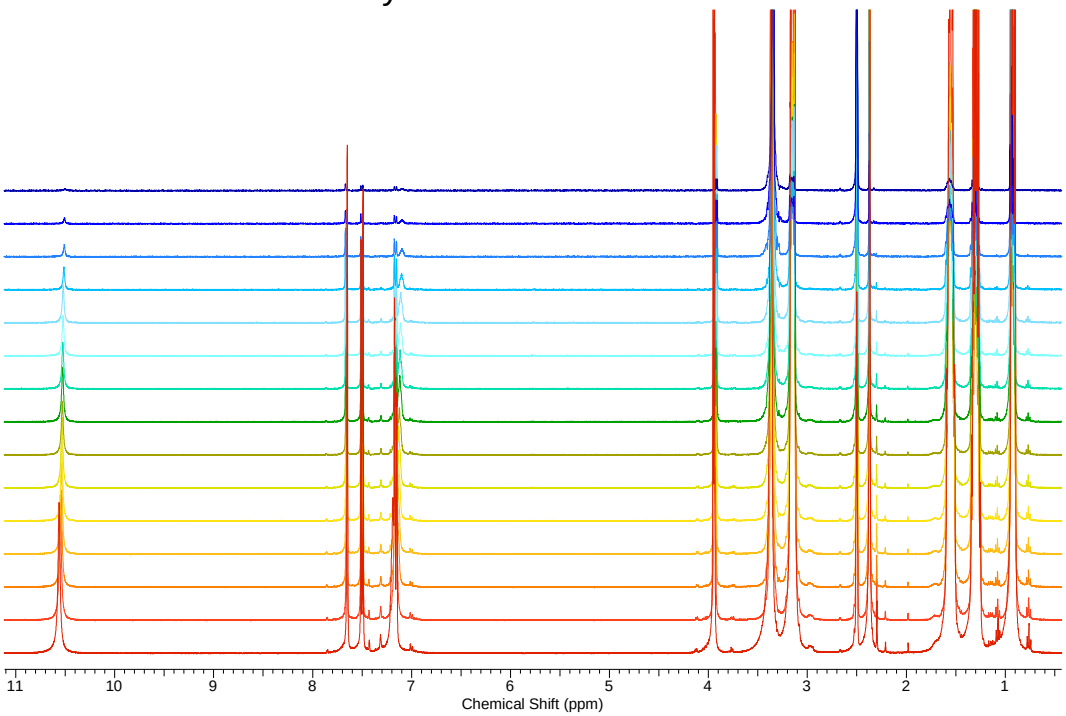

Figure S20 - ^{1}H NMR stack plot of SSA **1** in a DMSO-d_6 0.5 % H_2O solution. Samples were prepared in series with an aliquot of the most concentrated solution undergoing serial dilution.

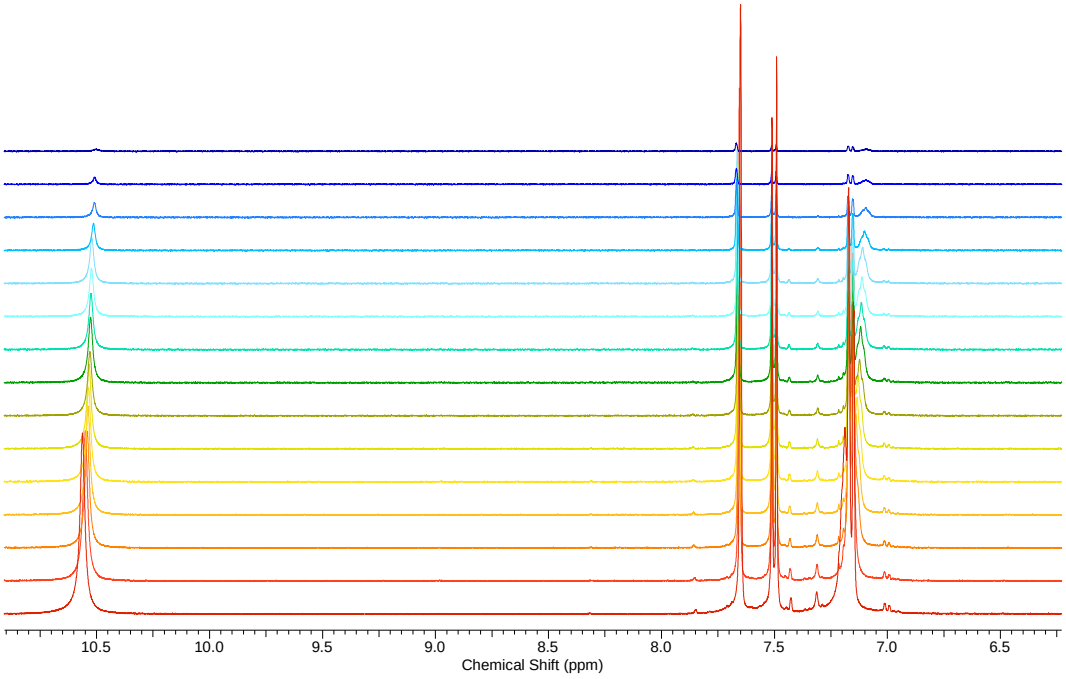

Figure S21 – Enlarged ^{1}H NMR stack plot of SSA **1** in a DMSO-d_6 0.5 % H_2O solution. Samples were prepared in series with an aliquot of the most concentrated solution undergoing serial dilution.

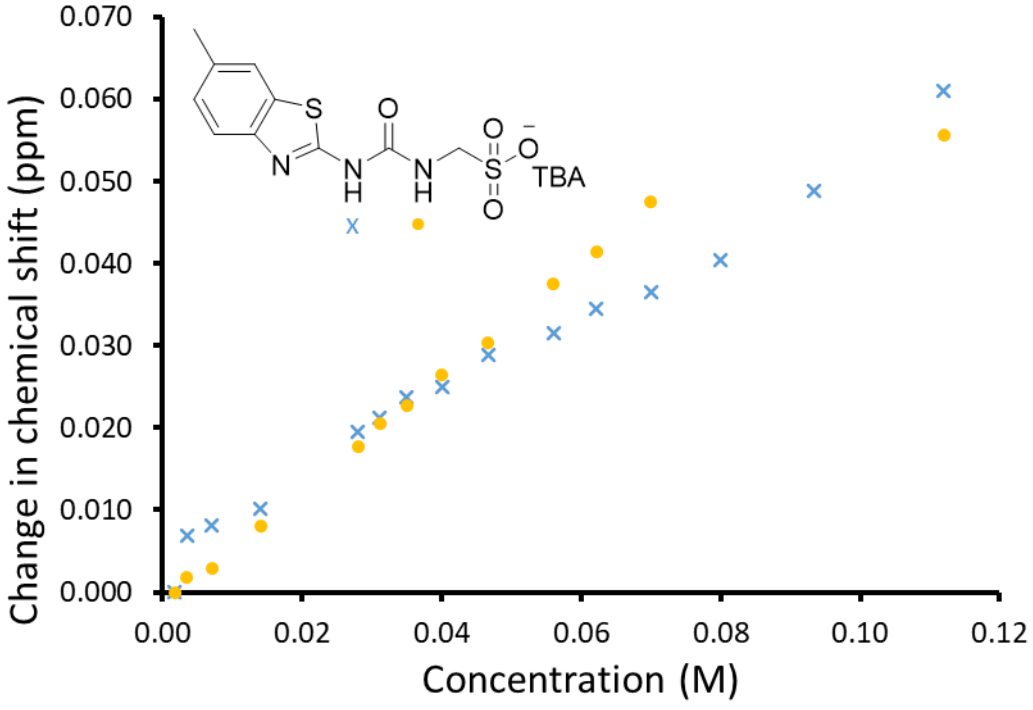

Figure S22 - Graph illustrating the ^{1}H NMR down-field change in chemical shift of urea NH resonances with increasing concentrations of SSA **1** in DMSO-d_6 0.5 % H_2O solution (298 K).

Self-association constant calculation

SSA **1** – Dilution study in DMSO-d_6 0.5 % H_2O. Values calculated from data gathered from both NH 1 and 2.

Equal K/Dimerisation mode

K_e = 0.18 M^{-1} ± 3.7764 % K_{dim} = 0.09 M^{-1} ± 1.8882 %

http://app.supramolecular.org/bindfit/view/6a664418-0fe3-40cb-8e35-ab26dbb81505

CoEK model

K_e = -0.68 M^{-1} ± 17.2912 % K_{dim} = -0.34 M^{-1} ± 8.6456 % ρ = -212.19 ± 14.8621 %

http://app.supramolecular.org/bindfit/view/493a2d8b-c6a2-4320-b45d-e4c75330c974

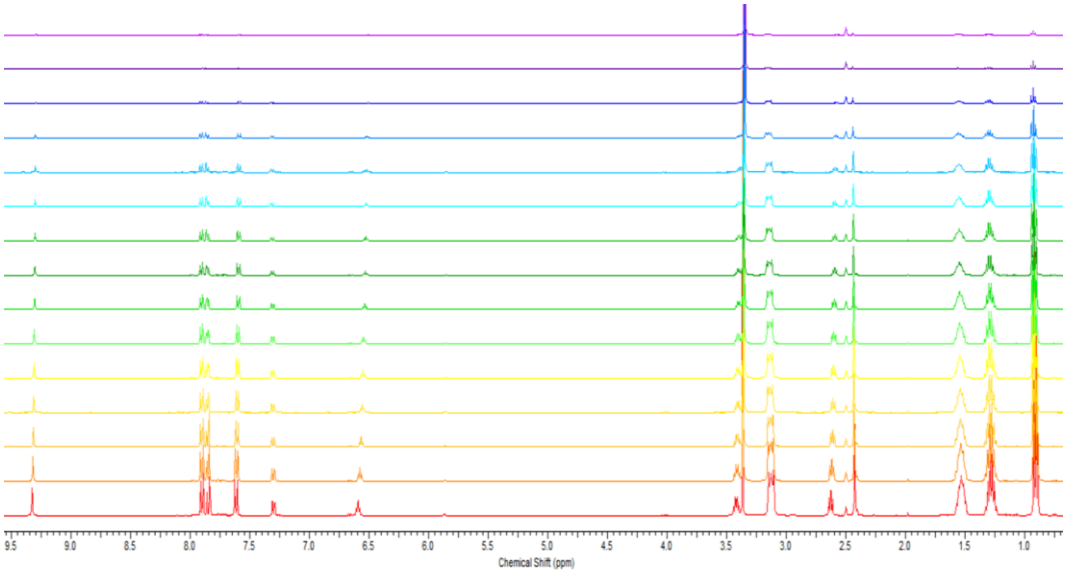

Figure S23 - ^{1}H NMR stack plot of SSA **3** in a DMSO-d_6 0.5 % H_2O solution. Samples were prepared in series with an aliquot of the most concentrated solution undergoing serial dilution.

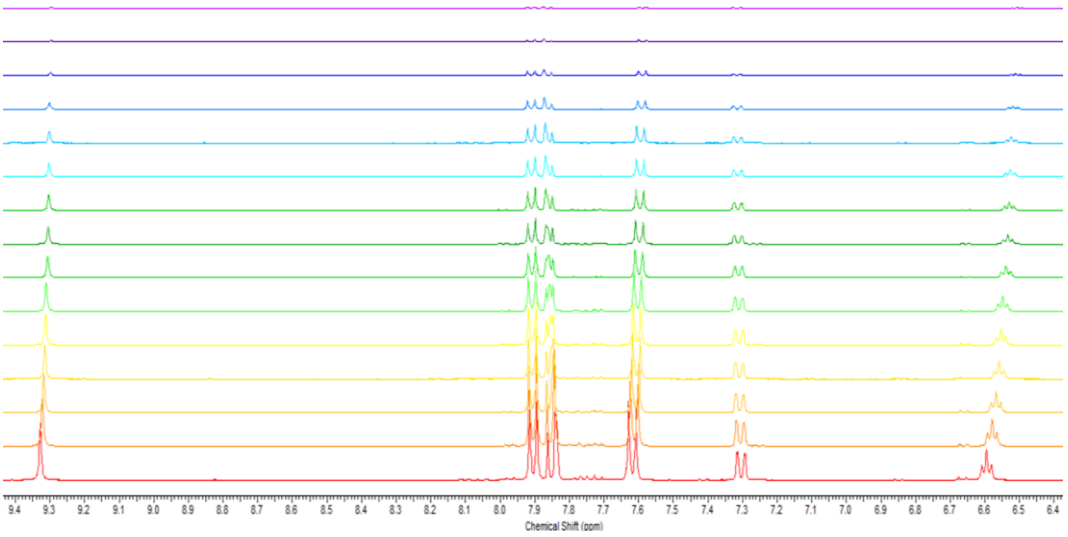

Figure S24 - Enlarged ^{1}H NMR stack plot of SSA **3** in a DMSO-d_6 0.5 % H_2O solution. Samples were prepared in series with an aliquot of the most concentrated solution undergoing serial dilution.

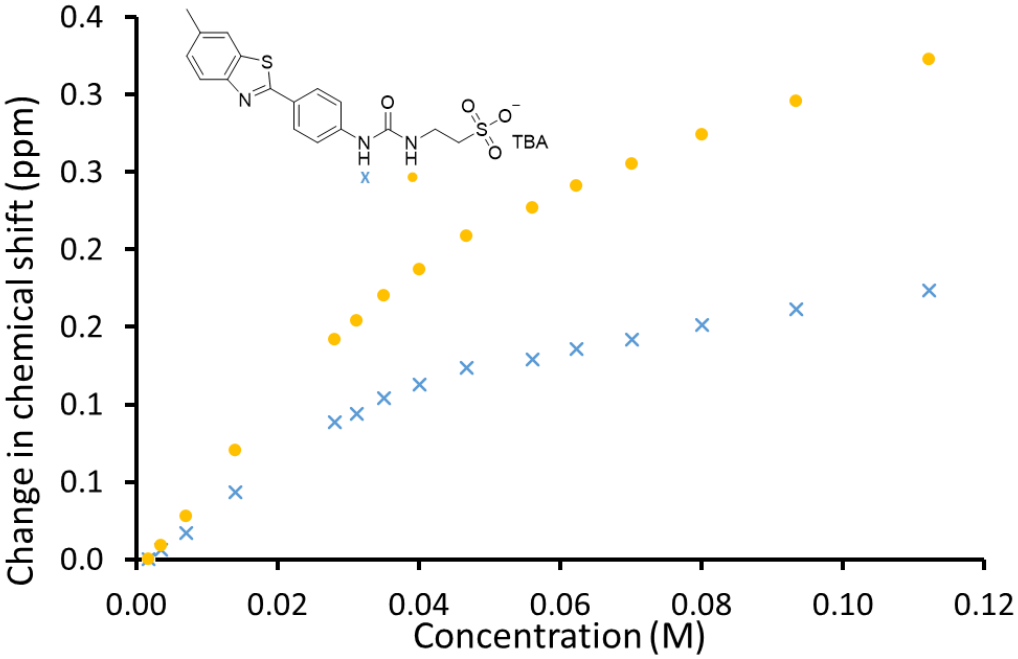

Figure S25 - Graph illustrating the ^{1}H NMR down-field change in chemical shift of urea NH resonances with increasing concentrations of SSA **3** in DMSO-d_6 0.5 % H_2O solution (298 K).

Self-association constant calculation

SSA **3** – Dilution study in DMSO-d_6 0.5 % H_2O. Values calculated from data gathered from both NH 1 and 2.

Equal K/Dimerisation mode

K_e = 8.01 x 10^{-5} M^{-1} ± 0.0879 % K_{dim} = 4.01 x 10^{-5} M^{-1} ± 4.3951 x 10^{-2} %

http://app.supramolecular.org/bindfit/view/fa96db32-f1f4-4cf6-bcc1-97bbcb17d141

CoEK model

K_e = 6.09 M^{-1} ± 4.4759 % K_{dim} = 3.04 M^{-1} ± 2.2238 % ρ = 0.22 ± 10.1476 %

http://app.supramolecular.org/bindfit/view/4ab2b3d9-dff7-4294-a191-400cf2ad9c74

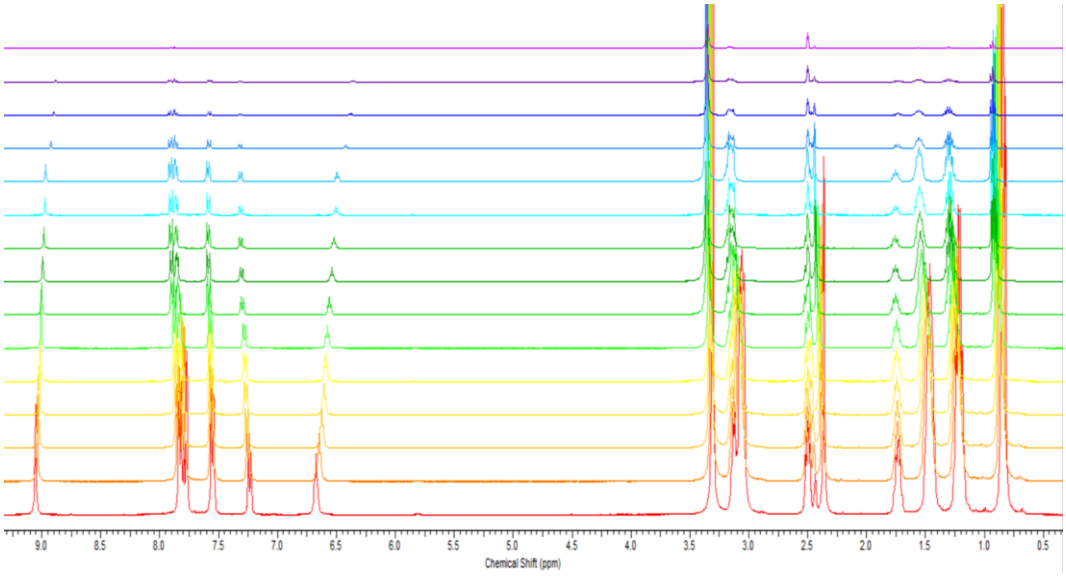

Figure S26 - ^{1}H NMR stack plot of SSA **4** in a DMSO-d_6 0.5 % H_2O solution. Samples were prepared in series with an aliquot of the most concentrated solution undergoing serial dilution.

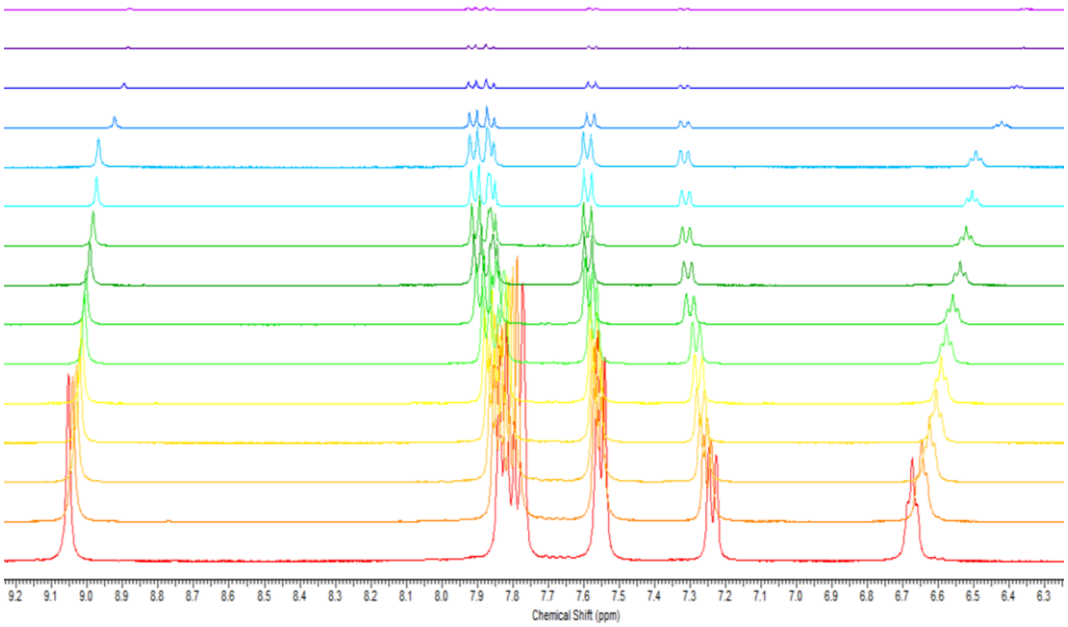

Figure S27 - Enlarged ^{1}H NMR stack plot of SSA **4** in a DMSO-d_6 0.5 % H_2O solution. Samples were prepared in series with an aliquot of the most concentrated solution undergoing serial dilution.

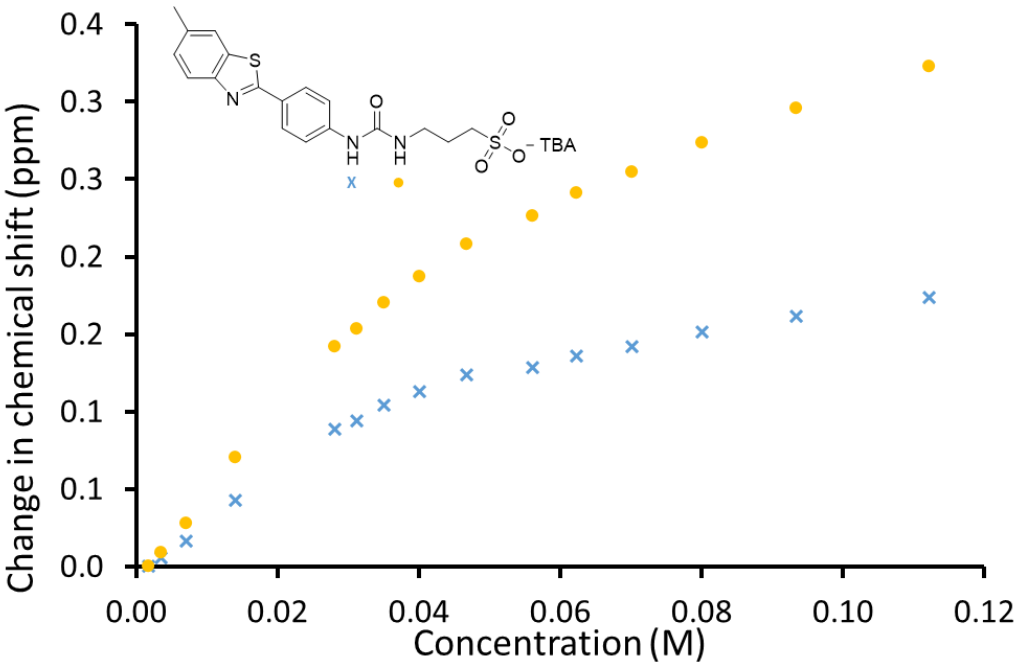

Figure S28 - Graph illustrating the ^{1}H NMR down-field change in chemical shift of urea NH resonances with increasing concentrations of SSA **4** in DMSO-*d*$_6$ 0.5 % H_2O solution (298 K).

Self-association constant calculation

SSA **4** – Dilution study in DMSO-*d*$_6$ 0.5 % H_2O. Values calculated from data gathered from both NH 1 and 2.

Equal K/Dimerisation mode

K_e = 12.55 M^{-1} ± 2.0388 % K_{dim} = 6.26 M^{-1} ± 1.0194 %

http://app.supramolecular.org/bindfit/view/c1a80133-529c-4560-a893-db3e0a4a0d22

CoEK model

K_e = 027.07 M^{-1} ± 2.2738 % K_{dim} = 13.54 M^{-1} ± 1.1369 % ρ = 0.40 ± 11.0863 %

http://app.supramolecular.org/bindfit/view/40e56a30-08db-4fd3-8fa8-1075d7fe1420

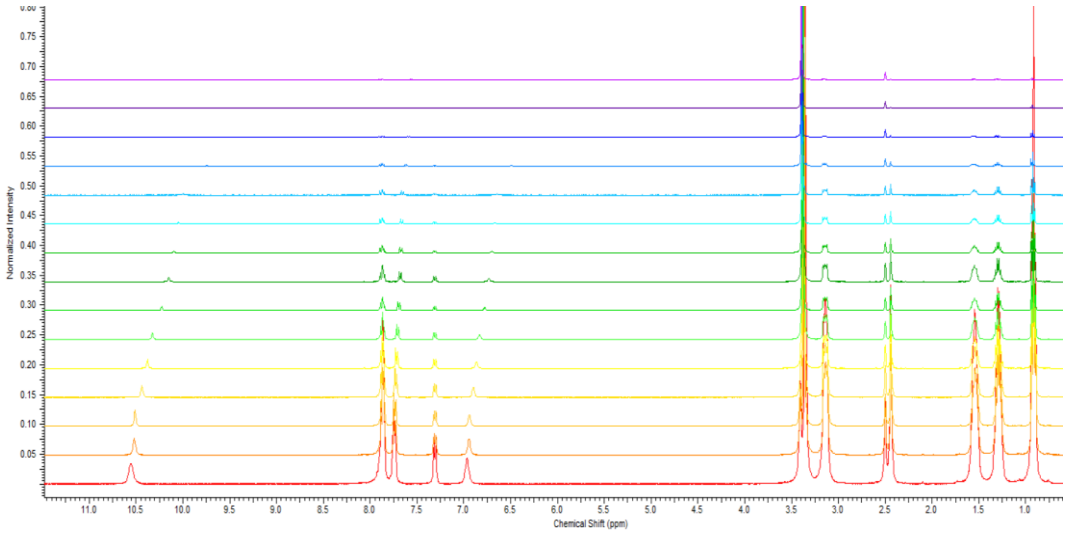

Figure S29 - ^{1}H NMR stack plot of SSA **6** in a DMSO-d_6 0.5 % H_2O solution. Samples were prepared in series with an aliquot of the most concentrated solution undergoing serial dilution.

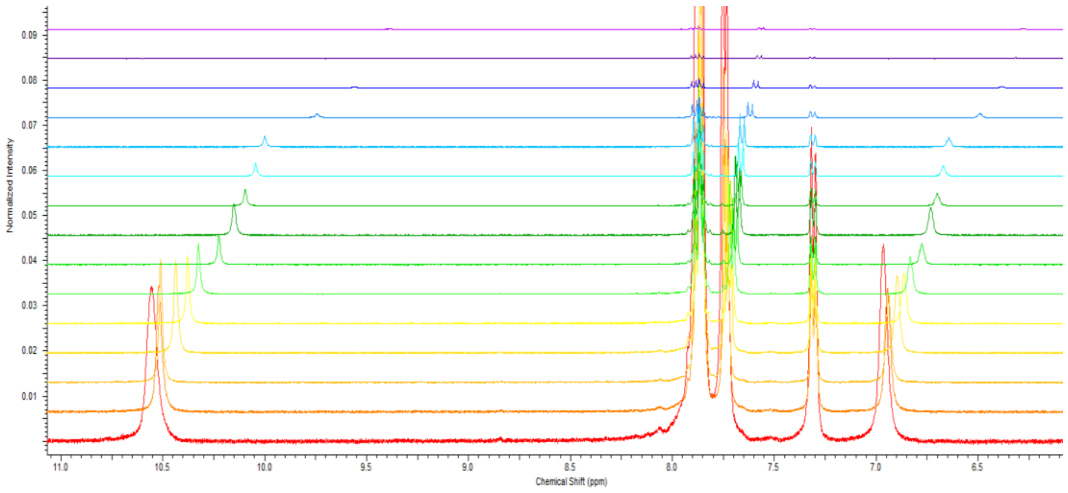

Figure S30 - Enlarged ^{1}H NMR stack plot of SSA **6** in a DMSO-d_6 0.5 % H_2O solution. Samples were prepared in series with an aliquot of the most concentrated solution undergoing serial dilution.

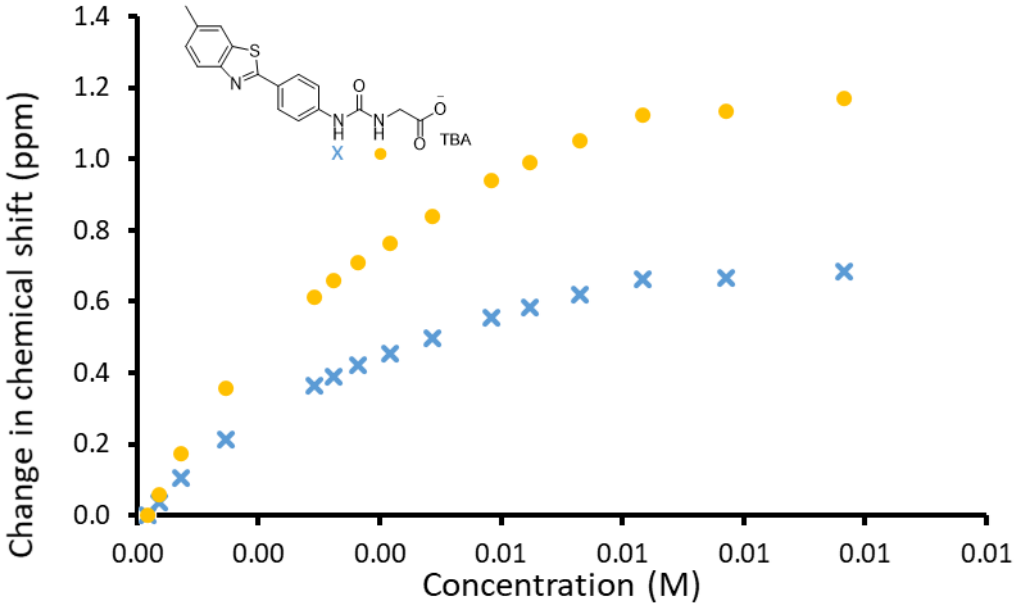

Figure S31 - Graph illustrating the ^{1}H NMR down-field change in chemical shift of urea NH resonances with increasing concentrations of SSA **6** in DMSO-*d*$_6$ 0.5 % H_2O solution (298 K).

Self-association constant calculation

SSA **6** – Dilution study in DMSO-*d*$_6$ 0.5 % H_2O. Values calculated from data gathered from both NH 1 and 2.

Equal K/Dimerisation mode

K_e = 185.32 M^{-1} ± 2.5334 % K_{dim} = 92.72 M^{-1} ± 1.2667 %

http://app.supramolecular.org/bindfit/view/4a40614b-b287-466e-a3f7-c60b6dfe06d8

CoEK model

K_e =333.13 M^{-1} ± 2.3717 % K_{dim} = 166.57 M^{-1} ± 1.1859 % ρ = 0.10 ± 12.3694 %

http://app.supramolecular.org/bindfit/view/96f38fd7-108c-4eba-a823-ec57fd9beb40

^{1}H DOSY NMR data

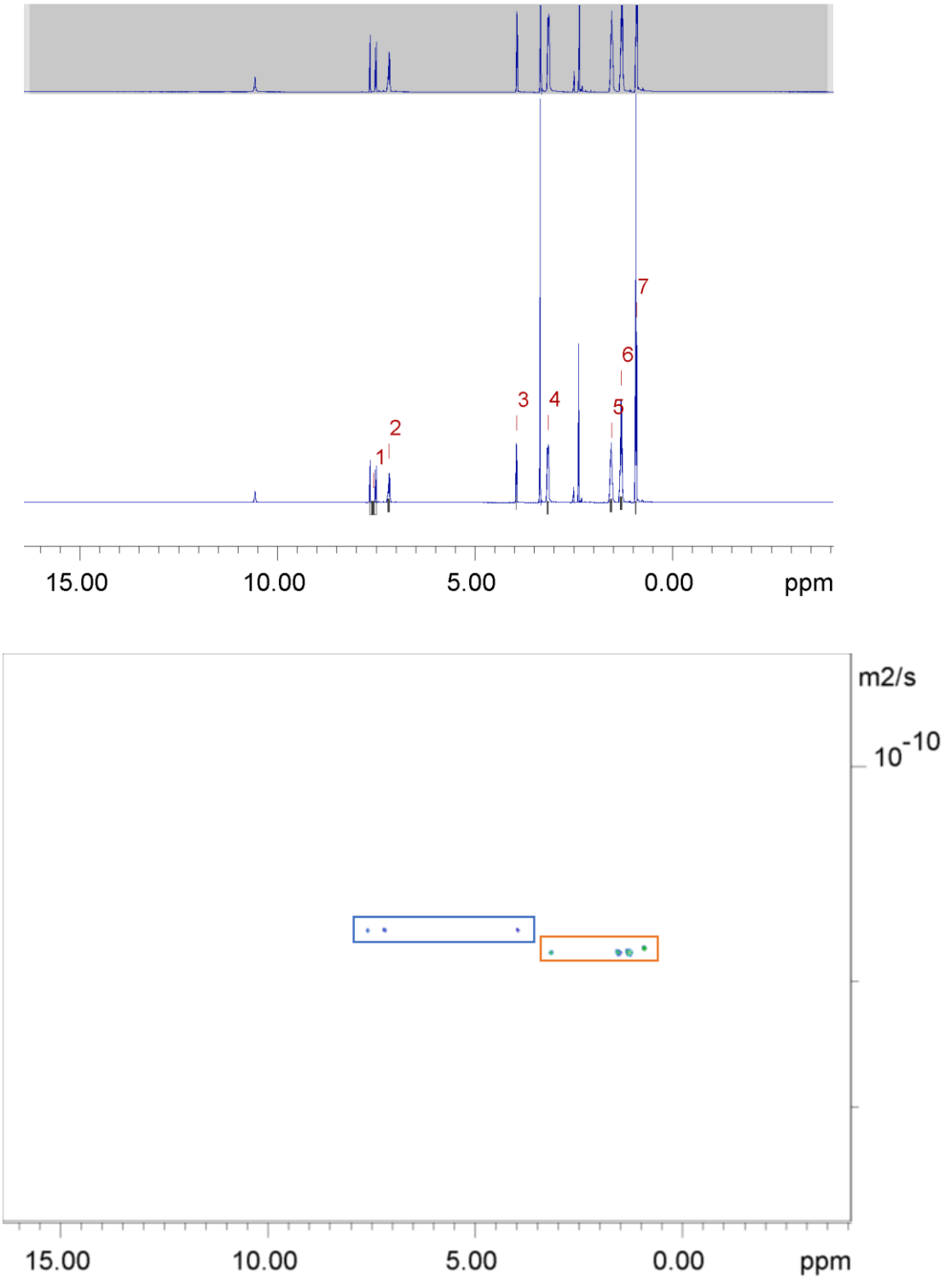

Figure S32 - ^{1}H DOSY NMR of SSA **1** (111.12 mM) in DMSO-d_6 conducted at 298 K. Anionic component highlighted in blue, TBA counter cation highlighted in orange.

Peak name	F2 [ppm]	Io	error	D [m2/s]	error
1	7.577	2.27e+09	1.184e+05	1.69e-10	1.877e-14
2	7.183	2.08e+09	7.218e+04	1.70e-10	1.261e-14
3	3.949	1.51e+09	3.684e+04	1.71e-10	8.860e-15
4	3.155	5.50e+09	6.090e+04	1.83e-10	4.290e-15
5	1.552	7.28e+09	7.607e+04	1.82e-10	4.016e-15
6	1.301	8.53e+09	7.062e+04	1.82e-10	3.182e-15
7	0.925	1.31e+10	5.645e+04	1.81e-10	1.651e-15

Figure S33 - ^{1}H DOSY NMR spectrum of the SSA **1** (111.12 mM) in DMSO-d_6 at 298 K and a table reporting the diffusion constants calculated for each peak used to determine the hydrodynamic diameter of the anionic component of **1** (d_H = 1.29 nm). Peaks 1 - 3 correspond to the anionic component of **1** while peaks 4 - 7 correspond to the cationic component of **1**.

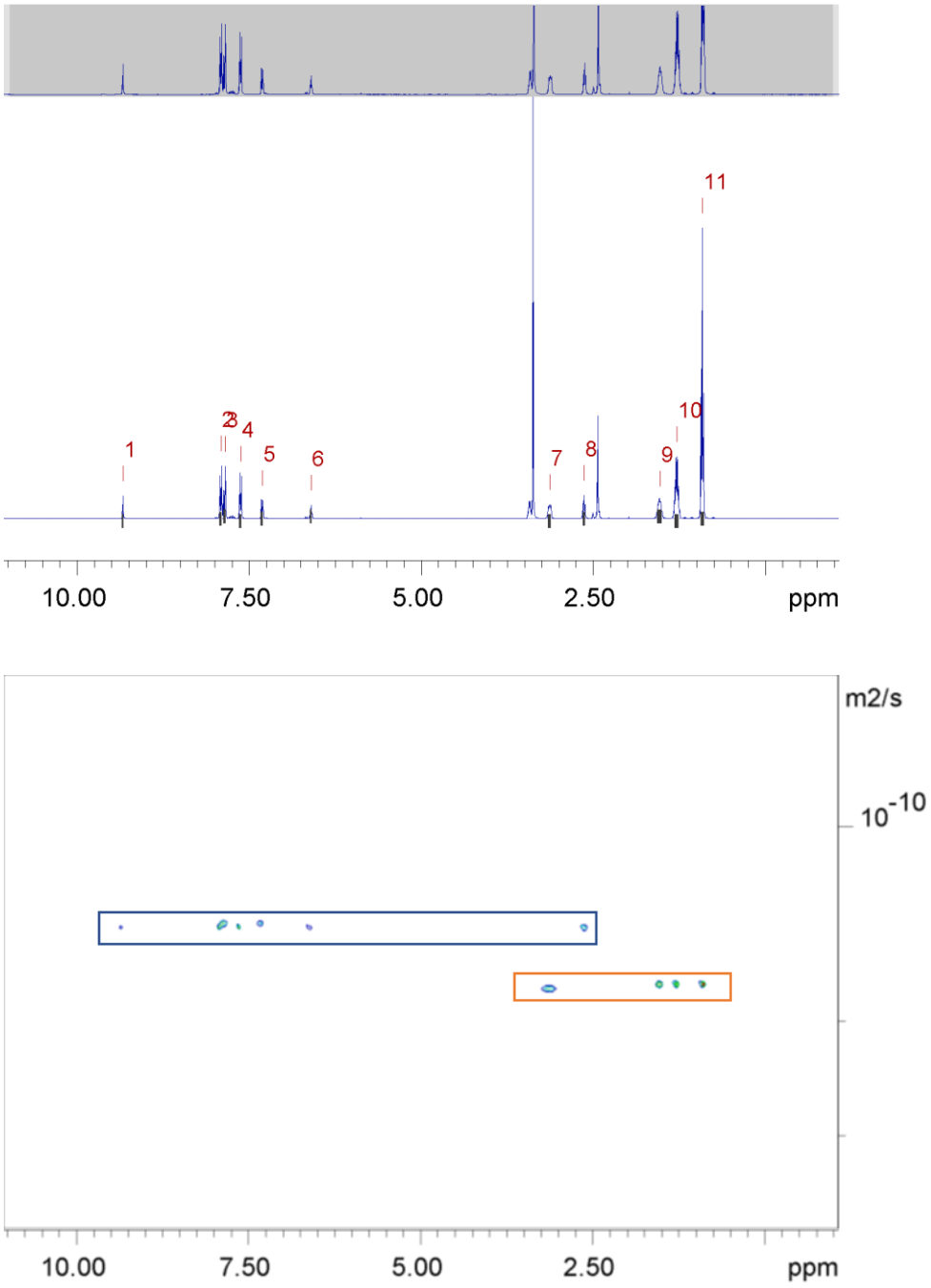

Figure S34 - ^{1}H DOSY NMR of SSA **3** (111.12 mM) in DMSO-d_6 conducted at 298 K. Anionic component highlighted in blue, TBA counter cation highlighted in orange.

Peak name	F2 [ppm]	Io	error	D [m2/s]	error
1	9.335	1.70e+08	1.413e+04	1.42e-10	2.376e-14
2	7.914	5.43e+08	1.631e+04	1.42e-10	8.569e-15
3	7.854	4.99e+08	1.630e+04	1.42e-10	9.285e-15
4	7.626	6.11e+08	1.930e+04	1.42e-10	9.012e-15
5	7.314	2.91e+08	1.747e+04	1.42e-10	1.705e-14
6	6.605	1.42e+08	1.504e+04	1.42e-10	3.021e-14
7	3.138	4.01e+08	2.146e+04	1.77e-10	1.859e-14
8	2.636	3.23e+08	1.711e+04	1.42e-10	1.510e-14
9	1.535	7.55e+08	2.712e+04	1.76e-10	1.246e-14
10	1.288	1.61e+09	2.626e+04	1.76e-10	5.670e-15
11	0.914	3.40e+09	2.349e+04	1.76e-10	2.394e-15

Figure S35 - ^{1}H DOSY NMR spectrum of the SSA **3** (111.12 mM) in DMSO-d_6 at 298 K and a table reporting the diffusion constants calculated for each peak used to determine the hydrodynamic diameter of the anionic component of **3** (d_H = 1.54 nm). Peaks 1 – 6 and 8 correspond to the anionic component of **3** while peaks 7, 9 - 11 correspond to the cationic component of **3**.

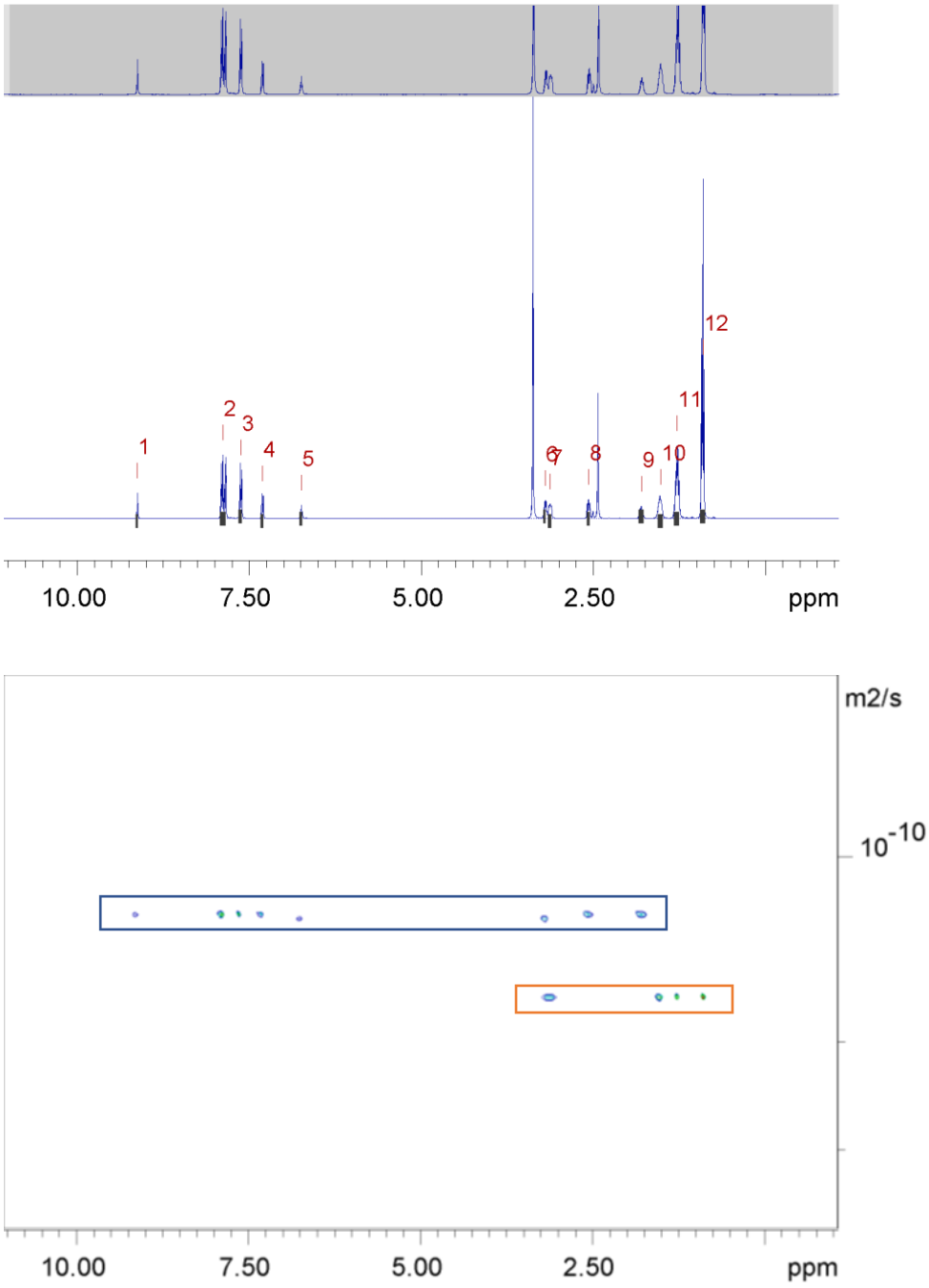

Figure S36 - ^{1}H DOSY NMR of SSA **4** (111.12 mM) in DMSO-d_6 conducted at 298 K. Anionic component highlighted in blue, TBA counter cation highlighted in orange.

Peak name	F2 [ppm]	Io	error	D [m2/s]	error
1	9.129	1.55e+08	1.892e+04	1.23e-10	2.839e-14
2	7.883	1.09e+09	3.171e+04	1.23e-10	6.729e-15
3	7.623	5.92e+08	2.409e+04	1.24e-10	9.472e-15
4	7.309	2.98e+08	2.263e+04	1.24e-10	1.768e-14
5	6.747	1.45e+08	2.158e+04	1.26e-10	3.511e-14
6	3.203	2.42e+08	2.074e+04	1.25e-10	2.021e-14
7	3.132	3.24e+08	2.592e+04	1.70e-10	2.517e-14
8	2.569	2.75e+08	2.108e+04	1.24e-10	1.788e-14
9	1.804	2.88e+08	2.922e+04	1.24e-10	2.367e-14
10	1.527	6.34e+08	3.309e+04	1.70e-10	1.647e-14
11	1.284	1.50e+09	3.341e+04	1.70e-10	7.056e-15
12	0.905	3.26e+09	3.277e+04	1.70e-10	3.174e-15

Figure S37 - ^{1}H DOSY NMR spectrum of the SSA **4** (111.12 mM) in DMSO-d_6 at 298 K and a table reporting the diffusion constants calculated for each peak used to determine the hydrodynamic diameter of the anionic component of **4** (d_H = 1.77 nm). Peaks 1 – 6, 8 and 9 correspond to the anionic component of **4** while peaks 7, 10 - 12 correspond to the cationic component of **4**.

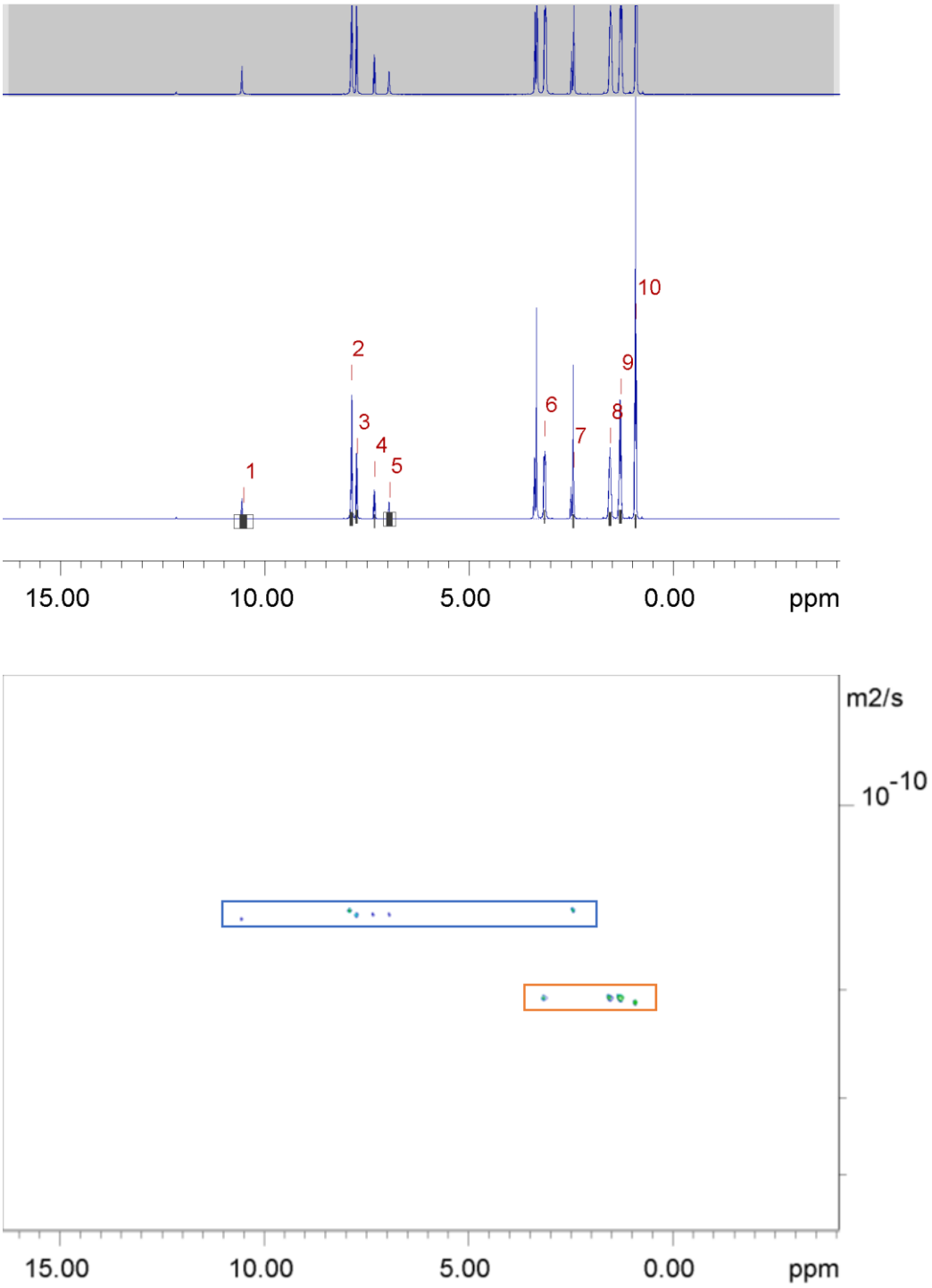

Figure S38 - ^{1}H DOSY NMR of SSA **6** (17 mM) in DMSO-d_6 conducted at 298 K. Anionic component highlighted in blue, TBA counter cation highlighted in orange.

Peak name	F2 [ppm]	Io	error	D [m2/s]	error
1	10.520	1.50e+09	7.329e+05	1.53e-10	1.657e-13
2	7.881	7.48e+09	3.145e+05	1.49e-10	1.398e-14
3	7.748	3.61e+09	2.410e+05	1.52e-10	2.253e-14
4	7.310	1.55e+09	2.048e+05	1.50e-10	4.414e-14
5	6.940	1.57e+09	5.792e+05	1.51e-10	1.241e-13
6	3.151	5.77e+09	2.237e+05	2.06e-10	1.736e-14
7	2.440	4.71e+09	2.045e+05	1.49e-10	1.445e-14
8	1.550	9.39e+09	3.149e+05	2.06e-10	1.501e-14
9	1.296	1.19e+10	3.112e+05	2.07e-10	1.174e-14
10	0.922	1.65e+10	2.299e+05	2.08e-10	6.280e-15

Figure S39 - ^{1}H DOSY NMR spectrum of the SSA **6** (17 mM) in DMSO-d_6 at 298 K and a table reporting the diffusion constants calculated for each peak used to determine the hydrodynamic diameter of the anionic component of **6** (d_H = 1.45 nm). Peaks 1 – 5 and 7 correspond to the anionic component of **6** while peaks 7, 8 - 10 correspond to the cationic component of **6**.

DOSY data overview

Table S8 - Overview of diffusion coefficients (m^2s^{-1}) of all SSAs in DMSO-d_6 at 298 K. Errors for diffusion constants are no greater than ± 1 x 10^{-13} m^2s^{-1}.

	Diffusion Coefficient (m^2 s^{-1})	
SSA	**Anion**	**TBA**
1	1.70 x 10^{-10}	1.82 x 10^{-10}
2	1.36 x 10^{-10}	1.45 x 10^{-10}
3	1.42 x 10^{-10}	1.76 x 10^{-10}
4	1.23 x 10^{-10}	1.70 x 10^{-10}
5	*a*	*a*
6	1.51 x 10^{-10}	2.07 x 10^{-10}
7	*b*	*b*

a – Compound was in slow exchange.
b – Compound showed loss in DMSO-d_6.

Table S9 - Overview of hydrodynamic diameters (nm) for all SSAs in DMSO-d_6 at 298 K.

	Hydrodynamic diameter (nm)	
SSA	**Anion**	**TBA**
1	1.29	1.20
2	1.61	1.51
3	1.54	1.25
4	1.77	1.28
5	*a*	*a*
6	1.45	1.06
7	*b*	*b*

a – Compound was in slow exchange.
b – Compound showed loss in DMSO-d_6

Section 8: DLS data

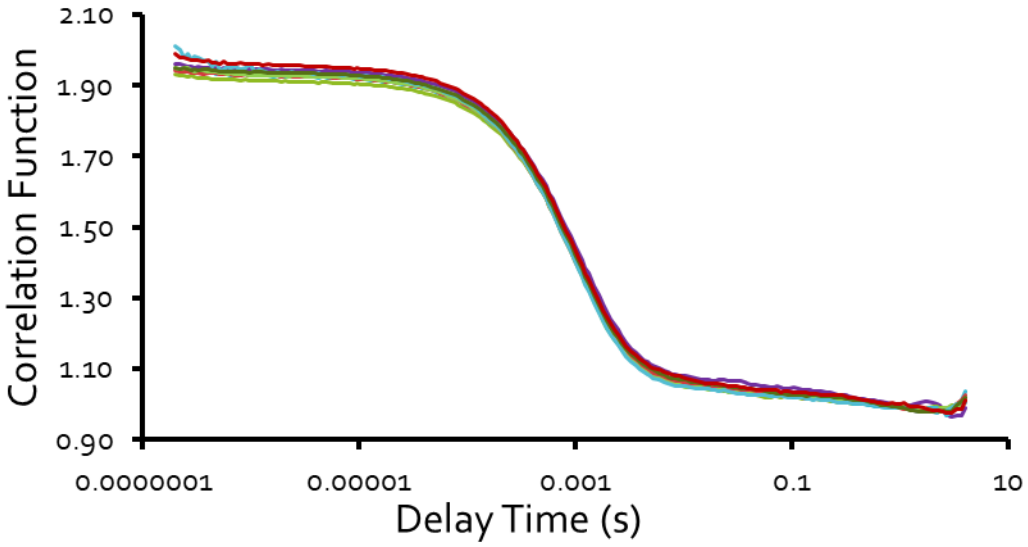

Figure S40 - Correlation function data for 10 DLS runs of SSA **1** (0.56 mM) in an EtOH:H_2O (1:19) solution at 298 K.

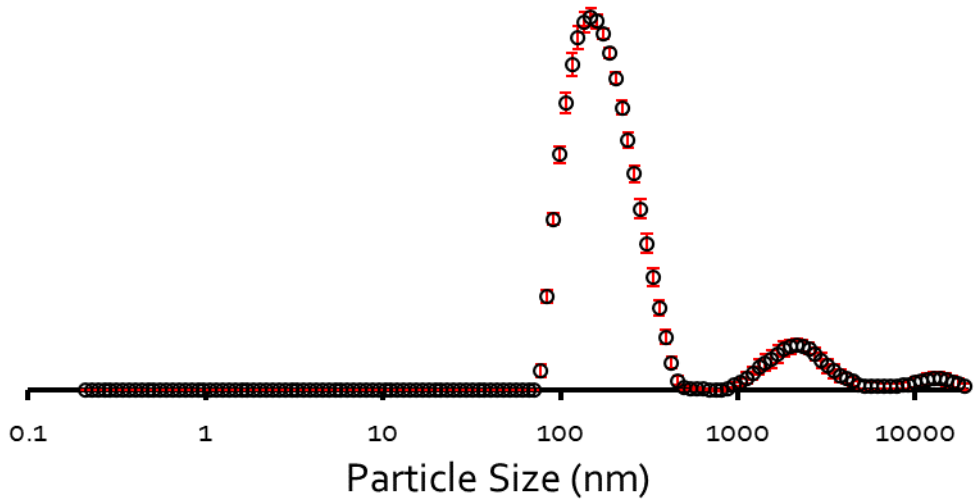

Figure S41 - The average intensity particle size distribution calculated (127 nm) using 10 DLS runs for SSA **1** (0.56 mM) in an EtOH:H_2O (1:19) solution at 298 K.

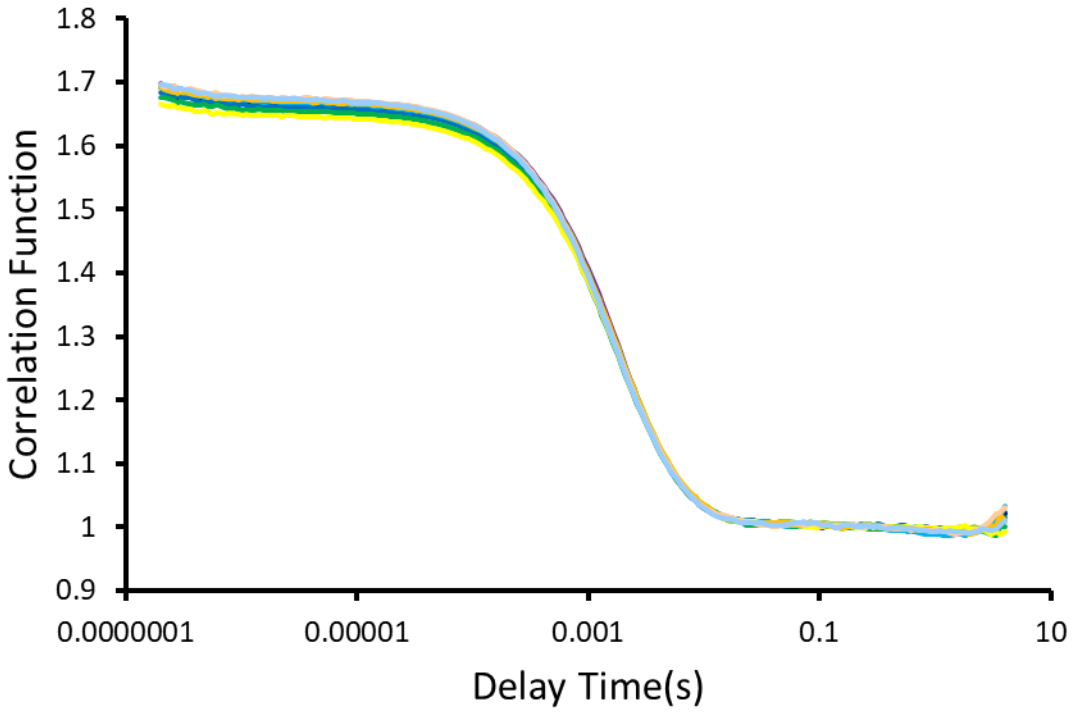

Figure S42 - Correlation function data for 10 DLS runs of SSA **3** (5.56 mM) in an EtOH:H_2O (1:19) solution at 298 K.

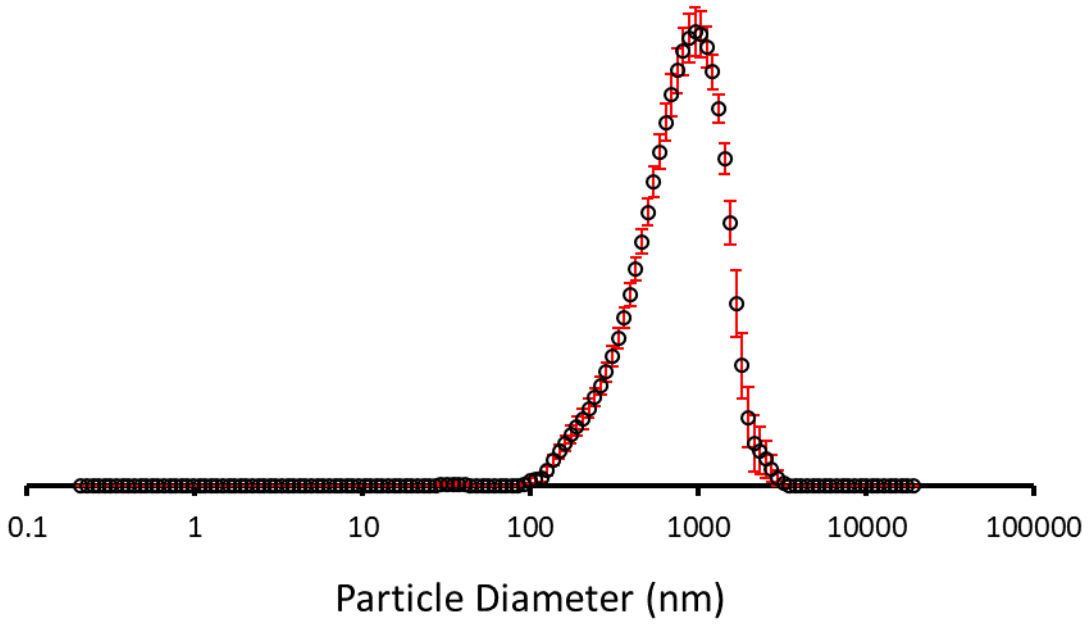

Figure S43 - The average intensity particle size distribution calculated (105 nm) using 10 DLS runs for SSA **3** (5.56 mM) in an EtOH:H_2O (1:19) solution at 298 K.

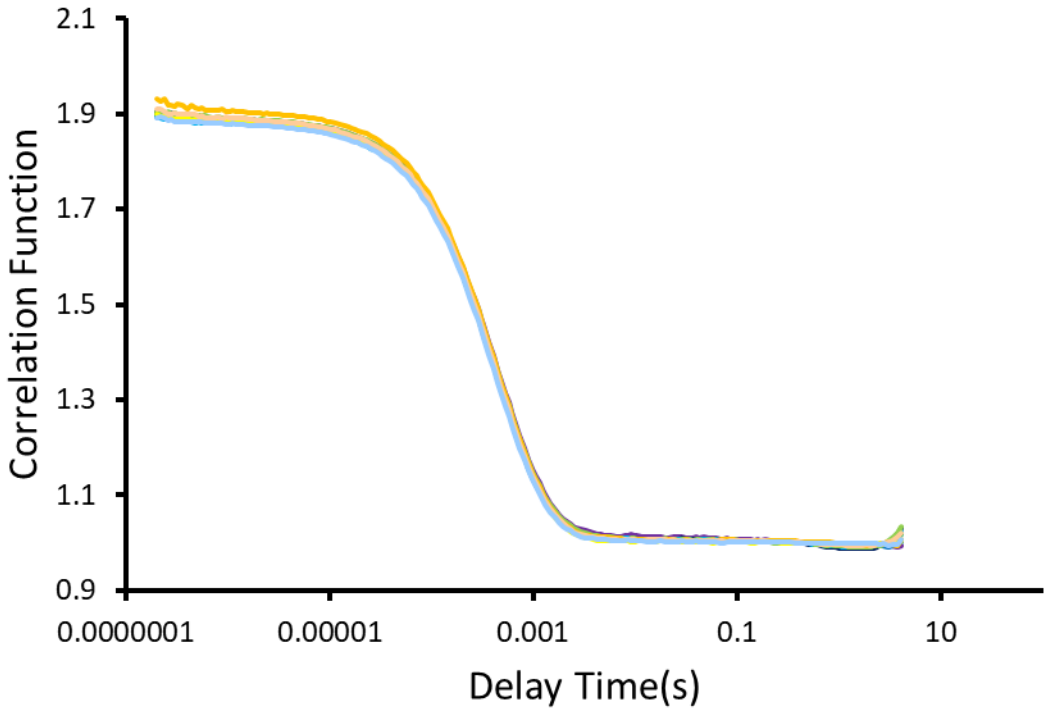

Figure S44 - Correlation function data for 10 DLS runs of SSA **3** (0.56 mM) in an EtOH:H_2O (1:19) solution at 298 K.

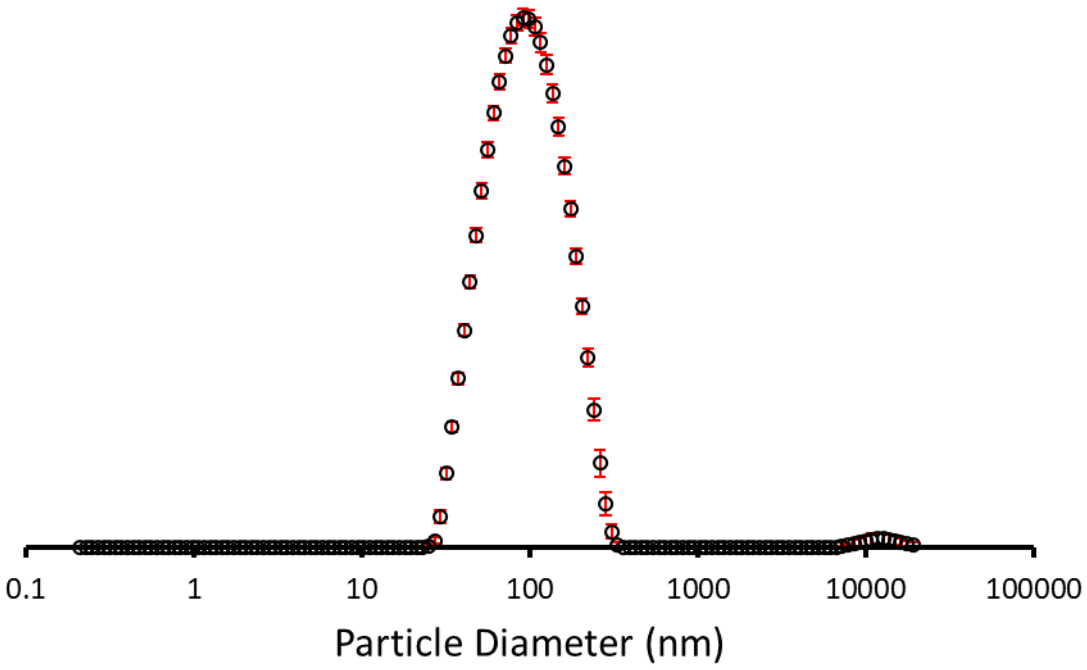

Figure S45 - The average intensity particle size distribution calculated (105 nm) using 10 DLS runs for SSA **3** (0.56 mM) in an EtOH:H_2O (1:19) solution at 298 K.

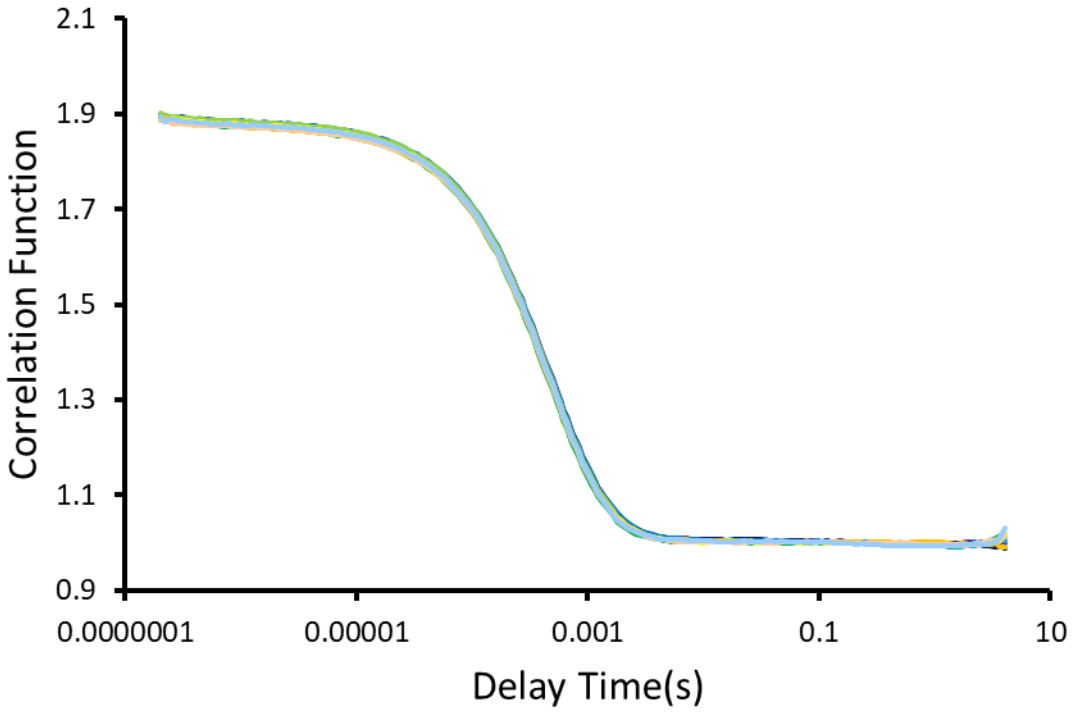

Figure S46 - Correlation function data for 10 DLS runs of SSA **4** (5.56 mM) in an EtOH:H_2O (1:19) solution at 298 K.

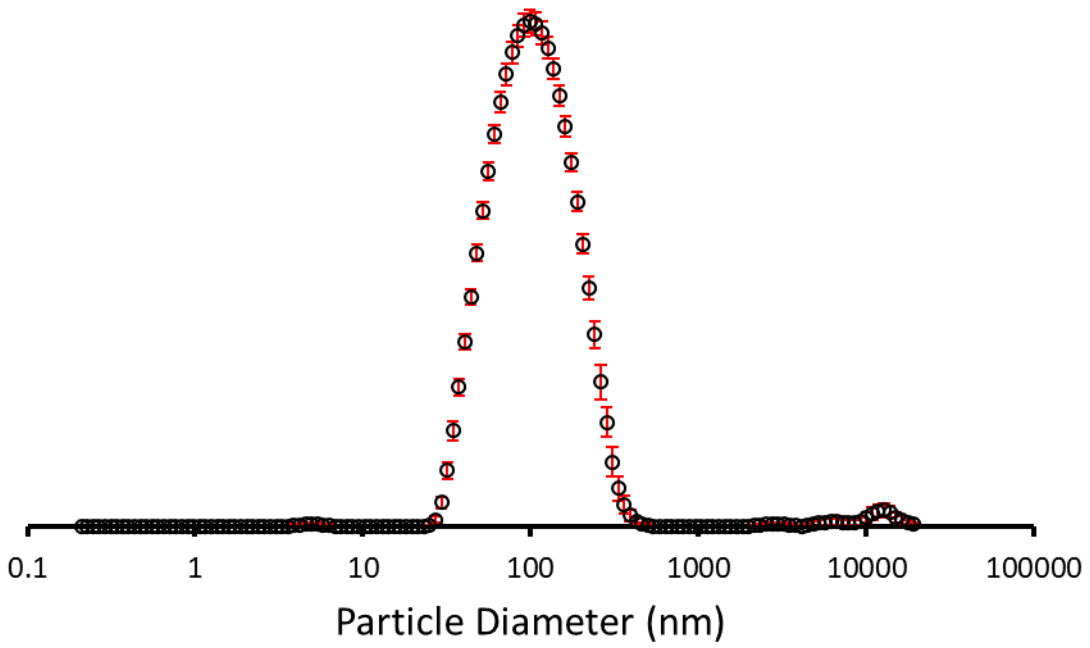

Figure S47 - The average intensity particle size distribution calculated (105 nm) using 10 DLS runs for SSA **4** (5.56 mM) in an EtOH:H_2O (1:19) solution at 298 K.

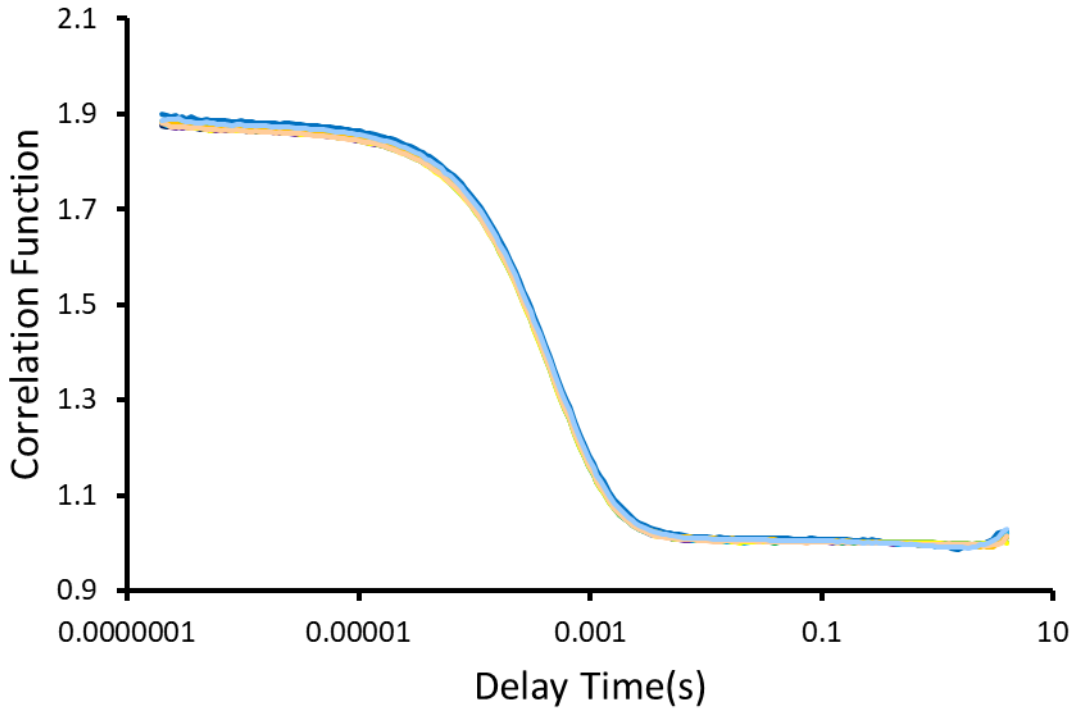

Figure S48 - Correlation function data for 10 DLS runs of SSA **4** (0.56 mM) in an EtOH:$_2$O (1:19) solution at 298 K.

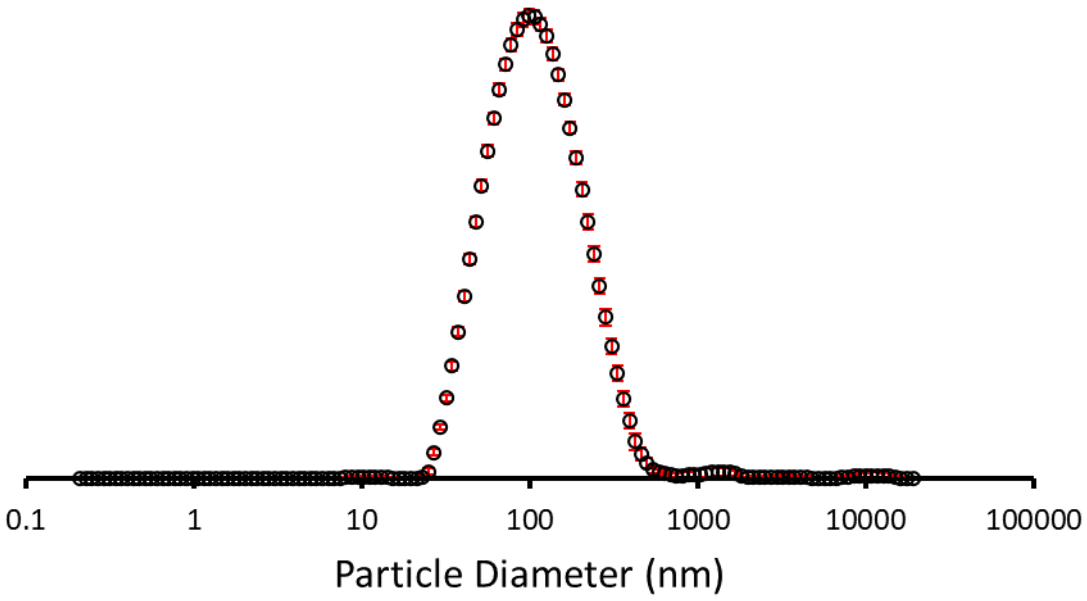

Figure S49 - The average intensity particle size distribution calculated (1320 nm) using 10 DLS runs for SSA **4** (0.56 mM) in an EtOH:H_2O (1:19) solution at 298 K.

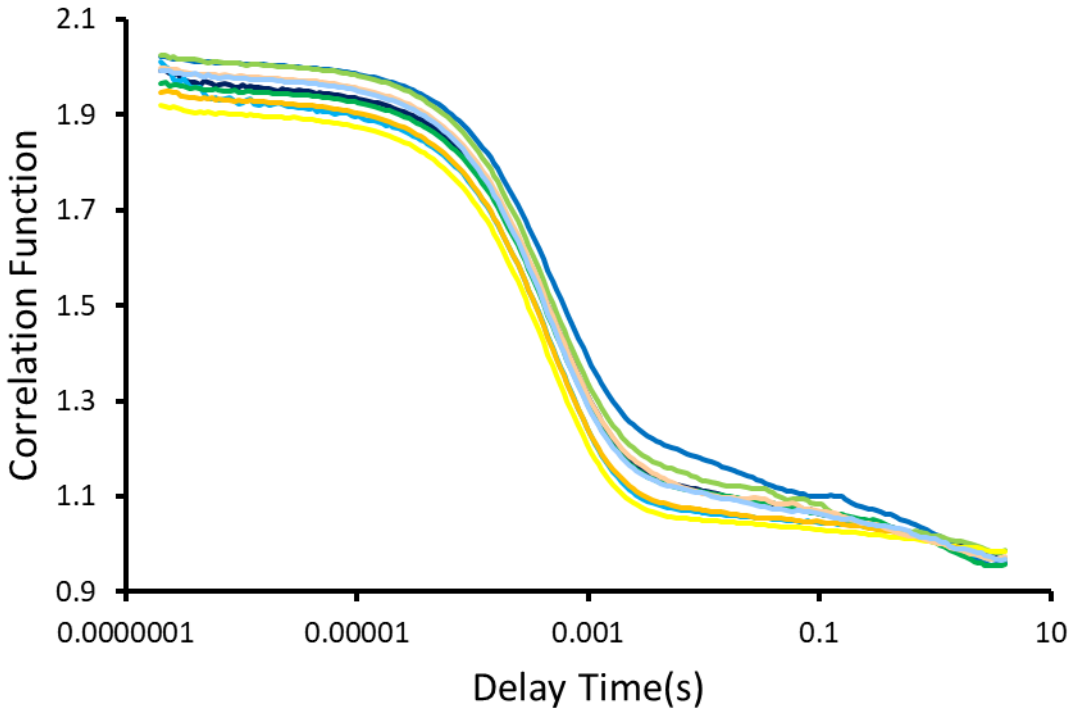

Figure S50 - Correlation function data for 10 DLS runs of SSA **6** (2.78 mM) in an EtOH:H_2O (1:19) solution at 298 K.

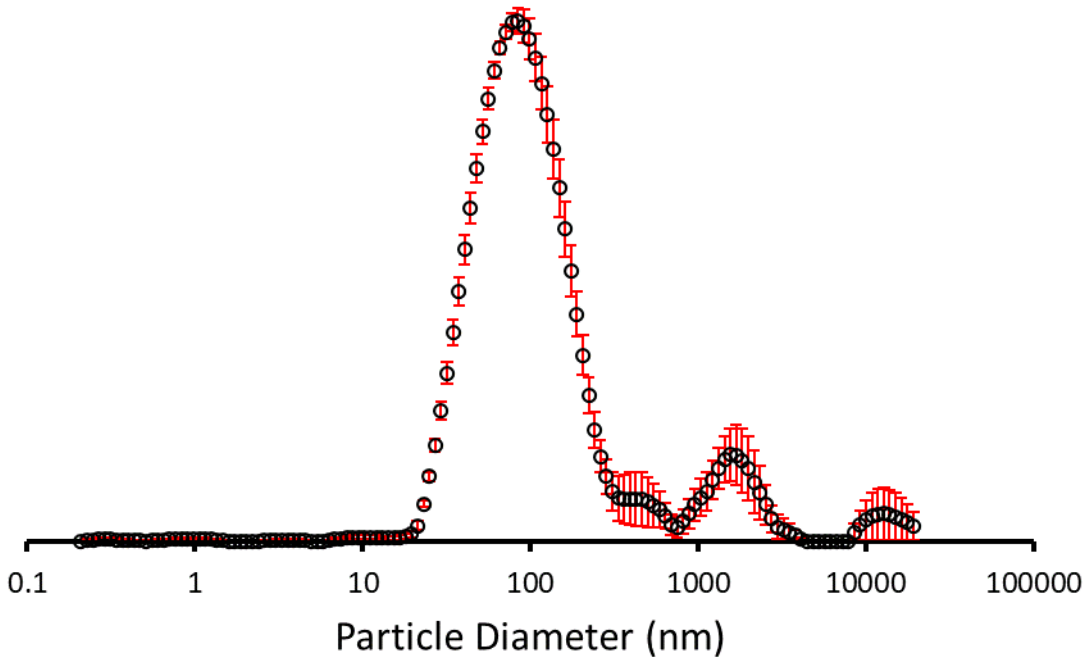

Figure S51 - The average intensity particle size distribution calculated (94 nm) using 10 DLS runs for SSA **6** (2.78 mM) in an EtOH:H_2O (1:19) solution at 298 K.

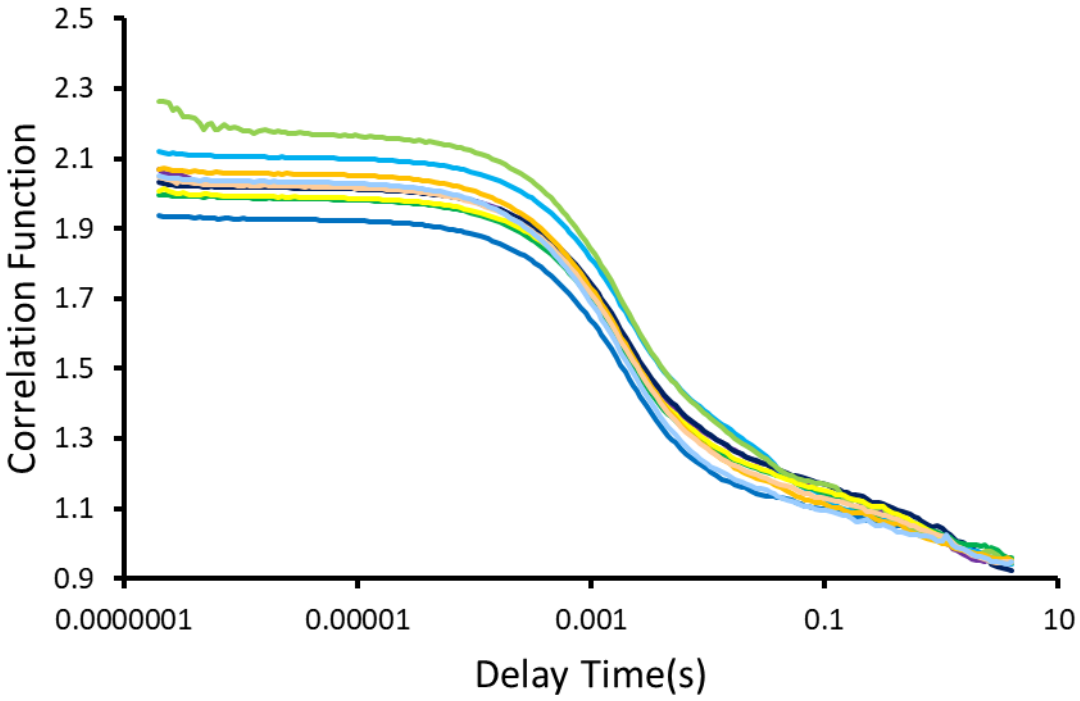

Figure S52 - Correlation function data for 10 DLS runs of SSA **6** (0.28 mM) in an EtOH:H_2O (1:19) solution at 298 K.

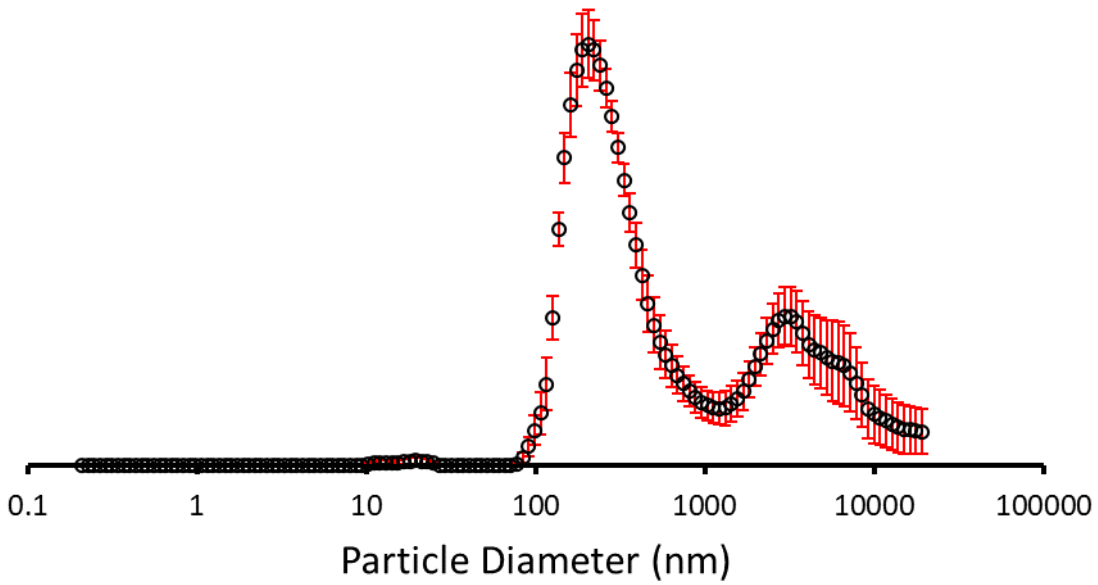

Figure S53 - The average intensity particle size distribution calculated (790 nm) using 10 DLS runs for SSA **6** (0.28 mM) in an EtOH:H_2O (1:19) solution at 298 K.

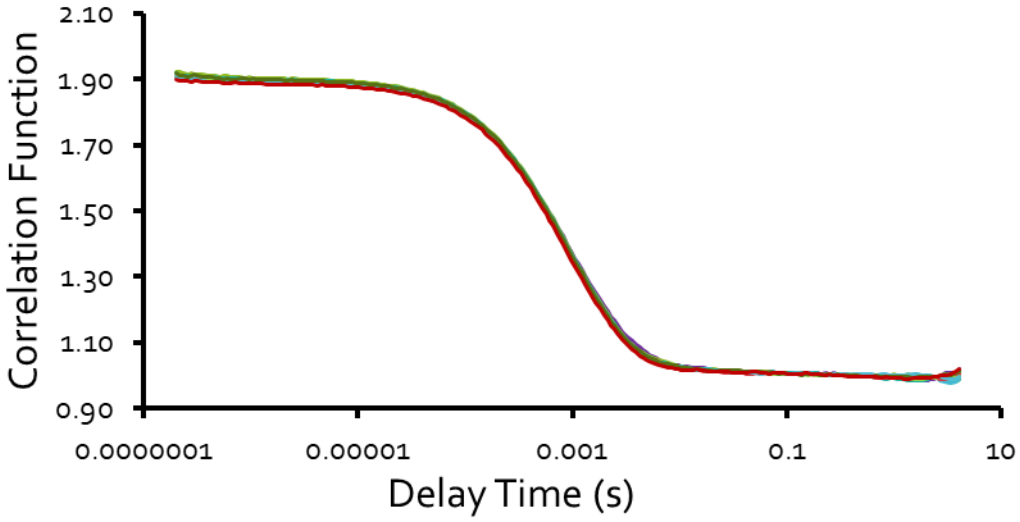

Figure S54 – Correlation function data for 10 DLS runs of SSA **7** (5.56 mM) in an EtOH: H_2O (1:19) solution at 298K.

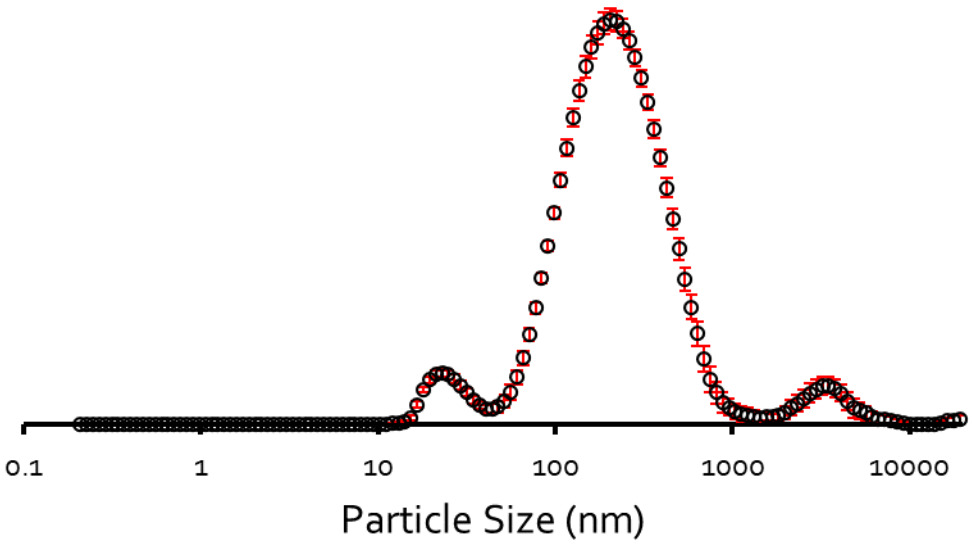

Figure S55 – The average intensity particle size distribution calculated (215 nm) using 10 DLS runs for SSA **7** (5.56 mM) in an EtOH:H_2O (1:19) solution at 298 K.

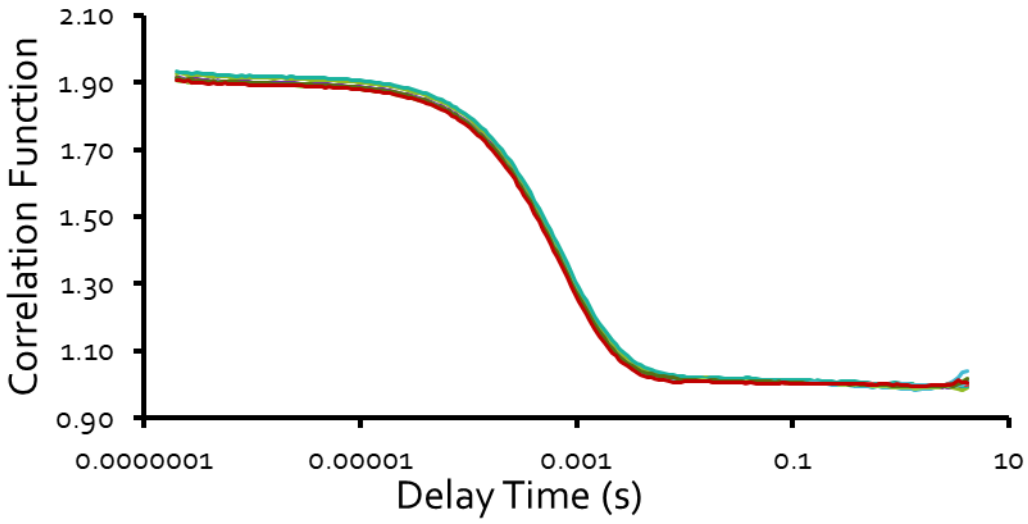

Figure S56 – Correlation function data for 10 DLS runs of SSA **7** (0.56 mM) in an EtOH:H_2O (1:19) solution at 298 K.

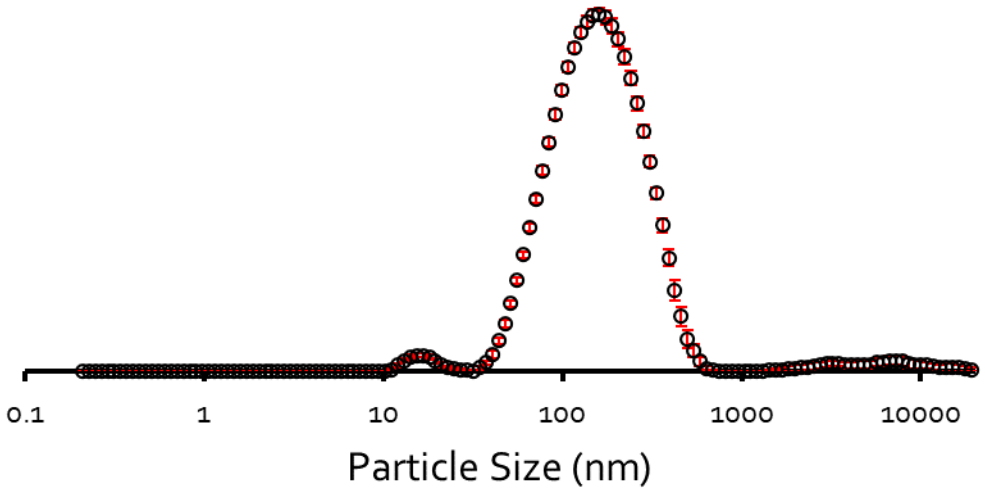

Figure S57 – The average intensity particle size distribution calculated (153 nm) using 10 DLS runs for SSA **7** (0.56 mM) in an EtOH:H_2O (1:19) solution at 298 K.

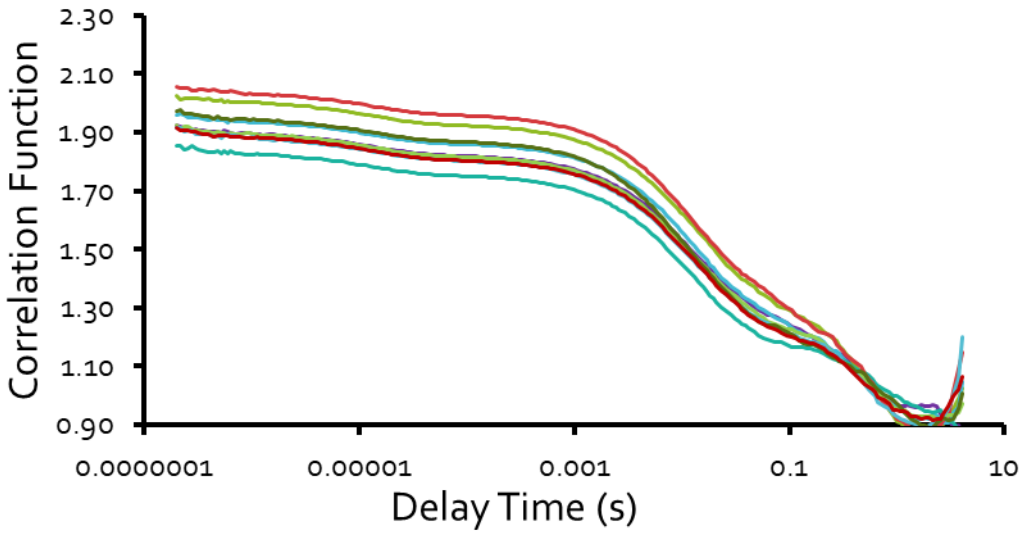

Figure S58 - Correlation function data for 10 DLS runs of SSA **7** (111.2 mM) in a DMSO solution at 298 K. These data should be treated with caution due high levels of polydispersity and amorphous nature of those aggregated species produced, as indicated by quality of the data collected.

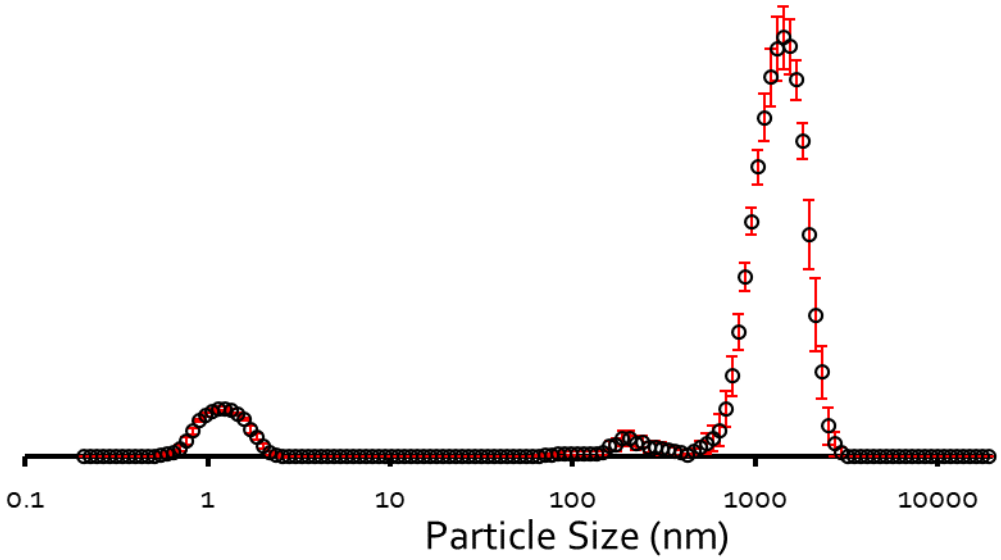

Figure S59 - The average intensity particle size distribution calculated (1380 nm) using 10 DLS runs for SSA **7** (111.2 mM) in a DMSO solution at 298 K. These data should be treated with caution due high levels of polydispersity and amorphous nature of those aggregated species produced, as indicated by quality of the data collected.

Overview

Table S10 - Summary of average intensity particle size distribution data in EtOH:H_2O 1:19 solution. Error = standard error of the mean given to 1 dp.

SSA	Concentration (mM)	Peak maxima (nm)	Polydisperity (%)
1	0.56	180.95 (± 2.5 %)	25.93 (±0.2 %)
2	5.56	300	*a*
	0.56	120	*a*
3	5.56	851.24 (± 25 %)	26.01 (± 0.5 %)
	0.56	105.29 (± 1.0 %)	23.57 (± 0.3 %)
4	5.56	115.39 (± 1.5 %)	24.25 (± 0.4 %)
	0.56	127.22 (± 1.9 %)	23.79 (± 0.7 %)
5	5.56	*b*	*b*
	0.56	*b*	*b*
6	2.78	127.22 (± 1.9 %)	23.79 (± 0.7 %)
	0.28	93.86 (± 3.0 %)	26.22 (± 0.6 %)
7	5.56	255.42 (± 7.1 %)	27.37 (± 0.2 %)
	0.56	177.46 (± 2.4 %)	25.96 (± 0.3 %)

a – Data could not be located.
b – Could not be calculated due to compound solubility.

Table S11 - Summary of average intensity particle size distribution data in DMSO. Error = standard error of the mean given to 1 dp.

SSA	Concentration (mM)	Peak maxima (nm)	Polydisperity (%)
1	*a*	*a*	*a*
2	*a*	*a*	*a*
3	*a*	*a*	*a*
4	*a*	*a*	*a*
5	*a*	*a*	*a*
6	*a*	*a*	*a*
7	111	1380 (± 23.17)	35.74 (± 1.4 %)

a – Study not performed due to no "*loss*" in qNMR.

Section 9: Zeta potential data

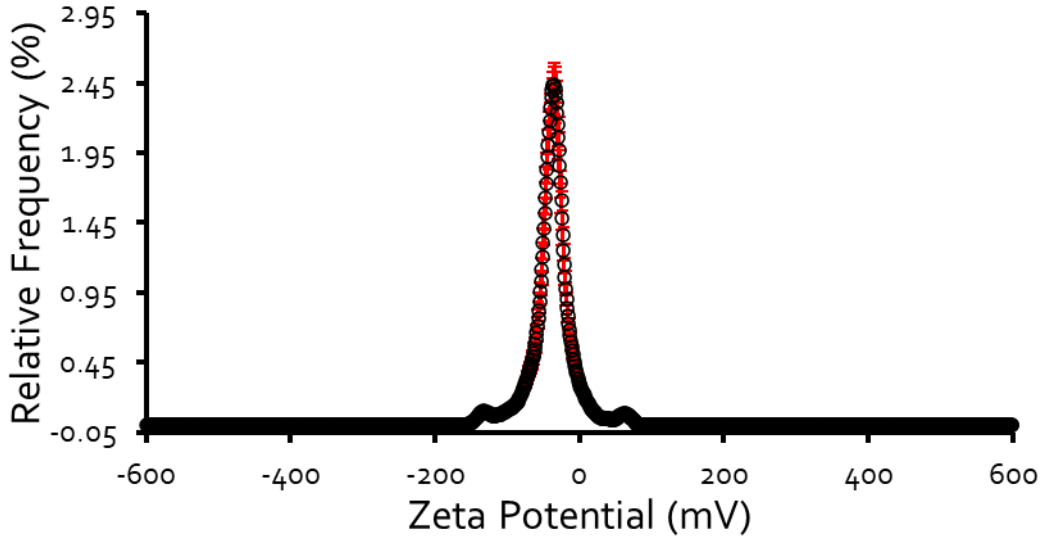

Figure S60 - The average zeta potential distribution calculated using 10 runs for SSA **1** (0.56 mM) in EtOH:H_2O (1:19) solution at 298 K. Average measurement value -42.71 mV.

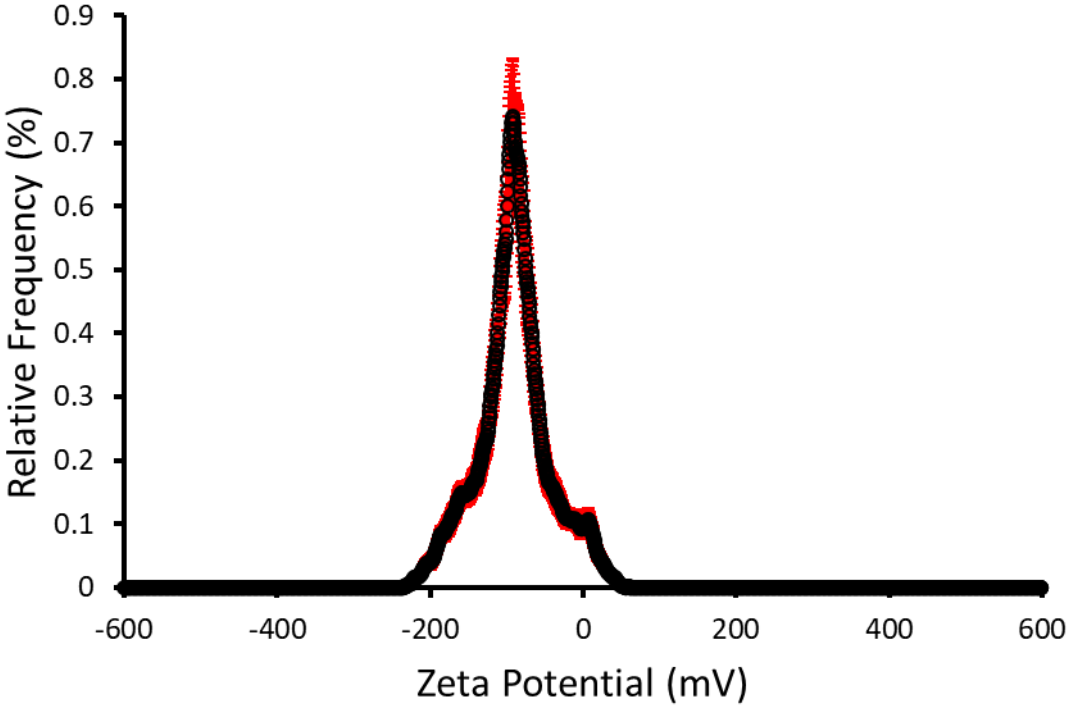

Figure S61 - The average zeta potential distribution calculated using 10 runs for SSA **3** (5.56 mM) in EtOH:H_2O (1:19) solution at 298 K. Average measurement value -88.29 mV.

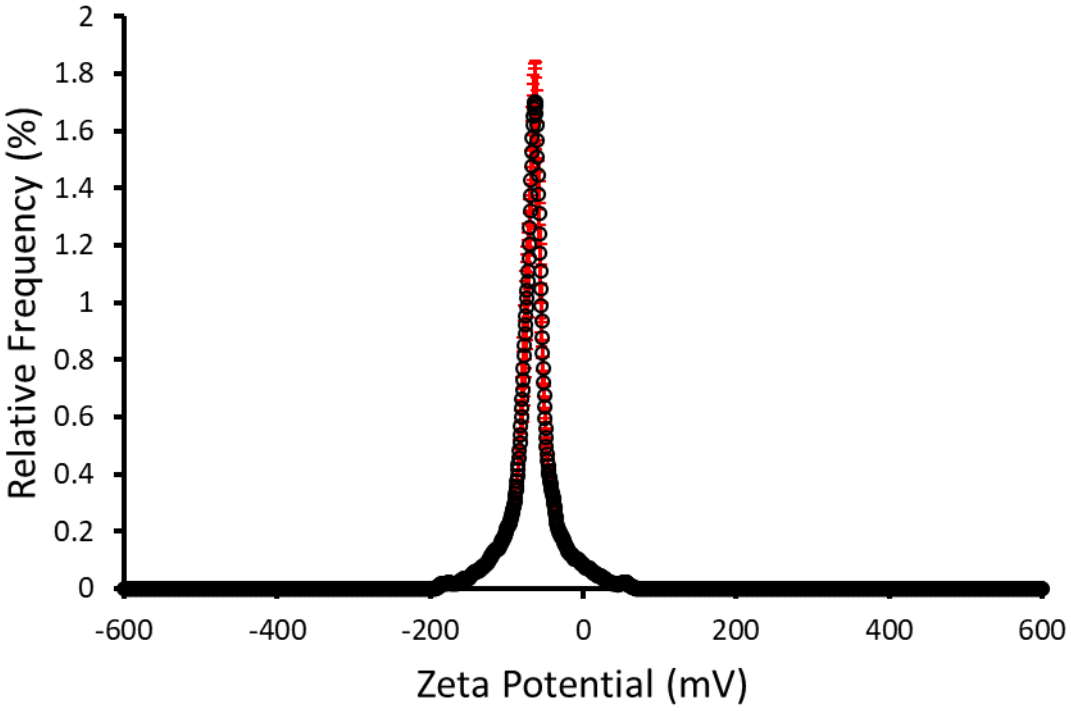

Figure S62 - The average zeta potential distribution calculated using 10 runs for SSA **4** (5.56 mM) in EtOH:H_2O (1:19) solution at 298 K. Average measurement value -74.80 mV.

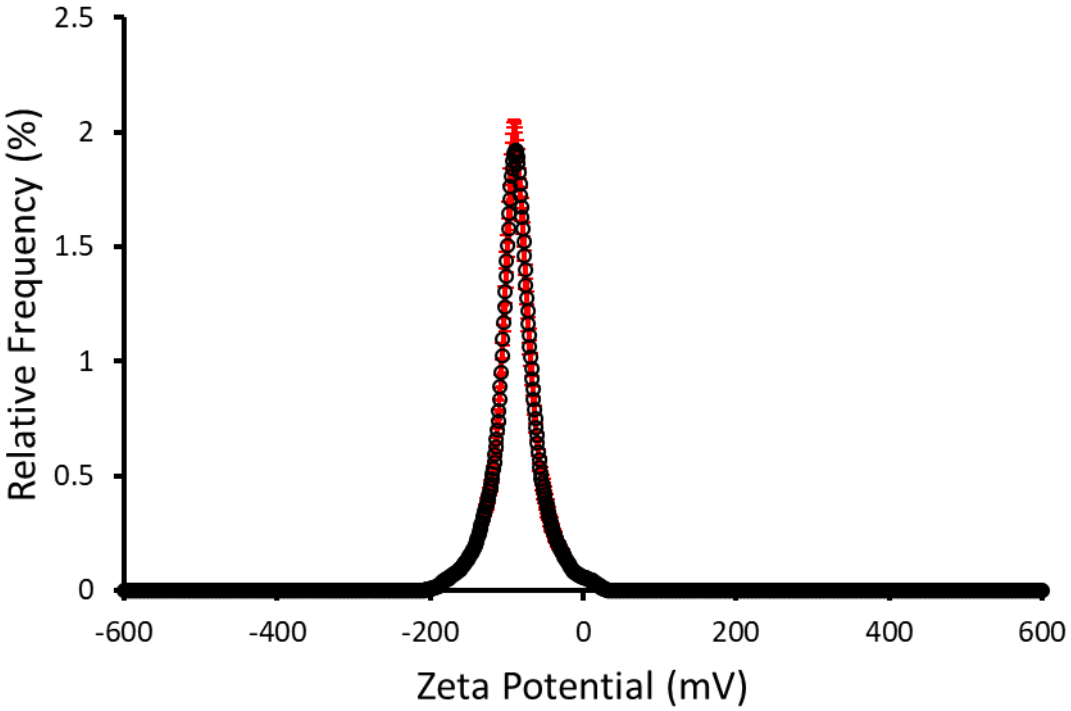

Figure S63 - The average zeta potential distribution calculated using 10 runs for SSA **6** (2.78 mM) in EtOH:H_2O (1:19) solution at 298 K. Average measurement value -84.22 mV.

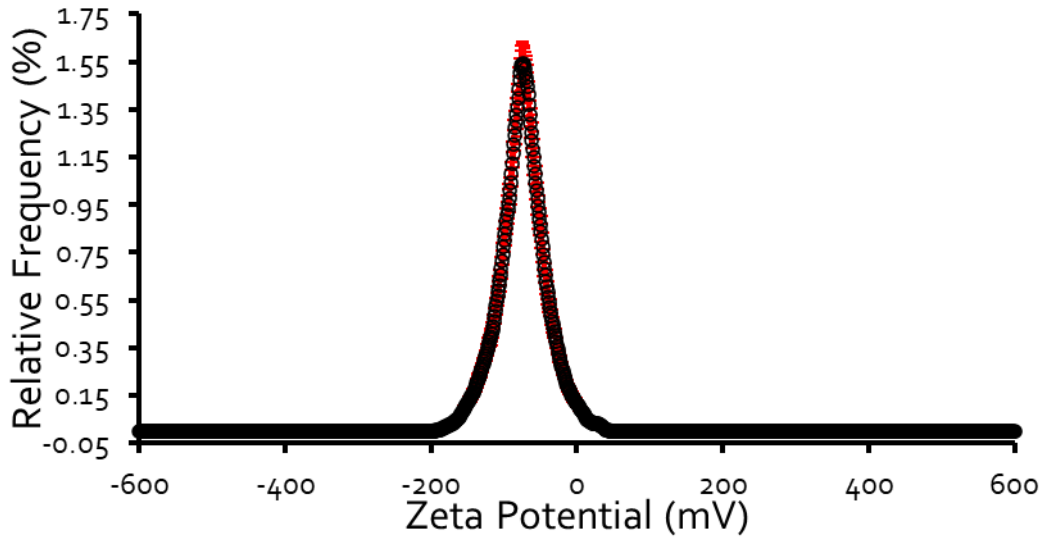

Figure S64 - The average zeta potential distribution calculated using 10 runs for SSA **7** (5.56 mM) in EtOH:H_2O (1:19) solution at 298 K. Average measurement value -67.13 mV.

Overview

Table S12 - Summary of zeta potential for all SSAs. Data obtained in an EtOH:H_2O (1:19) solution.

SSA	Zeta potential (mV)
1	-42.71
2	-101.00
3	-88.29
4	-74.80
5	*a*
6	-84.22
7	-67.13

a – Could not be completed due to compound solubility.

Section 10: Single crystal X-ray structures

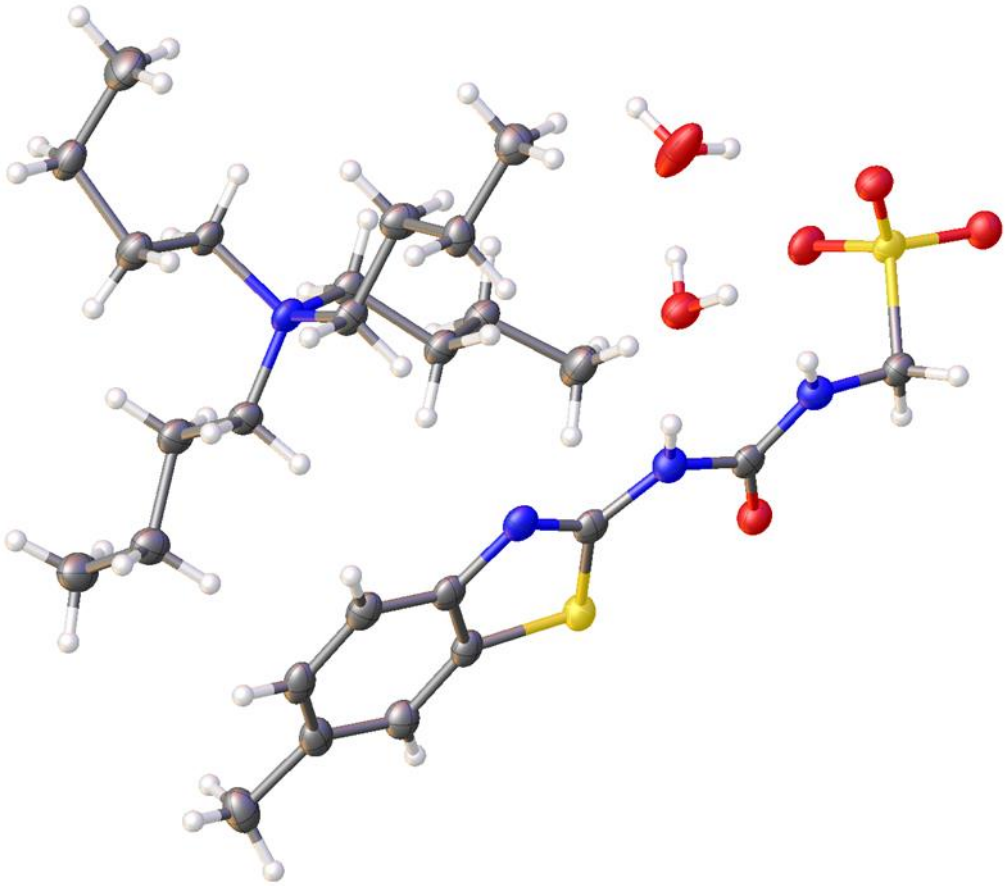

Figure S65 - Single crystal X-ray structure of **1**: red = oxygen; yellow = sulfur; blue = nitrogen; white = hydrogen; grey = carbon. CCDC 2022536, $C_{26}H_{50}N_4O_6S_2$ (M = 578.82): monoclinic, space group P 21/n, a = 8.4322(1) Å, b = 16.2622(2) Å, c = 23.0023(3) Å, α = 90°, β = 100.426(1)°, γ = 90°, V = 3102.14(7) $Å^3$, Z = 4, T = 100(1) K, CuK\α = 1.5418 Å, Dcalc = 1.239 g/cm^3, 21823 reflections measured (7.816 ≤ 2Θ ≤ 144.206), 6021 unique (R_{int} = 0.0513**,** R_{sigma} = 0.0427) which were used in all calculations. The final R_1 was 0.0392 (I > 2σ(I)) and wR_2 was 0.1069 (all data).

Table S13 - Hydrogen bond distances and angles observed for **1**, calculated from the single crystal X-ray structure shown in Figure S65.

Hydrogen bond donor	Hydrogen bond acceptor	Hydrogen bond length (D•••A) (Å)	Hydrogen bond angle (D-H•••A) (°)
N1	O1	3.0716(10)	3.0716(18)
N1	O5	3.125(2)	140.8 (1)
N2	O5	2.7277(18)	163.64 (10)
O5	O2	2.7833(17)	173.60 (8)
O5	O6	2.7021(19)	169.88 (10)
O6	O1	2.8691(19)	152.52 (10)
O6	O3	2.8365 (18)	172.02 (12)

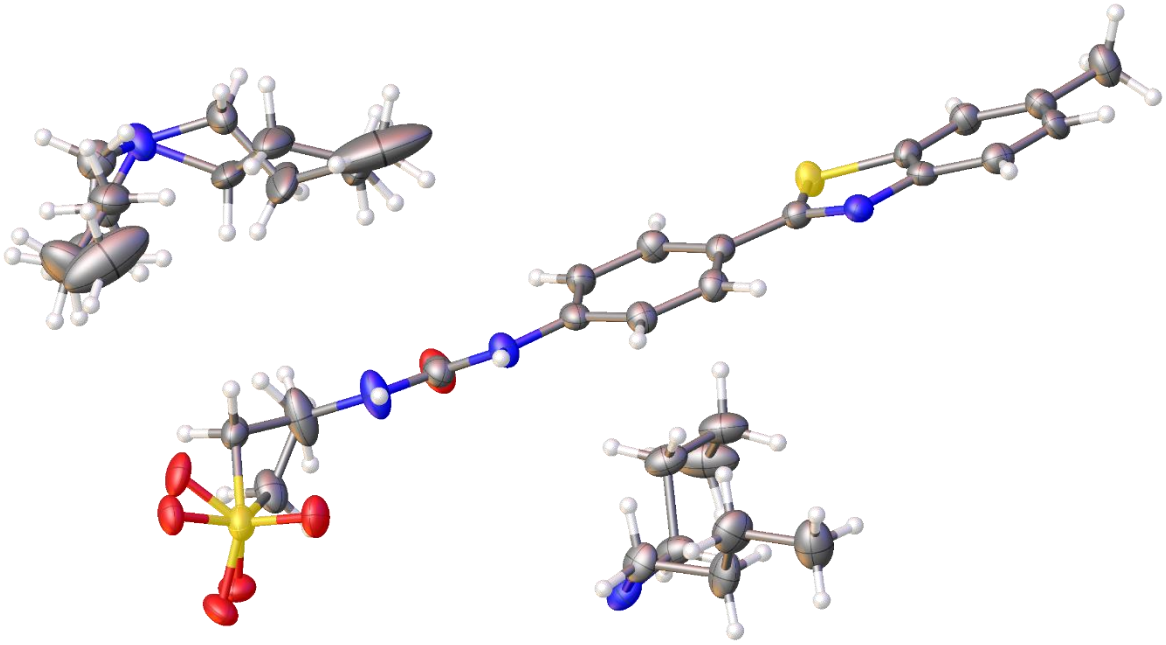

Figure S66 - Single crystal X-ray structure of **3**: red = oxygen; yellow = sulfur; blue = nitrogen; white = hydrogen; grey = carbon. CCDC 2023004, $C_{33}H_{52}N_4O_4S_2$ (M = 632.90): monoclinic, space group P 2/n, a = 16.4865(13) Å, b = 10.4507(7) Å, c = 20.0106(17) Å, α = 90°, β = 94.596(7)°, γ = 90°, V = 3436.7(4) $Å^3$, Z = 4, T = 100(1) K, CuK\α = 1.5418 Å, Dcalc = 1.223 g/cm^3, 22331 reflections measured (7.238 ≤ 2Θ ≤ 133.202), 6083 unique (R_{int} = 0.1112**,** R_{sigma} = 0.1299) which were used in all calculations. The final R_1 was 0.0622 (I > 2σ(I)) and wR_2 was 0.1341 (all data).

Table S14 – Hydrogen bond distances and angles observed for **3**, calculated from the single crystal X-ray structure shown in Figure S66.

Hydrogen bond donor	Hydrogen bond acceptor	Hydrogen bond length (D•••A) (Å)	Hydrogen bond angle (D-H•••A) (°)
N2	O4	2.839(4)	173.44(7)
N3	O4	2.995(4)	148.8(2)

Interior angle of dimerization = 135.4(4)°.

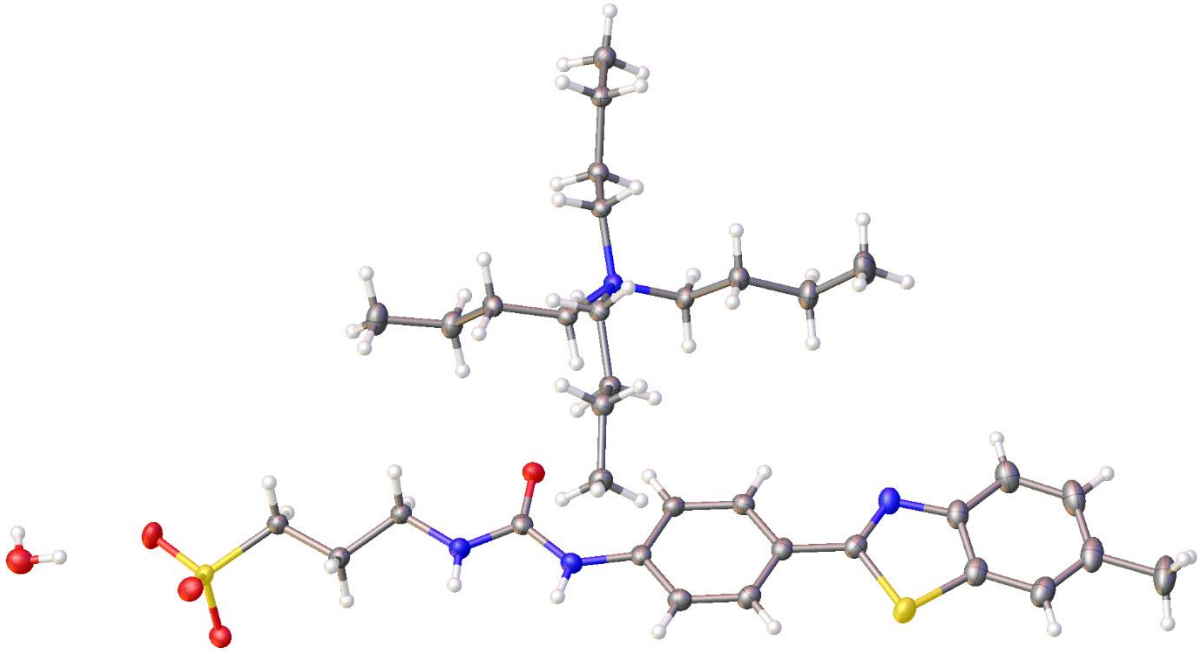

Figure S67 – Single crystal X-ray structure of **4**: red = oxygen; yellow = sulfur; blue = nitrogen; white = hydrogen; grey = carbon. CCDC 2033371, $C_{34}H_{56}N_4O_5S_2$ (M = 664.94): triclinic, space group P -1, a = 9.2701(2) Å, b = 9.2791(3) Å, c = 21.7492(7) Å, α = 91.169(3)°, β = 96.234(2)°, γ = 103.561(2)°, V = 1805.87(9) $Å^3$, Z = 2, T = 100(1) K, CuK\α = 1.5418 Å, Dcalc = 1.223 g/cm^3, 12423 reflections measured (8.184 ≤ 2Θ ≤ 143.716), 6885 unique (R_{int} = 0.0271, R_{sigma} = 0.0402**)** which were used in all calculations. The final R_1 was 0.0373 (I > 2σ(I)) and wR_2 was 0.0950 (all data).

Table S15 – Hydrogen bond distances and angles observed for **4**, calculated from the single crystal X-ray structure shown in Figure S67.

Hydrogen bond donor	Hydrogen bond acceptor	Hydrogen bond length (D•••A) (Å)	Hydrogen bond angle (D-H•••A) (°)
N1	O2	2.9478 (17)	154.64 (9)
N2	O1	2.9591 (17)	156.20 (9)
O5	O3	2.8719 (18)	173.45 (9)
O5	N3	2.9280 (19)	167.14 (10)

Interior angle of dimerization = 180.00(19)°.

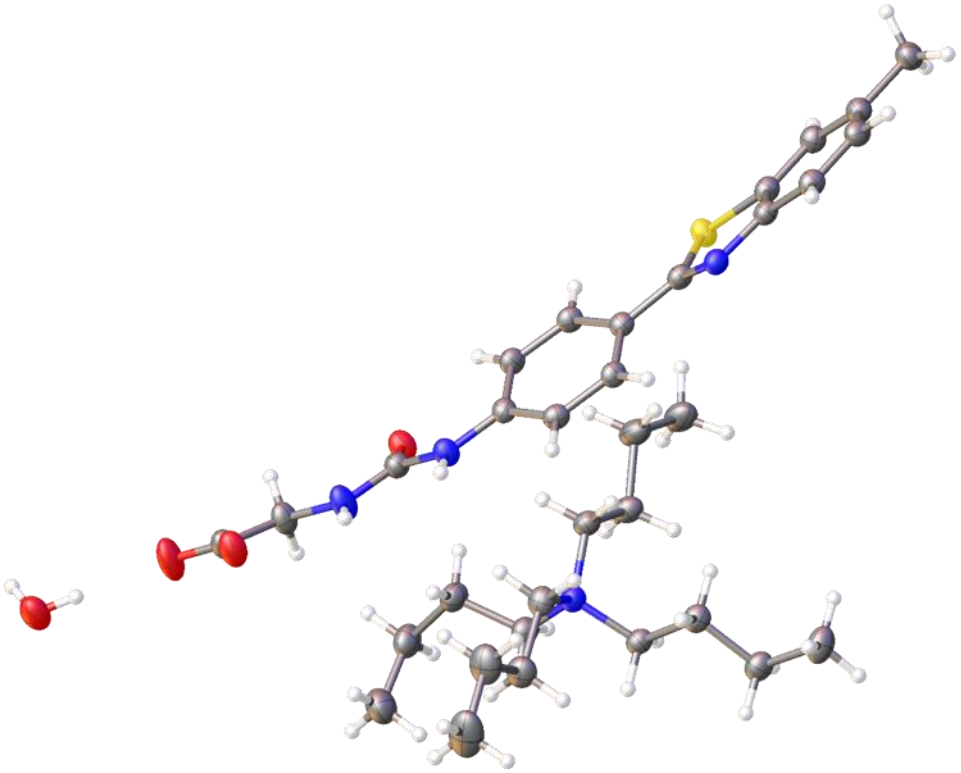

Figure S68 - Single crystal X-ray structure of **6**: red = oxygen; yellow = sulfur; blue = nitrogen; white = hydrogen; grey = carbon. CCDC 2106928, $C_{33}H_{52}N_4O_4S$ (M = 600.84): triclinic, space group P -1, a = 9.1985(4) Å, b = 11.8652(4) Å, c = 16.6048(6) Å, α = 80.985(3)°, β = 87.623(3)°, γ = 69.132(4)°, V = 1672.27(11) $Å^3$, Z = 2, T = 100(1) K, CuK\α = 1.5418 Å, Dcalc = 1.193 g/cm^3, 11602 reflections measured (8.068 ≤ 2Θ ≤ 144.196), 6341 unique (R_{int} = 0.0354**,** R_{sigma} = 0.0453) which were used in all calculations. The final R_1 was 0.0467 (I > 2σ(I)) and wR_2 was 0.1281 (all data).

Table S16 - Hydrogen bond distances and angles observed for **6**, calculated from the single crystal X-ray structure shown in Figure S68.

Hydrogen bond donor	Hydrogen atom	Hydrogen bond acceptor	Hydrogen bond length (D•••A) (Å)	Hydrogen bond angle (D-H•••A) (°)
N1	H1	O2	2.9892(19)	146.48(10)
N2	H2	O2	2.7332(18)	161.89(10)
O4	H4A	O1	2.8170(19)	170.68(11)
O4	H4B	O1	2.9025(19)	169.86(10)

Interior angle of dimerization = 180.00(12)°.

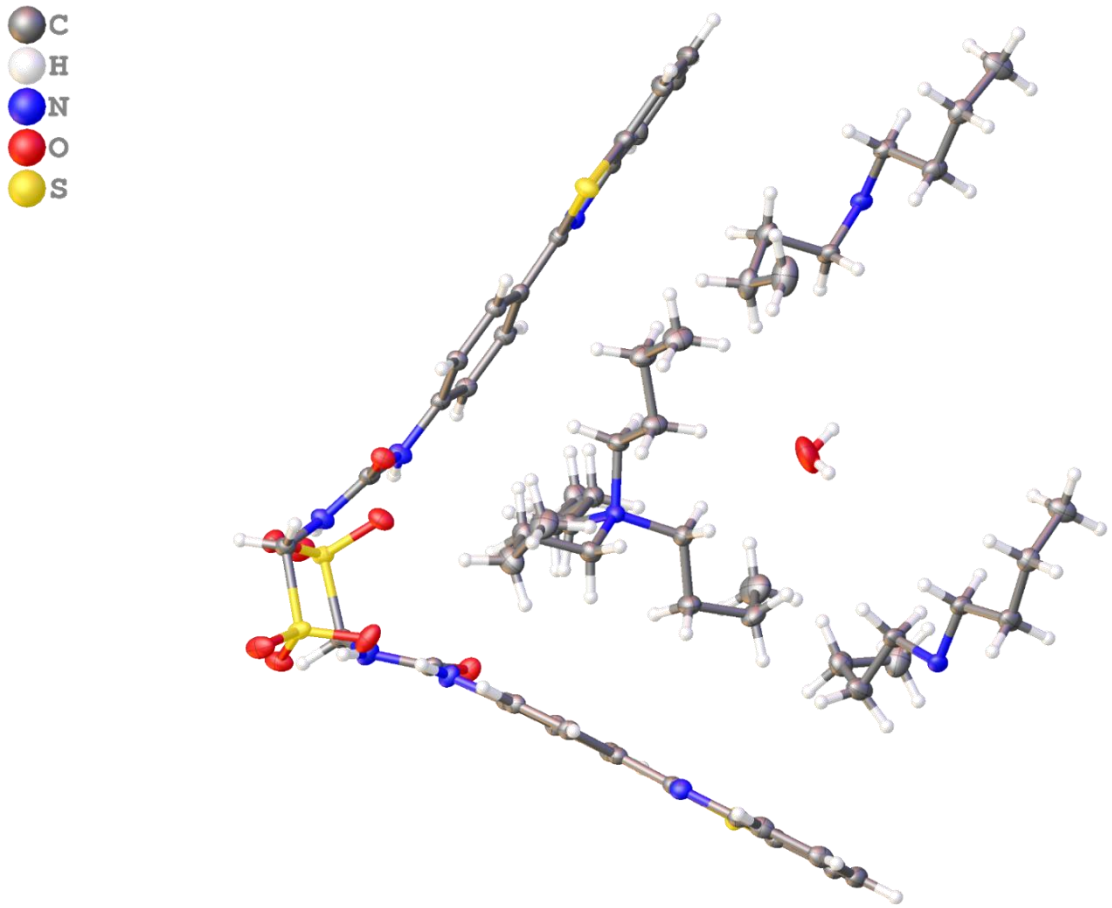

Figure S69 - Single crystal X-ray structure of **7**: red = oxygen; yellow = sulfur; blue = nitrogen; white = hydrogen; grey = carbon. CCDC 1997675, $C_{62}H_{98}N_8O_9S_4$ (M = 1227.72): monoclinic, space group P 2/n, a = 19.22676(16) Å, b = 13.73691(14) Å, c = 25.4779(2) Å, α = 90°, β = 107.0098(10)°, γ = 90°, V = 6434.76(11) $Å^3$, Z = 4, T = 148(1) K, CuK\α = 1.5418 Å, Dcalc = 1.267 g/cm^3, 42981 reflections measured (7.256 ≤ 2Θ ≤ 133.202), 11367 unique (R_{int} = 0.0440, R_{sigma} = 0.0365) which were used in all calculations. The final R_1 was 0.0379 (I > 2σ(I)) and wR_2 was 0.1033 (all data). Internal angel of dimerization = 53.65(8)°.

Table S17 - Hydrogen bond distances and angles observed for **7**, calculated from the single crystal X-ray structure shown in Figure S69.

Hydrogen bond donor	Hydrogen bond acceptor	Hydrogen bond length (D•••A) (Å)	Hydrogen bond angle (D-H•••A) (°)
N1	O5	2.9066(19)	163.53(11)
N2	O7	2.9093(19)	175.23(10)
N4	O3	2.2953(19)	178.69(12)
N5	O1	2.9089(19)	171.00(11)
O9	O5	2.827(2)	165.38(14)
O9	O3	2.852(2)	154.13(12)

Interior angle of dimerization = 95.12(13)°

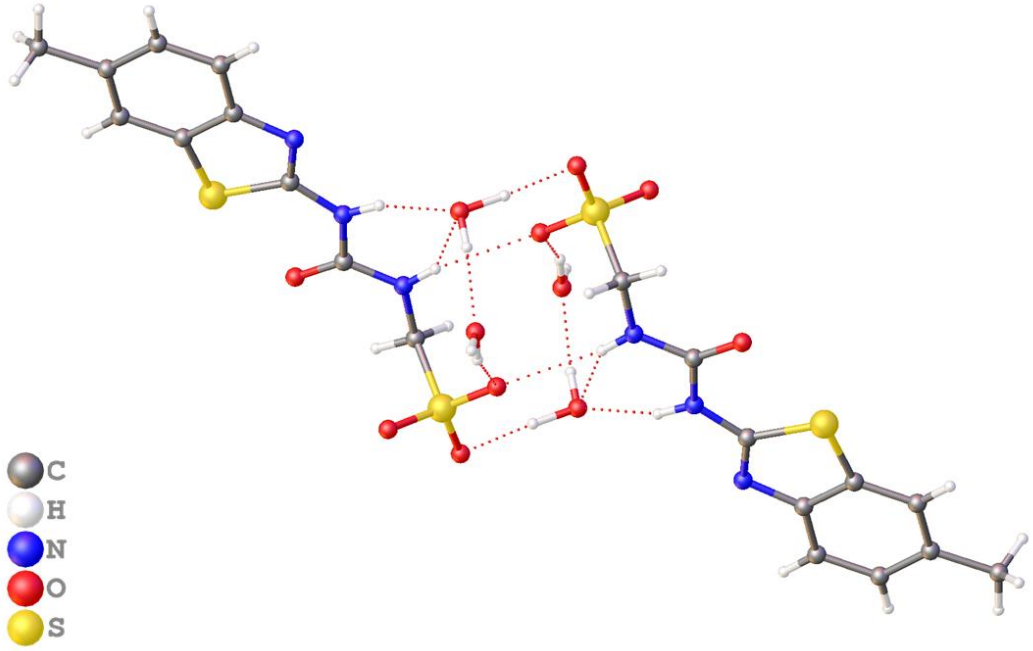

Figure S70 – Single crystal X-ray structure of **1**, exhibiting a hydrogen bonded dimer. TBA counter cation omitted for clarity.

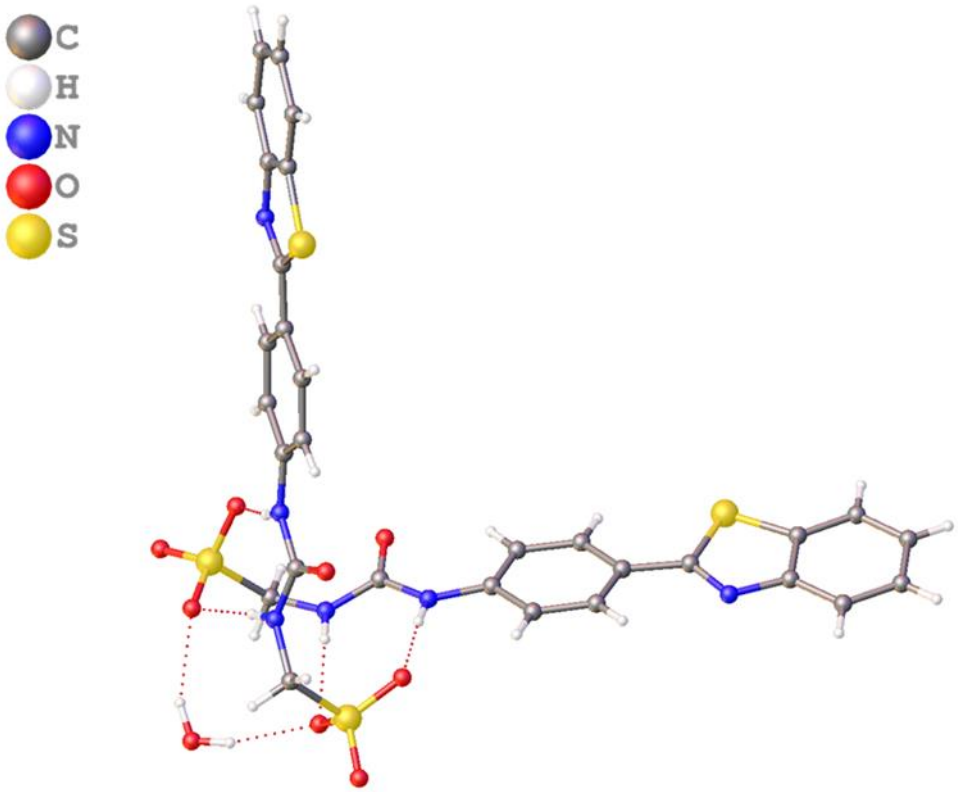

Figure S71 – Single crystal X-ray structure of **7**, exhibiting a hydrogen bonded dimer. TBA counter cation omitted for clarity.

Section 11: LogP calculation

http://www.vcclab.org/lab/alogps/[10,11]

Table S18 – Summary of LogP values for all SSAs.

SSA	Calculated LogP
1	1.22
2	2.58
3	2.62
4	2.81
5	*2.70*
6	3.58
7	2.45

Section 12: Mass spectrum data

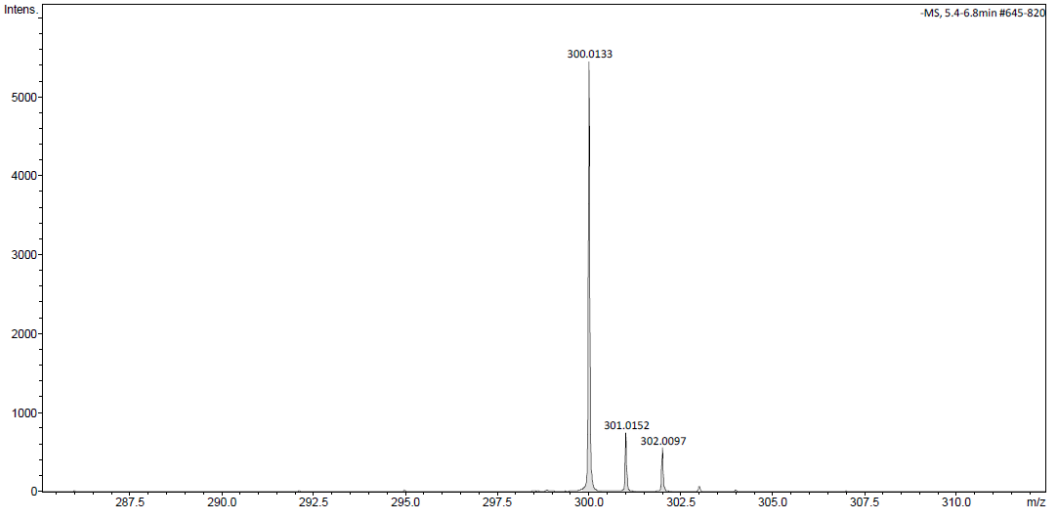

Figure S72 - A high-resolution mass spectrum (ESI^-) obtained for SSA **1** in methanol, *m/z* [M].

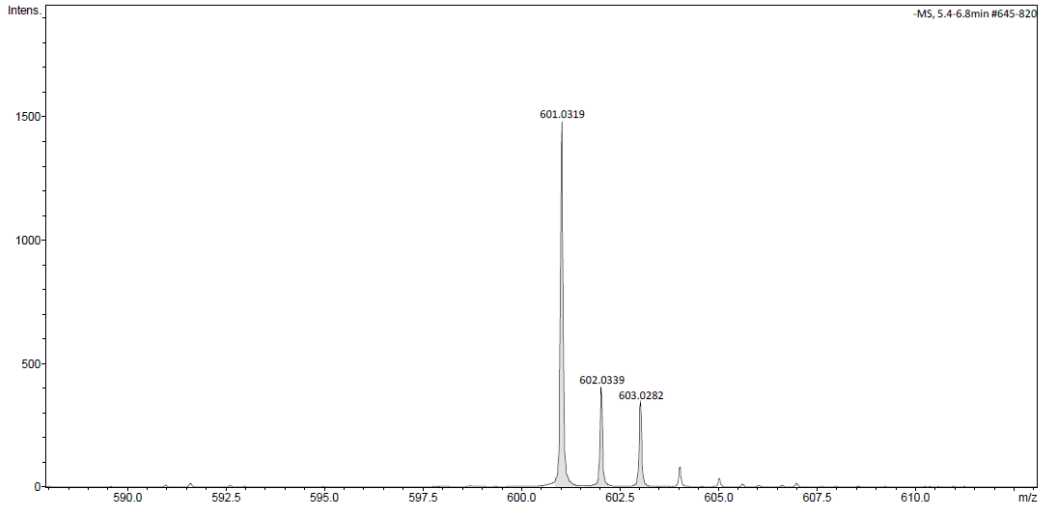

Figure S73 - A high-resolution mass spectrum (ESI^-) obtained for dimeric species of SSA **1** in methanol, *m/z* [M + M + H^+].

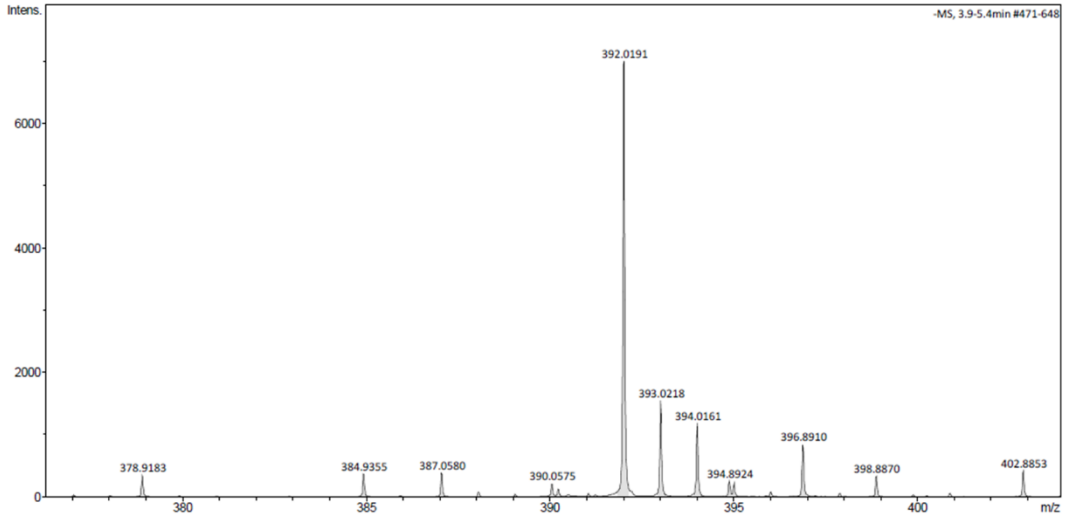

Figure S74 - A high-resolution mass spectrum (ESI$^-$) obtained for SSA **3** in methanol, *m/z* [M].

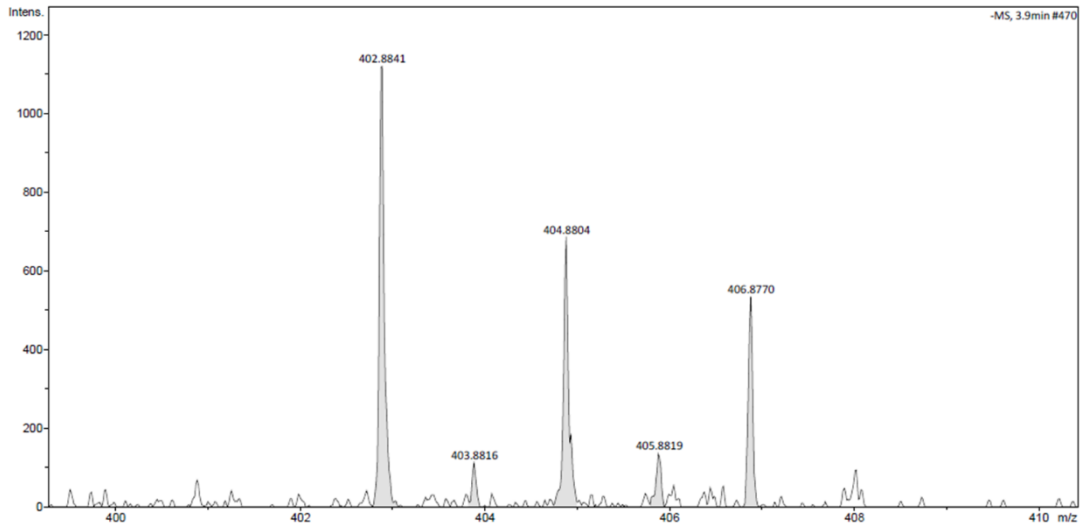

Figure S75 - A high-resolution mass spectrum (ESI$^-$) obtained for SSA **4** in methanol, *m/z* [M].

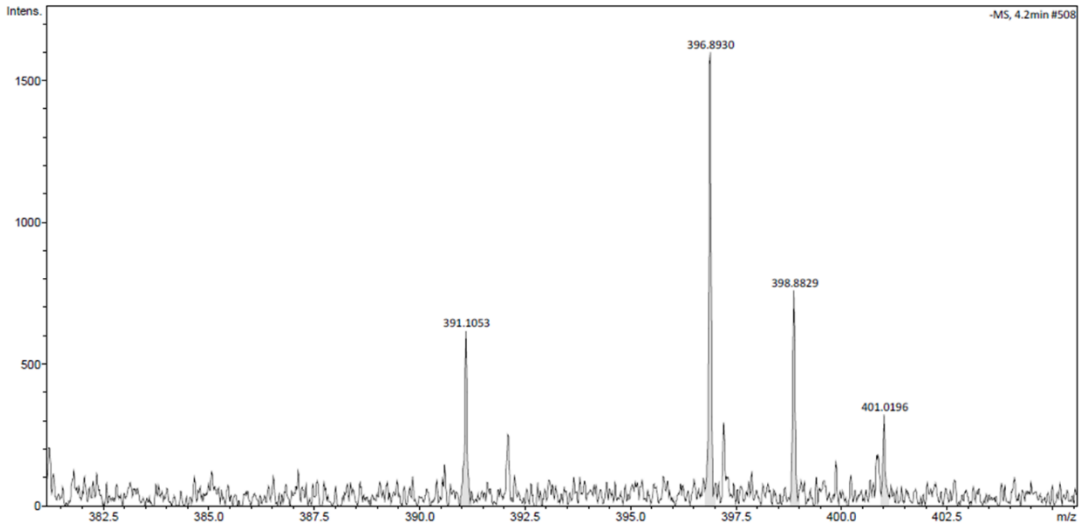

Figure S76 - A high-resolution mass spectrum (ESI$^-$) obtained for SSA **5** in methanol, *m/z* [M].

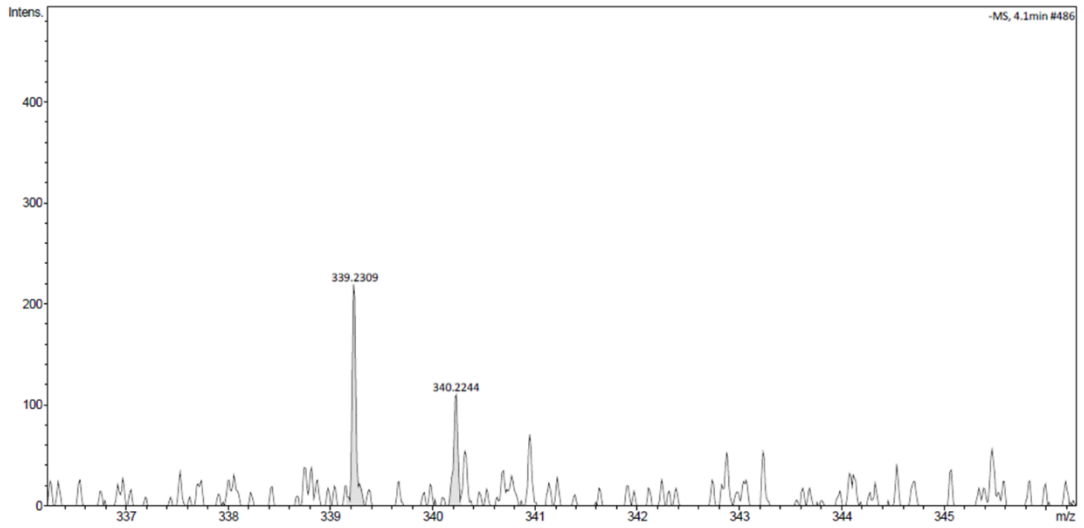

Figure S77 - A high-resolution mass spectrum (ESI$^-$) obtained for SSA **6** in methanol, *m/z* [M].

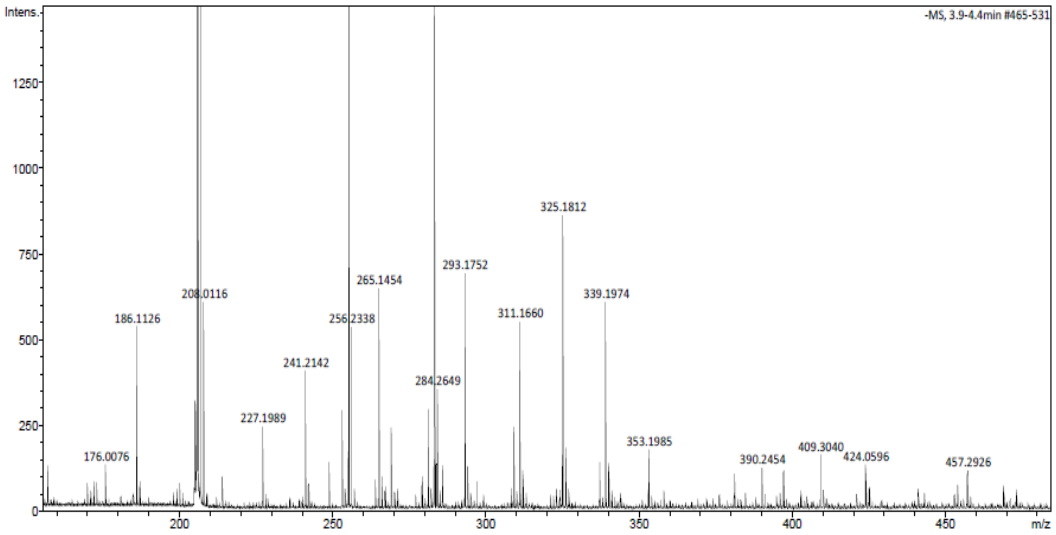

Figure S78 – A high-resolution mass spectrum (ESI$^-$) obtained for SSA **7** in methanol, *m/z* [M + C_2H_4].

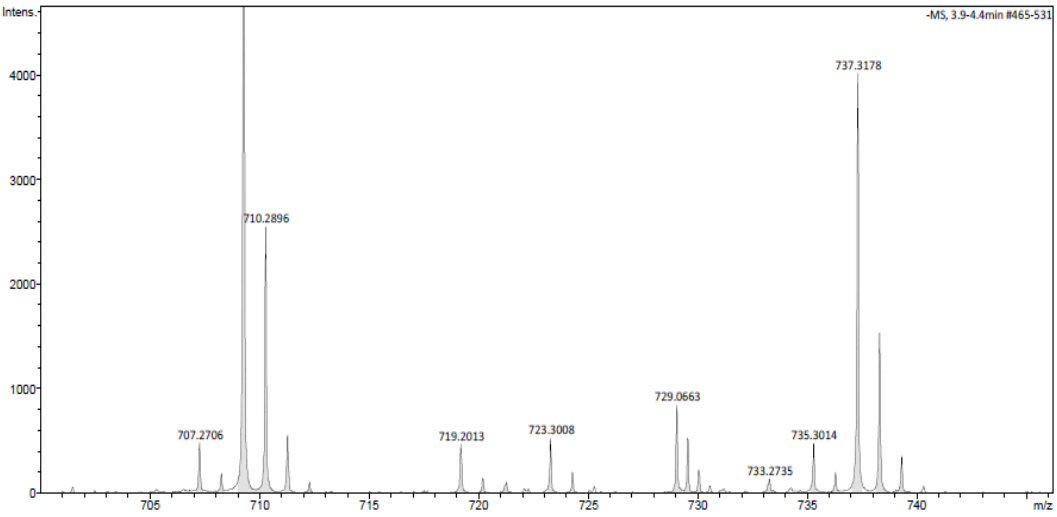

Figure S79 – A high-resolution mass spectrum (ESI$^-$) obtained for dimeric species of SSA **7** in methanol, *m/z* [M+ M + H$^+$].

Overview

Table S19 - High resolution ESI$^-$ mass spectrometry theoretical and experimentally derived values.

	m/z [M]		m/z [M + M + H]	
SSA	**Theoretical**	**Actual**	**Theoretical**	**Actual**
1	300.0118	300.0133	300.0236	601.0319
2	376.0431	376.0390	753.0862	753.0864
3	390.0588	390.0575	*a*	*a*
4	404.0744	403.8816	*a*	*a*
5	392.0203	391.1053*b*	*a*	*a*
6	340.0761	340.2244	*a*	*a*
7	362.0275	390.2425*c*	723.0550	723.3008

a – No dimer observed.
b – M$^-$ observed.

c – C_2H_2 adduct contaminate.[12]

Section 13: Hydrogel characterisation data

Minimum gelation concentration (MGC) determination

Figure S80 – SSA **3** MGC determination in 0.505 M aqueous NaCl. Liquid could be seen seeping out of the material and the meniscus could be seen. MGC is above 5 mg/mL.

Figure S81 – SSA **3** MGC determination in 0.505 M aqueous KCl. Liquid could be seen seeping out of the material and the meniscus could be seen. MGC is above 5 mg/mL.

Figure S82 – SSA **3** MGC determination in 0.505 M aqueous $NaNO_3$. Liquid could be seen seeping out of the material and the meniscus could be seen. MGC is above 5 mg/mL.

Figure S83 – SSA **3** MGC determination in 0.505 M aqueous NaH_2PO_4. Precipitation occurred so MGC could not be calculated.

Figure S84 – SSA **3** MGC determination in 0.505 M aqueous NOBz. Hydrogel not formed at 5 mg/mL.

Figure S85 – SSA **3** MGC determination in 0.505 M aqueous N_2SO_4. Liquid could be seen seeping out of the material and the meniscus could be seen. MGC is above 5 mg/mL.

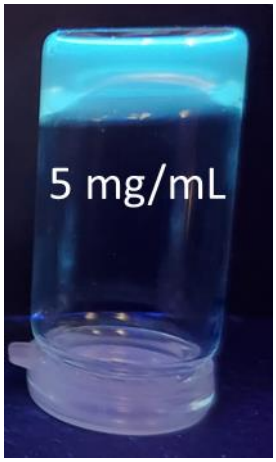

Figure S86 – SSA **4** MGC determination in 0.505 M aqueous NaCl. Liquid could be seen seeping out of the material and the meniscus could be seen. MGC is above 5 mg/mL.

e 

Figure S87 – SSA **4** MGC determination in 0.505 M aqueous KCl. Liquid could be seen seeping out of the material and the meniscus could be seen. MGC is above 5 mg/mL.

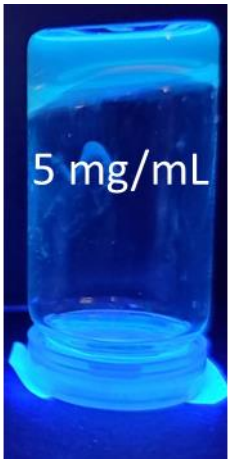

Figure S88 – SSA **4** MGC determination in 0.505 M aqueous $NaNO_3$. Liquid could be seen seeping out of the material and the meniscus could be seen. MGC is above 5 mg/mL.

Figure S89 – SSA **4** MGC determination in 0.505 M aqueous NaH_2PO_4. Liquid could be seen seeping out of the material and the meniscus could be seen. MGC is above 5 mg/mL.

Figure S90 – SSA **4** MGC determination in 0.505 M aqueous NaOBz. Liquid could be seen seeping out of the material and the meniscus could be seen. MGC is above 5 mg/mL.

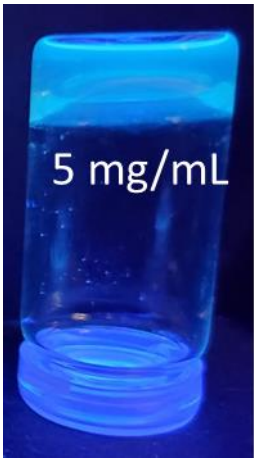

Figure S91 – SSA **4** MGC determination in 0.505 M aqueous NaH_2PO_4. Liquid could be seen seeping out of the material and the meniscus could be seen. MGC is above 5 mg/mL.

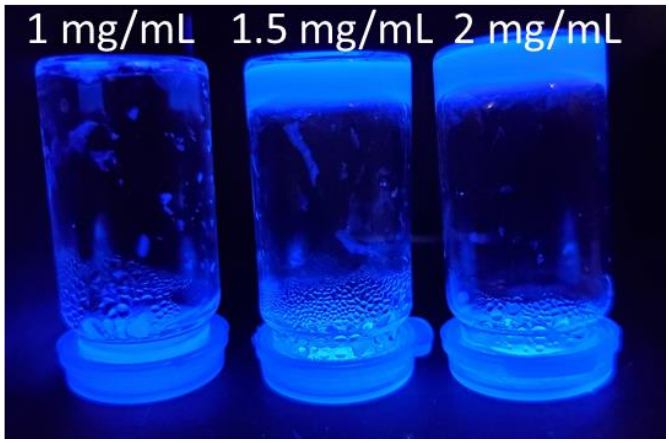

Figure S92 – SSA **7** MGC determination in 0.505 M aqueous NaCl. MGC determined to be 1.5 mg/mL.

Figure S93 – SSA **7** MGC determination in 0.505 M aqueous KCl. Precipitation occurred so MGC could not be calculated.

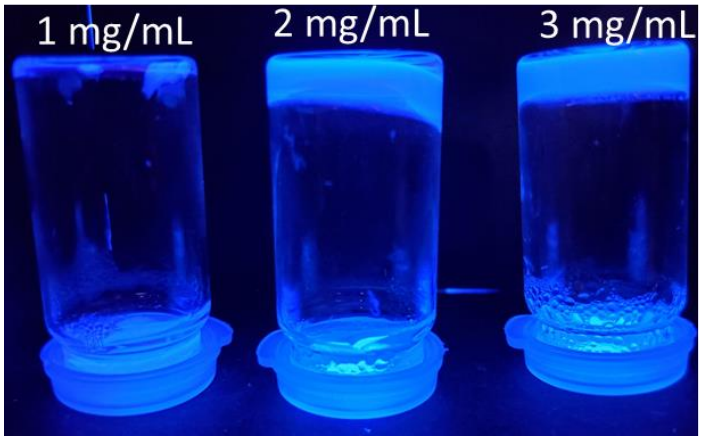

Figure S94 – SSA **7** MGC determination in 0.505 M aqueous $NaNO_3$. MGC determined to be 2 mg/mL.

Figure S95 – SSA **7** MGC determination in 0.505 M aqueous NaH_2PO_4. Hydrogel not formed at 5 mg/mL.

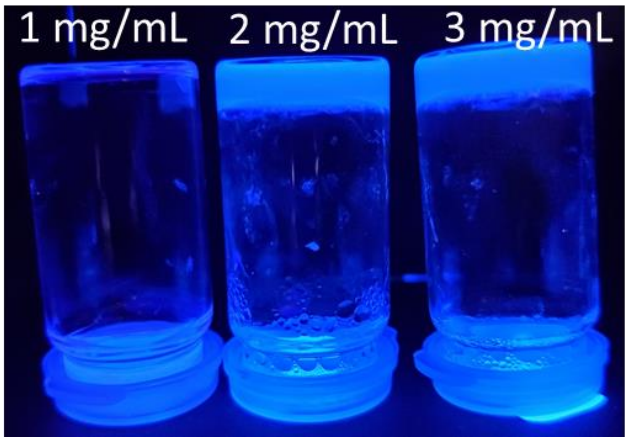

Figure S96 – SSA **7** MGC determination in 0.505 M aqueous NaOBz. MGC determined to be 2 mg/mL.

Figure S97 – SSA **7** MGC determination in 0.505 M aqueous Na_2SO_4. Hydrogel not formed at 5 mg/mL.

Amplitude sweep data

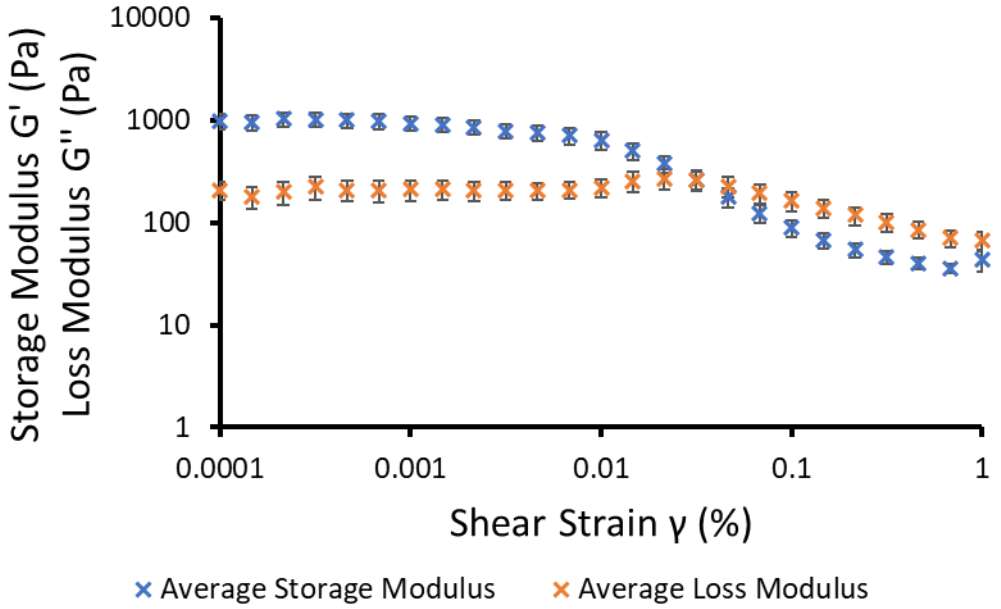

Figure S98 - Graph showing average results (n=3) from amplitude sweep experiments used to define the linear viscoelastic region of the sample at 298 K. SSA **7** (5 mg) in 1 mL of aqueous NaCl solution (0.505 M) (1 = 100 %). Error = standard deviation of the mean.

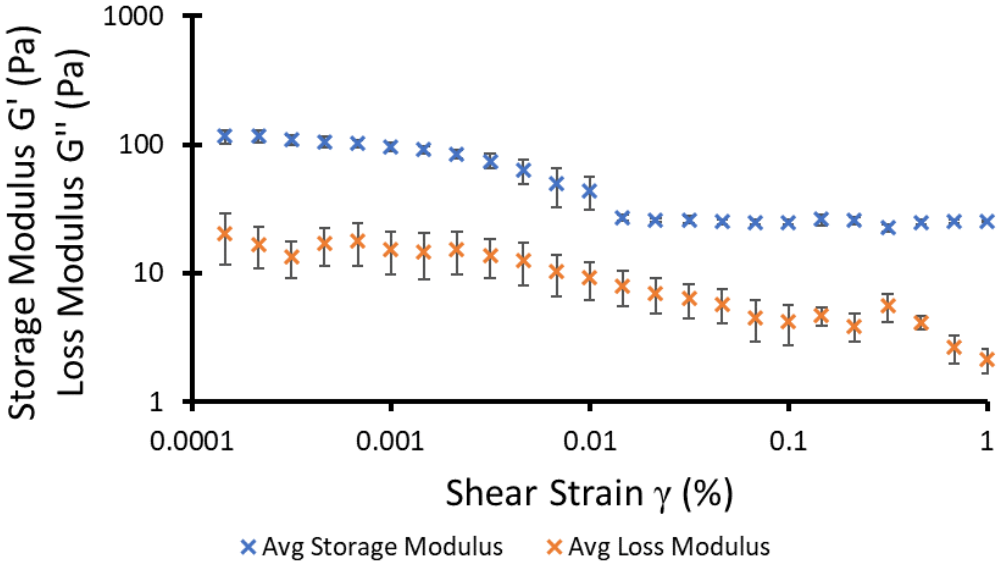

Figure S99 - Graph showing average results (n=3) from amplitude sweep experiments used to define the linear viscoelastic region of the sample at 298 K. SSA **7** (5 mg) in 1 mL of aqueous $NaNO_3$ solution (0.505 M) (1 = 100 %). Error = standard deviation of the mean.

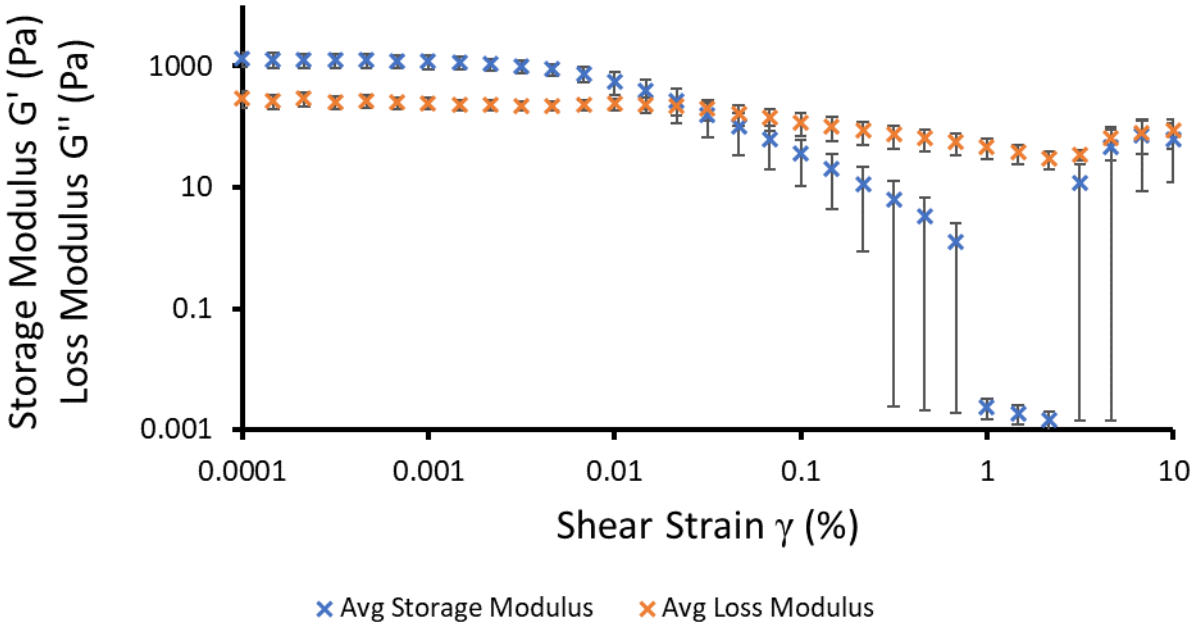

Figure S100 - Graph showing average results (n=3) from amplitude sweep experiments used to define the linear viscoelastic region of the sample at 298 K. SSA **7** (5 mg) in 1 mL of aqueous $NaNO_3$ solution (0.505 M) (10 = 1000 %). Error = standard deviation of the mean.

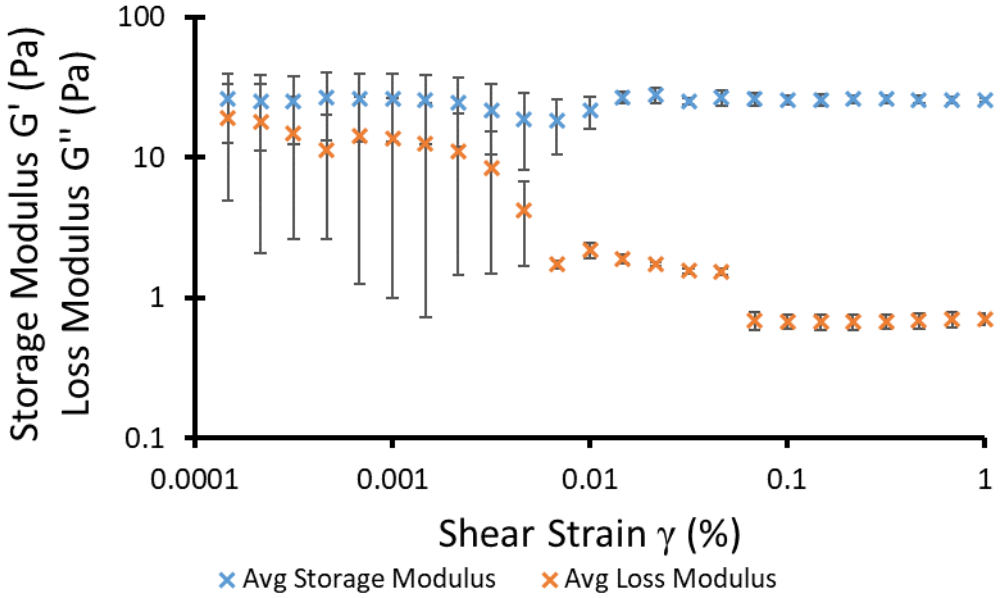

Figure S101 - Graph showing average results (n=3) from amplitude sweep experiments used to define the linear viscoelastic region of the sample at 298 K. SSA **7** (5 mg) in 1 mL of aqueous NaOBz solution (0.505 M) (1 = 100 %). Error = standard deviation of the mean.

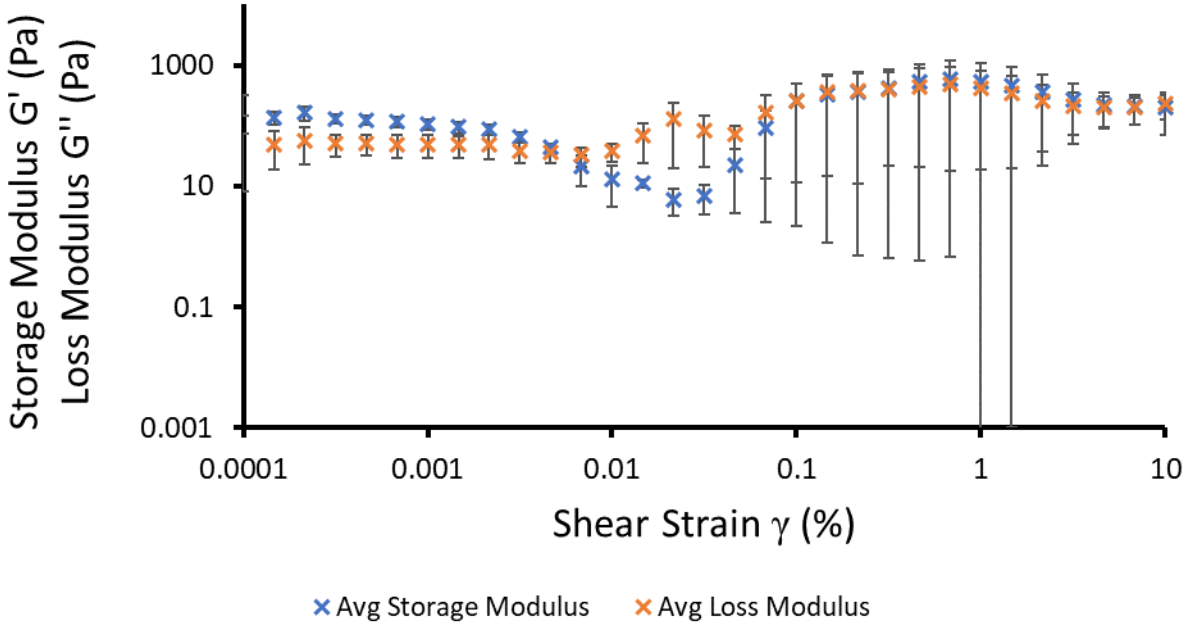

Figure S102 - Graph showing average results (n=3) from amplitude sweep experiments used to define the linear viscoelastic region of the sample at 298 K. SSA **7** (5 mg) in 1 mL of aqueous NaOBz solution (0.505 M) (10 = 1000 %). Error = standard deviation of the mean.

Frequency sweep data

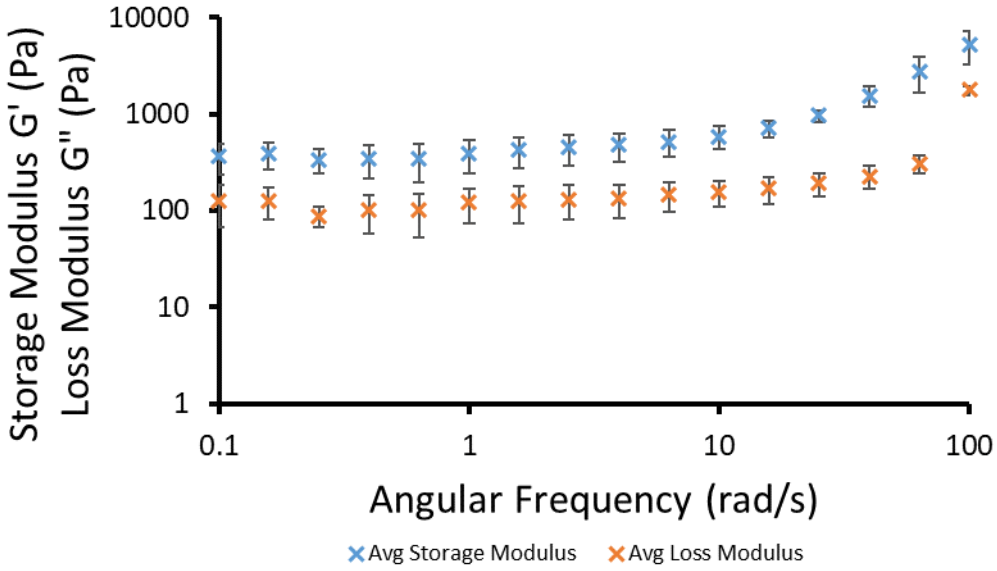

Figure S103 - Graph showing average results (n=3) from frequency sweep experiments obtained from the linear viscoelastic region under a constant shear strain (γ) of 0.0277 % (298 K). SSA **7** (5 mg) in 1 mL of aqueous NaCl solution (0.505 M). Error = standard deviation of the mean.

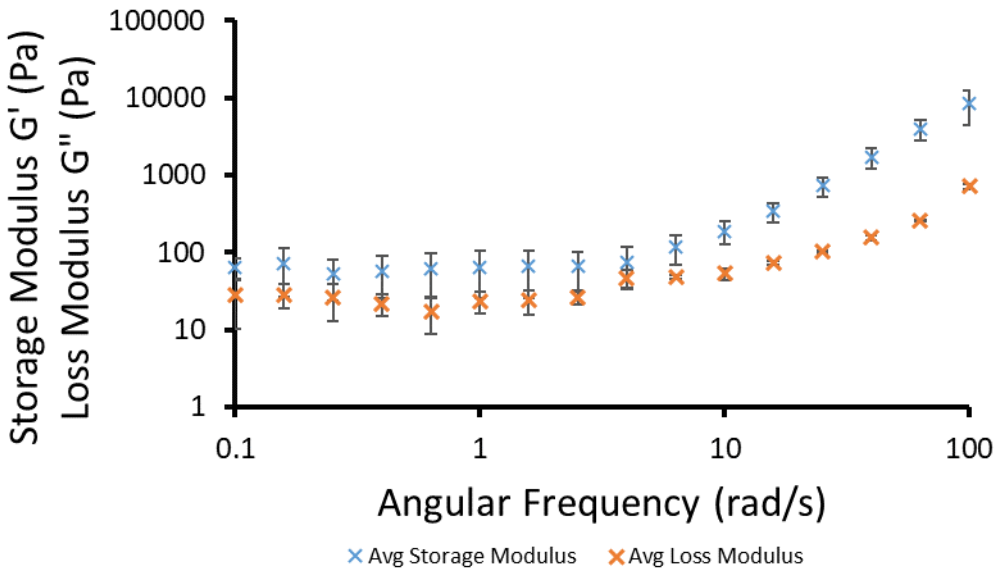

Figure S104 - Graph showing average results (n=3) from frequency sweep experiments obtained from the linear viscoelastic region under a constant shear strain (γ) of 0.0195 % (298 K). SSA **7** (5 mg) in 1 mL of aqueous $NaNO_3$ solution (0.505 M). Error = standard deviation of the mean.

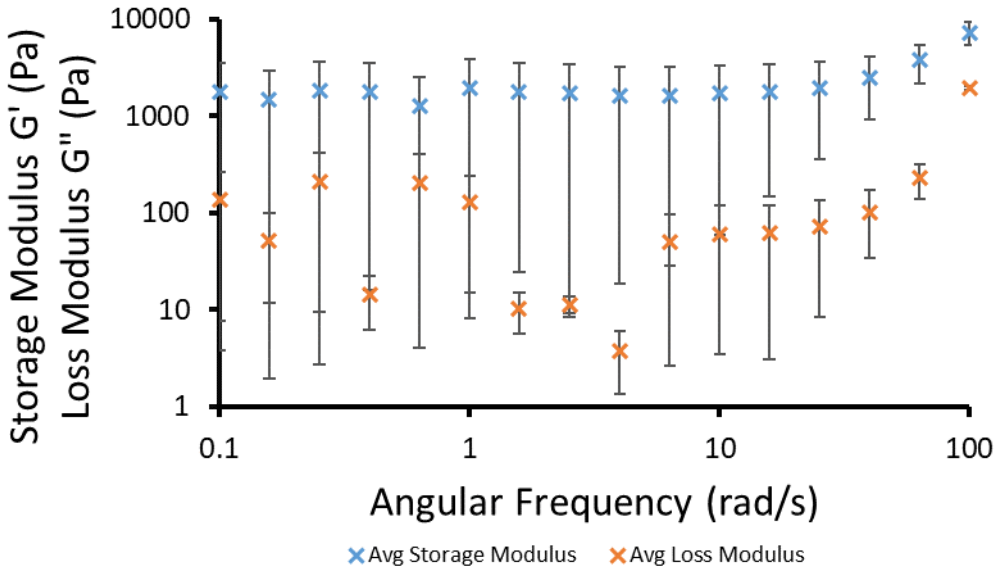

Figure S105 - Graph showing average results (n=3) from frequency sweep experiments obtained from the linear viscoelastic region under a constant shear strain (γ) of 0.0720 % (298 K). SSA **7** (5 mg) in 1 mL of aqueous NaOBz solution (0.505 M). Error = standard deviation of the mean.

Section 14: Widefield fluorescence microscopy data

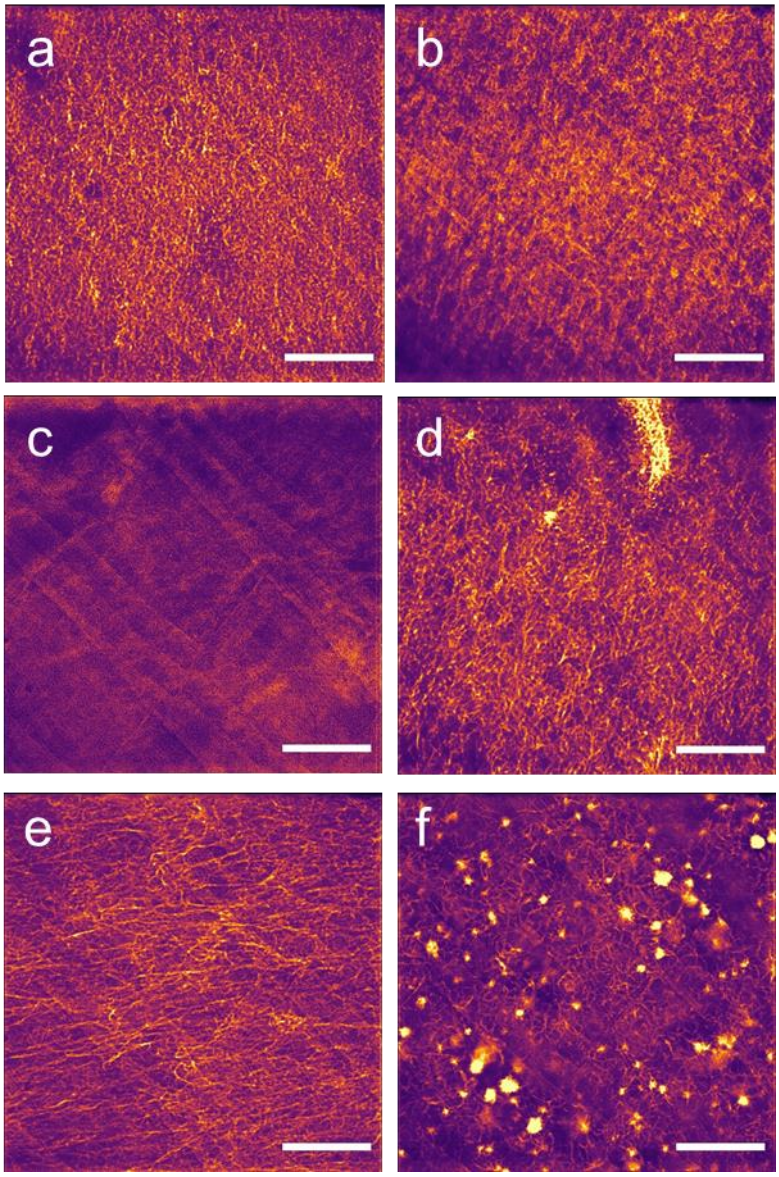

Figure S106 - Fluorescent microscopy image of **2** (5 mg/mL) in a) NaCl, b) KCl, c) $NaNO_3$, d) NaH_2PO_4, e) NaOBz, f) Na_2SO_4 at 0.505 M. Scale bar = 120 μm.

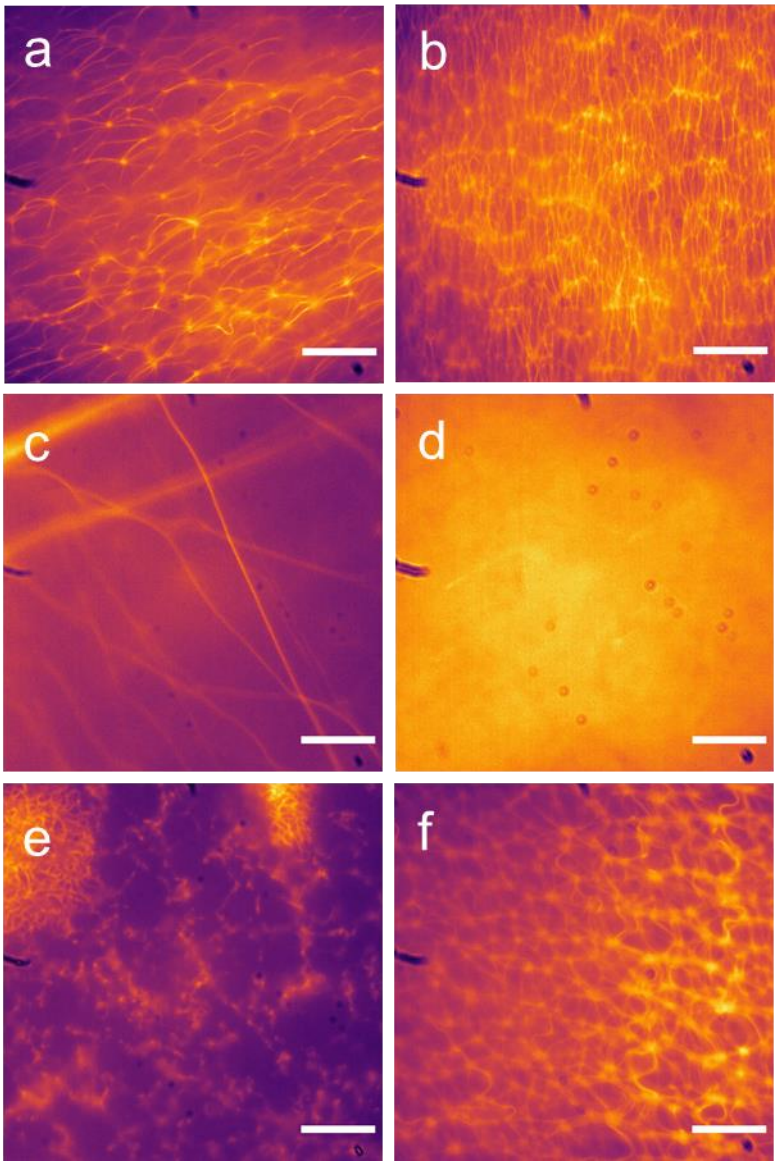

Figure S107 - Fluorescent microscopy image of **3** (5 mg/mL) in a) NaCl, b) KCl, c) $NaNO_3$, d) NaH_2PO_4, e) NaOBz, f) Na_2SO_4 at 0.505 M. Scale bar = 20 µm.

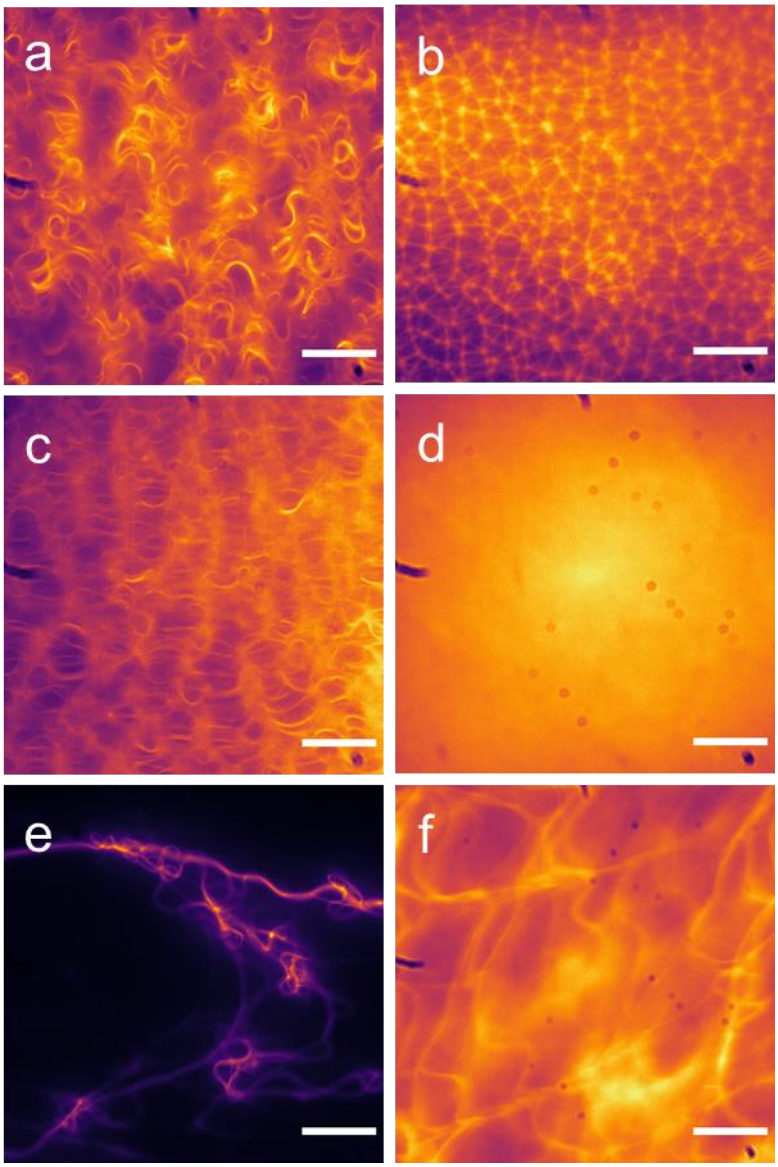

Figure S108 - Fluorescent microscopy image of **4** (5 mg/mL) in a) NaCl, b) KCl, c) $NaNO_3$, d) NaH_2PO_4, e) Na_2SO_4, f) NaOBz at 0.505 M. Scale bar = 20 μm.

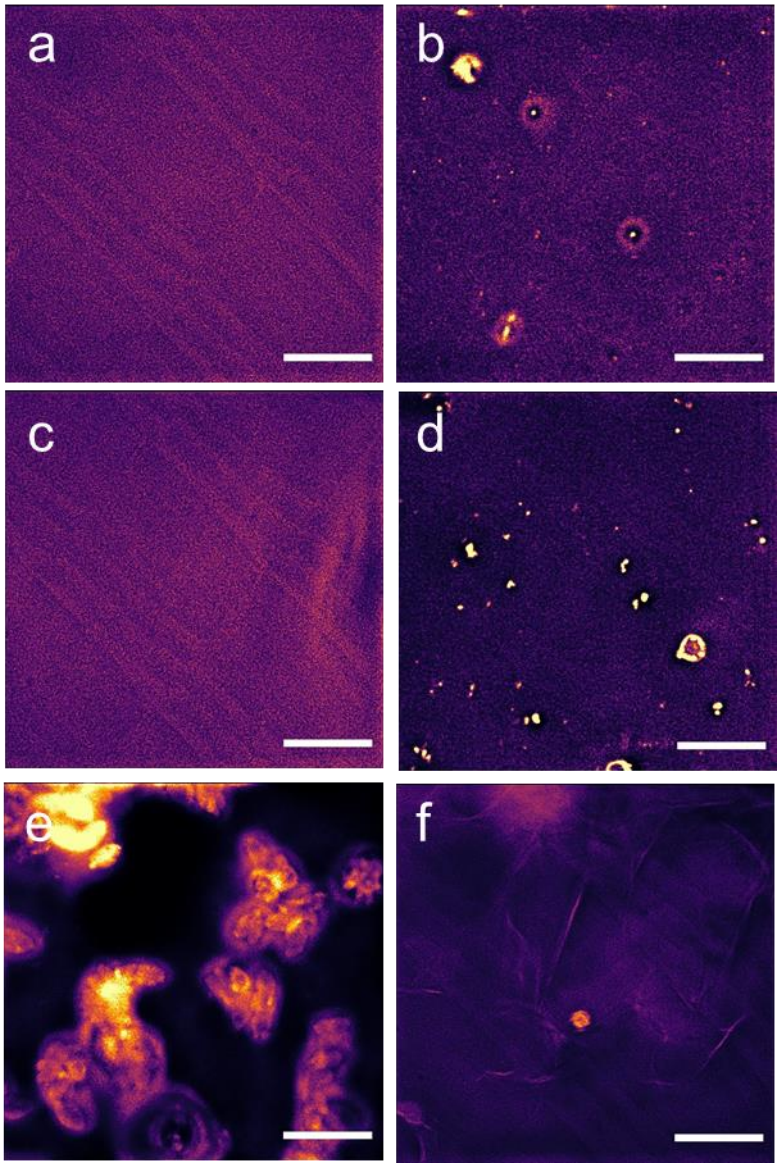

Figure S109 - Fluorescent microscopy image of **5** (5 mg/mL) in a) NaCl, b) KCl, c) $NaNO_3$, d) NaH_2PO_4, e) NaOBz, f) Na_2SO_4 at 0.505 M. Scale bar = 120 μm.

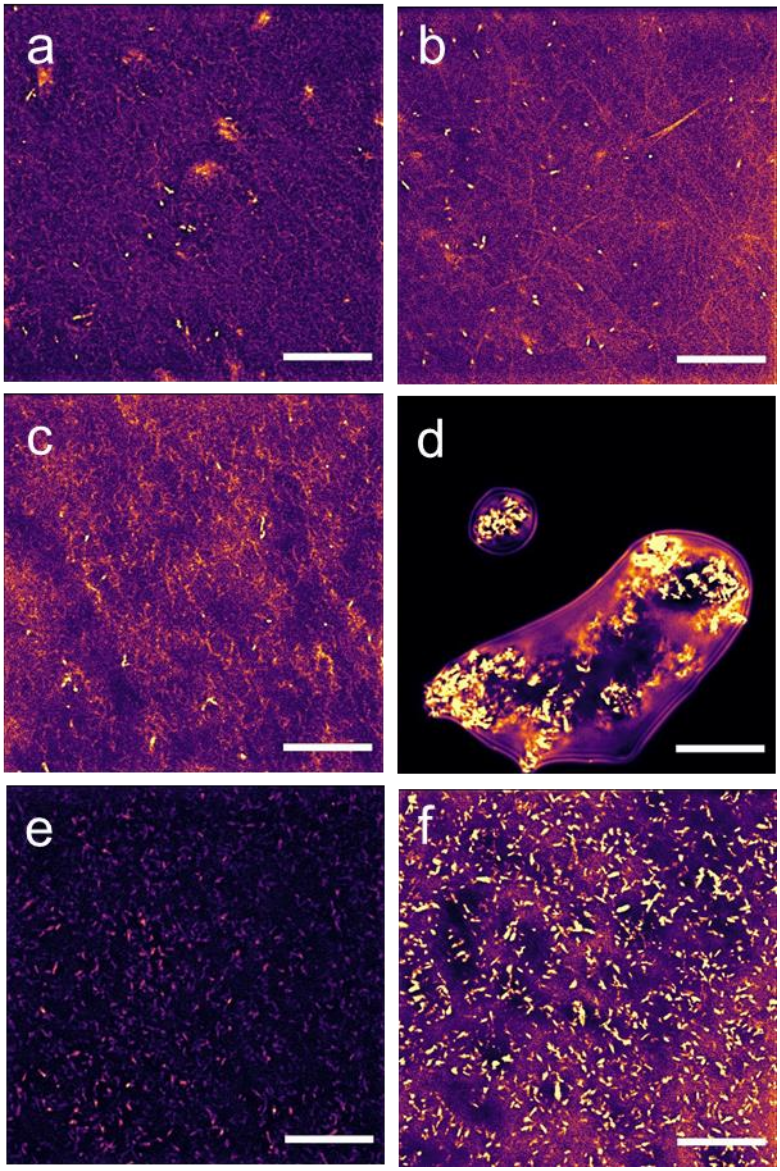

Figure S110 - Fluorescent microscopy image of **6** (5 mg/mL) in a) NaCl, b) KCl, c) $NaNO_3$, d) NaH_2PO_4, e) NaOBz, f) Na_2SO_4 at 0.505 M. Scale bar = 120 μm.

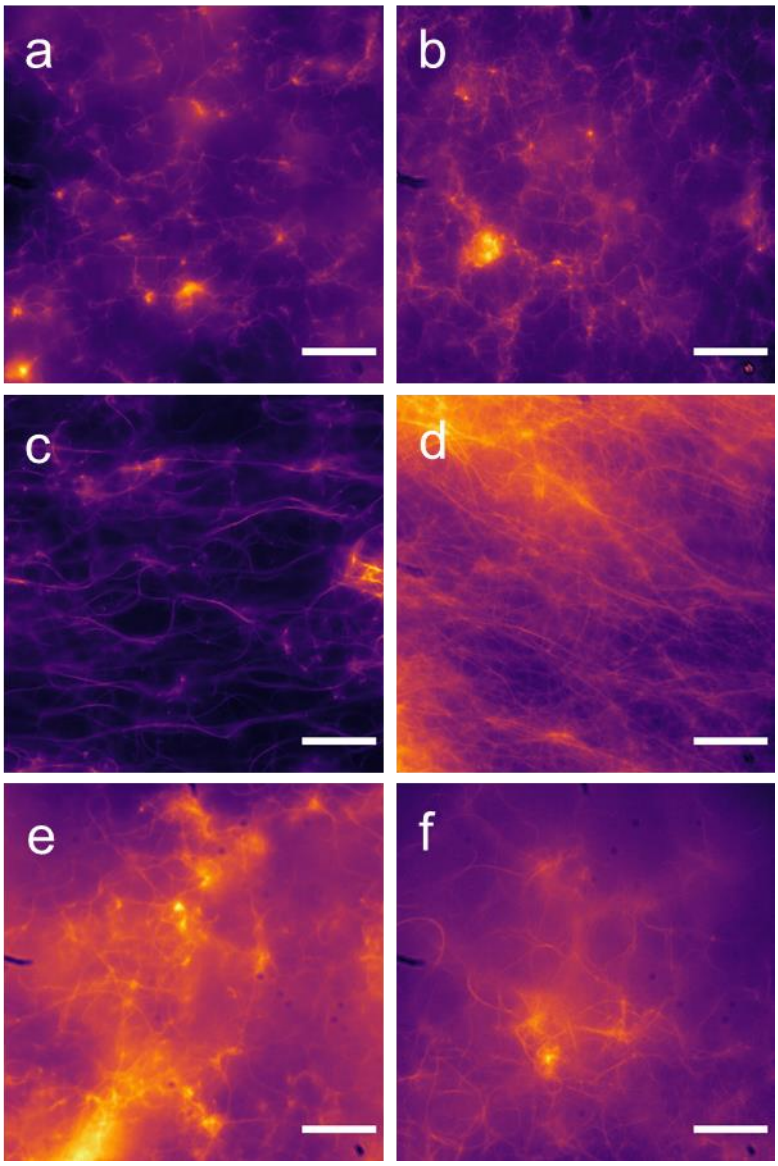

Figure S111 - Fluorescent microscopy image of **7** (5 mg/mL) in a) NaCl, b) KCl, c) $NaNO_3$, d) NaH_2PO_4, e) NaOBz, f) Na_2SO_4 at 0.505 M. Scale bar = 20 μm.

Quantitation of gel fibres

Table S20 - Observed gel fibres formed in various salt solutions. Strand formation of the final gel was defined by the following properties: straight (ST), curled (CL), crosslinked (LK), independent (IN), short (SH), long (LG), densely packed (DP), medium packing density (MP), low packing density (LP), uniform arrangement (UF), stochastic arrangement (SC), unidirectional strands (UD), multidirectional strands (MD).

		ST	CL	LK	IN	SH	LG	DP	MP	LP	UF	SC	UD	MD
1	NaCl													
	KCl													
	$NaNO_3$													
	NaH_2PO_4													
	NaOBz													
	Na_2SO_4													
2	NaCl													
	KCl													
	$NaNO_3$													
	NaH_2PO_4													
	NaOBz													
	Na_2SO_4													
3	NaCl													
	KCl													
	$NaNO_3$						b							
	NaH_2PO_4													
	NaOBz						a							
	Na_2SO_4													
4	NaCl													
	KCl													
	$NaNO_3$													
	NaH_2PO_4													
	NaOBz													
	Na_2SO_4						b							
5	NaCl													
	KCl													
	$NaNO_3$													
	NaH_2PO_4													
	NaOBz													
	Na_2SO_4													
6	NaCl													
	KCl													
	$NaNO_3$													
	NaH_2PO_4													
	NaOBz													
	Na_2SO_4													
7	NaCl													
	KCl													
	$NaNO_3$													
	NaH_2PO_4						a							
	NaOBz													
	Na_2SO_4						b							

	No gel present
	Structure not present
	Structure present

a – Larger than field of view.
b – Unable to discern individual fibres.

Section 15: Hydrogel antimicrobial efficacy experiment data

Figure S112 – 1 % agarose gel loaded with H_2O on the surface of agar inoculated with MRSA USA300 and incubated at 37 °C for 18 hours.

Figure S113 – 1 % agarose gel loaded with NaCl (0.505 M) on the surface of agar inoculated with MRSA USA300 and incubated at 37 °C for 18 hours.

Figure S114 – 1 % agarose gel loaded with NaCl (0.505 M) and oxacillin (8 mM) on the surface of agar inoculated with MRSA USA300 and incubated at 37 °C for 18 hours.

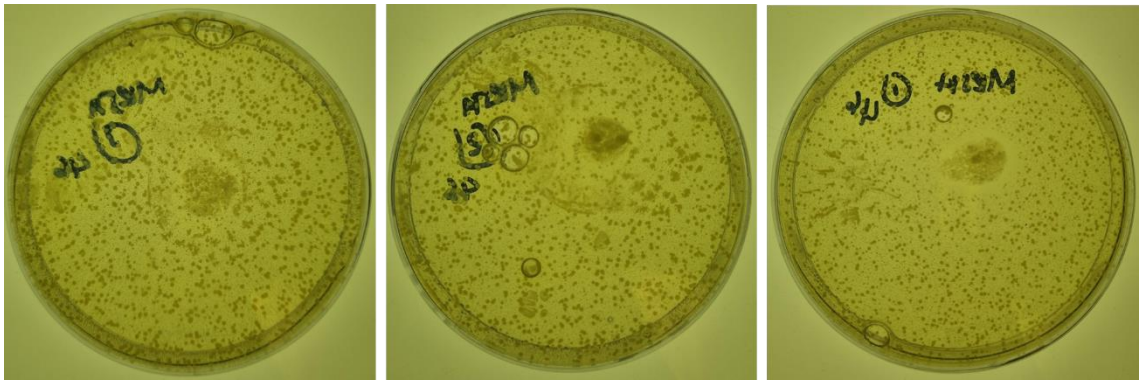

Figure S115 – Hydrogel of **7** (5 mg/mL) in NaCl (0.505 M) on the surface of agar inoculated with MRSA USA300 and incubated at 37 °C for 18 hours.

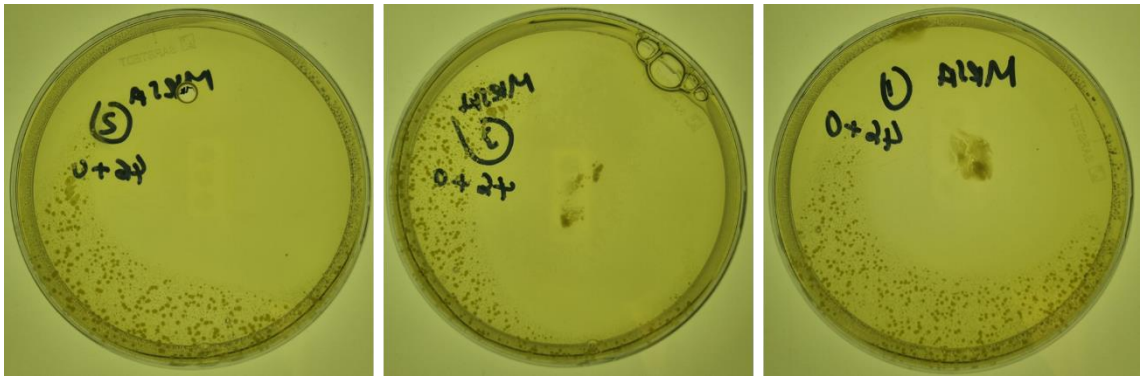

Figure S116 – Hydrogel of **7** (5 mg/mL) in NaCl (0.505 M) co-formulated with oxacillin (8 mM) on the surface of agar inoculated with MRSA USA300 and incubated at 37 °C for 18 hours.

Section 16: Porcine skin experiment data

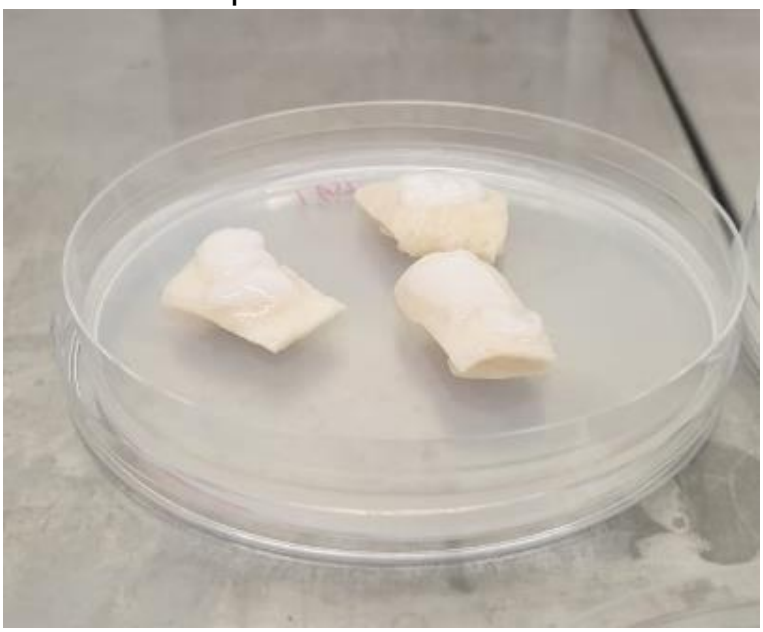

Figure S117 – NaCl (0.505 M) hydrogel of SSA **2** (5 mg/mL) on the surface of MRSA USA300 inoculated porcine skin on the top of an agar plate.

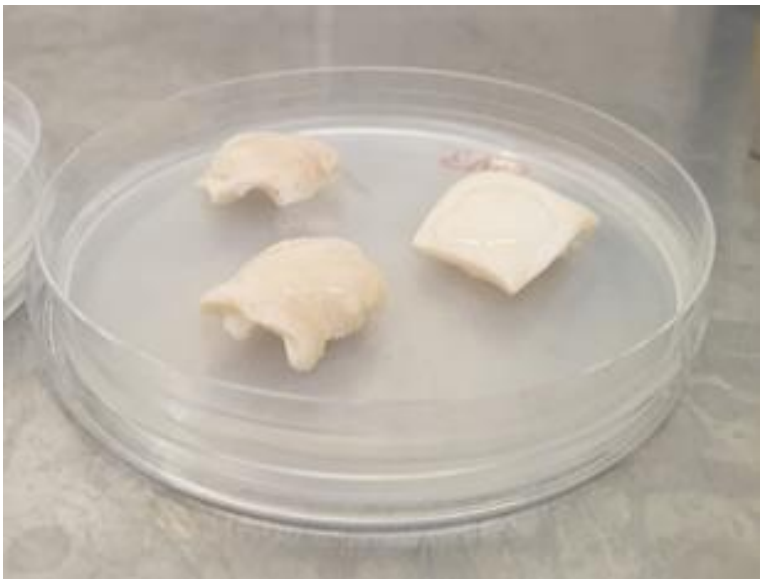

Figure S118 – NaCl (0.505 M) hydrogel of SSA **3** (5 mg/mL) on the surface of MRSA USA300 inoculated porcine skin on the top of an agar plate.

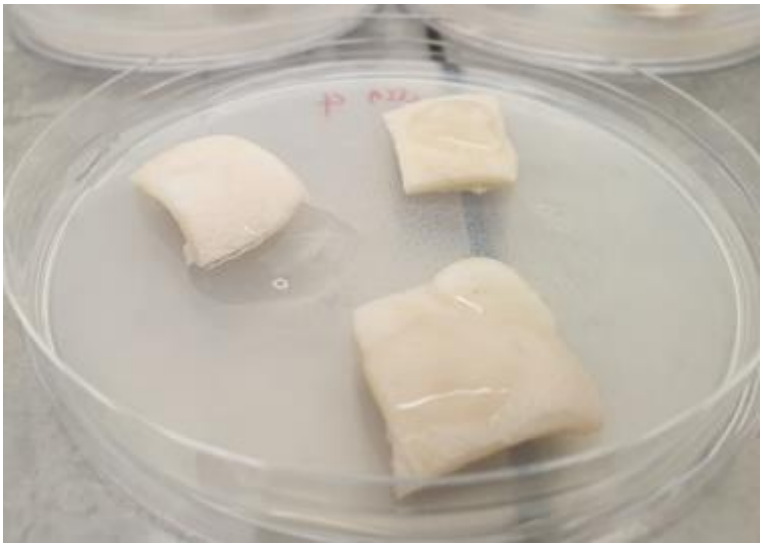

Figure S119 – NaCl (0.505 M) hydrogel of SSA **4** (5 mg/mL) on the surface of MRSA USA300 inoculated porcine skin on the top of an agar plate.

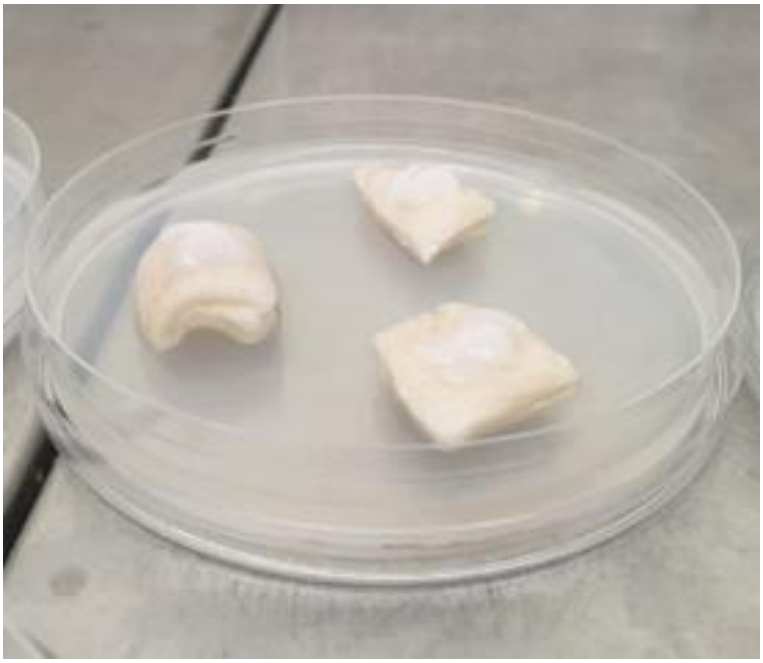

Figure S120 – NaCl (0.505 M) hydrogel of SSA **7** (5 mg/mL) on the surface of MRSA USA300 inoculated porcine skin on the top of an agar plate.

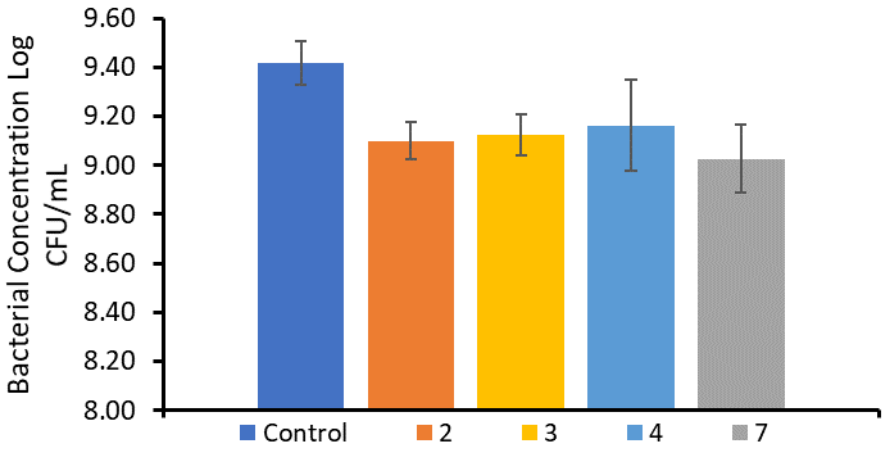

Figure S121 – MRSA USA300 colony forming units/mL after 18 hours incubation with gels.

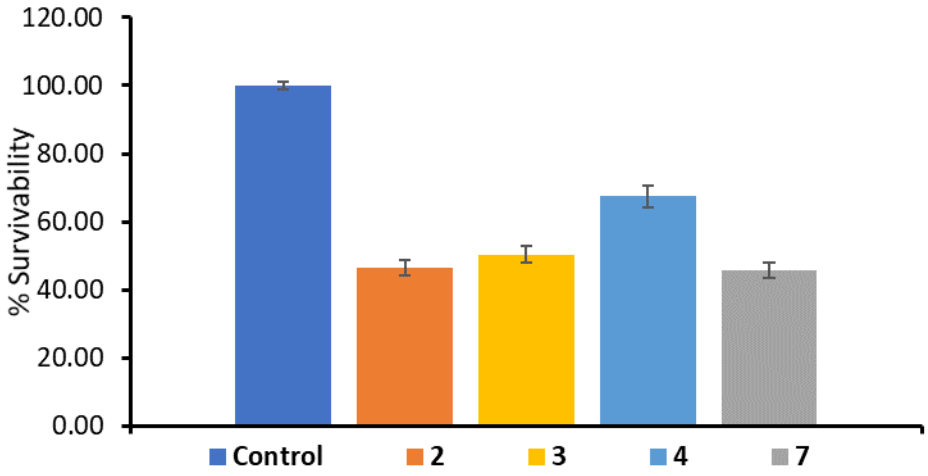

Figure S122 – Percentage survivability of MRSA USA300 after 18 hours incubation with gels.

Section 17: *C. elegans* data

Effect of SSAs on *C. elegans* food source

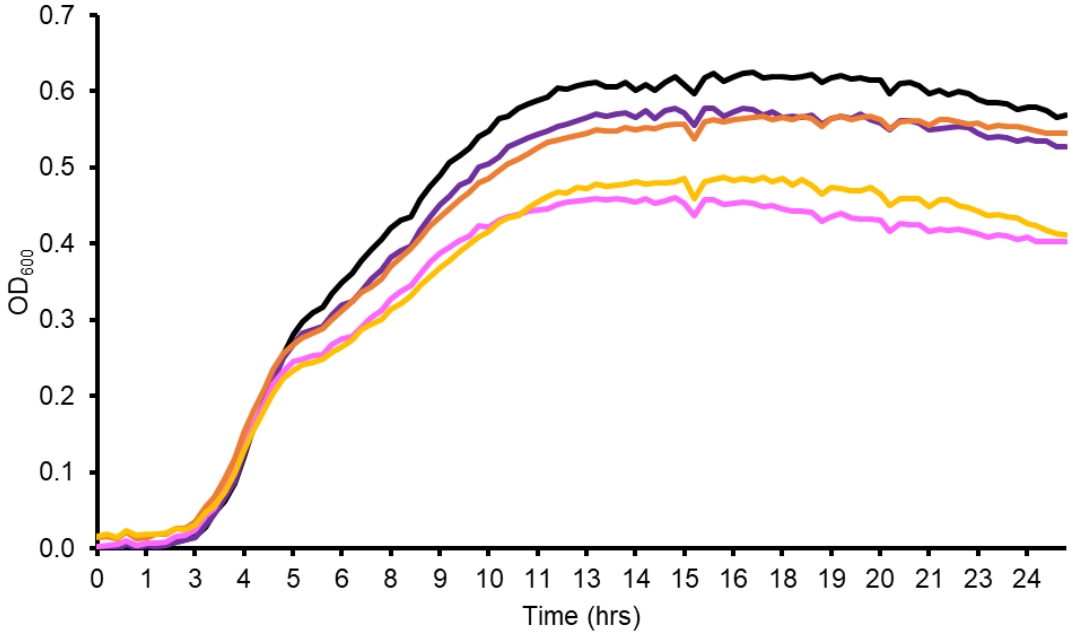

Figure S123 – Effect of **1** on *E. coli* OP50. Black = OP50, purple = **1** 0.1 mM, pink = **1** 0.2 mM, orange = 0.1 % EtOH, yellow = 0.2 % EtOH.

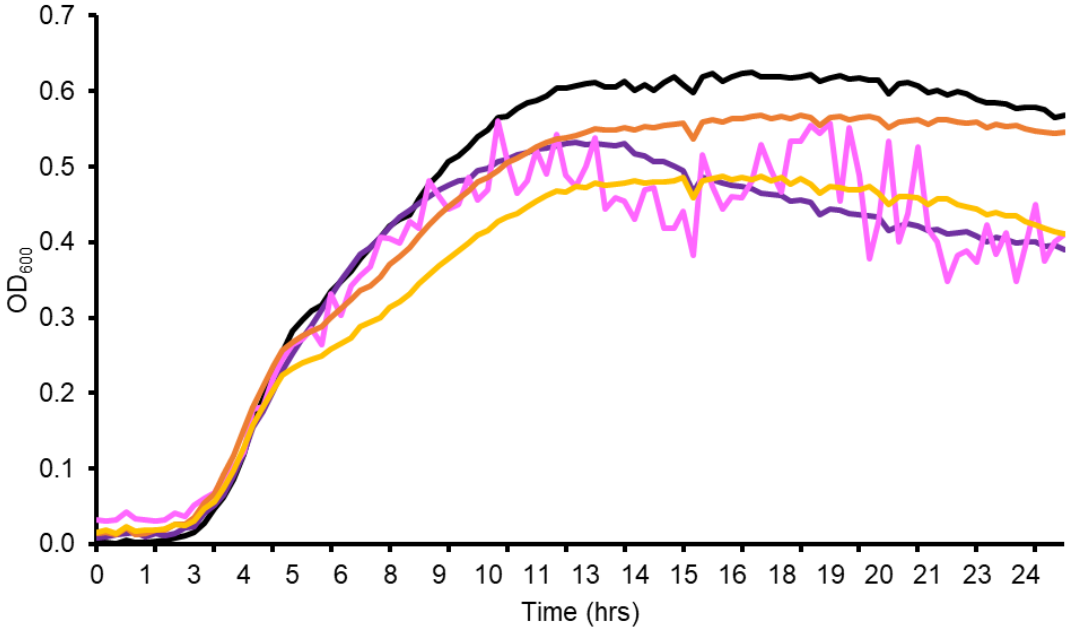

Figure S124 – Effect of **2** on *E. coli* OP50. Black = OP50, purple = **2** 0.1 mM, pink = **2** 0.2 mM, orange = 0.1 % EtOH, yellow = 0.2 % EtOH.

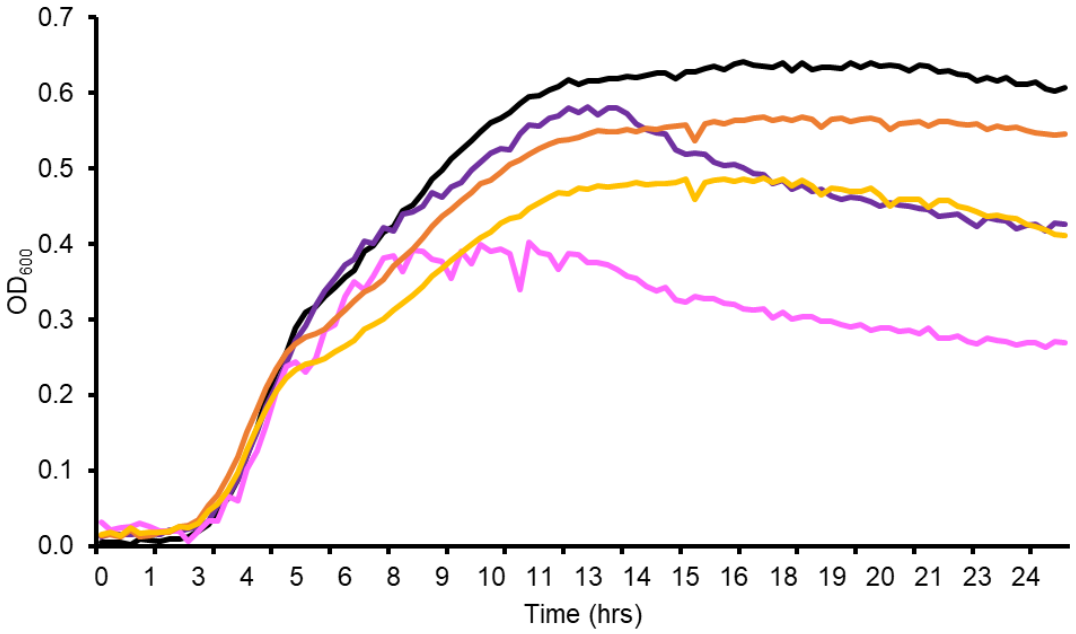

Figure S125 – Effect of **3** on *E. coli* OP50. Black = OP50, purple = **3** 0.1 mM, pink = **3** 0.2 mM, orange = 0.1 % EtOH, yellow = 0.2 % EtOH

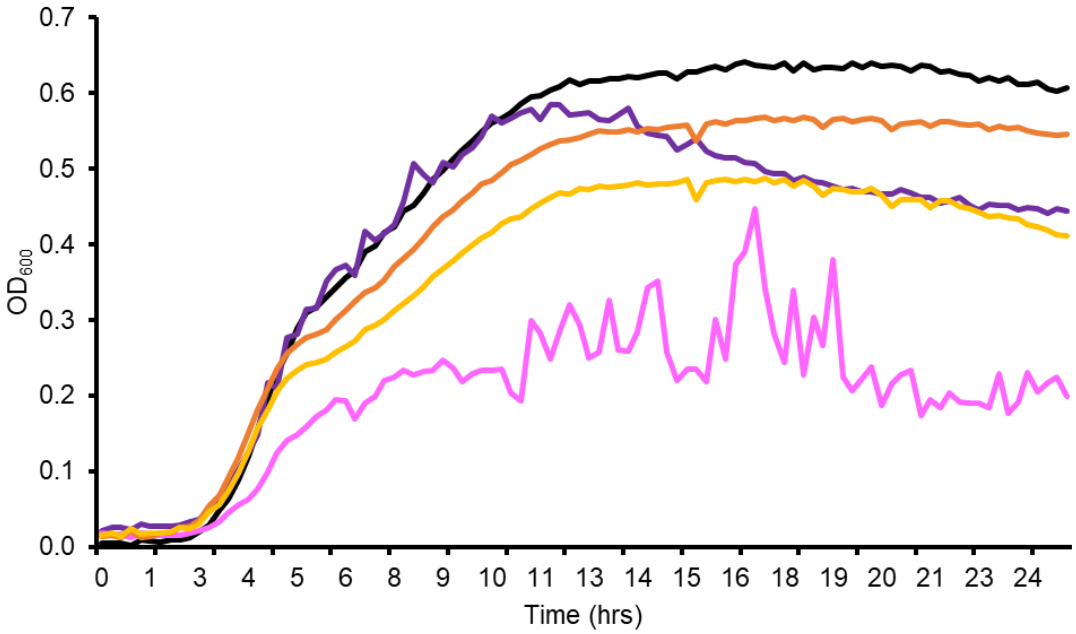

Figure S126 – Effect of **4** on *E. coli* OP50. Black = OP50, purple = **4** 0.1 mM, pink = **4** 0.2 mM, orange = 0.1 % EtOH, yellow = 0.2 % EtOH.

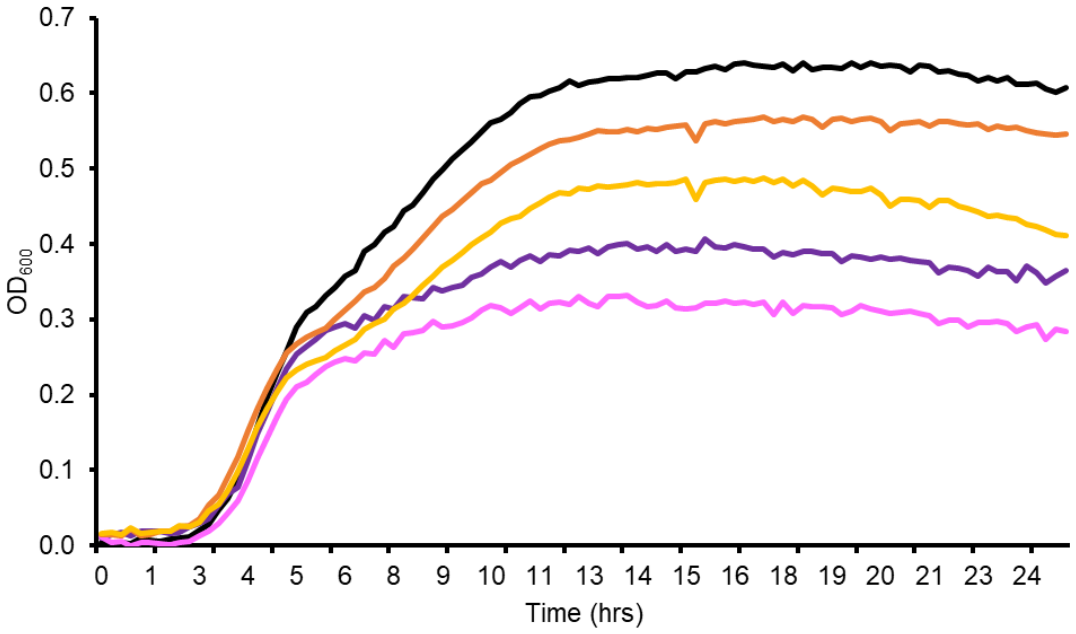

Figure S127 – Effect of **5** on *E. coli* OP50. Black = OP50, purple = **5** 0.1 mM, pink = **5** 0.2 mM, orange = 0.1 % EtOH, yellow = 0.2 % EtOH.

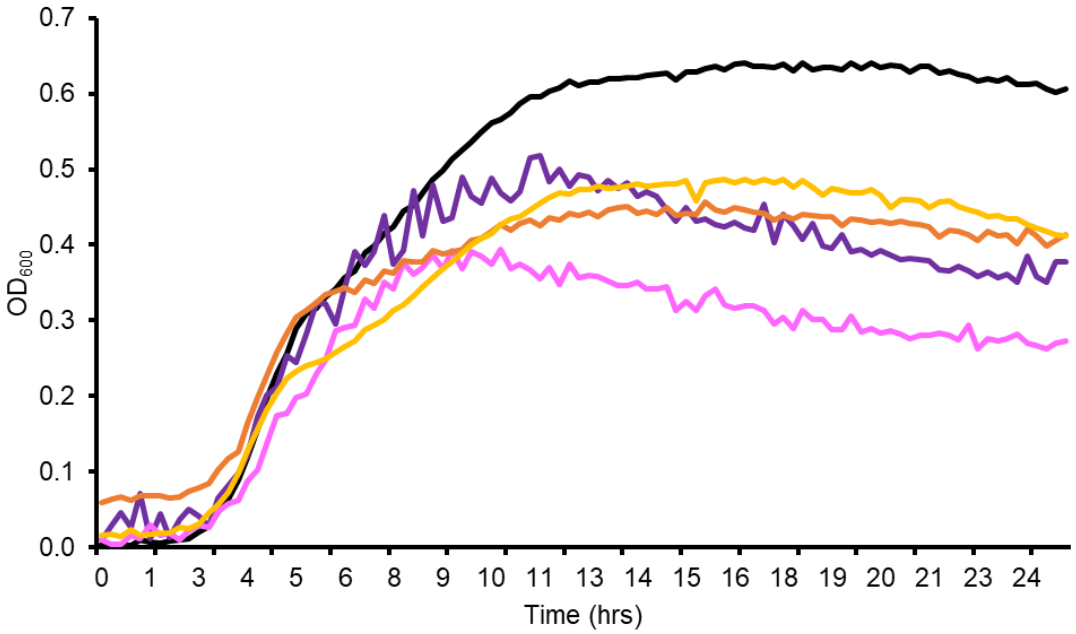

Figure S128 – Effect of **6** on *E. coli* OP50. Black = OP50, purple = **6** 0.1 mM, pink = **6** 0.2 mM, orange = 0.1 % EtOH, yellow = 0.2 % EtOH.

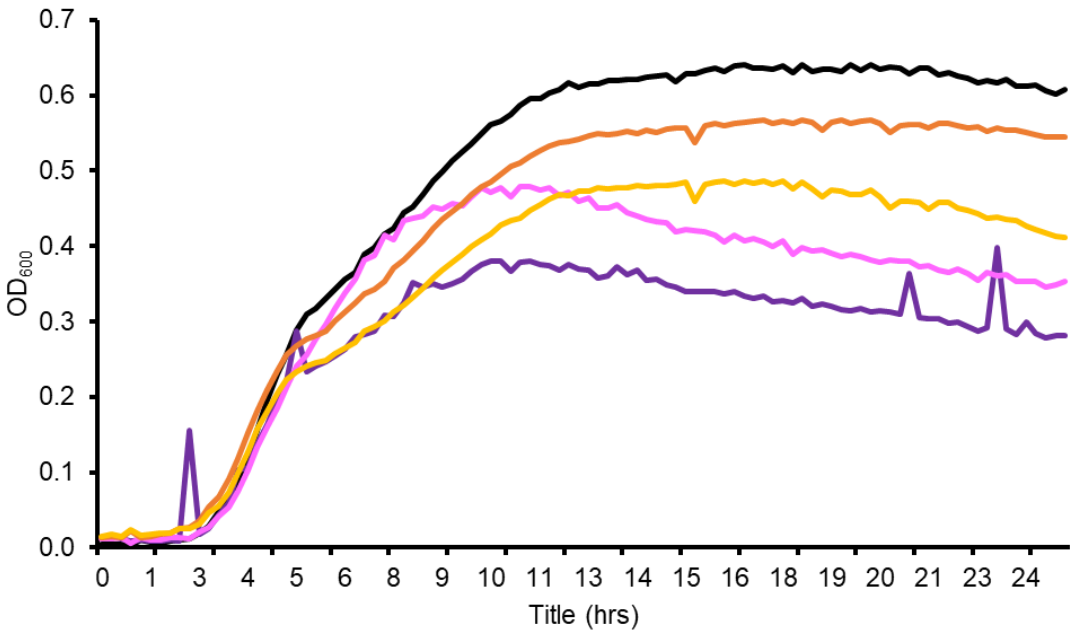

Figure S129 – Effect of **7** on *E. coli* OP50. Black = OP50, purple = **7** 0.1 mM, pink = **7** 0.2 mM, orange = 0.1 % EtOH, yellow = 0.2 % EtOH.

Effect of SSAs on *C. elegans* development

Table S21 – Effect of SSAs on development of *C. elegans* GLO-1 mutant. Error = standard deviation.

	Control	**4**	**6**
L3	0.637 ± 0.1	0.681 ± 0.1	0.647 ± 0.1
L4	0.363 ± 0.1	0.319 ± 0.1	0.353 ± 0.1

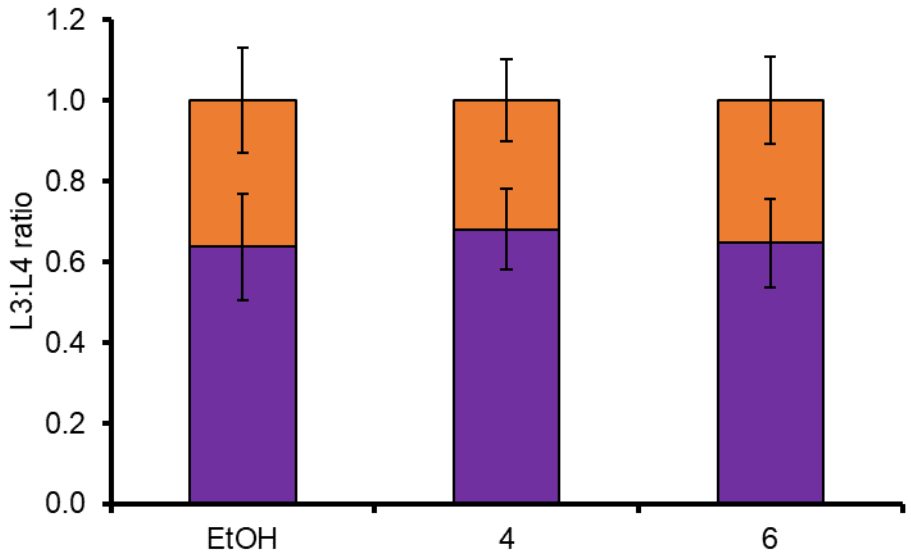

Figure S130 – Effect of SSAs on development of *C. elegans* GLO-1 mutant. Purple = L3 life stage, orange = L4 life stage. Error = standard deviation.

Effect of SSAs on *C. elegans* brood size

Table S22 – Overview of brood size assay against lab strain N2 *Caenorhabditis elegans* (*C. elegans*) and knock out mutant GLO-1 *C. elegans* against OP50 *E. coli* only and OP50 *E. coli* with 5 % ethanol in H_2O. Error = standard deviation.

	OP50		**Control**	
	Brood size	**Error**	**Brood size**	**Error**
N2	249.53	14.88	205.07	13.15
GLO-1	216.53	11.46	189.20	18.12

Table S23 – Overview of brood size of knock out mutant GLO-1 *C. elegans* against **4** and **6**. Error = standard deviation.

	Brood size	**Error**
4	168.86	9.69
6	156.33	9.21
Control	164.25	7.52

It is noted that the GLO-1 mutant has a lower brood size than N2 wild type *C. elegans*, and the addition of ethanol causes a further reduction in brood size in both N2[13] and GLO-1 mutant *C. elegans*.

C. elegans microscopy

C. elegans worms fed on solid plates of OP50 *E. coli* supplemented with SSA at a final concentration of 0.10 mM, grown from egg to adult. Images taken of day 1 young adult worms.

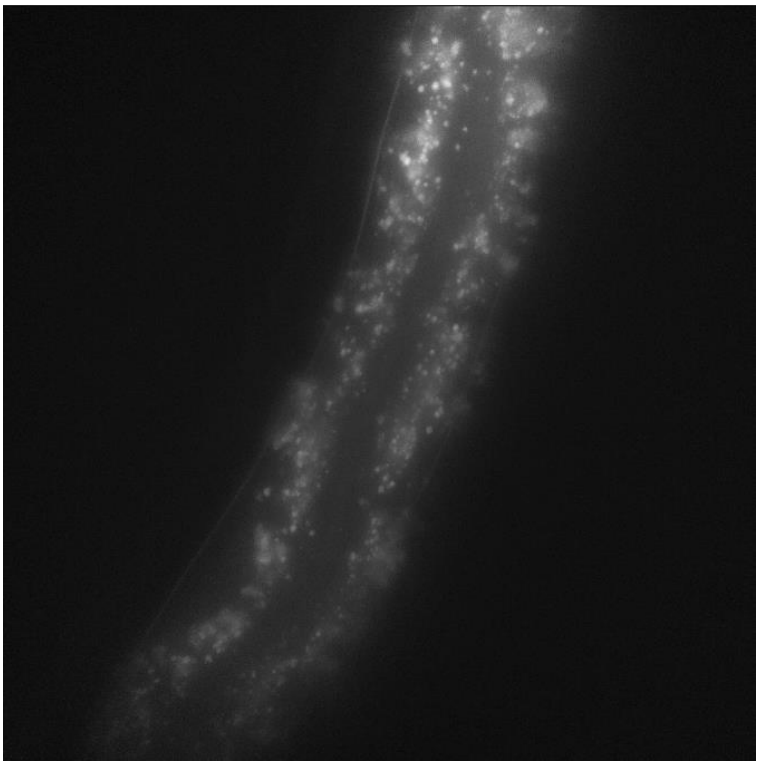

Figure S131 – Fluorescent microscopy image of *C. elegans* GLO-1 mutant supplemented with 0.1 % EtOH. Image taken with 200 ms exposure time.

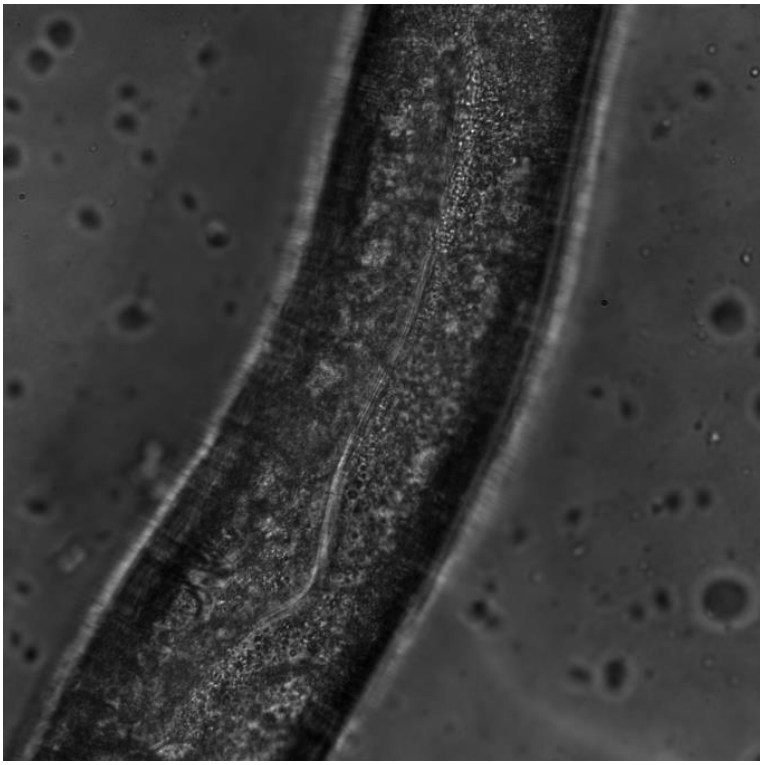

Figure S132 – Brightfield microscopy image of *C. elegans* GLO-1 mutant supplemented with 0.1 % EtOH. Image taken with 200 ms exposure time.

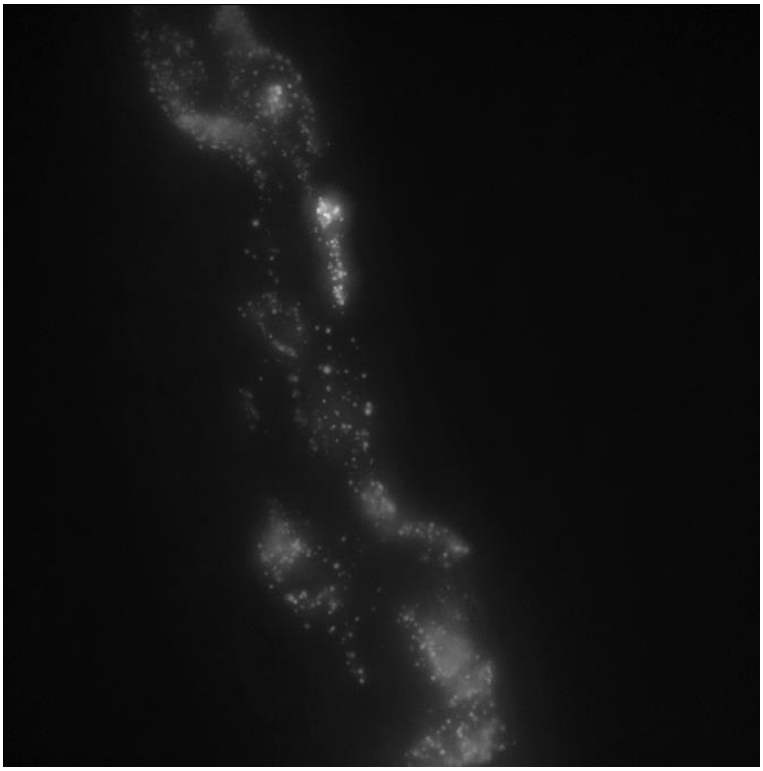

Figure S133 – Fluorescence microscopy image of *C. elegans* GLO-1 mutant supplemented with **1** at 0.10 mM in 5 % EtOH. Image taken with 200 ms exposure time.

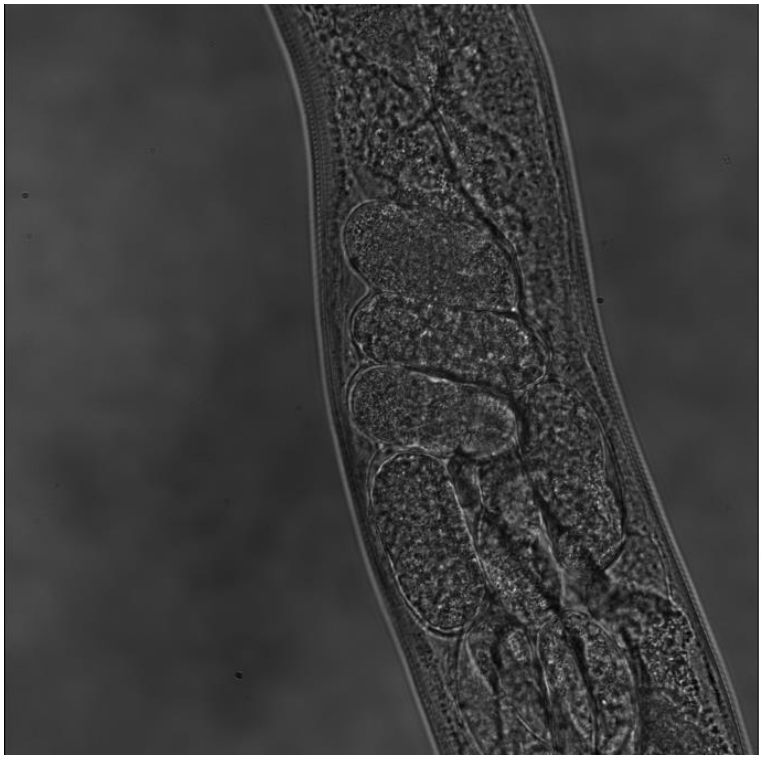

Figure S134 – Brightfield microscopy image of *C. elegans* GLO-1 mutant supplemented with **1** at 0.10 mM in 5 % EtOH. Image taken with 200 ms exposure time.

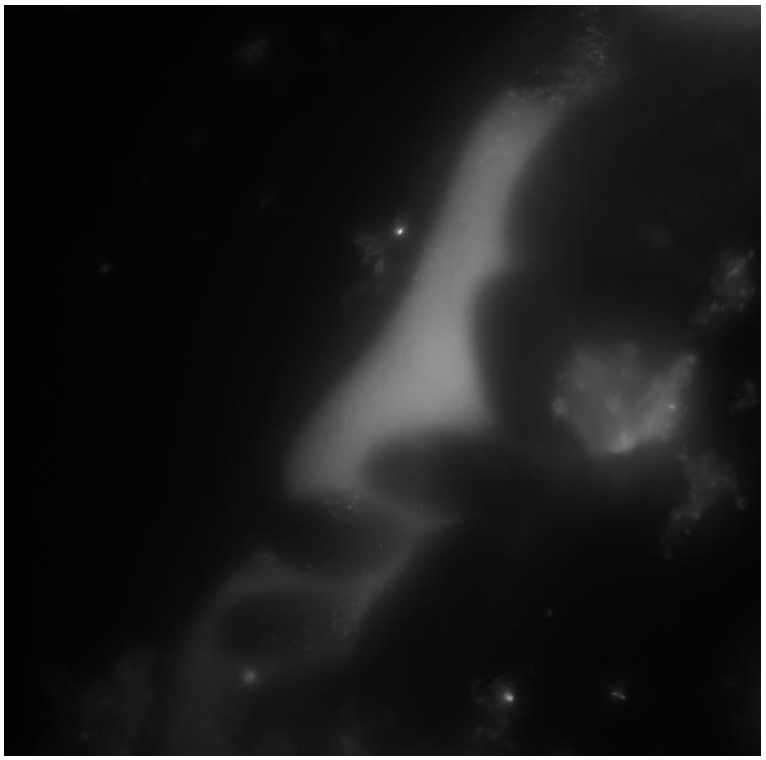

Figure S135 – Fluorescence microscopy image of *C. elegans* GLO-1 mutant supplemented with **2** at 0.10 mM in 5 % EtOH. Image taken with 200 ms exposure time.

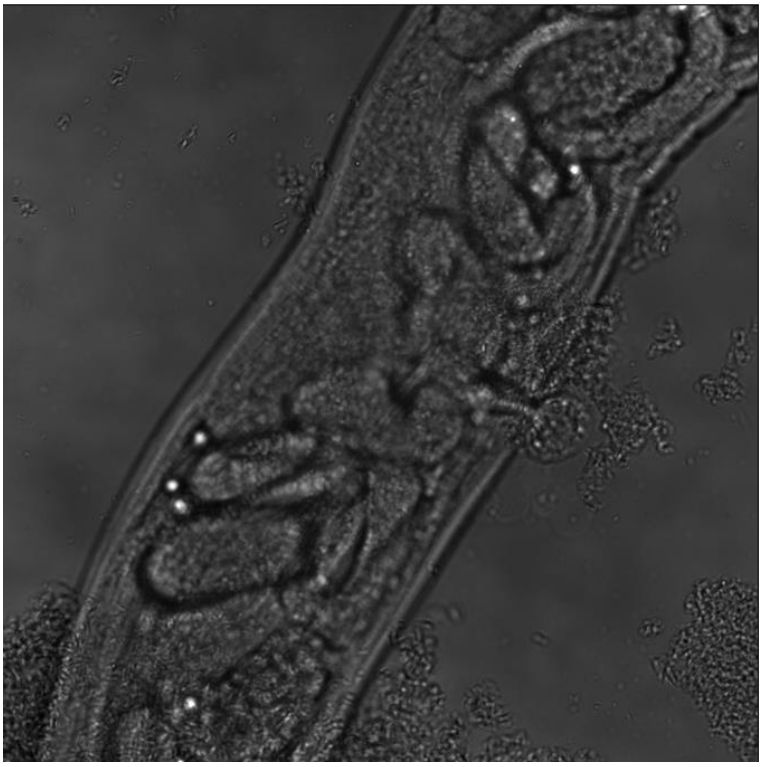

Figure S136 – Brightfield microscopy image of *C. elegans* GLO-1 mutant supplemented with **2** at 0.10 mM in 5 % EtOH. Image taken with 200 ms exposure time.

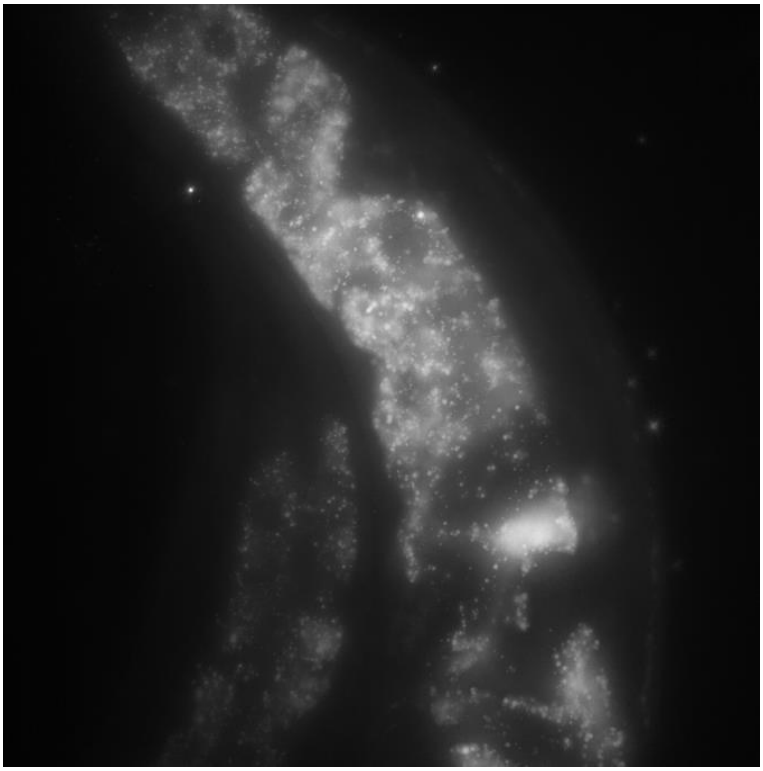

Figure S137 – Fluorescence microscopy image of *C. elegans* GLO-1 mutant supplemented with **3** at 0.10 mM in 5 % EtOH. Image taken with 200 ms exposure time.

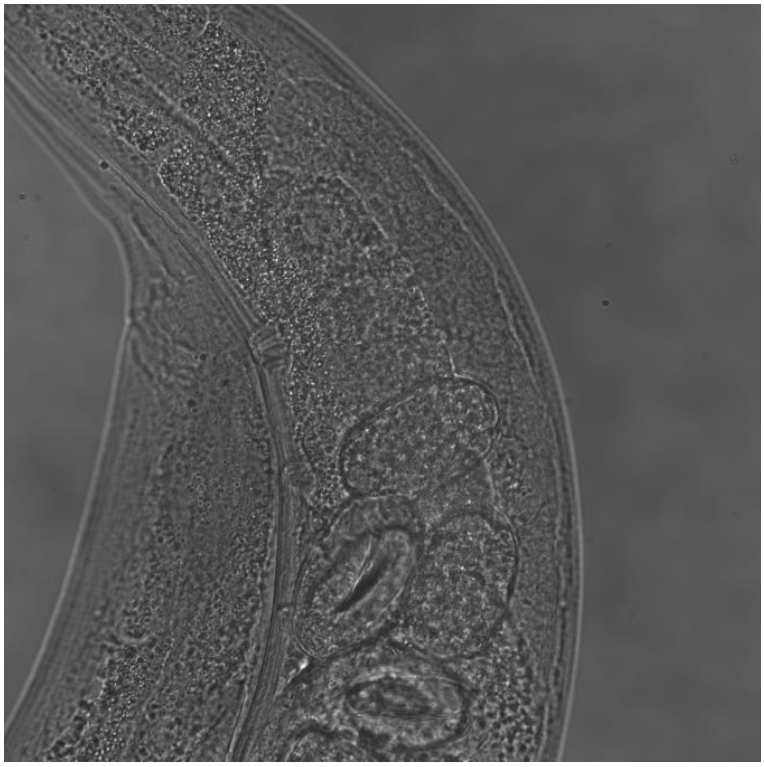

Figure S138 – Brightfield microscopy image of *C. elegans* GLO-1 mutant supplemented with **3** at 0.10 mM in 5 % EtOH. Image taken with 200 ms exposure time.

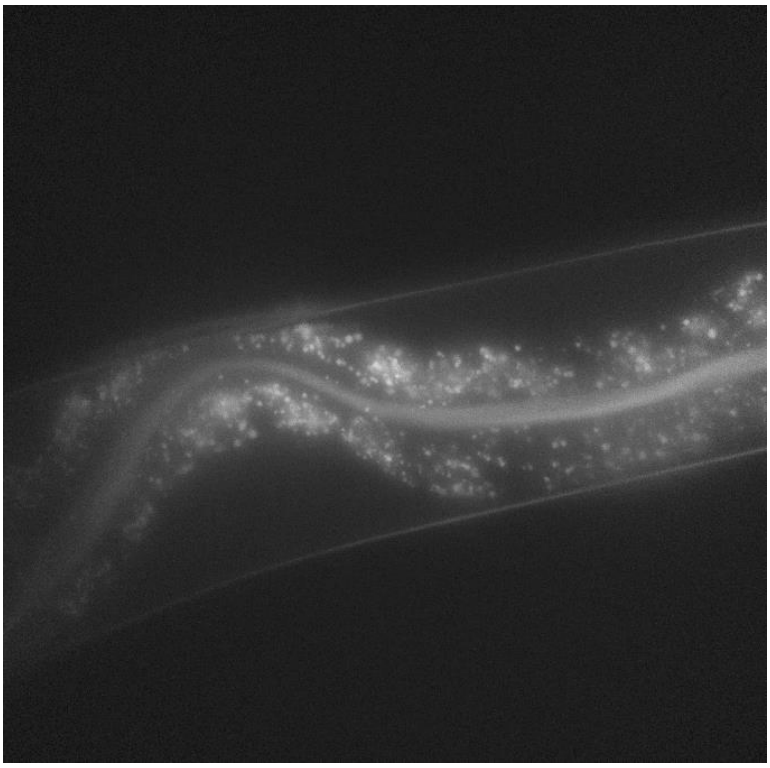

Figure S139 – Fluorescent microscopy image of *C. elegans* GLO-1 mutant supplemented with **4** at 0.10 mM in 5 % EtOH. Image taken with 200 ms exposure time.

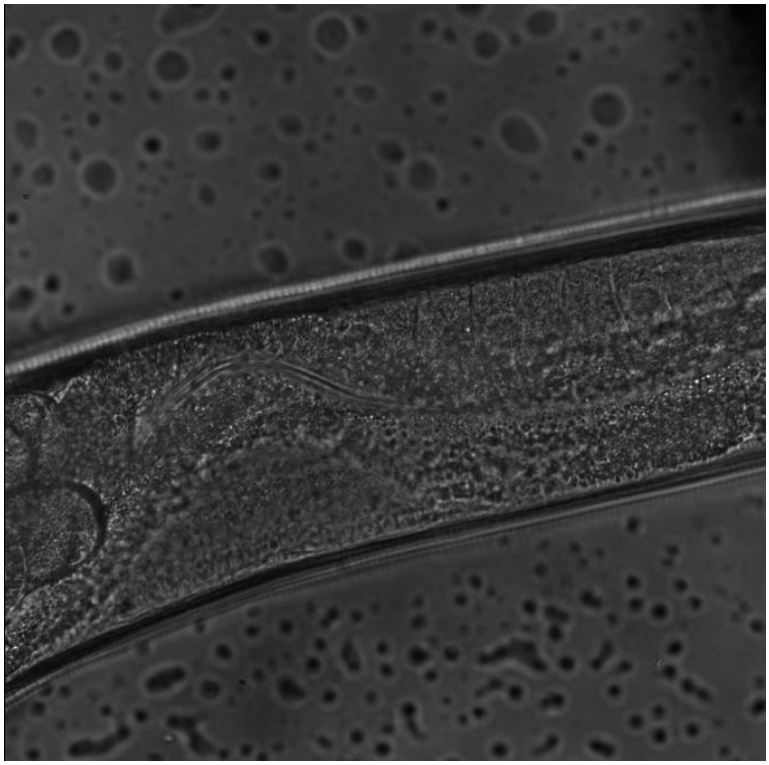

Figure S140 – Brightfield microscopy image of *C. elegans* GLO-1 mutant supplemented with **4** at 0.10 mM in 5 % EtOH. Image taken with 200 ms exposure time.

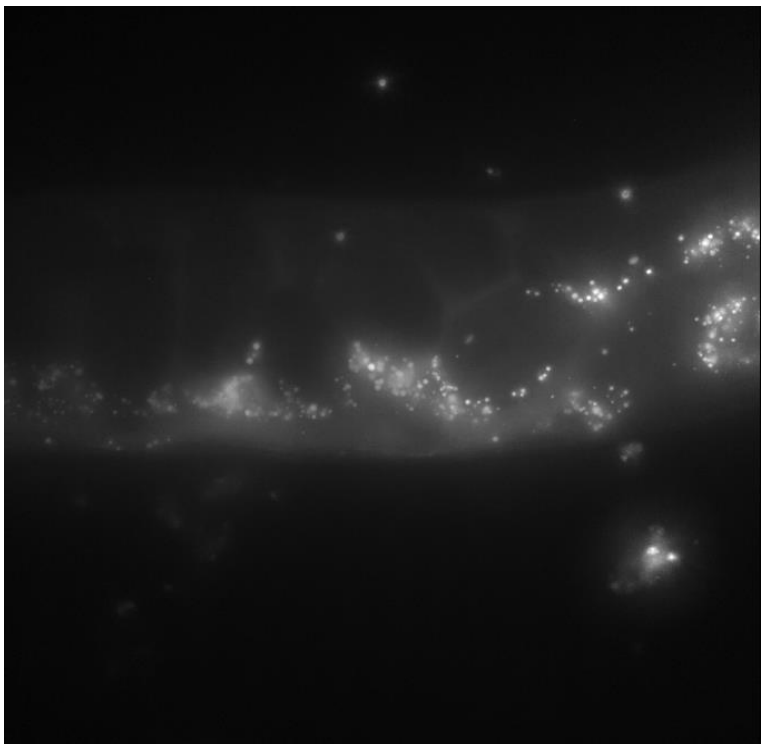

Figure S141 – Fluorescent microscopy image of *C. elegans* GLO-1 mutant supplemented with **5** at 0.10 mM in 5 % EtOH. Image taken with 200 ms exposure time.

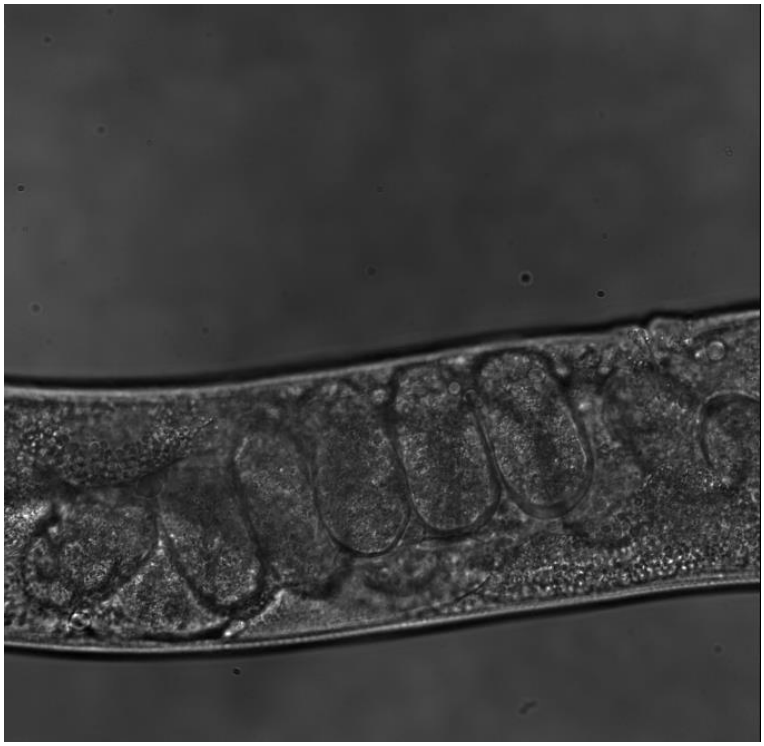

Figure S142 – Brightfield microscopy image of *C. elegans* GLO-1 mutant supplemented with **5** at 0.10 mM in 5 % EtOH. Image taken with 200 ms exposure time.

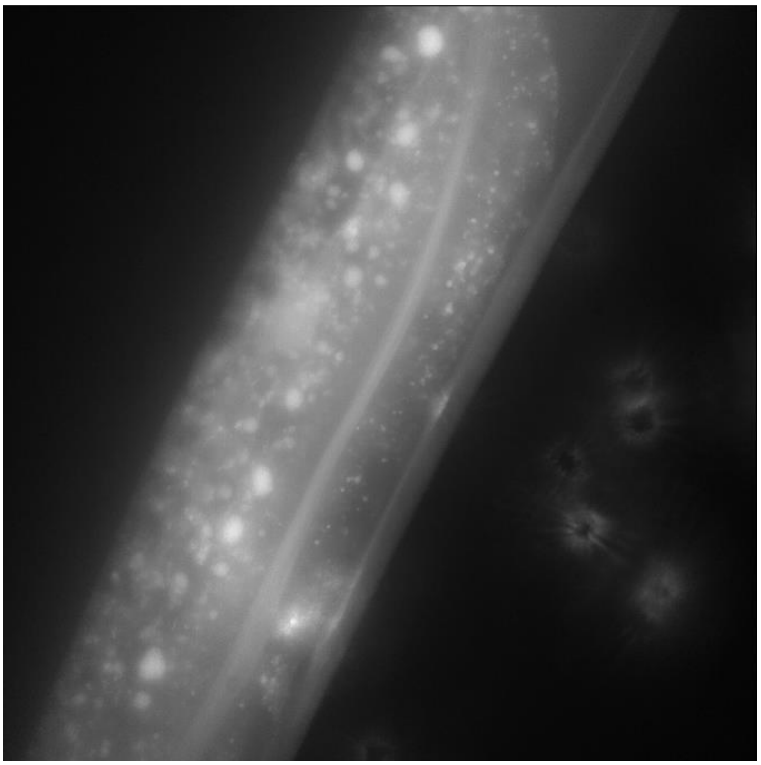

Figure S143 – Fluorescent microscopy image of *C. elegans* GLO-1 mutant supplemented with **6** at 0.10 mM in 5 % EtOH. Image taken with 200 ms exposure time.

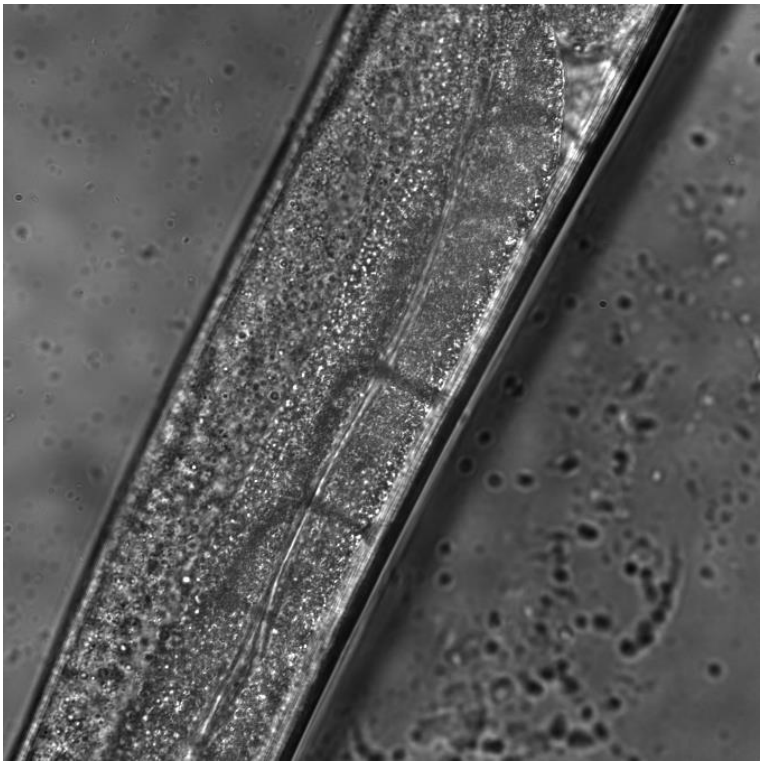

Figure S144 – Brightfield microscopy image of *C. elegans* GLO-1 mutant supplemented with **6** at 0.10 mM in 5 % EtOH. Image taken with 200 ms exposure time.

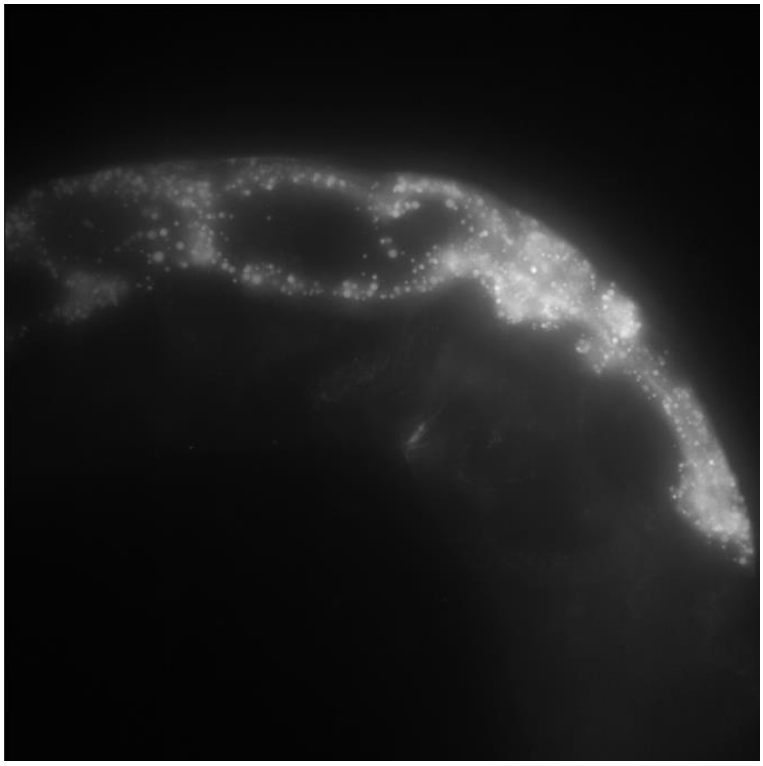

Figure S145 – Fluorescent microscopy image of *C. elegans* GLO-1 mutant supplemented with **7** at 0.10 mM in 5 % EtOH. Image taken with 200 ms exposure time.

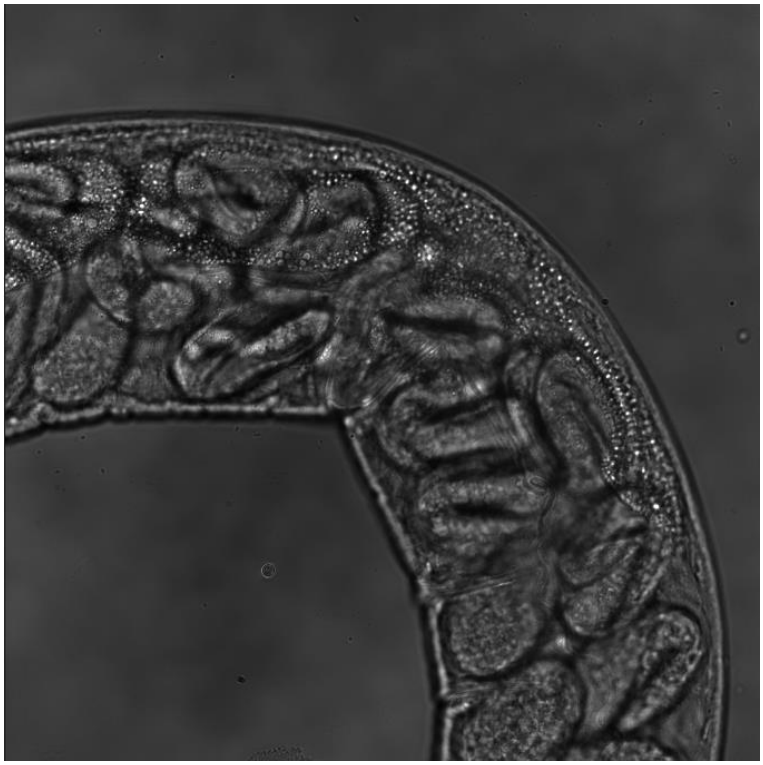

Figure S146 – Brightfield microscopy image of *C. elegans* GLO-1 mutant supplemented with **7** at 0.10 mM in 5 % EtOH. Image taken with 200 ms exposure time.

Section 18: Plate reader data

UV-Vis spectroscopy data

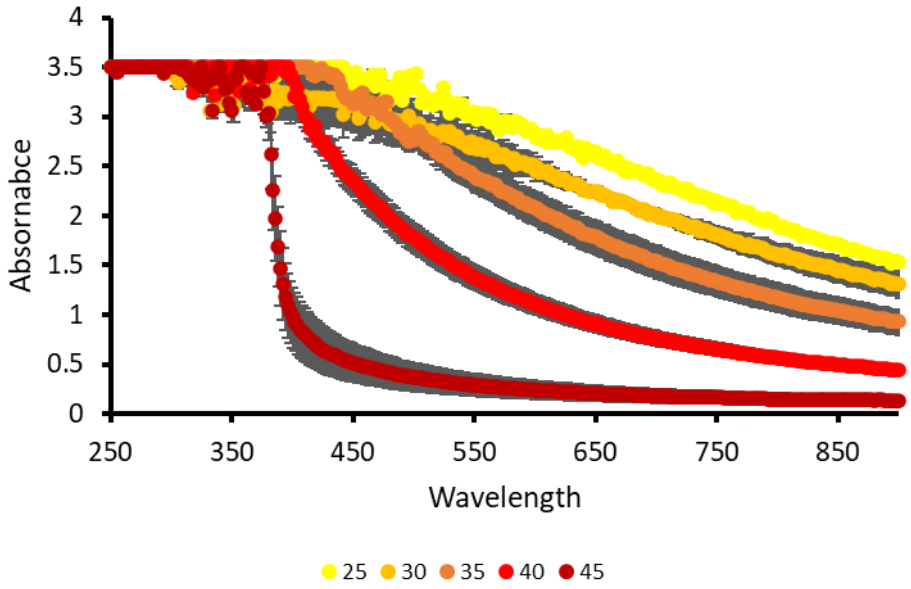

Figure S147 - Average (n=3) absorbance graph of **3** (1.5 mg/mL) in NaCl recorded for each 200 µL sample at 5-degree increments from 25-45 °C. Error = standard deviation of the mean.

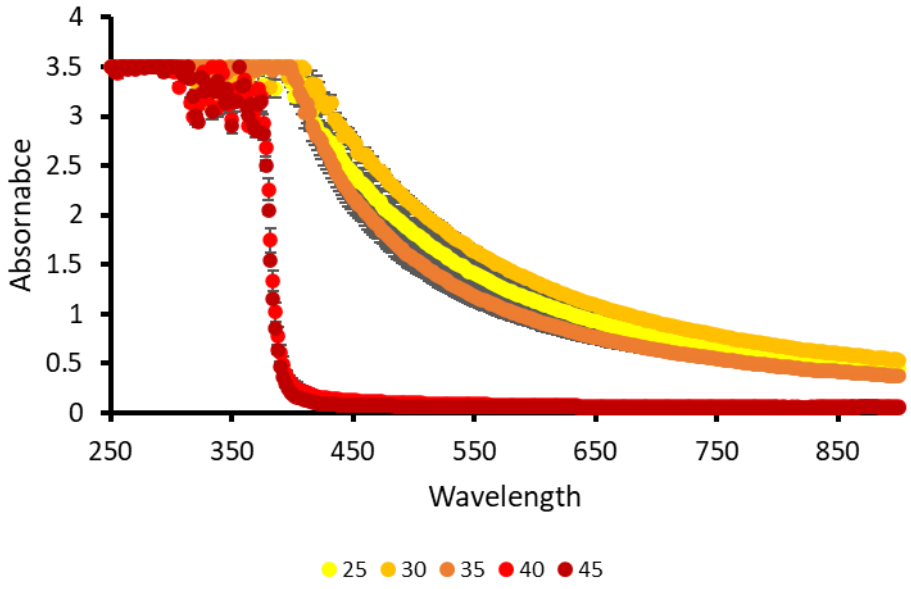

Figure S148 - Average (n=3) absorbance graph of **3** (1.5 mg/mL) in KCl recorded for each 200 µL sample at 5-degree increments from 25-45 °C. Error = standard deviation of the mean.

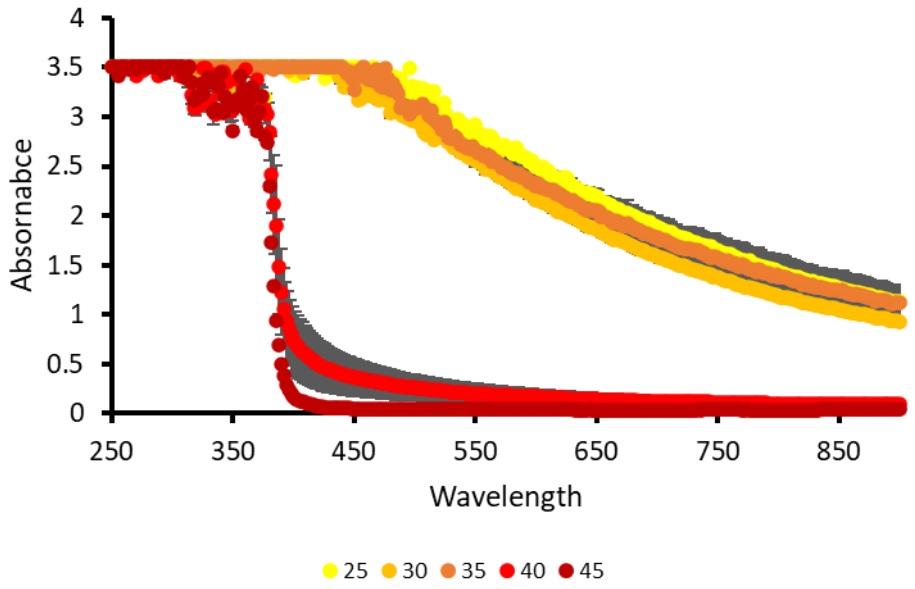

Figure S149 - Average (n=3) absorbance graph of **3** (1.5 mg/mL) in $NaNO_3$ recorded for each 200 µL sample at 5-degree increments from 25-45 °C. Error = standard deviation of the mean.

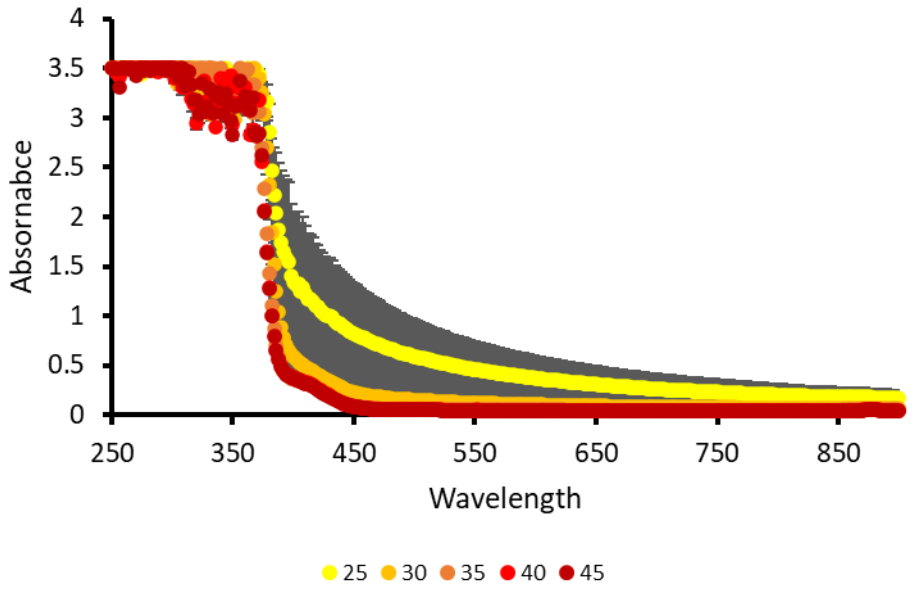

Figure S150 - Average (n=3) absorbance graph of **3** (1.5 mg/mL) in NaH_2PO_4 recorded for each 200 µL sample at 5-degree increments from 25-45 °C. Error = standard deviation of the mean.

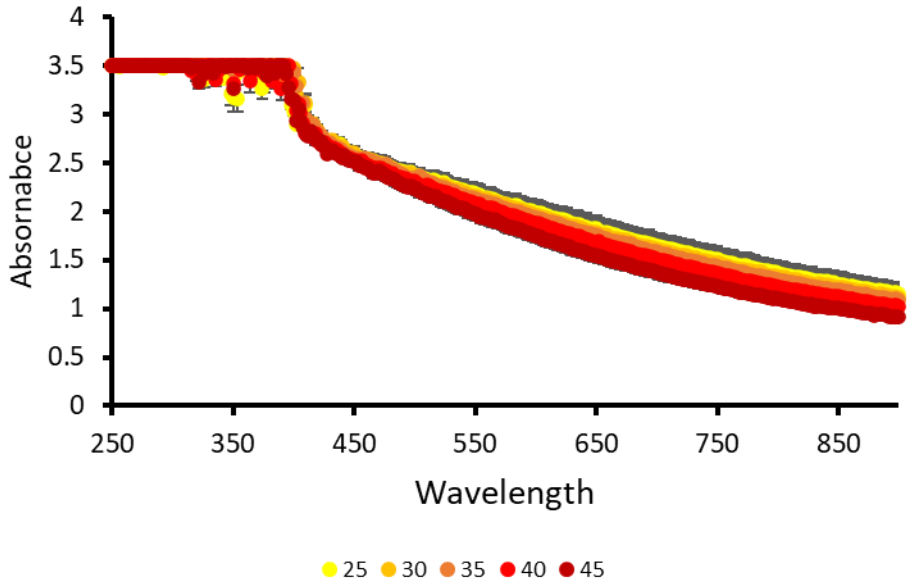

Figure S151 - Average (n=3) absorbance graph of **3** (1.5 mg/mL) in NaOBz recorded for each 200 µL sample at 5-degree increments from 25-45 °C. Error = standard deviation of the mean.

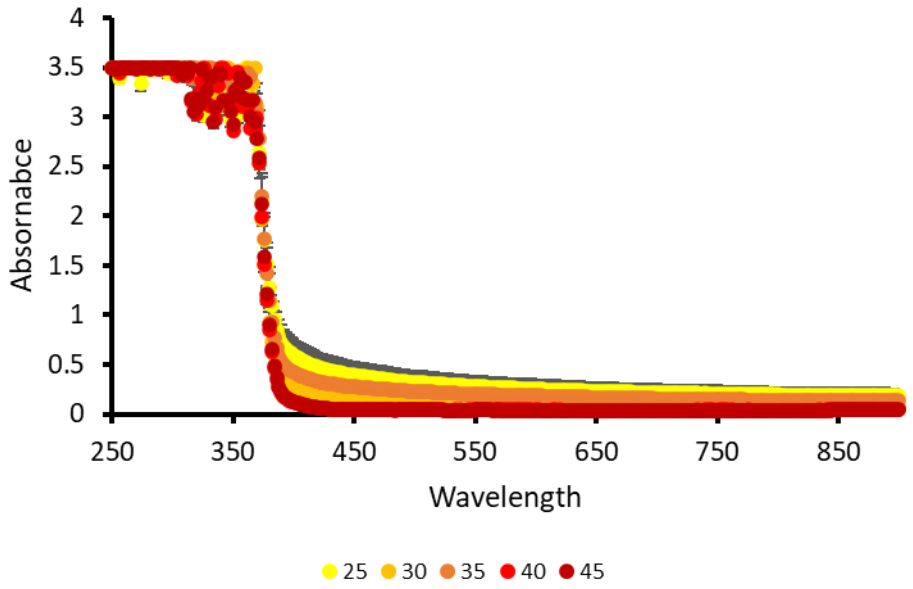

Figure S152 - Average (n=3) absorbance graph of **3** (1.5 mg/mL) in Na_2SO_4 recorded for each 200 µL sample at 5-degree increments from 25-45 °C. Error = standard deviation of the mean.

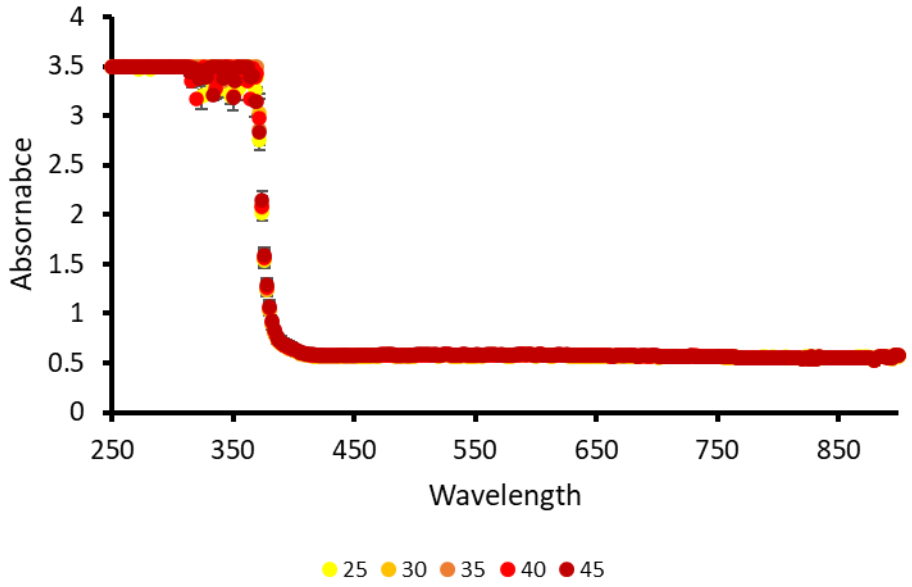

Figure S153 - Average (n=3) absorbance graph of **3** (1.5 mg/mL) in DMSO recorded for each 200 µL sample at 5-degree increments from 25-45 °C. Error = standard deviation of the mean.

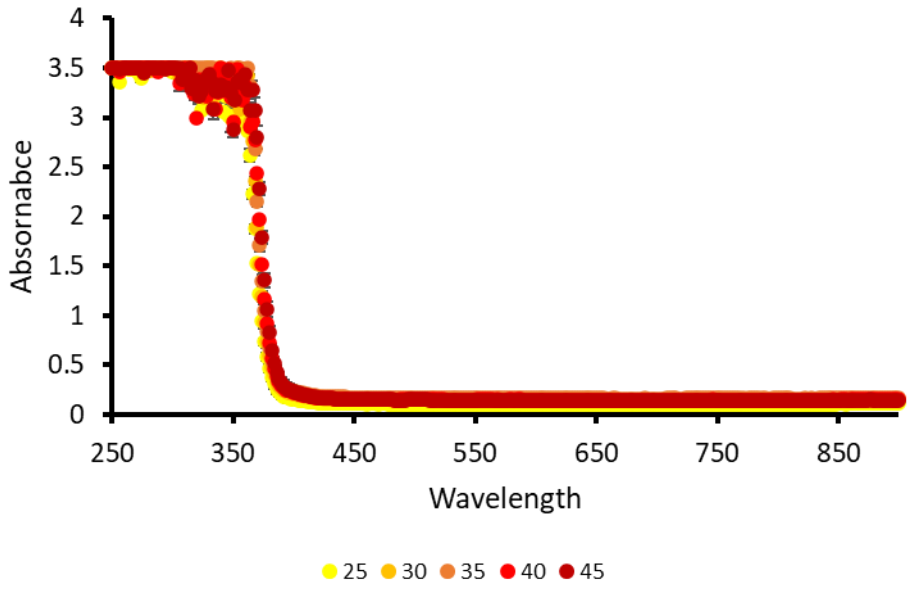

Figure S154 - Average (n=3) absorbance graph of **3** (1.5 mg/mL) in H_2O recorded for each 200 µL sample at 5-degree increments from 25-45 °C. Error = standard deviation of the mean.

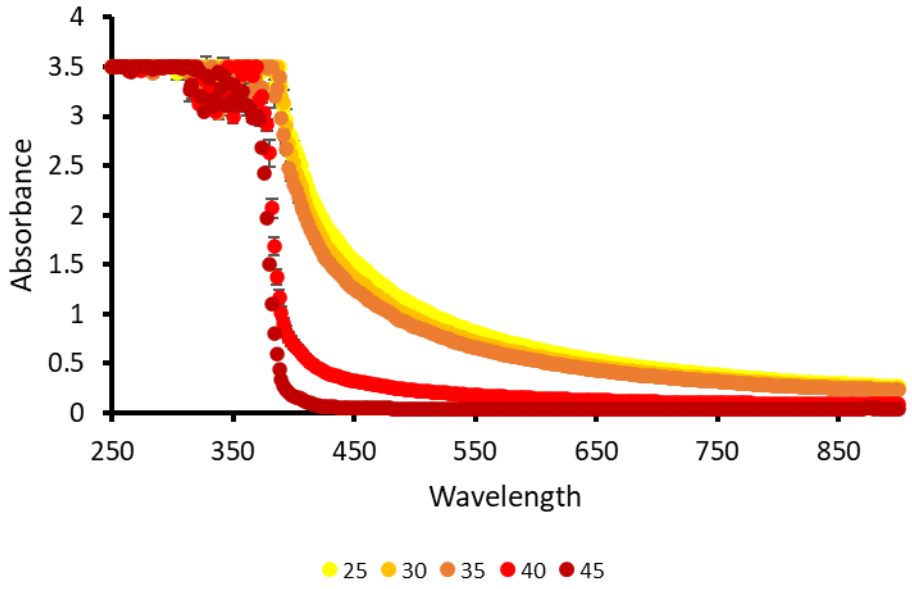

Figure S155 - Average (n=3) absorbance graph of **4** (1.5 mg/mL) in NaCl recorded for each 200 µL sample at 5-degree increments from 25-45 °C. Error = standard deviation of the mean.

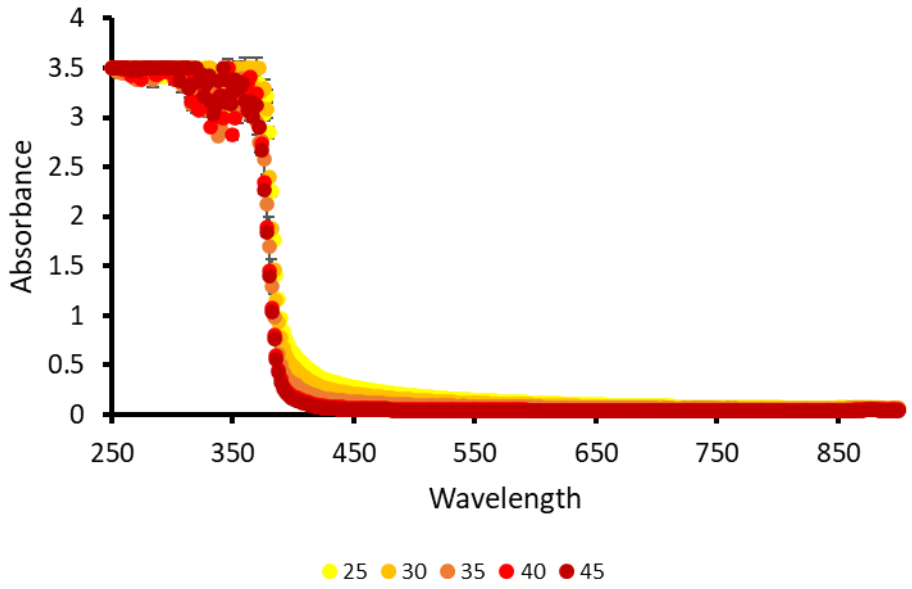

Figure S156 - Average (n=3) absorbance graph of **4** (1.5 mg/mL) in KCl recorded for each 200 µL sample at 5-degree increments from 25-45 °C. Error = standard deviation of the mean.

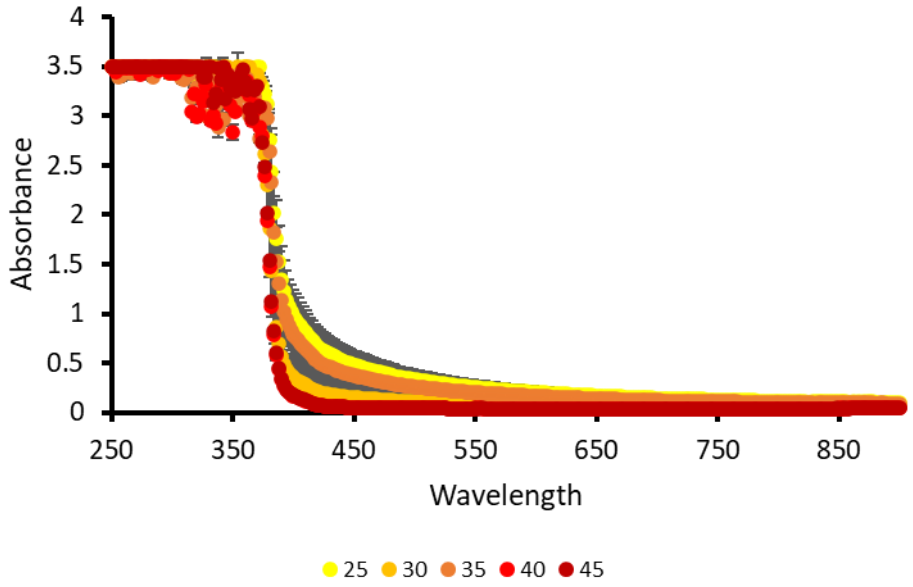

Figure S157 - Average (n=3) absorbance graph of **4** (1.5 mg/mL) in $NaNO_3$ recorded for each 200 µL sample at 5-degree increments from 25-45 °C. Error = standard deviation of the mean.

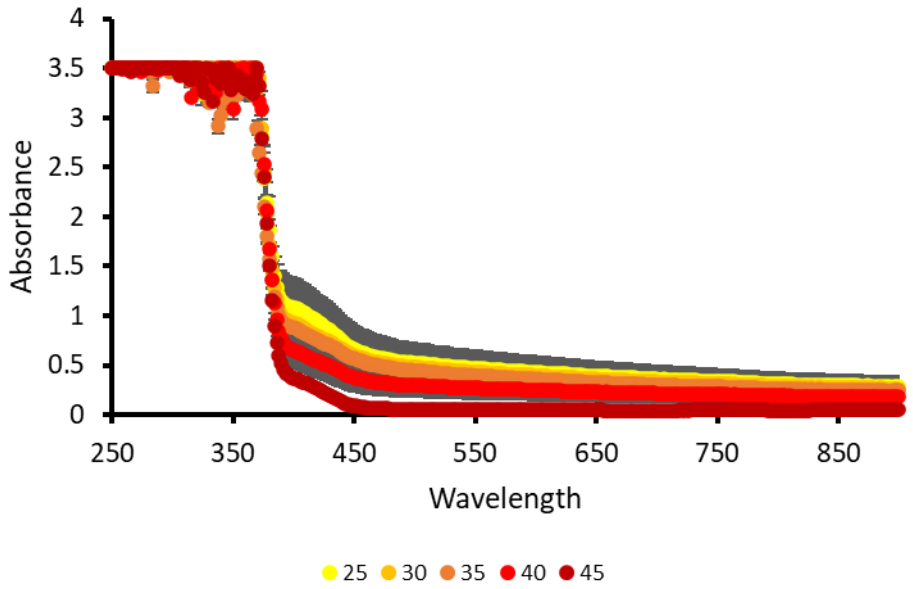

Figure S158 - Average (n=3) absorbance graph of **4** (1.5 mg/mL) in NaH_2PO_4 recorded for each 200 µL sample at 5-degree increments from 25-45 °C. Error = standard deviation of the mean.

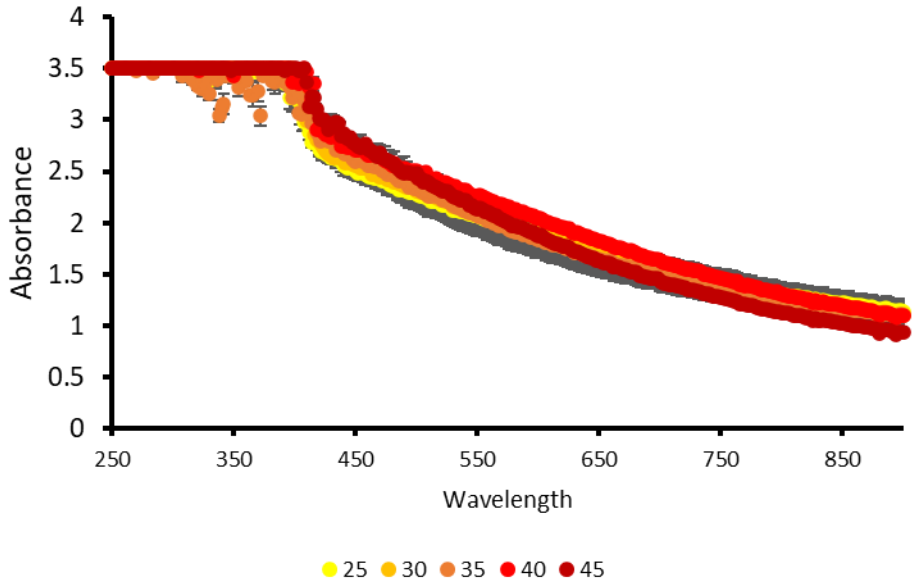

Figure S159 - Average (n=3) absorbance graph of **4** (1.5 mg/mL) in NaOBz recorded for each 200 µL sample at 5-degree increments from 25-45 °C. Error = standard deviation of the mean.

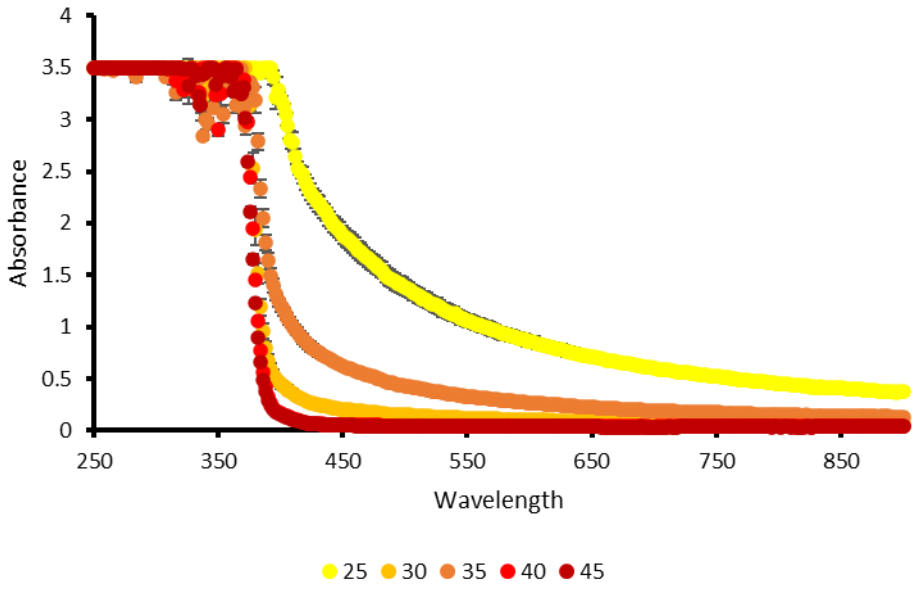

Figure S160 - Average (n=3) absorbance graph of **4** (1.5 mg/mL) in Na_2SO_4 recorded for each 200 µL sample at 5-degree increments from 25-45 °C. Error = standard deviation of the mean.

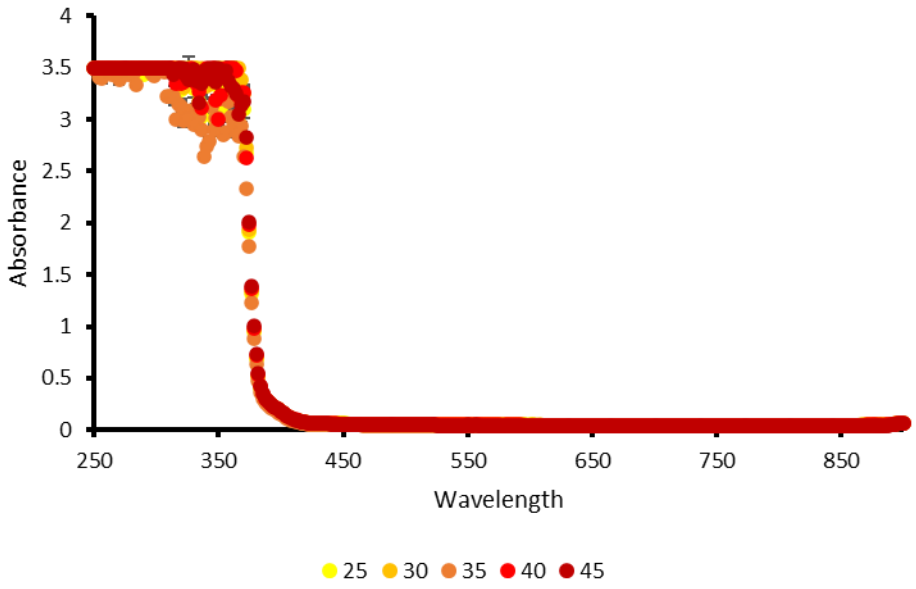

Figure S161 - Average (n=3) absorbance graph of **4** (1.5 mg/mL) in DMSO recorded for each 200 µL sample at 5-degree increments from 25-45 °C. Error = standard deviation of the mean.

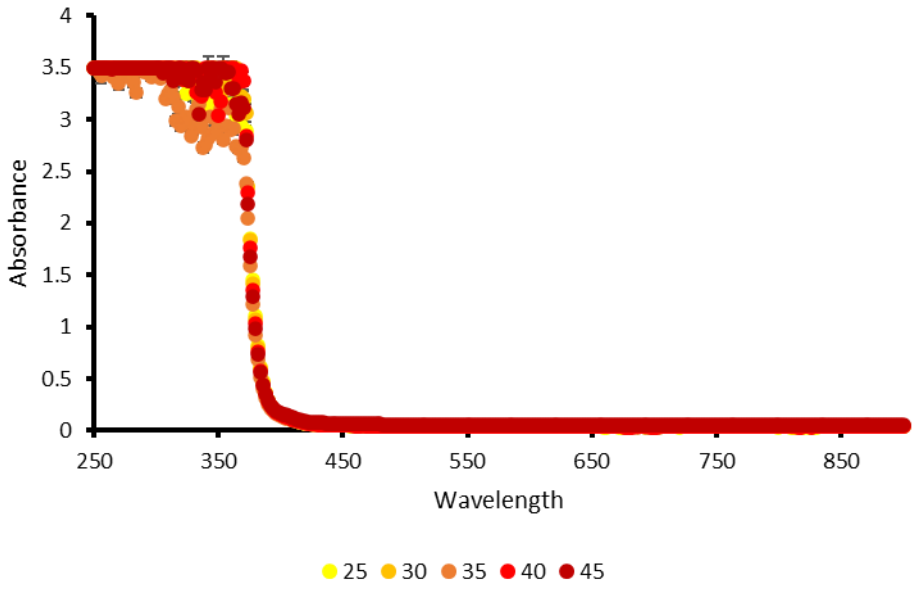

Figure S162 - Average (n=3) absorbance graph of **4** (1.5 mg/mL) in H_2O recorded for each 200 µL sample at 5-degree increments from 25-45 °C. Error = standard deviation of the mean.

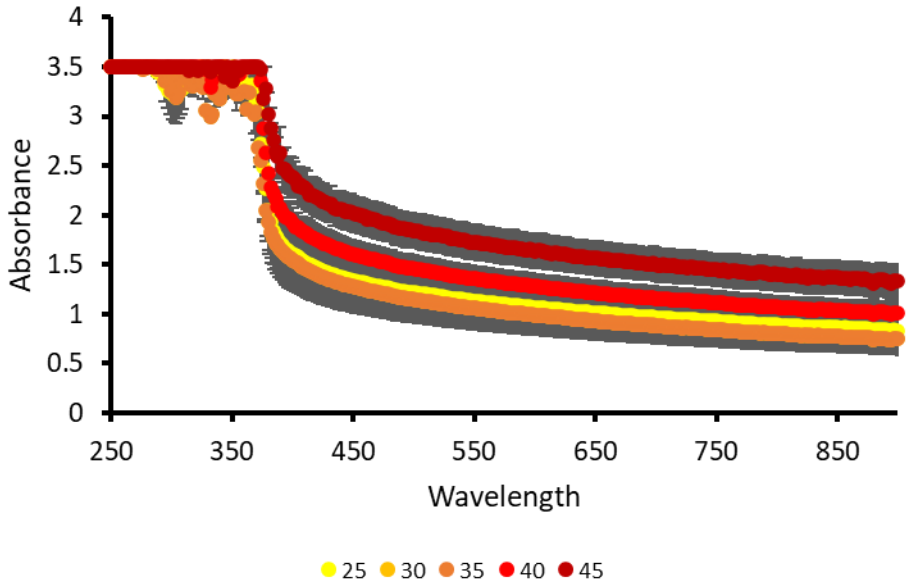

Figure S163 - Average (n=3) absorbance graph of **5** (1.5 mg/mL) in NaCl recorded for each 200 µL sample at 5-degree increments from 25-45 °C. Error = standard deviation of the mean.

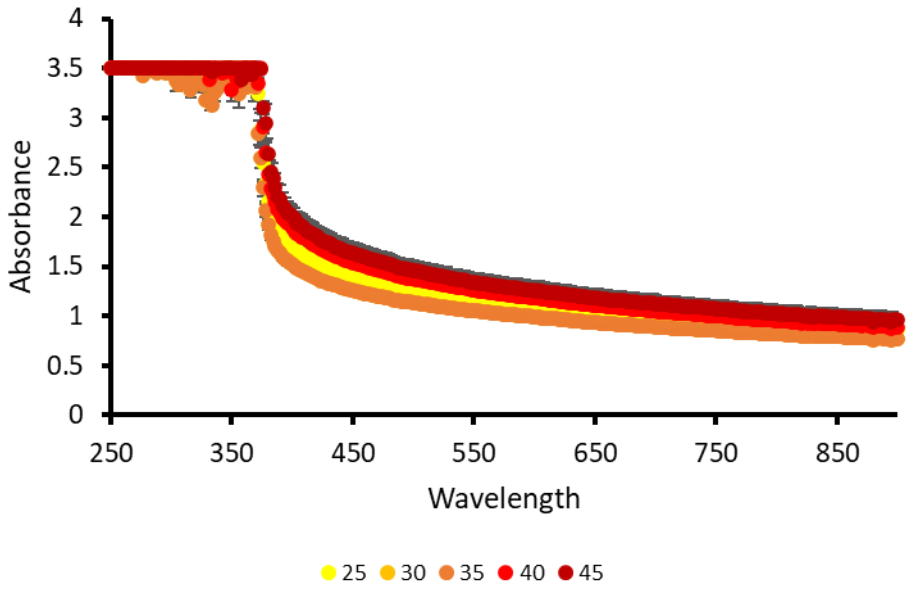

Figure S164 – Average (n=3) absorbance graph of **5** (1.5 mg/mL) in KCl recorded for each 200 µL sample at 5-degree increments from 25-45 °C. Error = standard deviation of the mean.

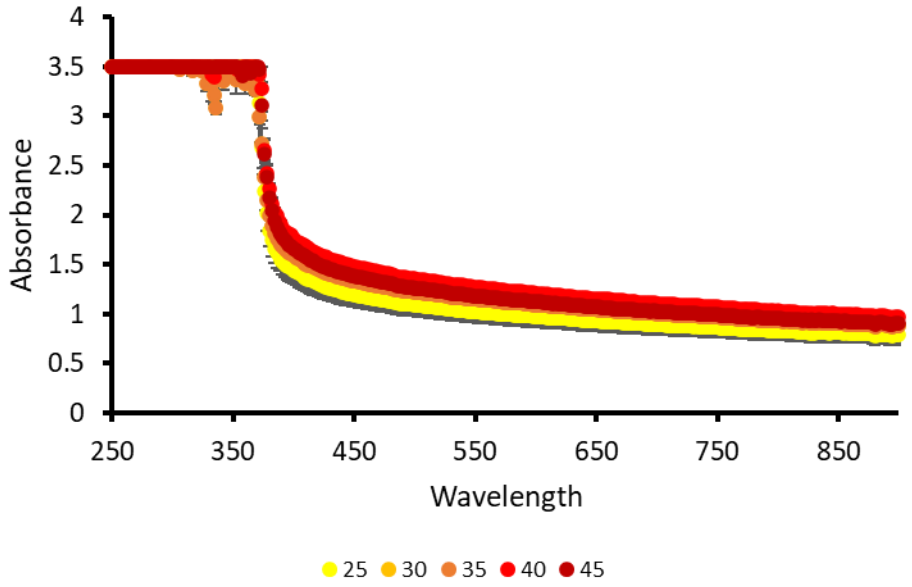

Figure S165 - Average (n=3) absorbance graph of **5** (1.5 mg/mL) in $NaNO_3$ recorded for each 200 µL sample at 5-degree increments from 25-45 °C. Error = standard deviation of the mean.

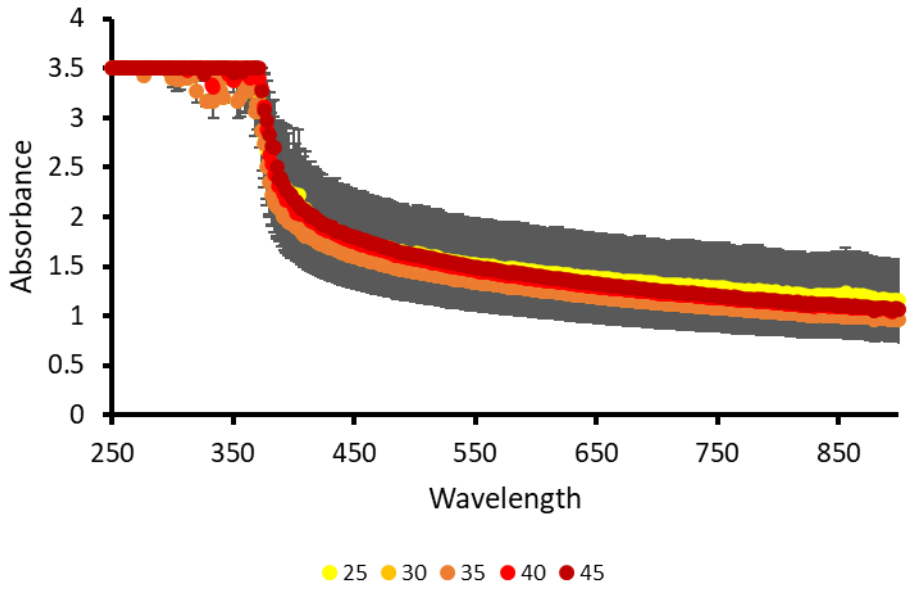

Figure S166 - Average (n=3) absorbance graph of **5** (1.5 mg/mL) in NaH_2PO_4 recorded for each 200 µL sample at 5-degree increments from 25-45 °C. Error = standard deviation of the mean.

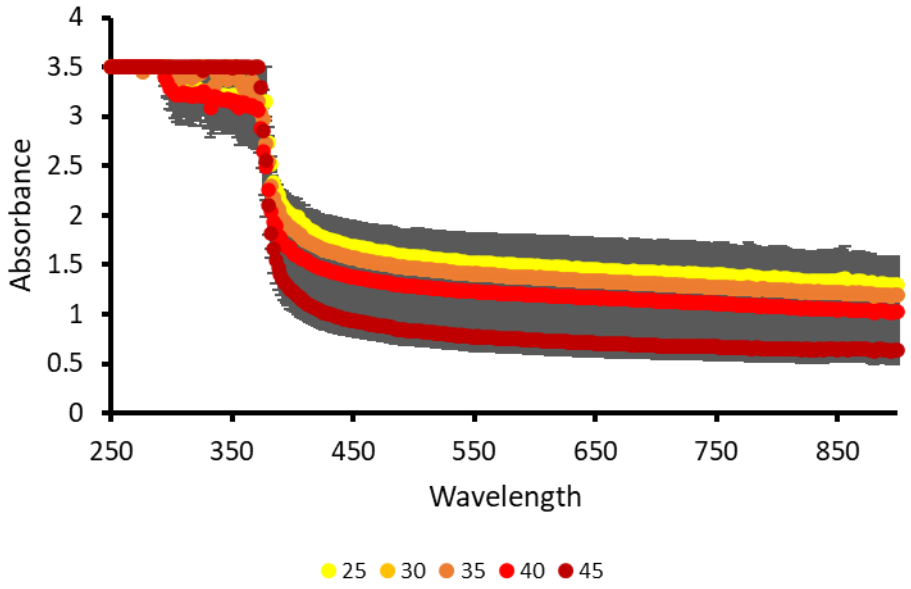

Figure S167 - Average (n=3) absorbance graph of **5** (1.5 mg/mL) in NaOBz recorded for each 200 µL sample at 5-degree increments from 25-45 °C. Error = standard deviation of the mean.

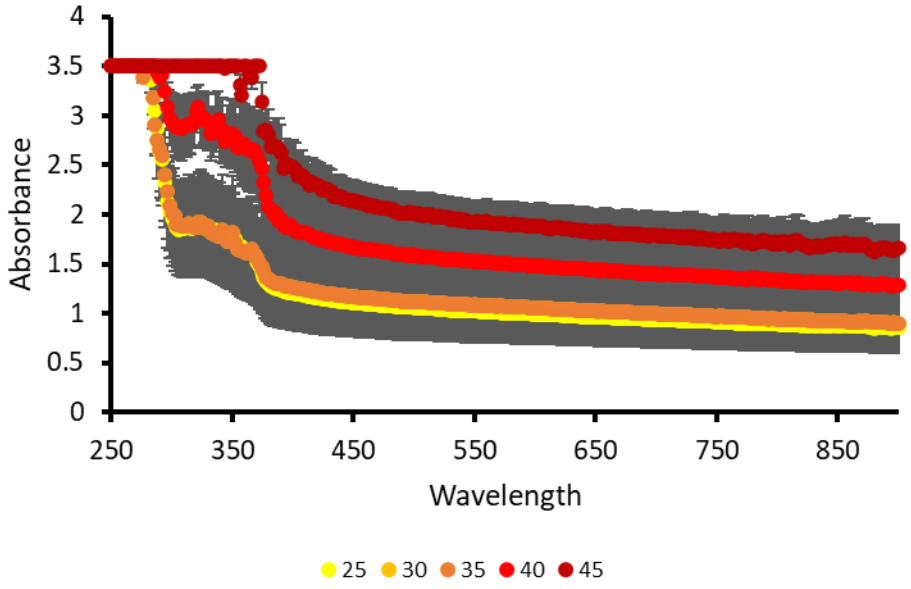

Figure S168 - Average (n=3) absorbance graph of **5** (1.5 mg/mL) in Na_2SO_4 recorded for each 200 µL sample at 5-degree increments from 25-45 °C. Error = standard deviation of the mean.

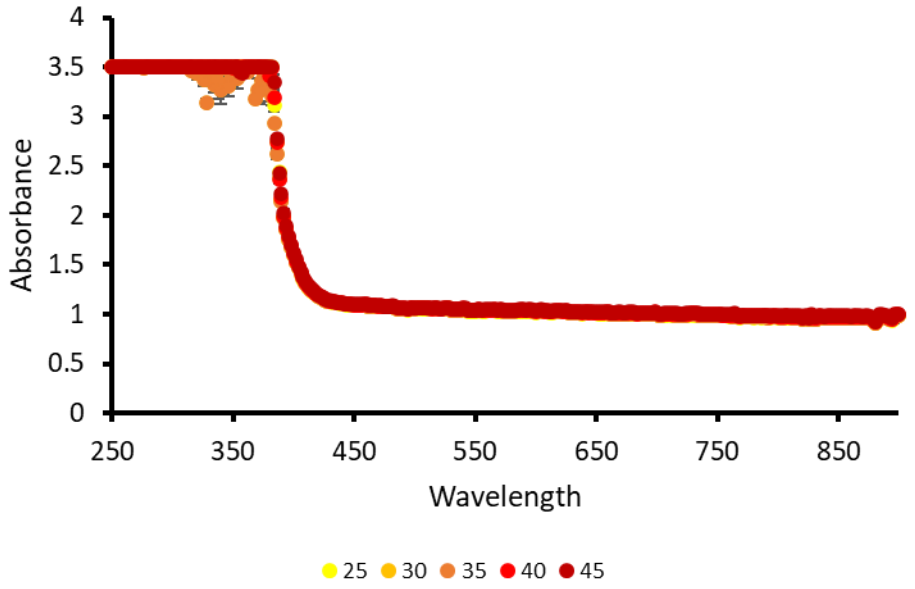

Figure S169 - Average (n=3) absorbance graph of **5** (1.5 mg/mL) in DMSO recorded for each 200 µL sample at 5-degree increments from 25-45 °C. Error = standard deviation of the mean.

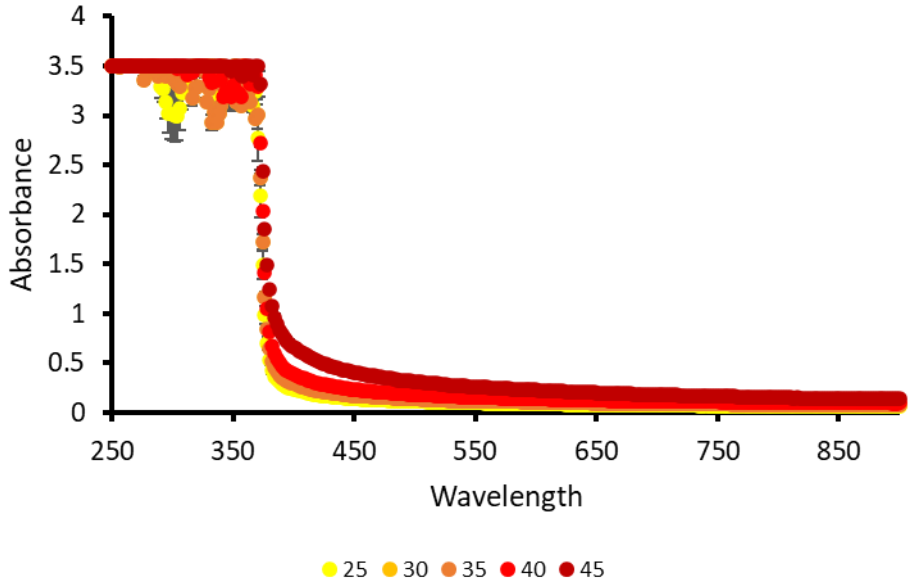

Figure S170 - Average (n=3) absorbance graph of **5** (1.5 mg/mL) inH_2O recorded for each 200 µL sample at 5-degree increments from 25-45 °C. Error = standard deviation of the mean.

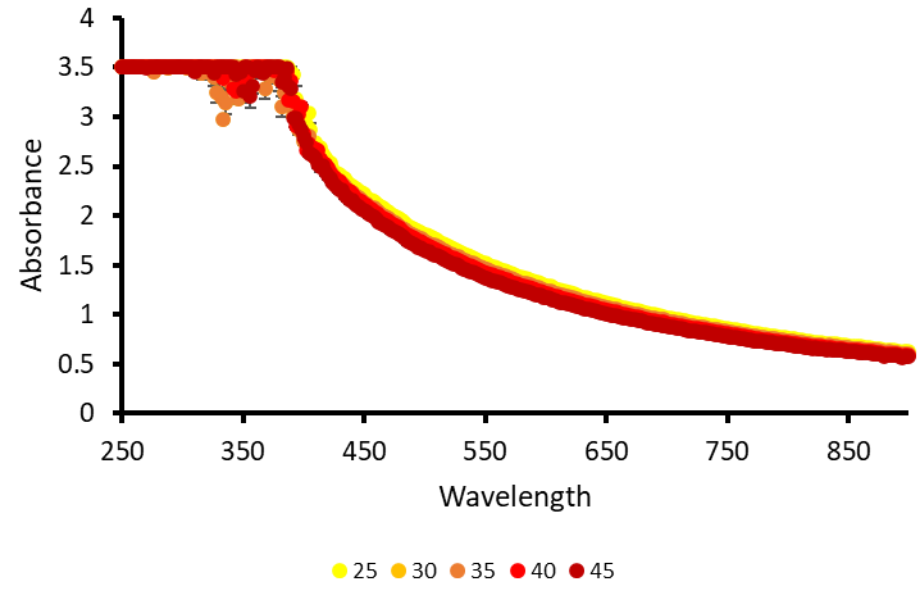

Figure S171 - Average (n=3) absorbance graph of **6** (1.5 mg/mL) in NaCl recorded for each 200 µL sample at 5-degree increments from 25-45 °C. Error = standard deviation of the mean.

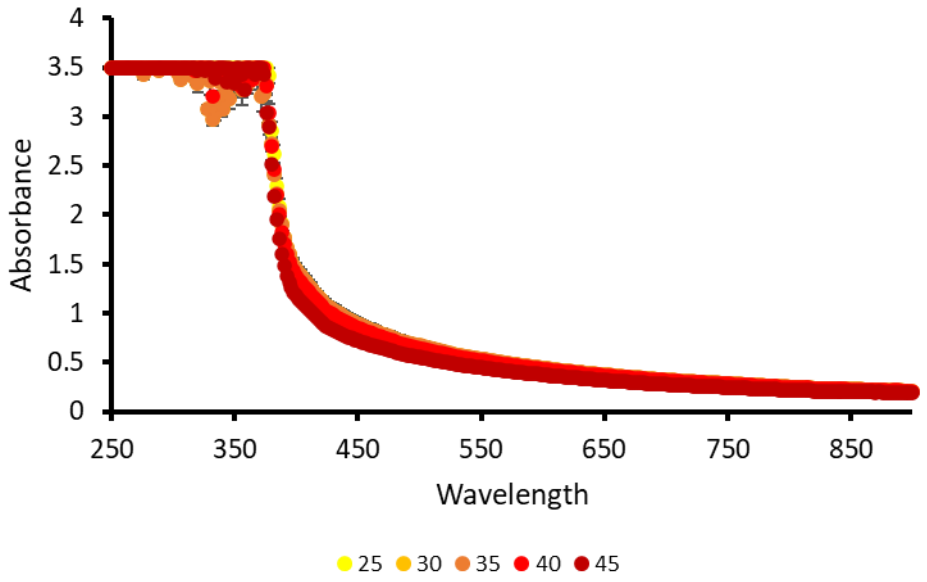

Figure S172 - Average (n=3) absorbance graph of **6** (1.5 mg/mL) in KCl recorded for each 200 µL sample at 5-degree increments from 25-45 °C. Error = standard deviation of the mean.

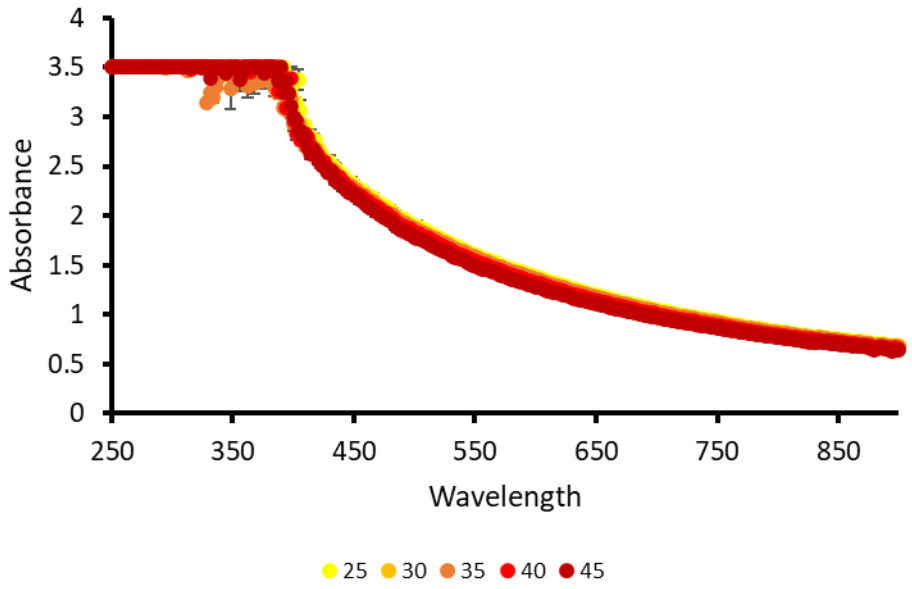

Figure S173 - Average (n=3) absorbance graph of **6** (1.5 mg/mL) in $NaNO_3$ recorded for each 200 µL sample at 5-degree increments from 25-45 °C. Error = standard deviation of the mean.

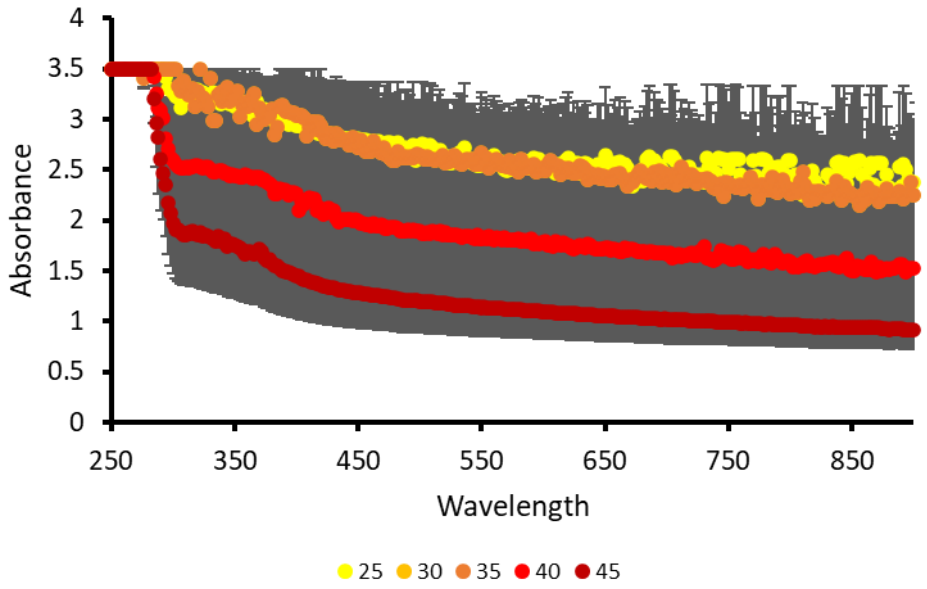

Figure S174 - Average (n=3) absorbance graph of **6** (1.5 mg/mL) in NaH_2PO_4 recorded for each 200 µL sample at 5-degree increments from 25-45 °C. Error = standard deviation of the mean.

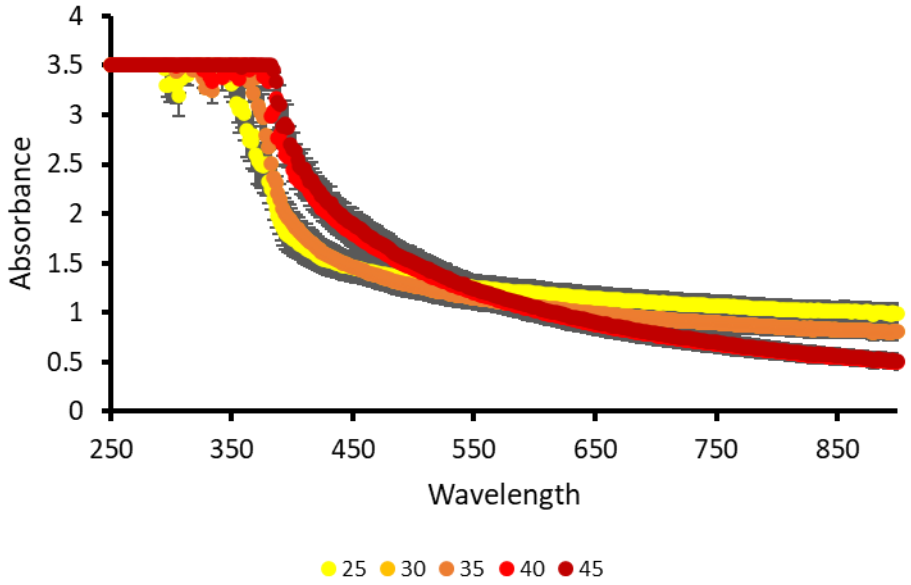

Figure S175 - Average (n=3) absorbance graph of **6** (1.5 mg/mL) in NaOBz recorded for each 200 µL sample at 5-degree increments from 25-45 °C. Error = standard deviation of the mean.

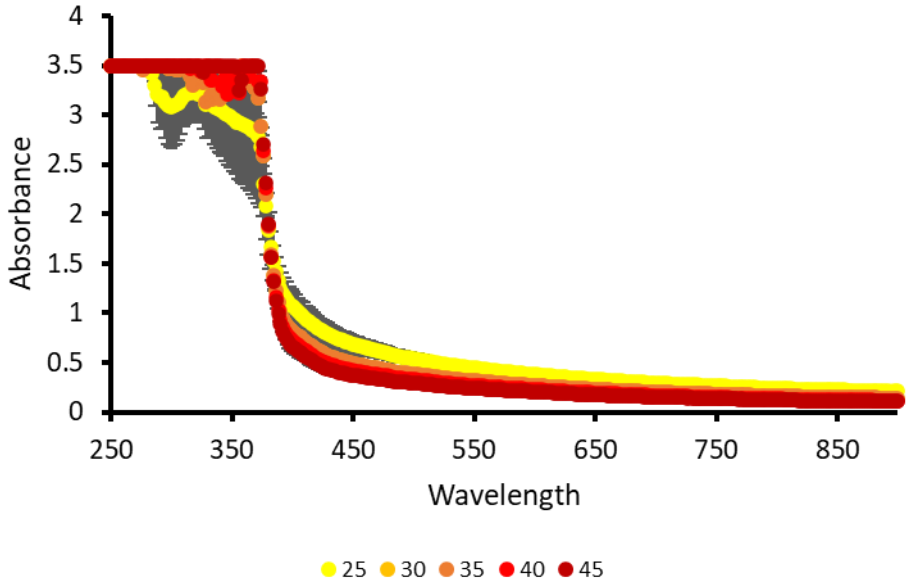

Figure S176 - Average (n=3) absorbance graph of **6** (1.5 mg/mL) in Na_2SO_4 recorded for each 200 µL sample at 5-degree increments from 25-45 °C. Error = standard deviation of the mean.

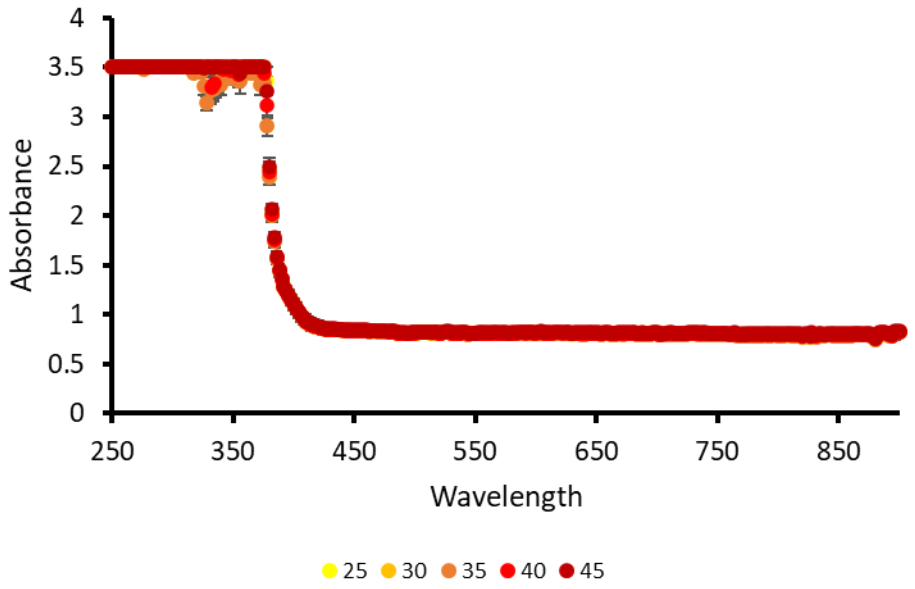

Figure S177 - Average (n=3) absorbance graph of **6** (1.5 mg/mL) in DMSO recorded for each 200 µL sample at 5-degree increments from 25-45 °C. Error = standard deviation of the mean.

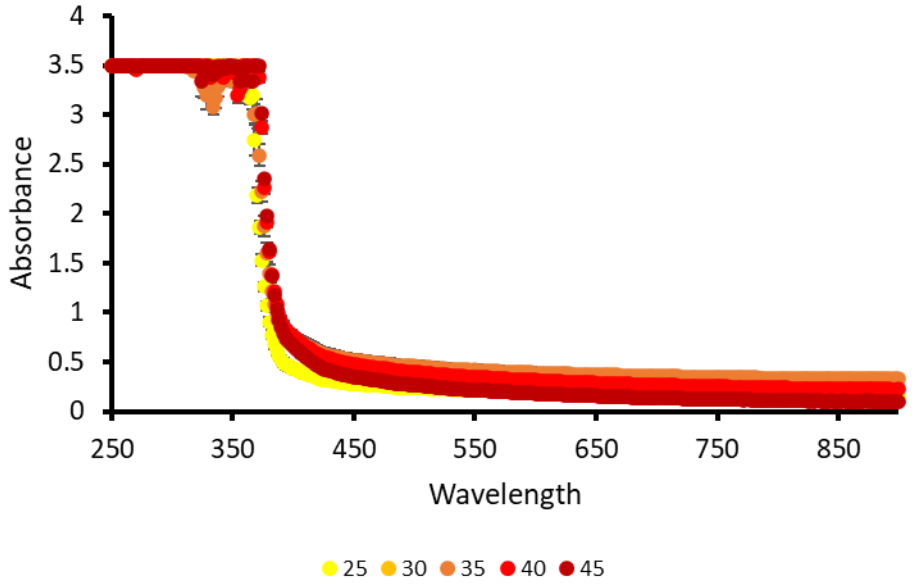

Figure S178 - Average (n=3) absorbance graph of **6** (1.5 mg/mL) in H_2O recorded for each 200 µL sample at 5-degree increments from 25-45 °C. Error = standard deviation of the mean.

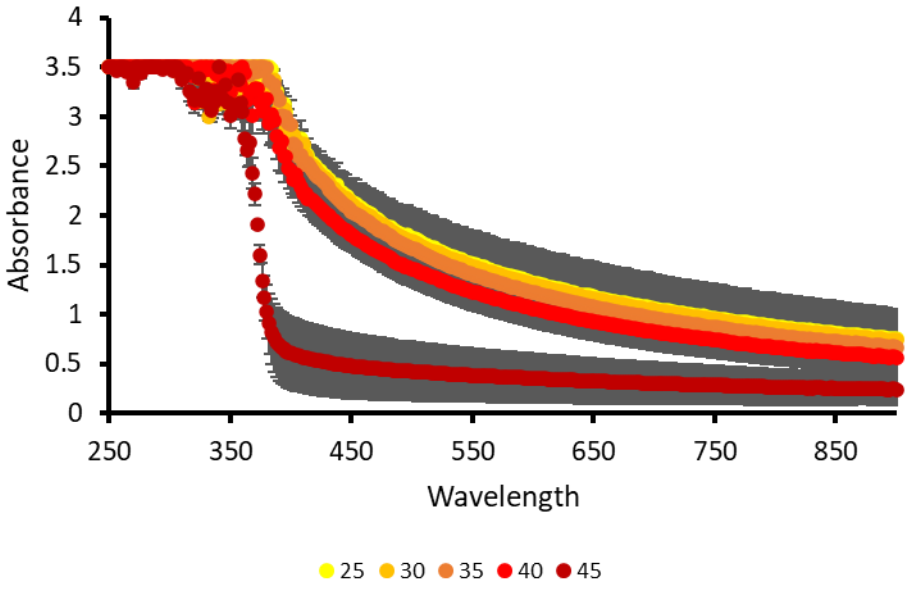

Figure S179 - Average (n=3) absorbance graph of **7** (1.5 mg/mL) in NaCl recorded for each 200 µL sample at 5-degree increments from 25-45 °C. Error = standard deviation of the mean.

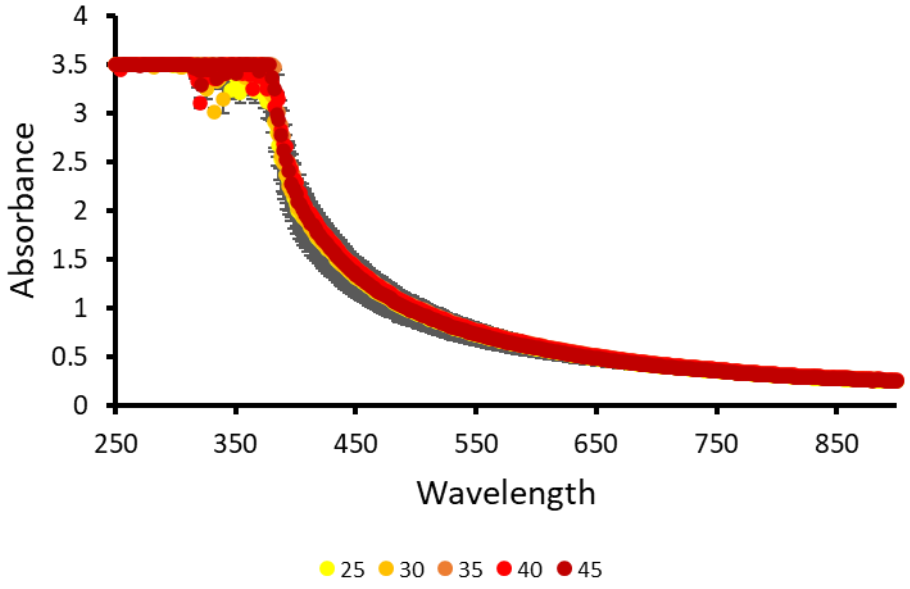

Figure S180 - Average (n=3) absorbance graph of **7** (1.5 mg/mL) in KCl recorded for each 200 µL sample at 5-degree increments from 25-45 °C. Error = standard deviation of the mean.

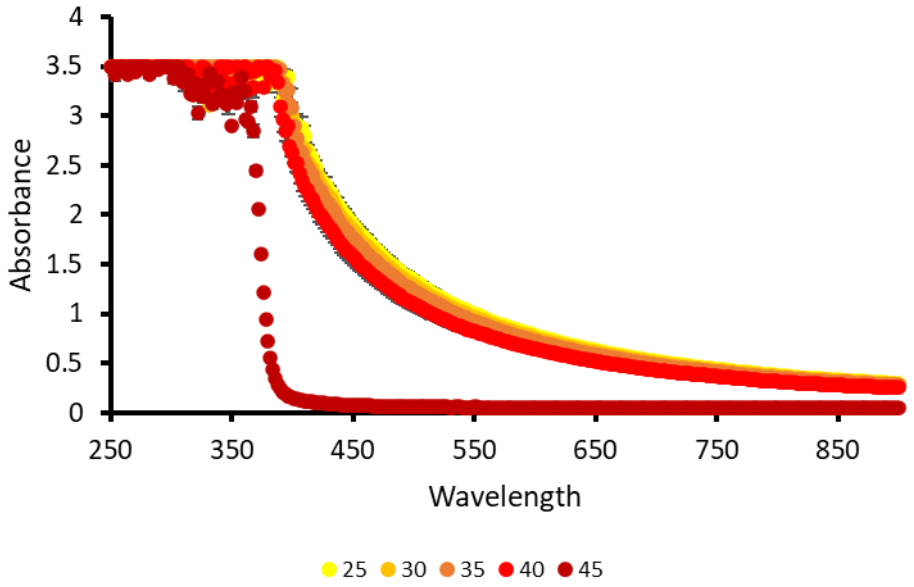

Figure S181 - Average (n=3) absorbance graph of **7** (1.5 mg/mL) in $NaNO_3$ recorded for each 200 µL sample at 5-degree increments from 25-45 °C. Error = standard deviation of the mean.

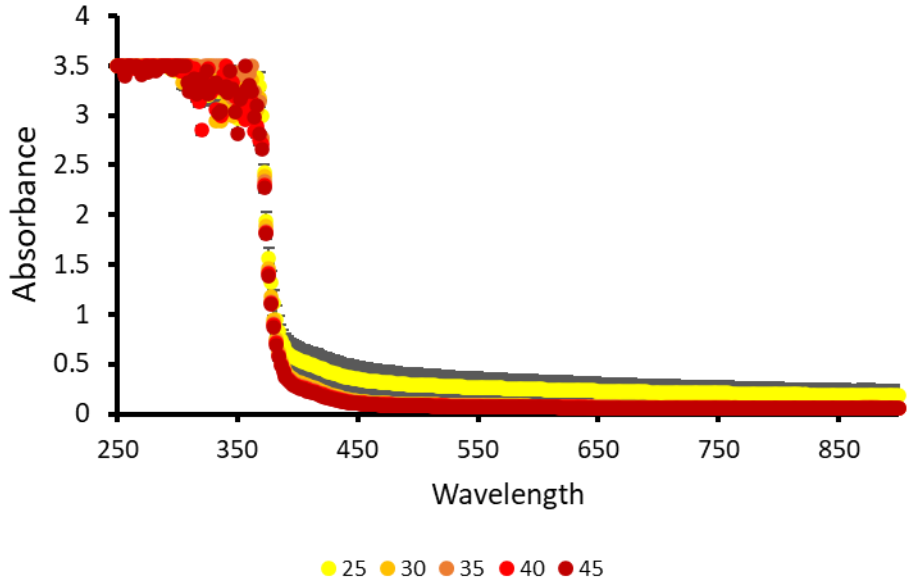

Figure S182 - Average (n=3) absorbance graph of **7** (1.5 mg/mL) in NaH_2PO_4 recorded for each 200 µL sample at 5-degree increments from 25-45 °C. Error = standard deviation of the mean.

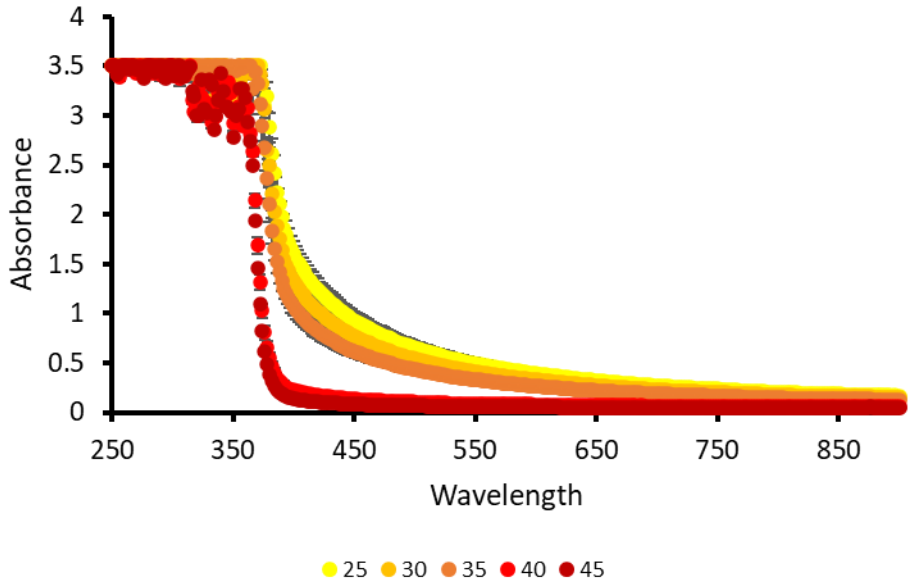

Figure S183 - Average (n=3) absorbance graph of **7** (1.5 mg/mL) in NaOBz recorded for each 200 µL sample at 5-degree increments from 25-45 °C. Error = standard deviation of the mean.

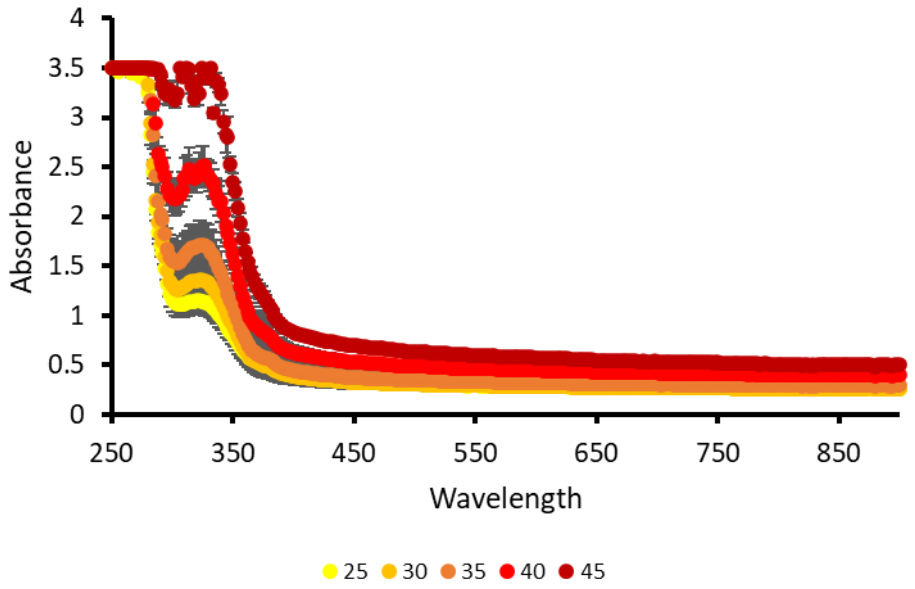

Figure S184 - Average (n=3) absorbance graph of **7** (1.5 mg/mL) in Na_2SO_4 recorded for each 200 µL sample at 5-degree increments from 25-45 °C. Error = standard deviation of the mean.

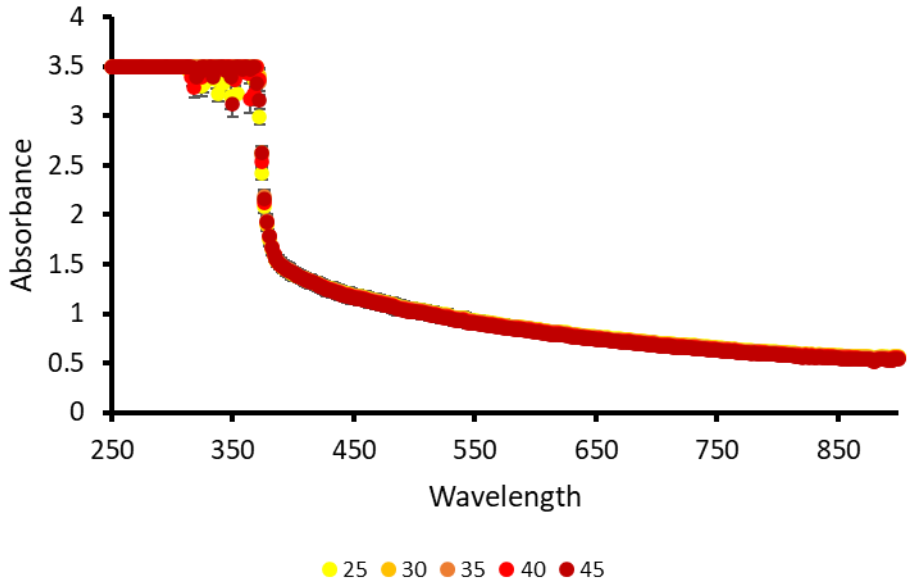

Figure S185 - Average (n=3) absorbance graph of **7** (1.5 mg/mL) in DMSO recorded for each 200 µL sample at 5-degree increments from 25-45 °C. Error = standard deviation of the mean.

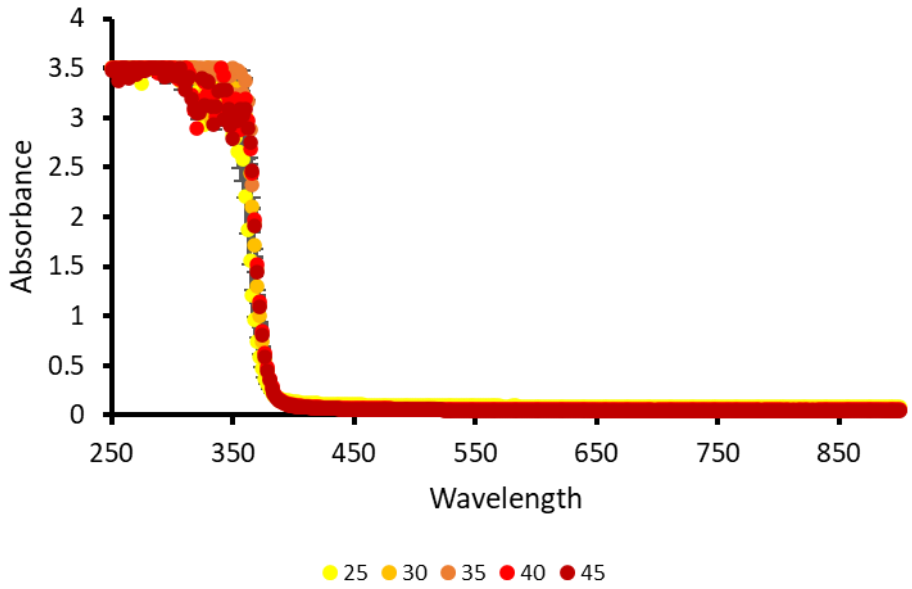

Figure S186 - Average (n=3) absorbance graph of **7** (1.5 mg/mL) in H_2O recorded for each 200 µL sample at 5-degree increments from 25-45 °C. Error = standard deviation of the mean.

Spectral well scans

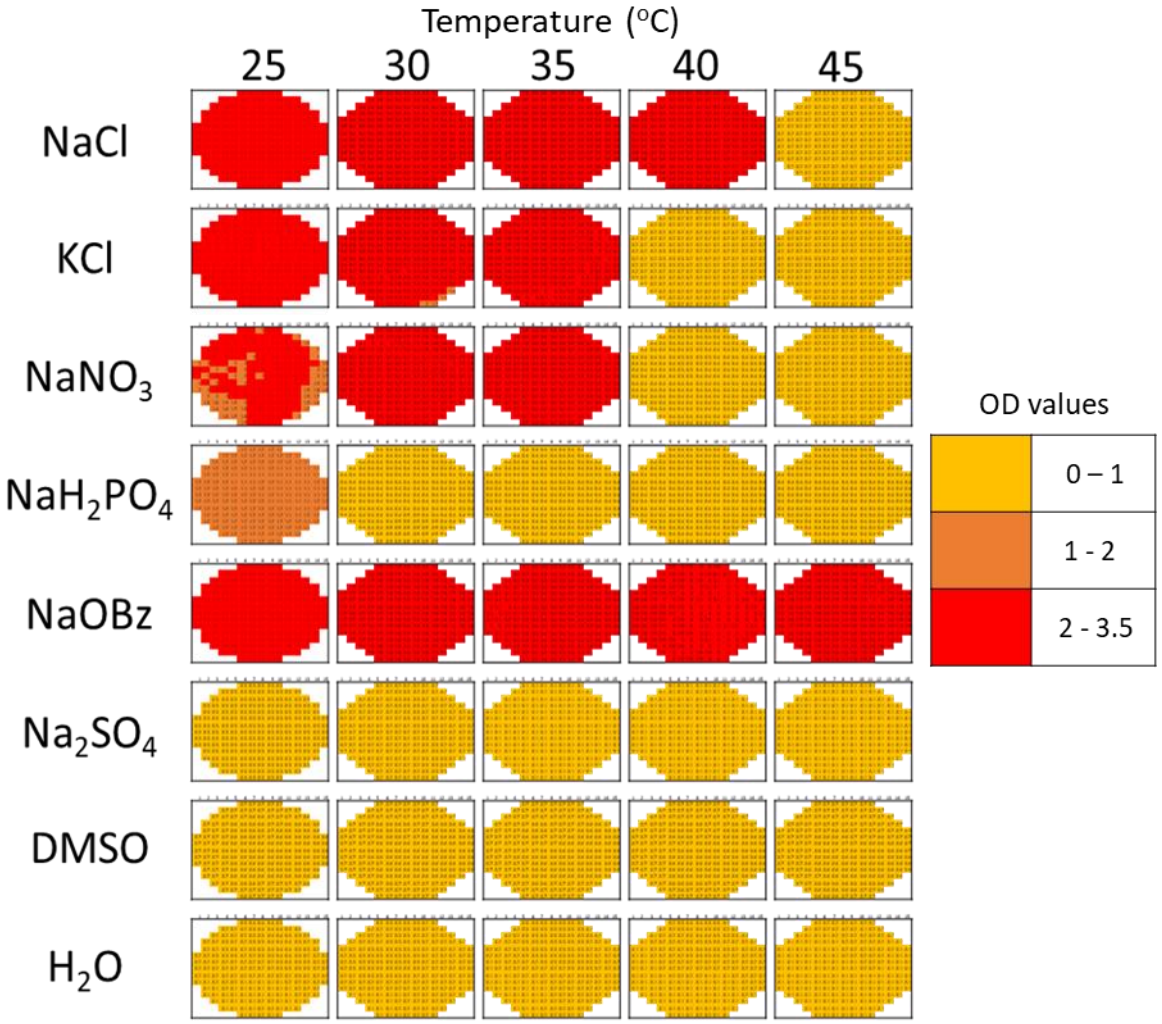

Figure S187 - Well scans (n=3) conducted at OD_{495} at a range of temperatures for SSA **3**.

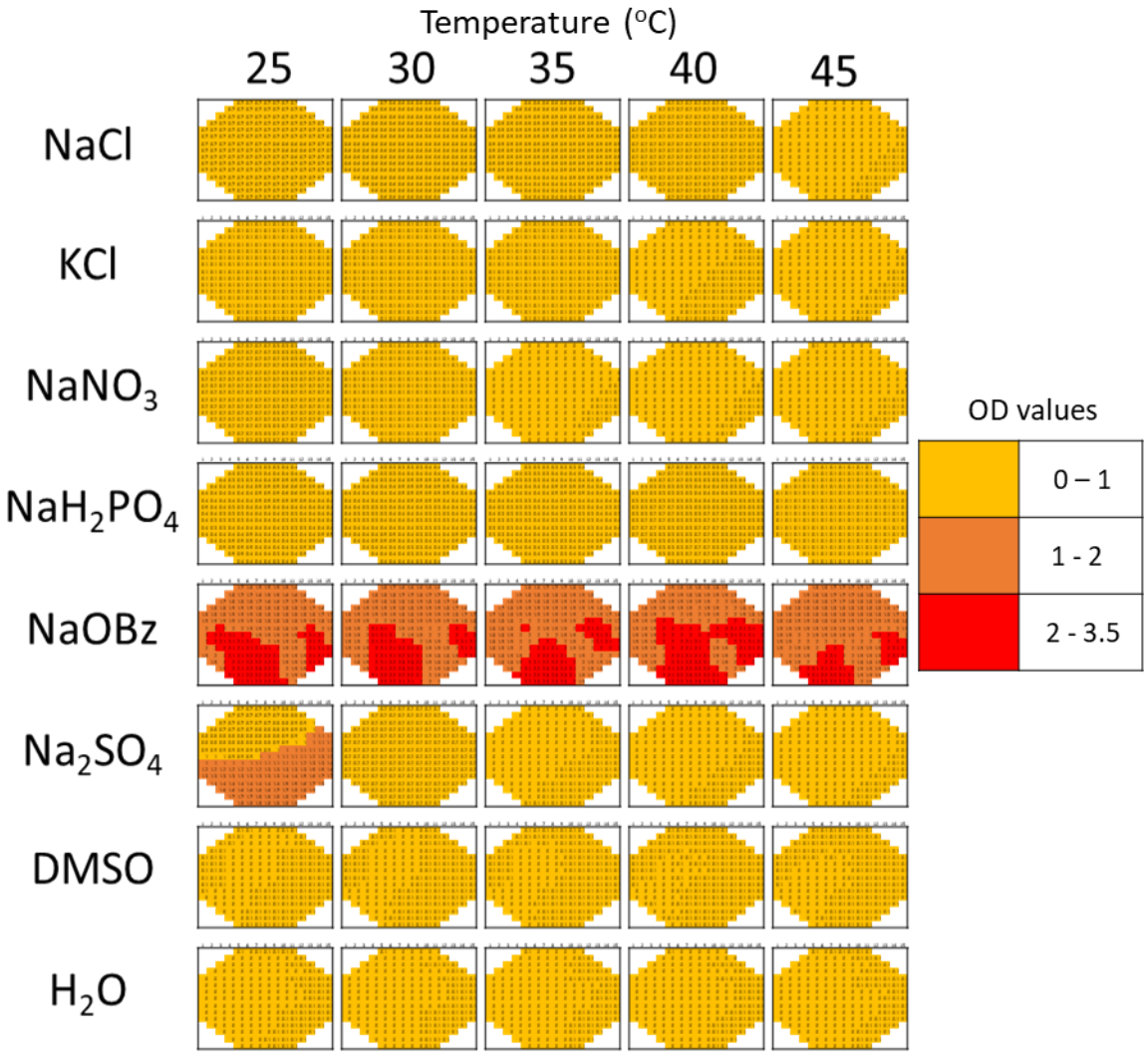

Figure S188 - Well scans (n=3) conducted at OD_{495} at a range of temperatures for SSA **4**.

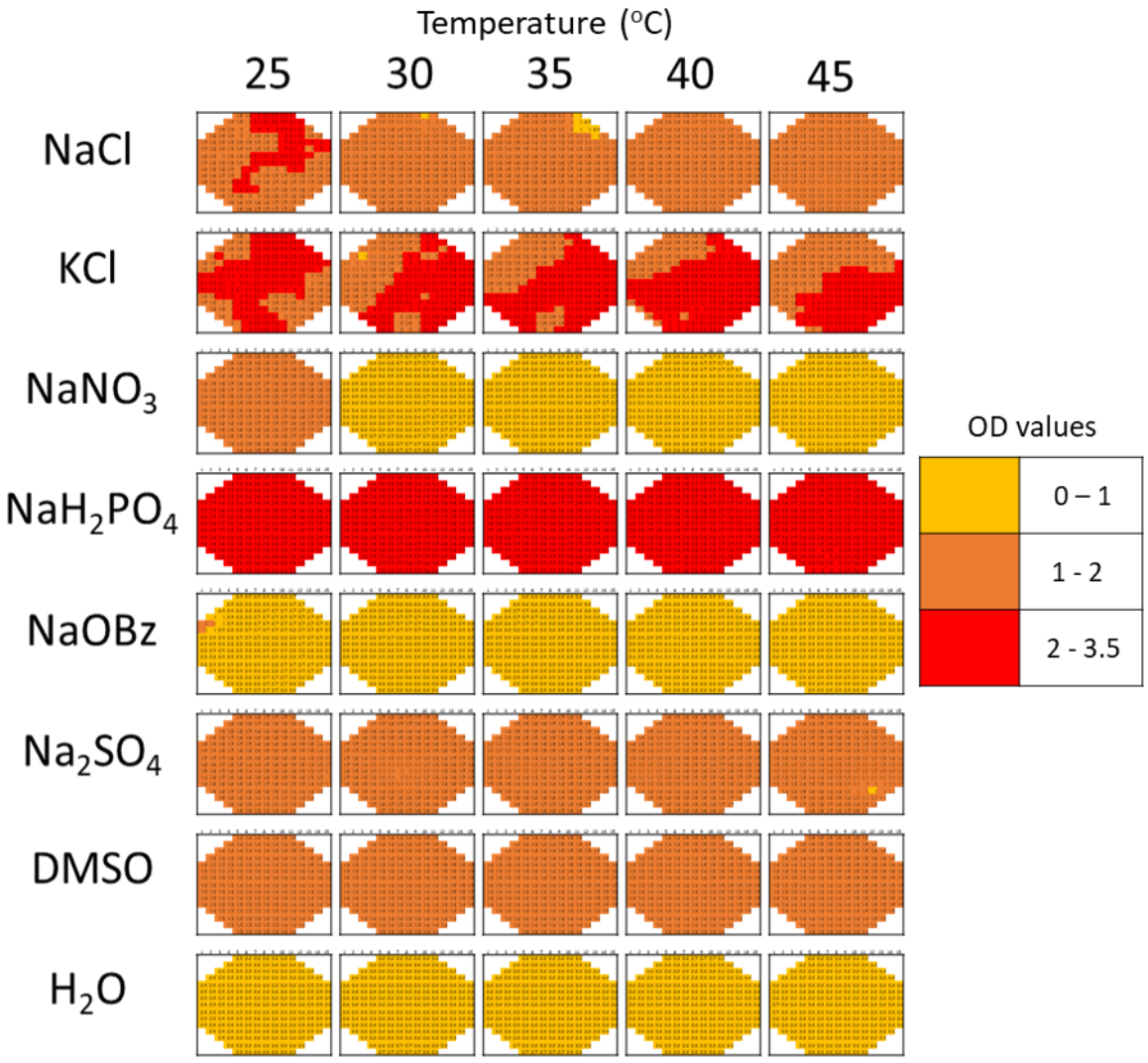

Figure S189 - Well scans (n=3) conducted at OD_{495} at a range of temperatures for SSA **5**.

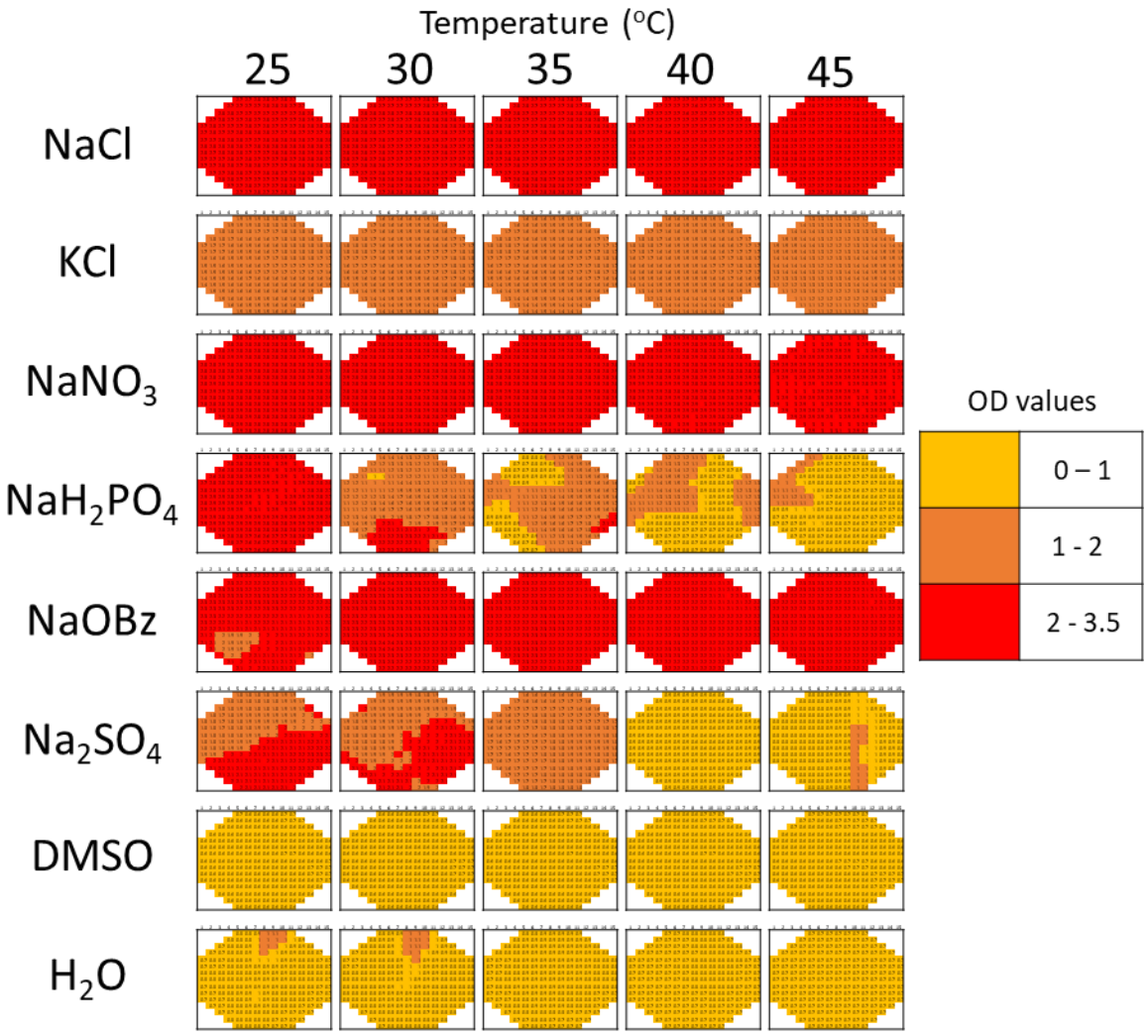

Figure S190 - Well scans (n=3) conducted at OD_{495} at a range of temperatures for SSA **6**.

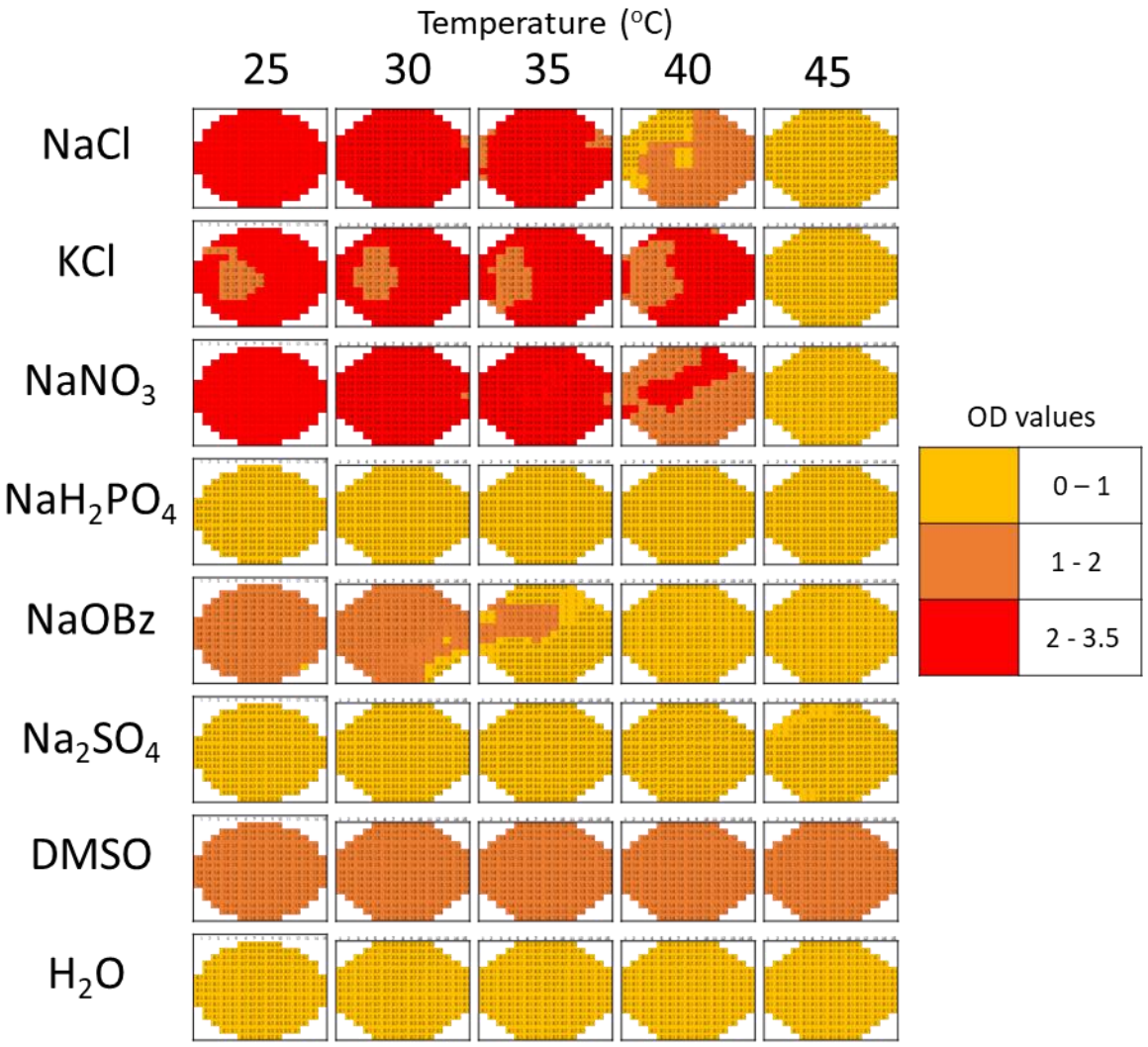

Figure S191 - Well scans (n=3) conducted at OD_{495} at a range of temperatures for SSA **7**.

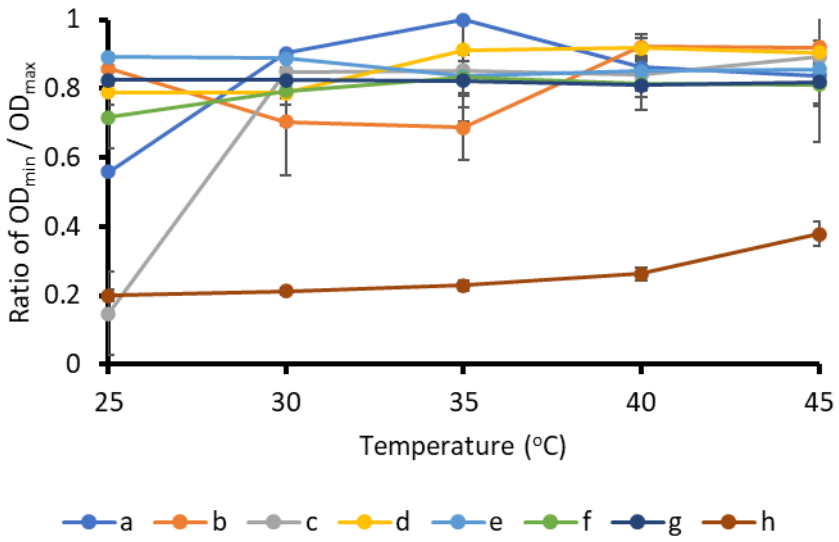

Figure S192 – Average (n=3) ratio values (OD_{495} minimum/OD_{495} maximum) taken from spectral well scan data of **3** (1.5 mg/mL). Error bars represent the full range of OD_{450} ratio values to be calculated from the n=3 OD_{495} maxima and minimum data. a = NaCl, b = KCl, c = $NaNO_3$ d = NaH_2PO_4 e = NaOBz, f = DMSO, g = H_2O.

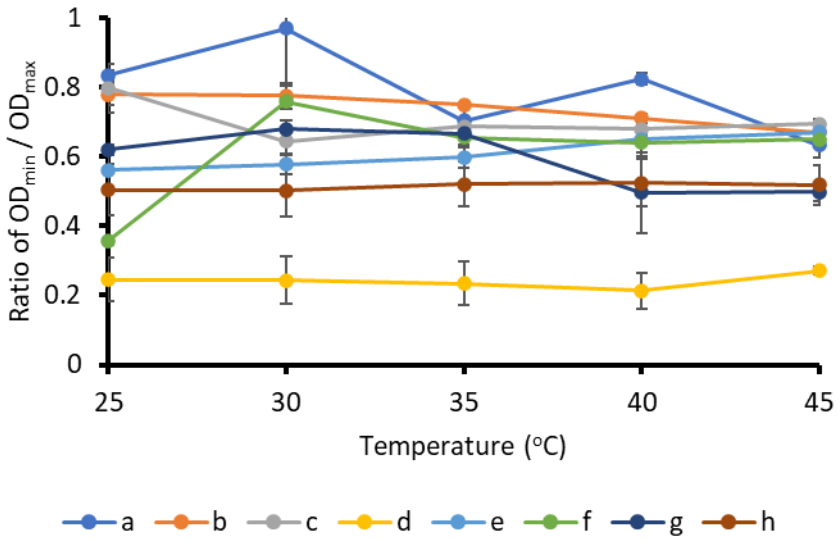

Figure S193 - Average (n=3) ratio values (OD_{495} minimum/OD_{495} maximum) taken from spectral well scan data of **4** (1.5 mg/mL). Error bars represent the full range of OD_{450} ratio values to be calculated from the n=3 OD_{495} maxima and minimum data. a = NaCl, b = KCl, c = $NaNO_3$ d = NaH_2PO_4 e = NaOBz, f = DMSO, g = H_2O.

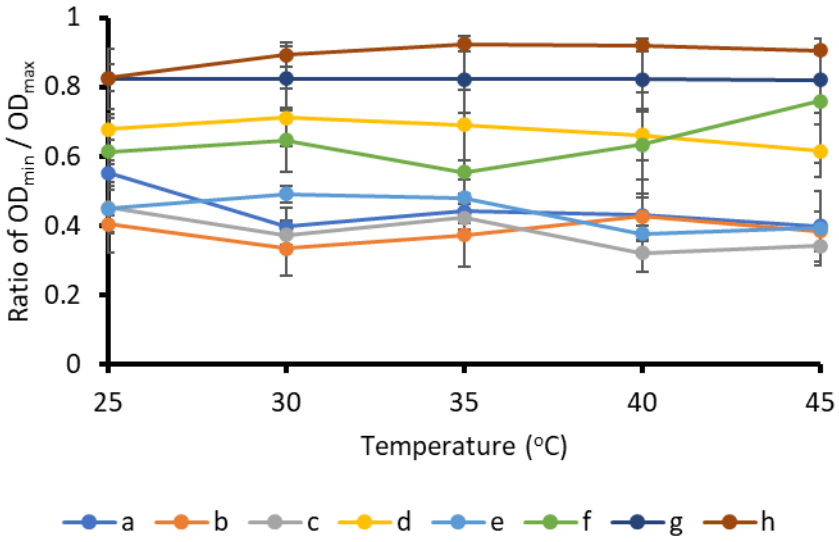

Figure S194 - Average (n=3) ratio values (OD_{495} minimum/OD_{495} maximum) taken from spectral well scan data of **5** (1.5 mg/mL). Error bars represent the full range of OD_{450} ratio values to be calculated from the n=3 OD_{495} maxima and minimum data. a = NaCl, b = KCl, c = $NaNO_3$ d = NaH_2PO_4 e = NaOBz, f = DMSO, g = H_2O.

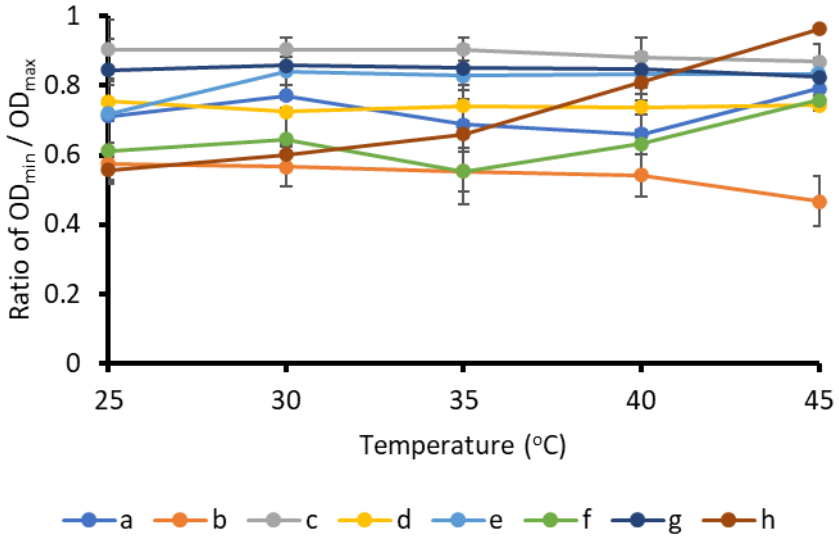

Figure S195 - Average (n=3) ratio values (OD_{495} minimum/OD_{495} maximum) taken from spectral well scan data of **6** (1.5 mg/mL). Error bars represent the full range of OD_{450} ratio values to be calculated from the n=3 OD_{495} maxima and minimum data. a = NaCl, b = KCl, c = $NaNO_3$ d = NaH_2PO_4 e = NaOBz, f = DMSO, g = H_2O.

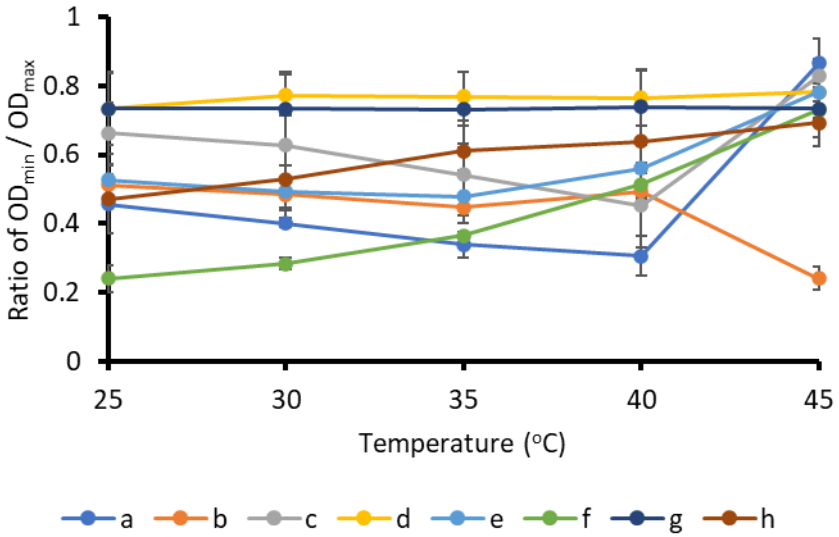

Figure S196 - Average (n=3) ratio values (OD_{495} minimum/OD_{495} maximum) taken from spectral well scan data of **7** (1.5 mg/mL). Error bars represent the full range of OD_{450} ratio values to be calculated from the n=3 OD_{495} maxima and minimum data. a = NaCl, b = KCl, c = $NaNO_3$ d = NaH_2PO_4 e = NaOBz, f = DMSO, g = H_2O.

Section 19: Low level in-silico modelling data

Computational calculations to identify primary hydrogen bond donating and accepting sites were conducted in line with studies reported by Hunter using Spartan 16"[14] Calculations were performed using semi-empirical PM6 methods, after energy minimisation calculations, to identify E_{max}, E_{min} and polarizability values. PM6 was used over AM1 in line with research conducted by Stewart.[15]

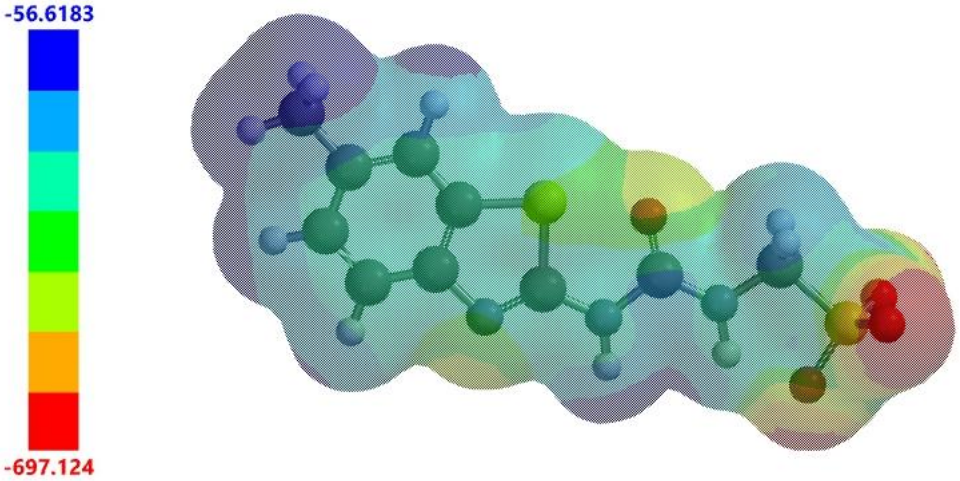

Figure S197 - Electrostatic potential map calculated for the anionic component of **1**. E_{max} and E_{min} values given in kJmol^{-1}.

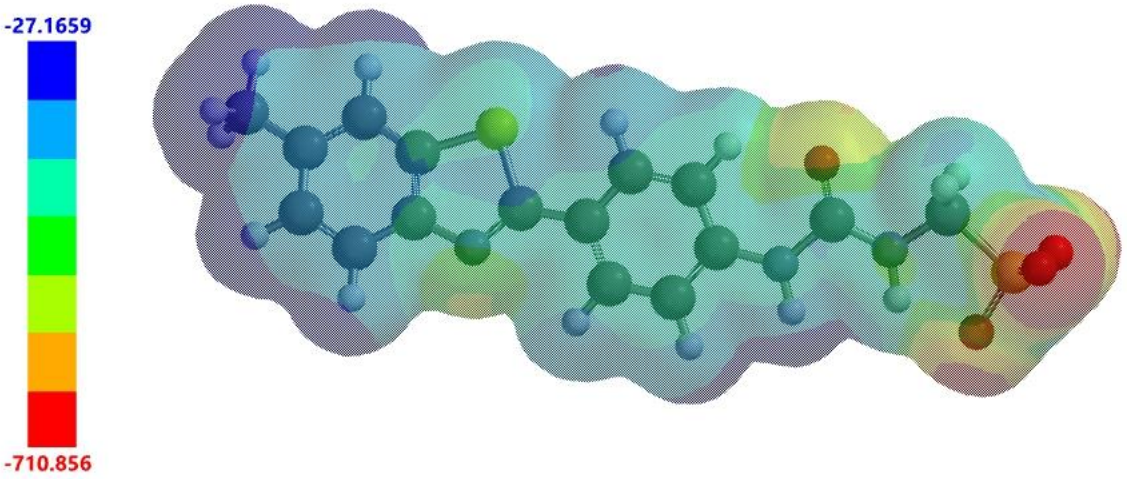

Figure S198 - Electrostatic potential map calculated for the anionic component of **2**. E_{max} and E_{min} values given in kJmol^{-1}.

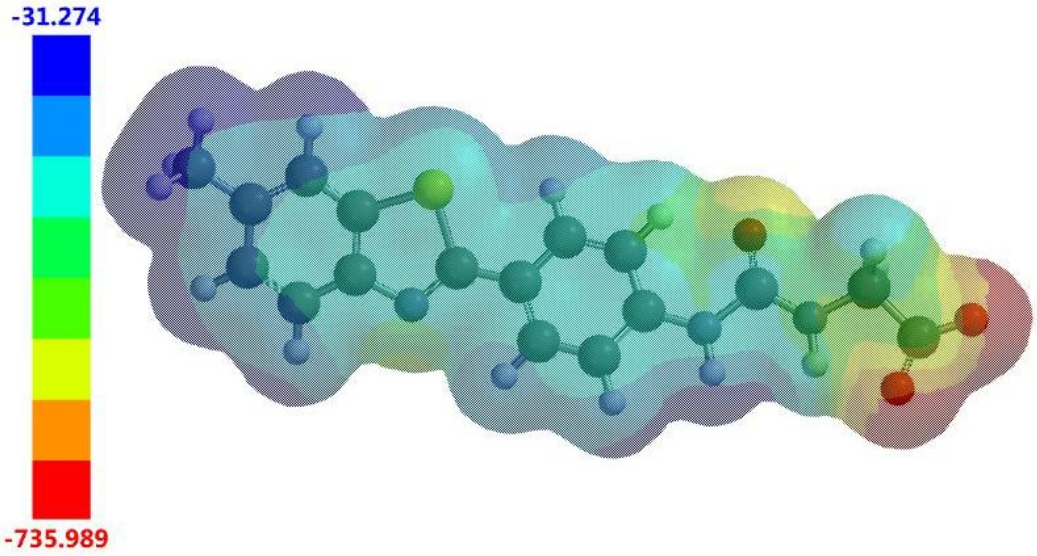

Figure S199 - Electrostatic potential map calculated for the anionic component of **6**. E_{max} and E_{min} values given in $kJmol^{-1}$.

Section 20: References

1 L. J. White, N. J. Wells, L. R. Blackholly, H. J. Shepherd, B. Wilson, G. P. Bustone, T. J. Runacres and J. R. Hiscock, *Chem. Sci.*, 2017, **8**, 7620–7630.

2 J. E. Boles, C. Bennett, J. Baker, K. L. F. Hilton, H. A. Kotak, E. R. Clark, Y. Long, L. J. White, H. Yuk Lai, C. K. Hind, J. Mark Sutton, M. D. Garrett, A. Cheasty, J. L. Ortega-Roldan, M. Charles, C. J. E. Haynes and J. R. Hiscock, *Chemical Science*, 2022, **13**, 9761–9773.

3 L. J. White, J. E. Boles, N. Allen, L. S. Alesbrook, M. J. Sutton, C. K. Hind, K. L. F. Hilton, L. R. Blackholly, R. J. Ellaby, G. T. Williams, D. P. Mulvihill and J. R. Hiscock, *Journal of Materials Chemistry B*, 2020, **8**, 4694–4700.

4 K. S. Thordarson and V. E. P. Thordarson, .

5 J. R. Hiscock, G. P. Bustone, B. Wilson, K. E. Belsey and L. R. Blackholly, *Soft Matter*, 2016, **12**, 4221–4228.

6 L. J. White, C. Wark, L. Croucher, E. R. Draper and J. R. Hiscock, *Chemical Communications*, 2020, **56**, 9557–9560.

7 J. E. Sulston and S. Brenner, *Genetics*, 1974, **77**, 95–104.

8 T. Komura, M. Yamanaka, K. Nishimura, K. Hara and Y. Nishikawa, *npj Aging Mech Dis*, 2021, **7**, 1–11.

9 C. Morris, O. K. Foster, S. Handa, K. Peloza, L. Voss, H. Somhegyi, Y. Jian, M. V. Vo, M. Harp, F. M. Rambo, C. Yang and G. J. Hermann, *PLOS Genetics*, 2018, **14**, e1007772.

10 On-line Lipophilicity/Aqueous Solubility Calculation Software, http://www.vcclab.org/lab/alogps/, (accessed 18 July 2022).

11 I. V. Tetko, J. Gasteiger, R. Todeschini, A. Mauri, D. Livingstone, P. Ertl, V. A. Palyulin, E. V. Radchenko, N. S. Zefirov, A. S. Makarenko, V. Yu. Tanchuk and V. V. Prokopenko, *J Comput Aided Mol Des*, 2005, **19**, 453–463.

12 B. O. Keller, J. Sui, A. B. Young and R. M. Whittal, *Analytica Chimica Acta*, 2008, **627**, 71–81.

13 M. Bilodeau, *All Theses*.

14 C. A. Hunter, *Angewandte Chemie International Edition*, 2004, **43**, 5310–5324.

15 J. J. P. Stewart, *Journal of Molecular modeling*, 2007, **13**, 1173–1213.